UNIVERSITÀ
DEGLI STUDI
DI PADOVA

Università degli Studi di Padova

Centro Interdipartimentale di Studi e Attività Spaziali (CISAS) 'G. Colombo'

SCUOLA DI DOTTORATO DI RICERCA IN: Scienze Tecnologie e Misure Spaziali

INDIRIZZO: Astronautica e Scienze da Satellite

CICLO: XXIII

TITOLO TESI

'STUDY AND PREPARATION OF SPACE MISSIONS FOR ASTEROSEISMOLOGY'

Direttore della Scuola: Ch.mo Prof. Giampiero Naletto

Supervisore: Ch.mo Prof. Francesco Marzari

Dottoranda: Serena Benatti

To Cinzia & Raffaele

Abstract

The PhD project presented in this thesis is aimed to exploit the great potential of Asteroseismology combined with the high precision photometry of present and future space satellites. The ESA-PLATO space mission [36] is proposed to be the next generation planet-finder, having its worth in the characterization of the parent stars thanks to asteroseismic analysis. The present work includes the feasibility study of PLATO, with particular attention on the analysis of simulated images, in order to evaluate the photometric quality of the optical design. Then the creation of procedures to perform seismic analysis allows us to measure useful asteroseismic observables which provide noticeable informations about the stellar structure. Finally we were able to constrain fundamental parameters of stars through the computation of stellar theoretical models supported by space-based observations with the NASA-Kepler satellite [29]. In the framework of Kepler and PLATO these results are of great importance, because the knowledge of global stellar parameters is the only way to characterize an extrasolar planet.

0.1 Asteroseismology

Asteroseismology analyses oscillation frequencies of stars, allowing to measure fundamental stellar parameters with an unprecedent accuracy. These pulsations are standing acoustic waves propagating between the surface and an inner point located in a position which depends on the characteristics of the oscillation mode, and therefore on the chemical and physical conditions of the stellar internal regions. Thanks to this peculiarity, Asteroseismology represents a remarkable diagnostic tool to constrain stellar structure.

By assuming adiabatic regime and neglecting any perturbations of gravitation potential (the so called *asymptotic theory*) it is possible to describe the general equation of stellar non-radial pulsations as:

$$\frac{d^2\xi_r}{dr^2} = -K(r)\xi_r \quad \text{where} \quad K(r) = \frac{\omega^2}{c^2}\left(\frac{N^2}{\omega^2} - 1\right)\left(\frac{S_l^2}{\omega^2} - 1\right). \tag{1}$$

N and S_l are the characteristic frequencies of two different pulsation regimes. The *buoyancy* frequency, N, is typical for modes driven by gravity (the so called 'g-modes'), occurring in the inner part of a star, whereas S_l is the *acoustic* frequency, typical for modes driven by pressure ('p-modes'), depending on l, the angular degree of the mode. The p-modes occur in the outer envelope of a star and undergo several refractions each time they pass through different layers, characterized by different values of the sound speed c. The bends of their trajectory affect the resulting frequencies providing thus a unique opportunity to map the stellar interiors.

Several driving mechanisms are responsible for stellar pulsations. The opacity mechanism acting in the partial ionization zone of elements of stellar matter produce p-, g-

(or both) oscillation modes for several type of stars, like Cepheids, Extreme Horizontal Branch stars, White Dwarfs and so on. The other mechanism, that mainly acts in the Sun, in Solar-like stars and in the Red Giants is the stochastic perturbation due to the turbolent convection in the outer envelope. The diagnostic potential of Asteroseismology is particularly important in the case of solar-like oscillations and it can be described by several relations between oscillation frequencies. According to the asymptotic theory the pulsation frequencies can be described by:

$$\nu_{nl} \simeq (n + \frac{l}{2} + \frac{1}{4} + \alpha)\Delta\nu - (AL^2 - \beta)\frac{\Delta\nu^2}{\nu_{nl}} \tag{2}$$

where

$$\Delta\nu \equiv \nu_{n+1,l} - \nu_{n,l} \simeq [2\int_0^R \frac{dr}{c}]^{-1} \text{ and } A \equiv \delta\nu \equiv \nu_{nl} - \nu_{n-1,l+2} \simeq \int_0^R \frac{dc}{dr}\frac{dr}{r} \tag{3}$$

are called *large frequency separation*, and $\delta\nu$ *small frequency separation*. The former is the inverse of twice the sound travel time between the centre and the stellar surface, providing thus informations about the mean properties of the stellar structure, the latter is sensitive to the conditions of the stellar core, through the gradient of the sound speed and thus the gradient of the mean molecular weight of the matter, providing a measure of the evolutionary state of the star. One of the most important diagnostic tools of Asteroseismology is the *asteroseismic HR diagram* that correlates the large and the small separations. As the star evolves, its position in this diagram varies creating an out-and-out evolutionary track. A particular feature of the solar-like oscillations is the presence of a Lorentian-shaped 'hump' in their power spectra that reveals the presence of a series of equally spaced frequencies. If we subdivide the spectrum in small portions with size equal to the large separation and stack them together we obtain the *echelle diagram*. According to the asymptotic theory, modes with the same value of the angular degree will be placed along vertical lines.

A large amount of stellar pulsating classes widely spread on the Hertzsprung-Russell diagram. Among them, besides the already mentioned solar-like oscillations, Subdwarf B stars show both gravity and pressure modes, in some case simultaneously, and are suited to search for possible planetary companion with the timing method, which represents the main goal of the observing network EXOTIME [138]. Finally, first Kepler observations allowed to discover the great variety of pulsation characteristics of hybrid γ Doradus and δ Scuti stars.

A strong connection exists between Asteroseismology and the search for Extrasolar planets. Both ground- and space-based instruments, dedicated to the detection of exoplanets provide valuable data for the asteroseismic research (e.g. HARPS [127] and SARG [74] spectrographs, the EXOTIME network [138], or CoRoT [8] and Kepler [29] satellites and the future PLATO Mission [36]). Furthermore space-based observations provide long and uninterrupted time series, so they are particularly suited to perform Asteroseismology.

The PhD project presented in this thesis has been developed in the scenario above mentioned, exploiting the asteroseismic potential provided by space instruments. In particular, the research follows several steps of a space mission project, contributing to the feasibility study of a satellite, passing through the analysis of the incoming data and the use of the results to determine reliable stellar parameters thanks to Asteroseismology.

0.2 PLATO Mission

The PLATO (*PLAnetary Transits and Oscillations of stars*) satellite is a space mission proposed for the ESA Cosmic Vision scientific plan for the years 2015-2025. Its main goal is the search for extrasolar planets with the transits method and their characterization through Asteroseismology. A full description of the project can be found in Catala et al. 2008 [36].

Part of the work presented in this thesis is focused on the preliminary study of PLATO satellite. Our aim was the estimation of the performances of the instrument by using a set of simulations (provided to us by Dr. Zima through an End-to-End Simulator [158]), which recreate the images at the focal plane of the telescope, adding all the possible sources of noise (sky background, readout noise from the detector, instrumental drift, ...). By calculating the noise budget for each simulated star in part per million per hour [ppm/h] for all of the 40 telescope units of PLATO, we are able to verify if the scientific requirements for the accepted noise levels (27 ppm/h for the stellar oscillations and 80 ppm/h for exoplanets detection) are fulfilled. We found that brighter stars ($m_V \sim 7 - 8$) show a low level of noise, but in some case this is due to their saturation on the detector. Stars with input magnitude less than $m_V \sim 11$ show a noise level less than 27 ppm/h, while the condition of the 80 ppm/h is fulfilled by stars with magnitude less than $m_V \sim 13$.

As secondary task we quantified the stellar crowding which affects the simulations, a problem that forced to abandon the preliminary idea of an observing strategy centred on the telescope defocussing. At first we estimated the shift of the luminosity function of the input catalog toward the brighter magnitudes. The amount of contaminating flux due to the neighbour sources for each star was estimated by using as input the dimensions of the Point Spread Function and the specified encircled energy. As expected, fainter stars are the most affected by crowding effect.

Finally, we present a procedure which, starting from a set of theoretical oscillation frequencies of a typical target, simulates the time series of the star as observed by PLATO. Then it adds this light curve to the time series of the noise described before and extracts the amplitude spectrum. This tool is useful to assure that these fluctuations can be actually observed by PLATO, and to evaluate the impact of the stellar noise on the detection of a planetary transit.

0.3 Seismic analysis

During the three years of PhD we created several IDL codes, aimed to perform seismic analysis of time series. We then applied these procedures to data obtained both from space (with the Kepler satellite) and from the ground (observations collected for the EXOTIME project).

Starting from raw time series data, these procedures extract the frequency spectrum by using the algorithm defined by Deeming [62], after a statistical analysis to investigate the properties of the time series. Then the frequencies extraction is performed through a prewhitening process. We tested the procedures with the Kepler data for a sample of hybrid γ Dor and δ Sct stars, in the framework of the collaboration with the WG 10 (The Working Group dedicated to the analysis of γ Doradus stars of KASC-Kepler Asteroseismic Science Consortium), having the purpose to compare the extracted frequencies of those targets among the members of the group. Other features were implemented to our procedures,

useful for the analysis of solar-like oscillations. Even in this case we had the opportunity to verify our codes with Kepler data, by using the preliminary observations of three solar-like stars reported by Chaplin et al. 2010 [37]. We modelled the background of the available power spectra through a least-square fit procedure and calculated the value of the large separation by evaluating of the *comb response* function (a tool able to reveal possible periodicities in the power spectrum in the frequency range of the Lorentian envelope). Finally we created the *echelle* diagram for the frequencies extracted by the prewhitening procedure.

Finally the data personally collected at the Asiago-Mt.Ekar Observatory, in the framework of the EXOTIME project, for the target HS0702+6043, already known as an hybrid Subdwarf B star [137], were used to test and verify the reliability of the codes. Besides the observations and data reduction, our contribution to this project includes the responsibility for the data collection and analysis of PG1325+101, another target of the EXOTIME sample.

0.4 Modelling solar-like stars with Asteroseismology

The last argument of the present thesis is the modelling of a sample of Solar-type stars observed by Kepler and show how, thanks to the computation of theoretical models, it is possible to obtain stellar fundamental parameters. The final goal is to search for the best candidate to be a solar-twin.

At first we computed stellar evolution models by using the code ASTEC [44], taking as input data stellar parameters available from the Kepler Input Catalog [103] and from literature. In order to reproduce the observed parameters we computed grids of evolutionary models starting with high steps of increments in mass, mixing-length parameters and metallicity, gradually approaching to the best set of models for each target star. Subsequently we computed the theoretical oscillation frequencies corresponding to the models, with the adiabatic oscillations code ADIPLS [43]. Finally the stellar models able to represent the set of frequencies observed with Kepler are selected through a chi-square minimization test. Our best result was obtained for the solar-like star KIC8379927. For this star we determined the following stellar parameters: mass equal to 1.2 $M_{\odot}$, age of 4.74 Gyr, radius of 1.15 $R_{\odot}$, $\log g$ equal to 4.39, effective temperature of 5696 K and luminosity of $1.26 L_{\odot}$.

In some case the comparison with the observed frequencies was further hampered by the poor or ambiguous mode identification. Because these stars behave like a distant Sun, they are expected to have very weak pulsations, leading to a difficult mode identification. The continuous collection of time series from space is expected to solve this problem and to provide unambiguous evidence of solar-like oscillations. On the other hand we found disagreement between KIC parameters, moreover affected by high uncertainties, and the corresponding ones from literature. This made the stellar modelling particularly difficult, producing erroneous or unexpected results. Actually the stellar mass of our best model indicates that KIC8379927 is not properly a solar-twin. This demonstrates that the KIC parameters should be verified and stresses the extreme necessity to know reliable values of stellar parameters, in addition to a high accuracy in their determination. In fact the possibility to obtain accurate determination of fundamental stellar parameters, provided by asteroseismic techniques, is a fundamental step toward exoplanets characterization, especially in consideration of the future space mission PLATO.

Sommario

Il progetto di dottorato di ricerca presentato in questa tesi si propone di sfruttare il potenziale dell'Asterosismologia combinato con l'alta precisione fotometrica fornita dai satelliti spaziali, sia quelli già operativi che in fase di progettazione. Il satellite ESA-PLATO (*PLAnetary Transits and Oscillations of stars*) [36] è stato proposto come uno strumento per la ricerca di pianeti extrasolari di prossima generazione, sfruttando l'analisi asterosismologica per la caratterizzazione della stella centrale del sistema planetario. Il presente lavoro include parte dello studio di fattibilità di PLATO, con particolare attenzione all'analisi di immagini simulate, al fine di valutare la qualità fotometrica del disegno ottico dei telescopi. Verrà quindi discussa la creazione di procedure per eseguire l'analisi sismica che permette di misurare gli osservabili asterosismologici che forniscono importanti informazioni riguardanti la struttura stellare. Infine siamo stati in grado di fissare i parametri fondamentali di alcune stelle attraverso il calcolo di modelli stellari teorici supportata da osservazioni dallo spazio con il satellite NASA-Kepler [29]. Nel quadro di Kepler e PLATO questi risultati sono di grande importanza, perché la conoscenza dei parametri stellari è l'unico modo per caratterizzare un pianeta extrasolare.

0.5 Asterosismologia

L'Asterosismologia è la scienza che analizza le frequenze di oscillazione delle stelle al fine di misurarne i parametri fondamentali con una precisione mai ottenuta finora. Queste pulsazioni sono onde acustiche stazionarie che si propagano tra la superficie e un punto interno, situato in una posizione che dipende dalle caratteristiche del modo di oscillazione, e quindi dalle condizioni chimico-fisiche degli strati stellari interni. Grazie a questa peculiarità, l'Asterosismologia rappresenta uno straordinario strumento di diagnostica per porre dei vincoli alla struttura stellare.

Assumendo un regime adiabatico e trascurando le perturbazioni del potenziale gravitazionale (ipotesi alla base della cosiddetta *teoria asintotica*) è possibile descrivere l'equazione generale delle pulsazioni stellari non radiali come:

$$\frac{d^2\xi_r}{dr^2} = -K(r)\xi_r \qquad \text{dove} \qquad K(r) = \frac{\omega^2}{c^2}\left(\frac{N^2}{\omega^2} - 1\right)\left(\frac{S_l^2}{\omega^2} - 1\right). \tag{4}$$

N e S_l sono le frequenze caratteristiche di due diversi regimi di pulsazione. La frequenza di *galleggiamento*, N, è tipica per i modi indotti dalla gravità (i cosiddetti 'modi-g'), che si verificano nella parte più interna di una stella, mentre S_l è la frequenza *acustica*, tipica per le pulsazioni indotte dalla pressione ('modi-p'), dipendente dal grado angolare del modo, l. I modi-p si propagano nell'inviluppo esterno di una stella e subiscono una serie di rifrazioni ogni volta che attraversano diversi strati di materia stellare, caratterizzati da differenti valori della velocità del suono c. La curvatura della loro traiettoria, causata da queste

rifrazioni influisce sulle frequenze di oscillazione risultanti, fornendo così un'occasione unica per mappare gli interni stellari.

Le pulsazioni stellari sono indotte da diversi meccanismi di eccitazione. Il meccanismo di opacità agisce nella zona di parziale ionizzazione degli elementi della materia stellare per produrre modi -p o -g (o anche entrambi) per diversi tipi di stelle, come le Cefeidi, stelle del Ramo Orizzontale Estremo (EHB), nane bianche e così via. L'altro meccanismo, che agisce principalmente nel Sole, in stelle di tipo solare e nelle giganti rosse è la perturbazione stocastica causata dalla convezione turbolenta nell'inviluppo esterno. Le potenzialità diagnostiche dell'Asterosismologia sono particolarmente importanti proprio nel caso di oscillazioni di tipo solare e derivano da alcune relazioni tra le frequenze di oscillazione. Secondo la teoria asintotica le frequenze di pulsazione possono essere descritte da:

$$\nu_{nl} \simeq (n + \frac{l}{2} + \frac{1}{4} + \alpha)\Delta\nu - (AL^2 - \beta)\frac{\Delta\nu^2}{\nu_{nl}} \tag{5}$$

dove n ed l sono rispettivamente l'ordine radiale e il grado angolare del modo, mentre:

$$\Delta\nu \equiv \nu_{n+1,l} - \nu_{n,l} \simeq [2\int_0^R \frac{dr}{c}]^{-1} \quad \text{e} \quad A \equiv \delta\nu \equiv \nu_{nl} - \nu_{n-1,l+2} \simeq \int_0^R \frac{dc}{dr}\frac{dr}{r}. \tag{6}$$

La quantità $\Delta\nu$ è chiamata *grande separazione*, e $\delta\nu$ *piccola separazione* in frequenza. La prima è l'inverso del doppio del tempo di percorrenza dell'onda fra il centro e la superficie stellare, fornendo così informazioni circa le proprietà globali della struttura stellare, mentre la piccola separazione è strettamente dipendente dalle condizioni del nucleo, attraverso il gradiente della velocità del suono e quindi del peso molecolare medio della materia, indicatore dello stato evolutivo della stella. Uno dei diagrammi diagnostici fondamentali dell'Asterosismologia è proprio quello che mette in relazione piccola e grande separazione: al variare dell'età di una stella varia anche la sua posizione in questo diagramma, descrivendo quindi una traccia evolutiva e per tale motivo viene chiamato *diagramma HR asterosismologico*. Una particolare caratteristica delle pulsazioni di tipo solare è la presenza di frequenze equispaziate di un valore pari a $\Delta\nu$, chiaramente riconoscibili nello spettro delle frequenze come un eccesso di potenza dalla forma di una lorenziana. In particolare se si suddivide tale spettro in porzioni di dimensione pari alla grande separazione e successivamente si dispongono una sull'altra si ottiene il *diagramma echelle*. Secondo la teoria asintotica i modi caratterizzati dallo stesso grado angolare si disporranno lungo linee verticali permettendone così l'identificazione.

Le classi di stelle pulsanti sono ampiamente diffuse nel diagramma HR. Tra queste, oltre che alle già citate stelle di tipo solare, troviamo le Subnane B che possono presentare sia modi-p che modi-g, anche contemporaneamente, e possono essere impiegate per la ricerca di possibili compagni planetari con il metodo del *timing*, che rappresenta l'obiettivo principale del progetto osservativo EXOTIME [138]. Le prime osservazioni di Kepler hanno permesso di scoprire la varietà delle caratteristiche pulsazionali delle stelle ibride γ Doradus e δ Scuti.

Tra l'Asterosismologia e la ricerca di pianeti extrasolari intercorre una profonda connessione, soprattutto dal punto di vista osservativo. Infatti la strumentazione dedicata alla rivelazione di pianeti extrasolari sia da terra che dallo spazio, è in grado di fornire dati preziosi per la ricerca asterosismologica (citiamo ad esempio gli spettrografi HARPS [127] e SARG [74], il network osservativo EXOTIME [138], o i satelliti CoRoT [8] e Kepler [29] e la

futura Missione PLATO [36]). Inoltre le osservazioni spaziali sono particolarmente adatte all'Asterosismologia, dato che possono fornire serie temporali lunghe ed ininterrotte.

Il progetto di dottorato di ricerca presentato in questa tesi è stato sviluppato nello scenario appena menzionato, avvalendosi del potenziale asterosismologico fornito dagli strumenti spaziali. In particolare questo lavoro attraversa varie fasi di un progetto di missione spaziale, contribuendo allo studio di fattibilità del satellite PLATO, passando attraverso l'analisi di dati Kepler e l'utilizzo di questi risultati per determinare con buona precisione i parametri stellari fondamentali, grazie alle tecniche asterosismologiche.

0.6 La missione PLATO

Il satellite PLATO (*PLAnetary Transits and Oscillations of stars*) è una delle missioni spaziali proposte per il piano scientifico dell'ESA 'Cosmic Vision 2015-2025'. L'obiettivo di PLATO è la ricerca di pianeti extrasolari con il metodo dei transiti e la loro caratterizzazione tramite l'Asterosismologia. Una descrizione completa del progetto si può trovare in Catala et al. 2008 [36].

Una parte del lavoro presentato in questa tesi è focalizzata proprio sullo studio di fattibilità di PLATO. Il nostro obiettivo era la valutazione delle prestazioni dello strumento utilizzando una serie di simulazioni (che ci sono state fornite dal Dr. Zima attraverso un simulatore End-To-End [158]), che ricrea le immagini del campo stellare sul piano focale del telescopio, con l'aggiunta di tutte le possibili fonti di rumore (il fondo cielo, il rumore di lettura del rivelatore, la deriva strumentale, ...). Attraverso il calcolo della quantità di rumore associata ad ogni stella simulata (calcolato in parti per milione per ora, [ppm/h]), è possibile verificare se siano soddisfatti i requisiti scientifici riguardanti il massimo livello di rumore consentito (e cioè 27 ppm/h per le oscillazioni stellari e 80 ppm/h per la rilevazione di pianeti extrasolari). Si è trovato che le stelle più luminose (con $m_V \sim 7-8$) mostrano un basso livello di rumore, anche se in alcuni casi questo è dovuto alla saturazione del rivelatore. Le stelle con magnitudine inferiore a $m_V \sim 11$ mostrano un livello di rumore minore di 27 ppm/h, mentre la condizione per la rivelazione dei pianeti viene soddisfatta da stelle con magnitudine inferiore a $m_V \sim 13$.

Come secondo compito abbiamo quantificato l'alta concentrazione stellare (*crowding*) che influenza la qualità delle simulazioni, un problema che ha costretto ad abbandonare l'idea preliminare di eseguire le osservazioni con i telescopi defocati. In un primo momento abbiamo stimato lo spostamento della funzione di luminosità del catalogo di input verso le magnitudini più luminose (si veda Figura (1), a sinistra), poi abbiamo quantificato il flusso contaminante per ogni stella, proveniente dalle sorgenti vicine tramite le dimensioni della PSF (Point Spread Function) e della *encircled energy*, la quantità di energia all'interno della PSF. Come previsto, le stelle più deboli sono le più colpite dall'effetto del crowding.

Infine, utilizzando una procedura da noi elaborata e partendo da un set di frequenze di oscillazione teoriche di un target tipico, abbiamo simulato la relativa serie temporale come fosse osservata da PLATO e successivamente aggiunto il rumore proveniente dalle curve di luce analizzate in precedenza estraendone quindi lo spettro delle ampiezze. Grazie a questo strumento è possibile assicurarsi che le oscillazioni stellari vengano effettivamente osservate da PLATO (si veda Figura (1), a destra), in cui i modi di pulsazione sono riconoscibili nell'intervallo di frequenze tra 2500 e 4500 μHz), come pure valutare l'impatto del rumore stellare sul rilevamento di un transito planetario.

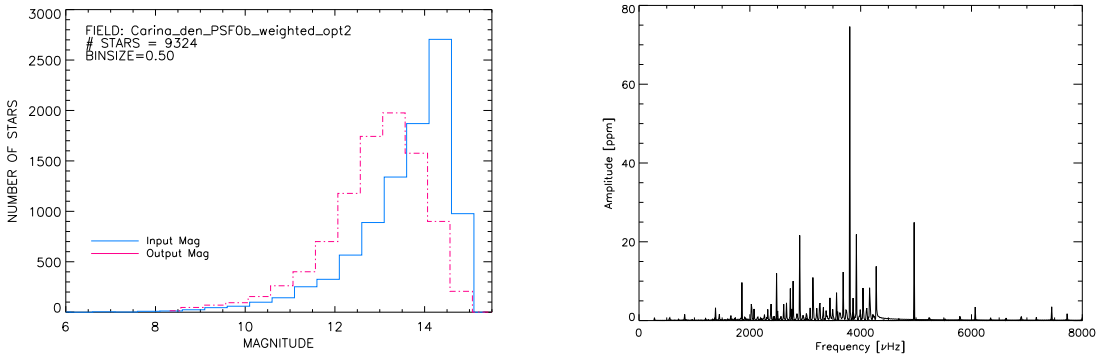

Figure 1: A sinistra: Istogramma delle magnitudini in input per le immagini simulate confrontato con quello delle magnitudini misurate e soggette al *crowding* stellare. A destra: Spettro delle frequenze del rumore simulato aggiunto alla serie temporale sintetica di un target tipico di PLATO.

0.7 Analisi sismica

Durante i tre anni di dottorato sono stati creati alcuni codici scritti in linguaggio IDL, finalizzati a svolgere l'analisi sismica di serie temporali, con applicazioni sia su dati provenienti dallo spazio (ottenuti dal satellite Kepler) che da terra (dalle osservazioni eseguite per il progetto EXOTIME).

A partire dai dati grezzi di serie temporali, queste procedure estraggono lo spettro delle frequenze di oscillazione utilizzando l'algoritmo definito da Deeming [62], a seguito di un'analisi statistica per valutare le proprietà delle serie temporali di input. Quindi viene eseguita l'estrazione delle frequenze tramite il metodo cosiddetto di *prewhitening*. Abbiamo avuto l'opportunità di testare queste procedure per un campione di stelle ibride γ Doradus e δ Scuti nell'ambito della collaborazione col Working Group 10 (il gruppo di lavoro del KASC-Kepler Asteroseismic Science Consortium che si occupa di stelle γ Doradus) al fine di confrontare le frequenze estratte di questi target tra i vari membri del gruppo. All'interno delle nostre procedure sono state implementate alcune funzionalità utili per l'analisi di stelle di tipo solare. Anche in questo caso abbiamo verificato la validità dei codici con i dati Kepler, in particolare utilizzando le prime osservazioni dei tre target presentati nell'articolo di Chaplin et al. 2010 [37]. Abbiamo quindi modellato il *background* dello spettro di potenza (cioè il rumore di fondo dello spettro generato da fenomeni come la granulazione e l'attività stellare) tramite una procedura di interpolazione ai minimi quadrati e calcolato il valore della grande separazione tramite l'analisi della funzione di *comb response*, che rivela eventuali periodocità nello spettro di potenza nella regione dell'inviluppo lorenziano tipico per queste stelle (si veda Figura (2), a sinistra). Infine abbiamo costruito il diagramma *echelle* per le frequenze estratte mediante il *prewhitening* (si veda Figura (2), a destra).

Abbiamo infine testato le nostre procedure anche per i dati raccolti personalmente presso l'Osservatorio di Asiago-Cima Ekar (VI), nell'ambito del progetto EXOTIME per la stella Subnana B HS0702+6043, già conosciuta come pulsatore ibrido [137]. Oltre che alle osservazioni e alla riduzione dati, il nostro contributo al progetto include la responsabilità di raccogliere e analizzare i dati per PG1325+101, un altro target del campione di EXOTIME.

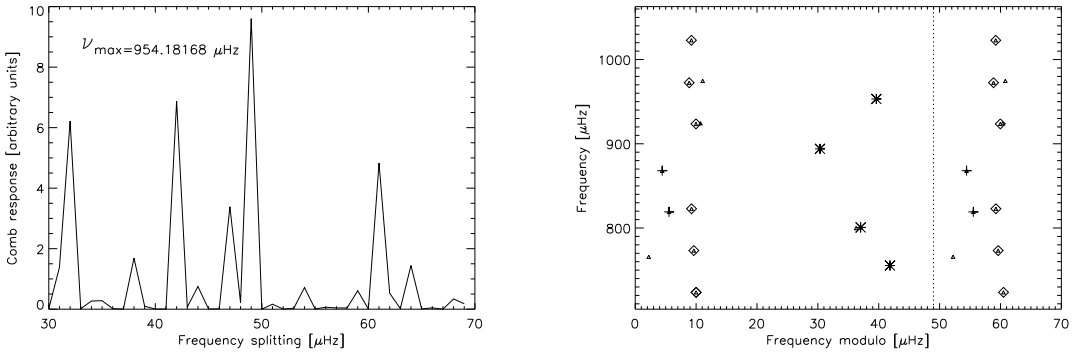

Figure 2: A sinistra: Andamento della funzione di *comb response* per uno dei target di tipo solare di Kepler: il valore massimo di questa funzione definisce la stima della grande separazione. A destra: Diagramma *echelle* delle frequenze estratte per lo stesso target.

0.8 Calcolo di modelli stellari con l'Asterosismologia

Come ultimo argomento di questa tesi viene presentata la modellizzazione di un campione di stelle di tipo solare osservato da Kepler e mostrare come, grazie all'elaborazione di modelli teorici, sia possibile ottenere parametri stellari fondamentali, con l'obiettivo di cercare il miglior candidato per essere un gemello solare.

In un primo momento abbiamo calcolato modelli di evoluzione stellare utilizzando il codice ASTEC [44], prendendo come dati di input i parametri stellari disponibili dal KIC (Kepler Input Catalog) [103] e dalla letteratura. Al fine di riprodurre i parametri osservati abbiamo calcolato le griglie di modelli evolutivi a partire da ampi incrementi in massa, parametro della mixing-length e metallicità, avvicinandoci gradualmente ai migliori modelli per ogni stella target. Successivamente abbiamo calcolato le frequenze di oscillazione teorica corrispondenti ai modelli, con il codice di pulsazioni adiabatiche ADIPLS [43]. Infine i modelli stellari in grado di rappresentare le frequenze osservate con Kepler (si veda Figura 3, a sinistra) sono stati selezionati attraverso un test di minimizzazione chi-quadro. Il nostro miglior risultato è stato ottenuto per la stella di tipo solare KIC8379927. Per questa stella abbiamo determinato i seguenti parametri: massa pari a 1.2 $M_{\odot}$, età di 4.74 miliardi di anni, raggio di 1.15 $R_{\odot}$, $\log g$ pari a 4.39, temperatura effettiva di 5696 K e una luminosità di 1.26 $L_{\odot}$ (si veda Figura 3, destra).

In qualche caso il confronto con le frequenze osservate è stato ostacolato da una scarsa o ambigua identificazione dei modi di oscillazione. Dato che queste stelle si comportano come un Sole molto distante, non è strano aspettarsi pulsazioni piuttosto deboli, che rischiano di rendere difficile l'identificazione dei modi. Ad ogni modo solo la raccolta continua di serie temporali dallo spazio permette di risolvere questo problema e rivelare oscillazioni di tipo solare senza ambiguità. D'altra parte abbiamo anche trovato disaccordo tra i parametri forniti dal KIC, in ogni caso soggetti ad alte incertezze, e quelli corrispondenti trovati in letteratura. Ciò ha reso la modellizzazione stellare particolarmente difficile, producendo risultati erronei o inattesi. A questo proposito la massa del nostro miglior modello per la stella KIC8379927 indica che quest'ultima non è propriamente un gemello solare. Ciò dimostra che i parametri forniti dal KIC devono essere verificati con altri disponibili, sottolinendo l'estrema necessità di conoscere valori attendibili dei parametri stellari, oltre che ad una elevata precisione nella loro determinazione. In effetti la possibilità

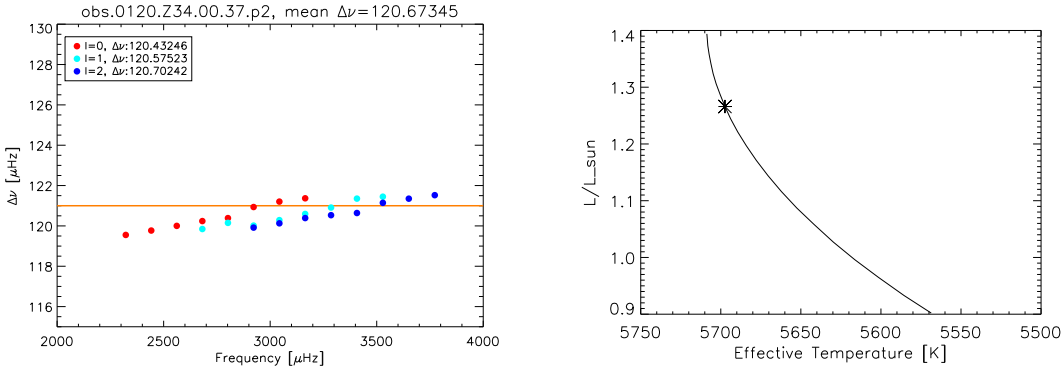

Figure 3: A sinistra: confronto tra la grande separazione media ottenuta dalle osservazioni con Kepler (linea orizzontale) e quella teorica calcolata per il miglior modello di KIC8379927. Destra: traccia evolutiva del miglior modello per KIC8379927, indicato dall'asterisco.

di ottenere un'accurata determinazione di parametri stellari fondamentali, con tecniche asterosismologiche, rappresenta un passo fondamentale verso la caratterizzazione pianeti extrasolari, soprattutto in vista della futura missione spaziale PLATO.

Contents

Introduction

Stellar pulsations represent a very important aspect in the study of stellar structure and dynamics. They are caused by changing in the thermodynamical state of the internal layers of the stars, so they are the only useful tool to know and quantify these variations. The behavior of the oscillations depends on their driving mechanism, typical of their evolutionary state and stellar characteristics. Pulsating stars are widely spread in the HR diagram, showing thus a great variety of oscillation features.

Thanks to the analysis of the solar pulsation frequencies, through Helioseismology, it was possible to obtain unprecedent informations about the structural parameters of the Sun, as well as the validation or not of the proposed solar models. The possibility to extend part of this knowledge to other stars is the main goal of Asteroseismology. Asteroseismology is a tool showing synergy with other types of research, putting constraints to the theories of stellar evolution, or, as in the purposes of the ESA-PLATO satellite, the characterization of the detected transiting planets.

On the observational point of view the strong constraint in the detection of stellar oscillations is their very low amplitude and the need to a regular and long sample in order to detect as many periodicities as possible. The observational scenario of Asteroseismology cannot be better than nowadays, since we are provided by a plenty of valuable incoming data from the space satellite like CoRoT and Kepler and the future might bring further opportunities with the already mentioned space mission PLATO.

This thesis is aimed to exploit the great potential of the asteroseismic research combined with the high precision instrumentation available. The ESA-PLATO satellite is the next generation planet-finder proposed for the *Cosmic Vision 2015-2025* plan of the European Space Agency. After the early proposal acceptation in 2008 and further reviews the final approvation from ESA is foreseen in June 2011. The main goal of this mission is to detect Earth-like planets with the transit method, while their characterization will be performed thanks to the asteroseismic analysis of the parent stars. At this moment PLATO is in its definition phase, in which the scientific and technical requirements are evaluated. In order to estimate the performances of the instrument a series of simulations were realized, trying to recreate the images at the focal plane of the telescope, adding all the possible sources of noise. The analysis of these images is an important task to perform in the framework of the feasibility study of PLATO and represents the main part of the work done in the first part of the PhD project. Thanks to this analysis the problem of crowding was revealed and quantified, allowing to study a different optical design and a different observing strategy. Indeed the high contamination due to brighter sources forced to give up the early idea of image defocussing. Using the image simulations, provided by our Belgian collaborators, we conceive a test on the detection threshold of typical solar-like oscillations with PLATO, in the case of the available noise budget. Starting from a set of theoretical oscillation frequencies, obtained with theoretical codes, simulations of time

series as observed by PLATO were created. The addition of the noise to this light curve and the extraction of the total amplitude spectrum allows to ensure if the oscillations (and then the planetary transits) can be actually observed by PLATO above the noise fluctuations.

The general purpose of this thesis is the creation of procedures to perform seismic analysis. Starting from raw data, these procedures, written in IDL code, extract the power spectrum using the algorithm of Deeming, after a statistical analysis to investigate the properties of the time series. Then the frequencies extraction is performed through a prewhitening process. The verification of the codes was performed applying them to light curves personally collected at the Asiago-Ekar Observatory in the framework of the EXOTIME project (see Chapter 2). Again the application of these codes to Kepler data of hybrid γ Doradus and δ Scuti stars as well as solar-like stars represents another test of the procedures with space data.

As deeply discussed in the first Chapter of this thesis, the importance of Asteroseismology resides on its diagnostic power of fundamental stellar parameters. Reliable values of mass, age, radius,..., can be obtained if one knows the pulsation frequencies of a star. Thanks to the four months experience at the Centro de Astrofísica da Universidade do Porto (Porto University, Portugal), under the supervision of Prof. M. Monteiro, it was possible to apply asteroseismic potential to constrain stellar fundamental parameters. The first step is to compute stellar evolution models in order to reproduce the observed stellar parameters and the corresponding theoretical oscillation frequencies. Subsequently, the comparison between Kepler data and theoretical predictions allow to select the model that better represents the target star.

In the framework of Kepler and PLATO this results are of great importance, because the knowledge of global stellar parameters is the only way to characterize an extrasolar planets. In fact both in the case of the transits and in radial velocities methods the achievable informations about radius and mass of the planet are always in function of stellar radius and mass.

The topics are subdivided as follows:

In the first Chapter the basic principles of Asteroseismology are presented. After a brief recall of the fundamental equations of stellar structure, hydrodynamics and stellar oscillations, the physical nature of the oscillation modes is reported, as well as the asymptotic theory. The diagnostic potential of asteroseismic observables are also presented and discussed. Finally the pulsation properties of some stellar classes are introduced.

The second Chapter reports about the synergy between Asteroseismology and the search for Extrasolar planets, with particular attention to the observational point of view. The state of the art for ground- and space-based observations together with the most important results are described (e.g. HARPS spectrograph and Kepler satellite).

The scientific and technical aspects of PLATO mission are introduced in the first part of the third Chapter. After that is described the work performed in order to analyse the simulated images that recreate part of the field of view, provided by Dr. W. Zima through the end-to-end simulator. These images were simulated in order to study all the possible sources of noise and to evaluate the impact of this noise on the photometric measurements to demonstrate the fulfill of the mission requirements. A preliminary evaluation of the telescopes defocussing is shown and the amount of the contaminating flux due to the high crowding is evaluated. Finally, the impact of the instrumental noise on the detection of stellar pulsation is discussed through the help of simulated time series.

In fourth Chapter the steps to perform a seismic analysis are presented. Within this

description are included the results obtained with personal procedures in order to evaluate the statistical behavior of a time series, to extract the corresponding power spectrum and to extract the frequencies. Further features are included with the aim to measure other important stellar parameters. These procedures were applied to the light curves of several objects and the results are reported as well.

In fifth Chapter the stellar modelling of a sample of *Kepler* solar-type targets is described. Thanks to its high precision photometry that allow modes identification it is possible to compare computed theoretical frequencies with the observed ones. With this method the validation of theoretical stellar models is performed and a first estimate of global parameters of a star is achieved.

Chapter 1

Asteroseismology and stellar oscillations

Observations of stellar variability has been performed for centuries, when it was clear that some types of stars showed variations in their luminosity and radius due to pulsations. These objects, as Cepheids or RR Lyrae, generally known as Classic Variables are characterized by a very stable oscillation periods and by a precise dependence between their luminosity and the period itself. This fact allows this stars to be one of the main distance indicators.

However it was only a few of tens ago that scientists found a sort of variability also in other type of stars: indeed almost all of them, with wide span in the Hertzsprung-Russell diagram. This variability however is quite different from the classical one, which is characterised by wide amplitudes that allow to detect them without ambiguity: while the Cepheids pulsate with radial oscillations that cover possible higher harmonics, other stars show non radial pulsations, which are difficult to recognize because of the very small effects that they induce on the observable stellar parameters. In spite of these and other difficulties, this research, called *Asteroseismology*, has obtained in the last decades very important results, starting with the study of the Sun (Helioseismology) to other type of stars (such as solar-like, subdwarf B, Giant stars...).

Asteroseismology, just like earth seismology, is the only research that allow to investigate the inner part of a star, and thus to know the main stellar parameters through the identification of the oscillation frequencies that are connected to them with precise laws. In this first Chapter we present the basic issues of Asteroseismology, following the guidelines established by several authors of important reviews in this field. In particular we will base our description drawing from the *Lecture notes on Stellar Oscillations* by J. Christensen-Dalsgaard 2003 [42], *Asteroseismology* by C. Aerts, J. Christensen-Dalsgaard and D.W. Kurtz 2010 [2], *Asteroseismology and interferometry* by M. Cunha et al. 2007 [58], *Stellar Stability and Asteroseismology* by R. Scuflaire and A. Thoul 2002 [139] as well as the paper by H. Kjeldsen and T. Bedding [99], and reference therein.

1.1 Equations of the stellar structure

Basic equations of the stellar structure are presented in the approximation of spherical symmetry, neglecting also rotational and magnetic field effects.

- The hydrostatic equilibrium between the pressure forces and the gravitational action is realised when the following condition is satisfied :

$$\frac{dP}{dr} = -\frac{Gm}{r^2}\rho \tag{1.1}$$

where r is the distance from the centre of the star, p is the pressure, ρ is the density and m is the mass contained in the sphere with radius equal to r.

- The mass conservation is assured by:

$$\frac{dM(r)}{dr} = 4\pi r^2 \rho. \tag{1.2}$$

- The energy balance is given by the sum of the energy sources. If ϵ_n is the contribution to the energy from nuclear burning, ϵ_g is the contribution from gravitational energy, and ϵ_ν is the energy loss by neutrinos, the total energy can be written as:

$$\frac{dL(r)}{dM(r)} = \epsilon_n + \epsilon_g - \epsilon_\nu. \tag{1.3}$$

$L(r)$ is the energy flux in unit of time through the sphere with radius equal to r. For stars in Main Sequence the energy is provided only by nuclear reactions, while the pre-Main Sequence stars are supported only by the gravitational contraction energy.

- The energy transport is defined as:

$$\frac{dT}{dr} = \nabla \frac{T}{P}\frac{dP}{dr} \tag{1.4}$$

The temperature gradient, ∇, depends on what kind of energy transport mechanism acts in a particular zone of the star. For radiative transfer the radiative gradient is:

$$\nabla_{rad} = \frac{3}{16\pi acG}\frac{\kappa\rho}{T^4}\frac{L(r)}{M(r)} \tag{1.5}$$

where κ is the opacity and a is the density radiation constant. For convective transport of the energy, the gradient can be written as:

$$\nabla_{conv} = 1 - \frac{1}{\Gamma_2}. \tag{1.6}$$

where Γ_2 is the adiabatic coefficient which links temperature and pressure. If ∇_{ad} is the adiabatic temperature gradient, when it is satisfied the condition:

$$\nabla_{rad} > \nabla_{ad},$$

the energy is transfer by the convective transport instead of the radiative one.

1.2 General equations of hydrodynamics

The treatment of the stellar oscillations find its background on the basic principles of hydrodynamics. There are two different descriptions of the problem: the first approach takes into account of the properties of the gas in a particular position and time, $(\mathbf{r}, t)$, the second one follows the motion of the particles starting from an initial position $\mathbf{r_0}$. The former is the *Eulerian* description, while the latter is the *Lagrangian* one.

- The mass conservation is expressed by the continuity equation:

$$\frac{\partial \rho}{\partial t} + \mathrm{div}(\rho \mathbf{v}) = 0 \tag{1.7}$$

with $\mathbf{v}$ and ρ are the local velocity and density. After simple computations, and taking into account the fact that the density is the inverse of the volume, $\rho = 1/V$, we can write Equation (1.7) in the form:

$$\frac{1}{V}\frac{dV}{dt} = \mathrm{div}\mathbf{v} = 0. \tag{1.8}$$

The divergence in Equation (1.8) defines the expansion rate of a certain volume of gas.

- In the equation of motion for a volume of gas under stellar conditions, viscosity is negligible. There are two types of acting forces: the surface forces (such as pressure), and the opposed body forces ($\mathbf{f}$, like gravity). The equation of motion is:

$$\rho \frac{d\mathbf{v}}{dt} = -\nabla p + \rho \mathbf{f}, \tag{1.9}$$

that becomes:

$$\rho \frac{\partial \mathbf{v}}{\partial t} + \rho \mathbf{v} \cdot \nabla \mathbf{v} = -\nabla p + \rho \mathbf{f}. \tag{1.10}$$

- Gravity is defined as the gradient of the gravitational potential Φ, $g = -\nabla\Phi$, that satisfy the Poisson equation:

$$\nabla^2 \Phi = 4\pi G \rho. \tag{1.11}$$

- We need another equation to link two stellar parameters such as pressure and density. According to the first law of thermodynamics:

$$\frac{dq}{dt} = \frac{dE}{dt} + p\frac{dV}{dt}, \tag{1.12}$$

the heat gain goes partly in the variation of the internal energy E, partly into work expanding or compressing the gas. Through the Equation (1.7) and taking into account of the adiabatic coefficients:

$$\Gamma_1 = (\frac{\partial \ln p}{\partial \ln \rho})_{ad}, \quad \frac{\Gamma_2 - 1}{\Gamma_2} = (\frac{\partial \ln T}{\partial \ln p})_{ad}, \quad \Gamma_3 - 1 = (\frac{\partial \ln T}{\partial \ln \rho})_{ad}, \tag{1.13}$$

Equation (1.12) can be rewritten as:

$$\frac{dq}{dt} = \frac{1}{\rho(\Gamma_3 - 1)}(\frac{dp}{dt} - \frac{\Gamma_1 p}{\rho}\frac{d\rho}{dt}) \tag{1.14}$$

$$= c_p(\frac{dT}{dt} - \frac{\Gamma_2 - 1}{\Gamma_2}\frac{T}{p}\frac{dp}{dt}) \tag{1.15}$$

$$= c_V[\frac{dT}{dt} - (\Gamma_3 - 1)\frac{T}{p}\frac{dp}{dt}], \tag{1.16}$$

where c_p and c_V are the specific heat per unit mass at constant pressure and volume. See Cox & Giuli 1968 [55] for further details about these relations.

Finally, in the case of adiabatic conditions, the equation for energy conservation is given by:

$$\frac{dp}{dt} = \frac{\Gamma_1 p}{\rho}\frac{d\rho}{dt}. \tag{1.17}$$

(See Christensen-Dalsgaard 2003 [42] and Aerts 2004 [1])

In conclusion, the continuity equation (1.7), the equation of motion (1.10), Poisson's equation (1.11) and the equation of the energy conservation (1.17) represents the complete set of equations for adiabatic motion. These are the basis for the stellar oscillations treatment.

1.3 Equations of radial and non-radial stellar oscillations

Stellar oscillations are treat as perturbations in the hydrodynamics equations. In a pulsating star, quantities like position, density, pressure and temperature of a mass element vary periodically around their equilibrium values. If X is a typical quantity, and X_0 is its equilibrium value, in *Lagrangian* description [1], the perturbation on X is:

$$\delta X(\vec{a}, t) \equiv X(\vec{a}, t) - X_0(\vec{a})$$

where $\vec{a}$ denotes a mass element. In the *Eulerian* description [2], the same variation is given by:

$$X'(\vec{r}, t) \equiv X(\vec{r}, t) - X_0(\vec{r}),$$

where $\vec{r}$ is a particular position in the space. Assuming very small variation of the considered quantities, it is possible to use also a linear approssimation, neglecting the higher order terms in the perturbation equations.

In the general discussion of non radial oscillations, the spherical symmetry of the perturbations is not assured, on the contrary of radial oscillations, which represent a particular case. While in the latter case the spatial displacement, δr, is only in the radial direction, in the non-radial oscillations it is divided in two contributions: radial and horizontal. With this distinction it is possible to write the equation of motion and the Poisson equation along these two components. Using the spherical polar coordinates, (r, θ, ϕ), the contribution of th radial amplitude function to the spatial displacement is $\xi_r(r, \theta, \phi, t)$, while the small pressure perturbation is $p'(r, \theta, \phi, t)$. These functions are the dependent variables of the obtained differential equations system.

The separation of the angular variables allow us to know the variation of the perturbations with θ and ϕ if the function which describes this variations, $f(\theta, \phi)$, is an eigenfunction in the horizontal Laplace operator, $\nabla_h^2 f$. After some computations, we can find the separated variables solution: $f(\theta, \phi) = f_1(\theta) f_2(\phi)$, where f_1 and f_2 are continuous and periodics. When these functions are separately substituted in the Laplace operator, we find a regular solution of the type:

$$f_1(\theta) = P_l^m(\cos\theta), \tag{1.18}$$

[1] The Lagrangian study in hydrodynamics describes the particles motion following the particular mass element.

[2] The Eulerian description, instead, studies the motion in a fixed point.

with P_l^m a Legendre function. With an appropriate scaling factor, eq. (1.18) yields:

$$f(\theta,\phi) = (-1)^m c_{lm} P_l^m(\cos\theta)\exp(im\phi) \equiv Y_l^m(\theta,\phi),$$

being Y_l^m a spherical armonic with the degree l and an azimuthal order m, and c_{lm} is a normalization constant. Using all of these results, the previously assigned variables, for the equation of motion and Poisson, can be written as:

$$\xi_r(r,\theta,\phi,t) = \sqrt{4\pi}\tilde{\xi}_r(r)Y_l^m(\theta,\phi)\exp(-i\omega t) \tag{1.19}$$

and

$$p'(r,\theta,\phi,t) = \sqrt{4\pi}\tilde{p'}(r)Y_l^m(\theta,\phi)\exp(-i\omega t), \tag{1.20}$$

which substituted in the equations system, yield another equation system independent from the azimuthal order m (because of the condition of spheric symmetry), which characterised the amplitude of the pulsations.

For radial oscillations, the degree l is equal to zero, and it is possible to neglect the perturbation in the gravitational field. Also the horizontal contribution is null, therefore the oscillation equations can be reduced to the more simple form of one equation:

$$\frac{1}{r^3}\frac{d}{dr}(r^4\Gamma_{1,0}p_0\frac{d\zeta}{dr}) + \frac{d}{dr}[(3\Gamma_{1,0}-4)p_0]\zeta + \rho_0\omega^2 r\zeta = \frac{d}{dr}[\rho_0(\Gamma_{3,0}-1)\delta\tilde{q}], \tag{1.21}$$

where $\zeta \equiv \tilde{\xi}_r/r$.

The produced heat is too much to be exchange with the environment in a short time, it means that the thermal relaxation time is longer than the oscillation period, so the entropy cannot change during the oscillation cycle. This fact leads to conclude that stellar oscillations could be assumed as adiabatic, and let us to neglect the term δq in the energy equation. The equations which rule the non-radial stellar oscillations are:

$$\begin{cases} \frac{d\xi_r}{dr} = -(\frac{2}{r} + \frac{1}{\Gamma_1 p}\frac{dp}{dr})\xi_r + \frac{1}{\rho c^2}(\frac{S_l^2}{\omega^2} - 1)p' + \frac{l(l+1)}{\omega^2 r^2}\Phi' \\ \frac{dp'}{dr} = -\rho(\omega^2 - N^2)\xi_r + \frac{1}{\Gamma_1 p}\frac{dp}{dr}p' - \rho\frac{d\Phi'}{dr} \\ \frac{1}{r^2}\frac{d}{dr}(r^2\frac{d\Phi'}{dr}) = 4\pi G(\frac{p'}{c^2} + \frac{\rho\xi_r}{g}N^2) + \frac{l(l+1)}{r^2}\Phi' \end{cases} \tag{1.22}$$

which represent a fourth-order equation system of ordinary differential equations for the dependent variables: ξ_r, p', Ψ and $d\Psi/dr$.

The numbers utilized to describe the spherical harmonics, form a set of three numbers that characterize the oscillation modes. In particular:

- the degree l, which determine the nodal lines on the surface oscillations;
- the order m, the number of the nodes along the equator;
- the radial order n which indicates the properties of radial direction.

Figure (1.1) shows some examples of spherical harmonics Y_l^m characterized by different orders and angular degrees. In general the frequencies ω_{nlm} of stellar oscillations depend on all of these numbers, but it is convenient to separate them in the multiplet frequency ω_{nl} and the rotational splitting $\Delta\omega_m$. The more the degree l is high, the less the modes go deep in the internal part of the Sun. As we can see in Figure (1.2), the only mode which pass in the centre of the Sun is the mode with $l = 0$, and it corresponds to the purely radial oscillation. The same Figure shows that modes with lower l degree value (e.g. $l = 2$) are deeper than the modes with higher l degree value (e.g. $l = 75$). This characteristic makes p-mode a powerful diagnostic for probing layers of different depth in the stellar interior.

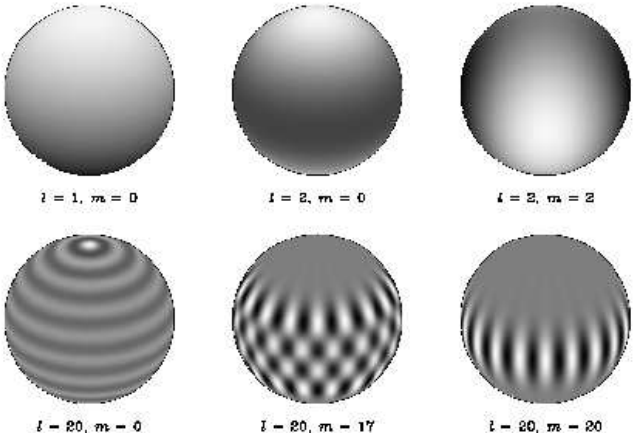

Figure 1.1: Spherical harmonics

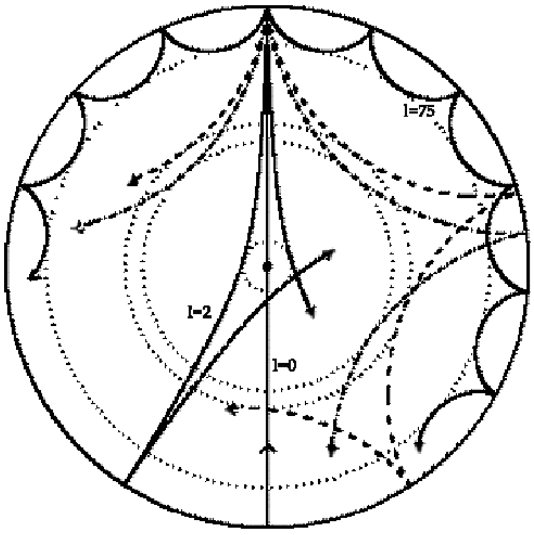

Figure 1.2: Some examples of propagating sound waves through a cross section of the solar model. The inner turning point for each mode is represent with the dotted curve (taken from Christensen-Dalsgaard 2003 [42]). Higher l degree modes are those with circle closer to the surface.

1.4 Stellar oscillations

1.4.1 The physical nature of the oscillation modes

The analytical approach to the stellar pulsations is based on the perturbations theory applied to the hydrodynamics equations, whose describe and rule the behavior the stellar matter. Stellar oscillation equations are mainly solved with numerical techniques, for the extreme complexity of the full equation system. In analytic form we can find solutions only for restricted cases, and these specific values of frequencies ω, correspond to the eigenvalues that describe the modes of oscillation. The resulting eigenfrequencies give the distibution of the amplitudes with the position in the star.

The computation of stellar models is based on some assumptions that make simpler the complex mechanisms in the interior of the star. For example, it is possible to treat the convection in an approximate way, through a parametrization of the stellar layers in whose it acts, and neglect its dynamical effects. Also the outer mechanism and the effects of the magnetic field are ignored. Another important assumption, in the calculation of oscillation frequencies, is to treat them as adiabatic.

According to the asymptotic theory of the stellar oscillations (see Section 1.4.3) it is possible to neglect the perturbations due to the gravitational potential. This assumption, called *Cowling approximation* (see Cowling 1941 [54]), reduces the equation system of stellar oscillations from the fourth to the second order. In Christensen-Dalsgaard and Gough 2001 [49] is provided a justification of this approssimation as the deletion of the contributions, due to the opposite signs of the perturbations.

The general equation for non radial oscillation is:

$$\frac{d^2\xi_r}{dr^2} = \frac{\omega^2}{c^2}(1 - \frac{N^2}{\omega^2})(\frac{S_l^2}{\omega^2} - 1)\xi_r \tag{1.23}$$

where the characteristic acoustic frequency S_l, and the buoyancy frequency N, are defined as:

$$S_l^2 = \frac{l(l+1)c^2}{r^2} = k_h^2 c^2 \tag{1.24}$$

$$N^2 = g(\frac{1}{\Gamma_1 p}\frac{dp}{dr} - \frac{1}{\rho}\frac{d\rho}{dr}) \tag{1.25}$$

where k_h is the horizontal wavenumber, and Γ_1 is the adiabatic exponent. The behaviour of S_l and N is shown in Figure (1.3), plotted using a standard solar model. We can see that the frequency S_l tends to infinity for null values of the radius, and decreases as r/R tends to the unity, also for the decrease of the sound speed. N^2 is negative in the regions interested to the convection mechanism, and it is larger than zero elsewhere. For a standard solar model the convectively instable regions is located in the outer envelope, at about 30 per cent of the radius. The increase of N, toward the centre of the star is also due to the increase of helium abundance, produced by the nuclear burning, which makes the inner part of the star stable to the convection [3].

Writing Eq. (1.23) as:

$$\frac{d^2\xi_r}{dr^2} = -K(r)\xi_r \tag{1.26}$$

[3] Writing the buoyancy frequency using the equation of state of the ionized gas, we obtain $N^2 \simeq \frac{g^2\rho}{p}(\nabla_{ad} - \nabla + \nabla_\mu)$, where $\nabla = \frac{d\ln T}{d\ln p}$, $\nabla_{ad} = (\frac{\partial \ln T}{\partial \ln p})_{ad}$ and $\nabla_\mu = \frac{d\ln\mu}{d\ln p}$. In the nuclear burning regions the molecular weight, μ, increases with the depth and hence with the pressure. The term ∇_μ, therefore, gives a positive contribution to N^2

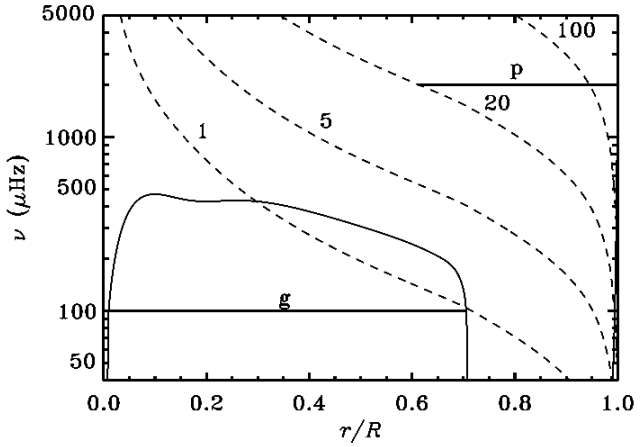

Figure 1.3: Plot of the buoyancy frequency, N (continuous line), and the characteristic acoustic frequency, S_l (dashed line), in terms of the corresponding cyclic frequency, against fractional radius r/R for a solar model. The horizontal lines indicate the trapping regions for p- and g-mode (taken from Christensen-Dalsgaard 2003 [42]).

where

$$K(r) = \frac{\omega^2}{c^2}\left(\frac{N^2}{\omega^2} - 1\right)\left(\frac{S_l^2}{\omega^2} - 1\right) \tag{1.27}$$

it is possible to study the behavior of the oscillation ξ_r, depending on the sign of K.

- If K **is larger than zero**, ξ_r is locally an oscillating function of r. The approximate solution is:

$$\xi_r \sim \cos\left(\int K^{1/2} dr + \phi\right) \tag{1.28}$$

  where the phase ϕ is determined by the boundary conditions.
  So we can find oscillating solutions when

$$|\omega| > |N| \quad \text{and} \quad |\omega| > |S_l|, \tag{1.29}$$

  or

$$|\omega| < |N| \quad \text{and} \quad |\omega| < |S_l|. \tag{1.30}$$

- If K **is lower than zero**, ξ_r is locally an increasing or decreasing exponential function of r. In this case the solution is of the type:

$$\xi_r \sim \exp\left(\pm \int |K|^{1/2} dr\right). \tag{1.31}$$

  Therefore the exponential solution is find when the following conditions are satisfied:

$$|N| < |\omega| < S_l, \tag{1.32}$$

  or

$$S_l < |\omega| < |N|. \tag{1.33}$$

For a wider discussion of the problem see Unno et al. 1989 [152].

In the regions where the oscillating solution is dominant, the solution itself is said to be *trapped*. The point characterized by a null value of $K(r)$ correspond to the borderline of the trapping region, and it is called *turning point*. From eq. (1.28) we can deduce that within the trapping region the mode oscillates the more rapidly the higher the value of K. Thus if the order of the mode depends on the number of zeros of the function ξ_r^2, the order increases with the increasing of K.

According to the behavior of the frequencies S_l and N, and the just obtained conditions, we may expect two main classes of modes: modes with high frequencies which satisfy the condition in Eq. (1.29), called *p-modes*; modes with low frequencies which satisfy the condition in Eq. (1.30), called *g-modes*. An intermediate type of modes, between p-modes and g-modes, are called *f-modes*.

P-modes

The p-modes are standing acoustic waves, with the restoring force dominated by pressure. This is the reason because they are labelled as "p"-modes. They are trapped in the region between the stellar surface and the inner turning point r_t. This point is characterized by the condition $K(r_t) = 0$, that, according to eq. (1.27), can be rewritten as $S_l(r_t) = \omega$, which, using Eq. (1.24) produces:

$$\frac{c^2(r_t)}{r_t^2} = \frac{\omega^2}{l(l+1)} \tag{1.34}$$

that yields the dependence of r_t by l and ω. In the solar case this result gives indications on the interpretation of the solar five-minutes oscillations. For small values of l, the turning point is very close to the centre, while for high degrees r_t is closer to the surface. According to Christensen-Dalsgaard 2003 [42], modes with $l \geq 40$ are trapped in the convection zone (located between $r = 0.72R$ and the surface, $r = R$, being R the solar radius), and they are the more suitable to investigate the properties of the equation of state of the stellar matter and the solar composition.

The observed five-minutes modes of the Sun are characterized by $\omega \gg N$, and the value of K is about:

$$K(r) \simeq \frac{1}{c^2}(\omega^2 - S_l^2). \tag{1.35}$$

This means that the dynamic of the p-modes is determined by the variation of the sound speed with the radius. We can determine the dispersion relation for p-modes, taking into account that they are simple acoustic standing waves, tipically characterized by the dispersion relation: $\omega^2 = c_0^2|\mathbf{k}|^2$, and that the wave vector $\mathbf{k}$ can be write as the sum of the radial and horizontal contribution:

$$|\mathbf{k}|^2 = \frac{\omega^2}{c^2} = k_r^2 + k_h^2$$

As in Christensen-Dalsgaard 2003 [42] in the case of local plane waves, we substitute k_h^2 with $l(l+1)/r^2$, therefore, using also Eq. (1.24), the dispersion relation is given by:

$$k_r^2 = \frac{1}{c^2}(\omega^2 - S_l^2). \tag{1.36}$$

Since the equation (1.35) and (1.36) are the same we can conclude that the function K could be identified with the radial wave vector. The interior reflection of p-modes can

be explained in terms of ray theory. A mode can be considered as a superposition of propagating sound waves. As they propagate into the star (see as reference Figure (1.2)), the deeper parts of the wave fronts cross regions with higher values of the sound speed, and therefore travel faster. Consequently the direction of propagation bends away from radial direction, in the same way in which a light ray is refracted when it travels into a mean with higher speed of light.

The dependence of the turning point position r_t on mode degree and frequency is of great importance: for small l, r_t is very close to the centre of the star, while for higher degrees the turning point moves toward the surface, constraining modes in the outer convection zone (in the solar case this is true for modes with $l \leq 40$).

From the equation (1.35) we can see that, for the p-modes, K increases with the frequency ω. This increases the the number of zeroes of the eigenfunction, that represent the radial order n. Consequently, the frequency increases with the mode order.

G-modes

For the g-modes the restoring force is the gravity, therefore they are gravity waves, and this is the reason that why they are called "g-modes". Their turning point is defined with the condition $N = \omega$. As seen in Figure (1.3), for low frequencies this condition generates one turning point very close to the centre, and a second one just below to the base of the convection zone. At higher frequencies the upper turning point is deeper, and for frequencies near to the maximum of N the modes are trapped in the deep interior. With this approssimation r_t is independent from the degree l.

For high order g-modes a typical condition is $\omega^2 \ll S_l^2$, so K can be approximate by:

$$K(r) \simeq \frac{1}{\omega^2}(N^2 - \omega^2)\frac{l(l+1)}{r^2}. \tag{1.37}$$

The dynamic is dominated by the variation of the buoyancy frequency. Even in this case we can find a dispersion relation for gravity waves, with the radial component of the wave number given by.

$$k_r^2 = \frac{l(l+1)}{r^2}(\frac{N^2}{\omega} - 1) \tag{1.38}$$

that is equal to the Eq. (1.37). K increases with the decreasing of the frequency ω, and the same for the order n.

F-modes

Modes with radial order $n = 0$ and degree $l \geq 20$, behave like the p-modes, but they are physically different. These modes are the intermediate between p- and g-modes, and they are called f-modes, "f" stays for fundamental. In practice they are surface gravity waves, and therefore they don't penetrate deep into the star. The f-mode frequencies are determined by the following equation, according to Christensen-Dalsgaard 2002 [41]:

$$\omega^2 \simeq g_s k_h = \frac{GM}{R^3}L \tag{1.39}$$

where g_s is the surface gravity. As it is possible to see, this equation is independent from internal structure parameters of the star. Equation (1.39) is the relation dispersion for a surface gravity waves.

The eigenfunctions of the f-modes are approximately exponential:

$$\xi_r \propto \exp(k_h r). \tag{1.40}$$

***

The radial order n provides the the number of the zeroes in the amplitude function ξ_r. For the three kind of modes, n can assume values from minus to plus infinity, and, more precisely, it obeys to the following conditions:

- $n > 0$ for p-modes;
- $n = 0$ for f-modes;
- $n < 0$ for g-modes.

They are consistent with the fact that the frequencies increase with the number of radial nodes, therefore they confirm that ω increases with n for the p-modes, while it decreases for the g-modes, and that ω doesn't depend on the number of the zeroes of the eigenfunction for the f-modes.

Figures (1.4) and (1.5) show the typical behaviors of p-modes and g-modes scaled radial displacement eigenfuncions for different values of n, l and ν. In particular the quantity plotted, $r\rho^{1/2}\xi_r$, is related to the contribution to the energy density from the radial component (see Christensen-Dalsgaard 2003 [42]) We can clearly see that for the p-modes the turning point moves toward the surface with the increasing of the degree, trapping the modes, and thus the energy in the outer parts of the star. For low degrees, instead, the energy is distribuited in a more homogeneous way. A different situation is shown for the g-modes: here the larger amplitudes are located in the deep interior of the star. The number of radial zeroes increase with l. The distribution of the energy has it's maximum very near to the centre, and it doesn't show large variations with the degrees, because the turning point depends only on the frequency.

Rotational effects on the oscillation frequencies

The previous discussion has been carry on neglecting the velocity fields, which, in reality exist, because the Sun and the stars rotate. In particular the observed frequencies of the modes are influenced by such rotation. If Ω is the uniform angular velocity and ω_0 is the frequency of the oscillation which is independent from the order m in a solid reference system with the rotating star (r, θ, ϕ), another frame (r', θ', ϕ') is related to the former in an inertial system through

$$(r', \theta', \phi') = (r, \theta, \phi - \Omega t). \tag{1.41}$$

The perturbation dependence on ϕ' and t is $\cos(m\phi' - \omega_0 t)$ in the rotating frame, while it is $\cos(m\phi - \omega_m t)$ in the inertial frame, being

$$\omega_m = \omega_0 + m\Omega, \tag{1.42}$$

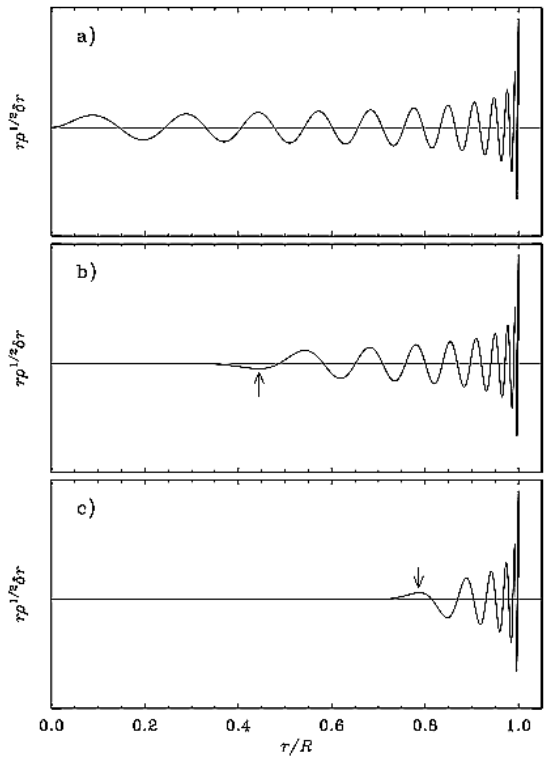

Figure 1.4: Plot of the scaled radial displacement eigenfunction for p-modes in a solar model, for three different set of l and n. *Panel a)* $l = 0$, $n = 23$, $\nu = 3310\mu$Hz; *Panel b)* $l = 20$, $n = 17$, $\nu = 3375\mu$Hz; *Panel c)* $l = 60$, $n = 10$, $\nu = 3234\mu$Hz (taken from Christensen-Dalsgaard 2003 [42]).

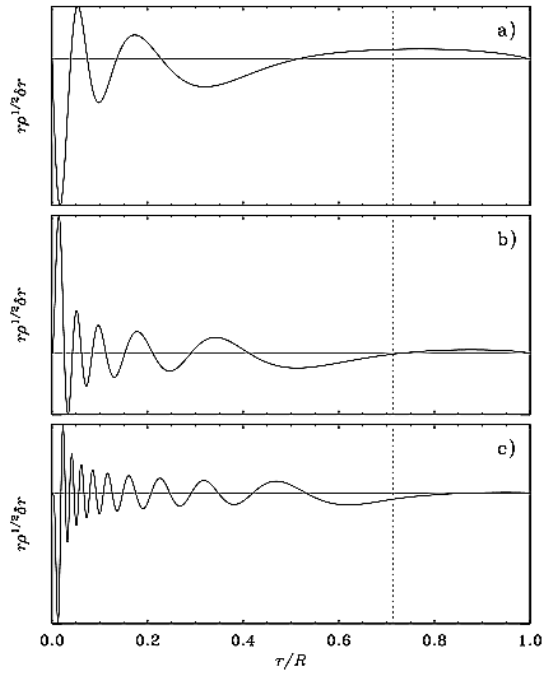

Figure 1.5: Plot of the scaled radial displacement eigenfunction for g-modes in a solar model, for three different set of l and n. *Panel a)* $l = 1$, $n = -5$, $\nu = 110\mu$Hz; *Panel b)* $l = 2$, $n = -10$, $\nu = 103\mu$Hz; *Panel c)* $l = 4$, $n = -19$, $\nu = 100\mu$Hz. The vertical dotted line locates the base of the convection zone (taken from Christensen-Dalsgaard 2003 [42]).

that provides the direct dependence of the frequency splitting on m.

As shown in Christensen-Dalsgaard 2003 [42], the effect of the pure rotation can be obtain re-computing the derivation of perturbation equations, this time taking into account of the velocity fields, always approssimating at the first order, since the quadratic term in v_0 can be neglect. After the computations we obtain the perturbation of the frequencies caused by the rotation:

$$\delta\omega_{nlm} = m\frac{R_{nlm}}{I_{nlm}} \tag{1.43}$$

where the functions R_{nlm} and I_{nlm} are defined by resolving the integrals at numerator and denominator of:

$$\delta\omega = -i\frac{\int_V \rho_0 \delta\mathbf{r}^* \cdot (\mathbf{v_0} \cdot \nabla)\delta\mathbf{r} dV}{\int_V \rho_0 |\delta\mathbf{r^2}|^2 dV}. \tag{1.44}$$

Since the function R_{nlm}/I_{nlm} is an even function of m and thus $\delta\omega_{nlm}$ is an odd function of m, it follows:

$$\delta\omega_{nl-m} = -\delta\omega_{nlm}. \tag{1.45}$$

It is also important to note that the rotational frequency splitting is sensitive only to the symmetrical part of Ω around the equator.

In the particular case of spherically symmetric rotation with the angular velocity Ω_s, the splitting is directly proportional to m:

$$\delta\omega_{nlm} = m\beta_{nl}\Omega_s, \tag{1.46}$$

where β_{nl} is a constant. Therefore in the two cases the rotational splitting between adiacent m-values is approximately given by the rotation rate.

Even the Coriolis force contributes to the splitting, but in a neglecting way.

1.4.2 Driving mechanisms

Modes in a star must to be excited to be detected, and exist different exciting mechanisms which do that. Analysing these mechanisms we are able to know which modes are excited and their expected amplitudes, but to obtain this we should use a full non-linear and non-adiabatic analysis. To go round the difficulties involved in this kind of discussion, it is possible to solve the problems separately. The main mode-excitation mechanisms are the *self-excitation*, which is responsible for the pulsations of the classical variables as the Cepheids, and the *stochastic excitation*, which occurs in the Sun and in the solar-like stars, due to the convective envelope.

Self-excitation

The estimation of the growth rate of the oscillations, due to the self-excitation mechanism, can be performed and understand treating the oscillations equations as a linear eigenvalues problem. To taking into account the departure from the adiabatic approssimation of the pulsations, the equation of the perturbed motion can be turned into non-adiabatic adding a sutable term. After calculations (see Christensen-Dalsgaard 2003 [42]), the resulting equation is of the type:

$$\omega^2\delta\mathbf{r} = \mathcal{F}_{ad}(\delta\mathbf{r}) + \delta\mathcal{F}(\delta\mathbf{r}) \tag{1.47}$$

where $\mathcal{F}_{ad}$ and $\delta\mathcal{F}$ are linear operators of the eigenfunction $\delta\mathbf{r}$, and they described the adiabatic and the non adiabatic behavior. They are defined as:

$$\mathcal{F}_{ad} = \frac{1}{\rho}\nabla p'_{ad} - g' - \frac{\rho'}{\rho}g$$

and

$$\delta\mathcal{F}(\delta\mathbf{r}) = \frac{i}{\omega\rho}\nabla[(\Gamma_3 - 1)(\rho\epsilon - \mathrm{div}\mathbf{F})'],$$

where the apexes denote the perturbate quantities. Assuming $\delta\mathcal{F}$ small and imaginary, the frequency variation is itself imaginary, therefore it doesn't change. Considering the frequency given by the sum of its real and imaginary part, and since the growth rate of the oscillation is provided by the imaginary part of the frequency, the growth rate is given by $\delta\mathcal{F}(\delta\mathbf{r})$. After calculations we can find that this contribution can be written as:

$$\delta\omega = \frac{i}{2\omega^2}\frac{\int_V \frac{\delta\rho^*}{\rho}(\Gamma_3 - 1)(\rho\epsilon - \mathrm{div}\mathbf{F})' dV}{\int_V \rho|\delta\mathbf{r^2}|^2 dV} \tag{1.48}$$

where $\delta\rho^*$ is the solution for adiabatic oscillations equation. The coefficient $\Gamma_3 - 1$ is given by

$$\Gamma_3 - 1 \equiv (\frac{\partial \ln T}{\partial \ln \rho})$$

To evaluate the integral in the numerator of Eq. (1.48) it is assumed the so called quasi-adiabatic approssimation, because it depends on the perturbed operator, expressing the non-adiabatic part. If the growth rate is negative, the oscillation mode is stable and it is characterized by very small amplitudes, almost undetectables if it doesn't occur an external excitation mechanism. If it is positive the mode is unstable, and the amplitudes are faded by non-linear effects.

Dividing the real and imaginary terms of the frequency in Eq. (1.48) into $\omega = \omega_r + i\eta$ we could obtain an approximate expression of the type:

$$\eta \simeq \frac{C_r}{2\omega_r^2 I}$$

being

$$C_r = \mathrm{Re}[\int_V \frac{\delta\rho^*}{\rho}(\Gamma_3 - 1)(\rho\epsilon - (div)\mathbf{F})' dV] \quad \text{and} \quad I = \int_V \rho|\delta\mathbf{r^2}|^2 dV.$$

If $C_r > 0$ the mode is unstable;
If $C_r < 0$ the mode is stable.

Considering only the outer part of the star, where are excited the p-modes, we have to assume some conditions: to neglect the nuclear reactions, and consider the quasi-adiabatic approssimation or even the non-adiabatic regime. With these hypothesis the approximated value of C_r is:

$$C_r \simeq -L\int_M \frac{\delta\rho}{\rho}(\Gamma_3 - 1)\frac{d}{dm}(\frac{\delta L}{L})dm. \tag{1.49}$$

Assuming the compression, given by the condition $\delta\rho > 0$, it follows from Eq. (1.49) that the contribution to the damping or excitation depends only on the rate of change of δL. If δL increases towards the surface, much more energy leaves the layer, compare to the

one that enters, so the particular layer give a negative contribution to C_r, increasing the damping during the compression. If δL decreases towards the surface, the reverse occurs, and the layer contributes to the excitation.

Considering the radiative luminosity given by the expression obtained from the radiative transport,

$$L = -\frac{4ac}{3\kappa} 16\pi^2 r^4 T^4 \frac{d\ln T}{dm},$$

with the assumption of the nearly adiabatic condition, the luminosity perturbation can be write as:

$$\frac{\delta L}{L} \simeq (\frac{\delta L}{L})_a = [(4-\kappa_T)(\Gamma_3 - 1) - \kappa_\rho]\frac{\delta\rho}{\rho}.$$

For typical values, in many cases δL increases towards the surface and, for what we have just said, it tends to the stability. The decreasing of $(\delta L)_a$ occurs, in fact, only when are reached some particular conditions, like a strong decrease of Γ_3 or a strong increase of κ_T, conditions that could rise in the ionization zones. In such regions, characterized by a low value of the coefficient $\Gamma_3 - 1$, the heat carried by radiative transport is stored as ionization energy. In this process the opacity of gas increases with the compression, despite of what usually happens, giving a further contribution to the excitation. The exciting processes are therefore called γ- and κ-mechanism.

If the ionization zone is deep into the star, at high optical depth, the variation of quantities like pressure, density and luminosity are small and this induce small driving mechanism. Therefore the excitation in superficial regions could be mitigated by other zones of the star. Even when the ionization zone is characterized by low optical depth the driving contribution is neglected, because the radiation is not keeped by the layers. This means that the existence of such a region doesn't suffice to the driving mechanism. What is necessary is that the location of the ionization region is between the zone where radiative energy is generated by the compression and the region that is able to radiate such an energy. If we consider Δm_i the mass of the ionization region, containing the energy $\langle c_V T_i\rangle \Delta m_i$, where c_V is the specific heat at constant volume, and T_i is the characteristic temperature of the ionization of a particular element, we can express a parameter, Ψ, as:

$$\Psi = \frac{\langle c_V T_i\rangle \Delta m_i}{\Pi L}$$

being Π the pulsation period. Ψ is therefore the ratio between the thermal energy stored in the layer outside the point considered, in the ionization region, and the energy radiated by the star in a pulsation period. The ratio is lower than one near the surface, so the energy contained in the region is insufficient to perturb the luminosity, which is therefore constant. This is the non-adiabatic case. Instead, at grater depth, $\Psi \gg 1$ the energy content is so large than the radiative transfer doesn't affect its variation. This is the adiabatic case. The transition region between the adiabatic and non-adiabatic behaviour is then the region where is satisfied the condition:

$$\frac{(\langle c_V T\rangle)_{TR}(\Delta m)_{TR}}{\Pi L} \sim 1. \tag{1.50}$$

The position of the transition zone compared with the ionization one decides the stability rather than the instability. For example, for a star with a small radius (and high effective temperature), the helium ionization zone is near the surface above the transition region. While in the inner part of the star the quantity $\delta L/L$ increases towards the surface and

contibutes to the damping, above the transition region it is constant and gives no contribution to the driving. Resulting $C_r < 0$, the star is stable. The position of the transition region varies with the increasing of the radius of the star, and for a radius equal to a critical radius R_{crit}, it coincides with the helium ionization region. The internal parts of the star still contribute to the damping, but the ionization zone provides a strong contribution to the excitation, and since the luminosity perturbation is now "frozen" in the upper part of the ionization zone, the damping mechanism is absent, and rises the instability. For stars with larger radius (with lower T_{eff}), the ionization zone is located in the quasi-adiabatic zone, giving both positive and negative contributions to the excitation, with a possible tendency to the damping of the modes.

In Cox 1967 [56] and Cox 1974 [57] this discussion is made in relation to the position of the variable stars in the Hertzsprung-Russell diagram. In fact from eq. (1.50) it is possible to obtain the slope of some strips crossing the H-R diagram where the instability is developed. They are quite steep, being $L \propto T_{eff}^{-\alpha}$, with α a large value, and three main bands are distinguished, corresponding to: *a)* the ionization of HI and HeI at low effective temperatures (Mira variable are located in this strip); *b)* the ionization of singly ionized helium (here we found the classical Cepheids); *c)* the ionization of iron (for variables with spectral type B).

Stochastic excitation

The Sun (and likely also in the solar-like stars) shows pulsations which aren't compatible with the driving mechanisms seen before. In these stars the outer envelope is convective, and the energy coming from convective motions could be turned into oscillation motions, making the convection itself the responsible for the pulsations. The convective motion near the surface reaches velocity very close to the sound speed, and this turbolent motion acts as source of acoustic waves. Because of the excitation is due to the very large number of convective eddies, the driving mechanism is random, i.e. stochastic. According to Batchelor 1953 [14], in which is discussed the problem of the damped oscillator driven by random forces, the power spectrum resulting for a mode of frequency ω_0, and a damping rate η is of the type:

$$\langle P(\omega)\rangle \simeq \frac{1}{4\omega_0^2}\frac{\langle P_f(\omega)\rangle}{(\omega-\omega_0)^2+\eta^2} \tag{1.51}$$

where $\langle P_f(\omega)\rangle$ is the average power spectrum of the forcing function. It consists of an ensemble of intrinsecally damped harmonic oscillators. If the spectrum is a slowly variating function of the frequencies, it appears like a Lorentian profile, and the damping rate of the mode gives the width of the profile. In Figure (1.6) is shown the power spectrum of a single mode and the fitted Lorentian profile, which, in reality, is not the right interpolation function, because of the asymmetries of the observed spectrum. These asymmetries are however to taking into account because without them can occur some sistematic errors, and they also provide constrains to the surface convection.

The stochastic nature of the excitation makes the observed amplitudes of the modes to vary in time. The observation of modes performed on a short time scale compared with the damping time, provides an exponential energy distribution:

$$p(E)dE = \langle E\rangle^{-1}\exp(-\frac{E}{\langle E\rangle})dE \tag{1.52}$$

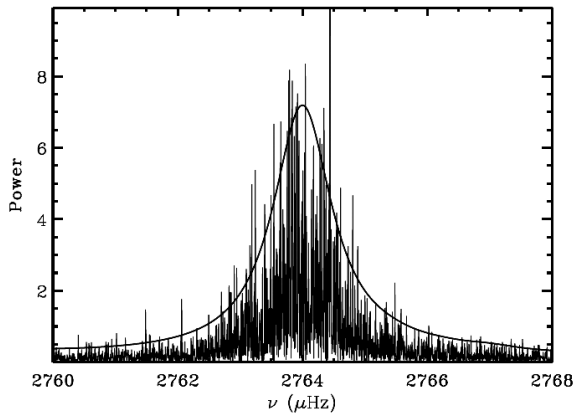

Figure 1.6: Power spectrum of a single radial mode, fitted with a Lorentian profile (taken from Christensen-Dalsgaard 2003 [42]).

being the energy E proportional to the squared amplitudes, and $\langle E \rangle$ the average energy. The kinetic energy density in convection is great near the surface, so p-modes are likely the modes excited primarily.

Simulations has been made for a better study of the behavior of these modes and, as it was easily intuitable, the amplitudes change in an irregular way, and there is the probability that a mode could be invisible, as shown in Figure (1.7). This fact is of fundamental importance when these kind of stars are analysed.

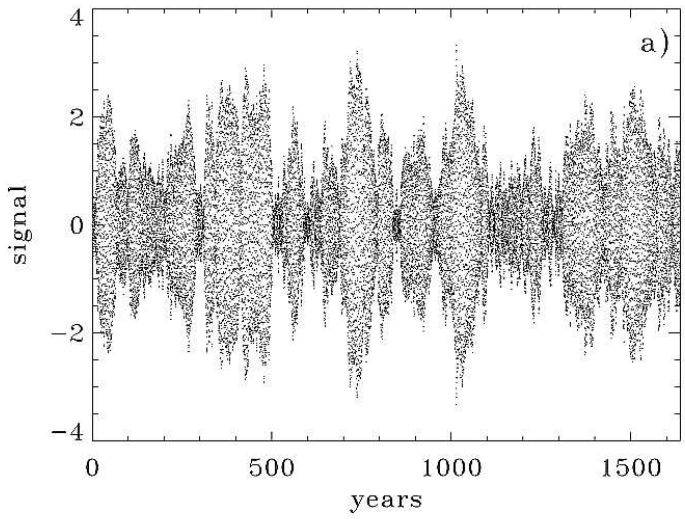

Figure 1.7: Artificial time series covering about 1600 years (see Christensen-Dalsgaard et al. 2001 [52].

The amplitude of these oscillations is difficult to predict since it depends on the interaction of waves and convective turbulent motion which is very difficult to describe and model. It is generally accepted that the strength of driving as a function of position in the star depends quite strongly on the expectation value of the energy density of the convective

motion. For stars with relatively low effective temperatures that have a surface convective zone (like the Sun), the kinetic energy density in the convection is largest very close to the visible surface and therefore the driving of oscillations is strongly concentrated very close to the surface. It is therefore likely that it is primarily p-modes that are excited because these have appreciable amplitudes close to the surface. Higher mass stars without a surface convective zone are expected to have a convective core. It seems reasonable to expect that in such stars g-modes are quite likely to be excited : the argument again being that there is coincidence of the region that can drive oscillations with the region where the amplitude of the modes is high. This excitation mechanism is less restrictive than the self-excitation of the previous section in terms of the frequencies of the modes that can be excited. Since turbulent convection produces motions with a very broad spectrum, both in terms of spatial and temporal frequency, it is likely to excite oscillations over a broad range of frequencies, as is observed in the Sun. The modes are damped so once energy has been put into a mode by the convection the mode slowly decays again until the next excitation event (see Pijpers 2003 [128]).

1.4.3 Asymptotic theory of the oscillations

Equation (1.23), defined in Section (1.4) as the general expression for a non-radial oscillation, is not specific for the eigenfunctions description in the stellar case. This situation, therefore, demands an adequate theory which could better interpret the behavior of the stellar oscillations. The asymptotic theory satisfies to this requirement, providing a better interpretation of the observations of stellar pulsations. Also, since the observed modes are in many case of high order, asymptotic expressions are sufficiently precise to provide useful quantitative results. After the first attempts to develop this theory (as the JWKB method [4] , see Unno et al. 1989 [152] for a description), the ultimate versions, which have correct the previous of their problems, are by Deubner and Gough 1984 [65] and subsequentely Gough 1993 [73].

The asymptotic analysis is based on the Cowling approximation (already mentioned in Section 1.4.1), neglecting the perturbation to the gravitational potential which in fact has a significant effect on the frequencies of the lowest order modes (e.g., Robe 1968 [132]; Christensen-Dalsgaard 1991 [40]). Being the observed modes of high radial order, this approximation is suitable to describe the stellar oscillation frequencies obtained from our observations.

From the dispersion relation Eq. (1.36) we derive:

$$k_r^2 = \frac{\omega^2}{c^2}(1 - \frac{S_l^2}{\omega^2}). \tag{1.53}$$

Thanks to Eq. (1.53) it is possible to justify an approximate but useful exression for the frequencies of acoustic oscillations. The requirement for standing waves in the radial direction implies that the integral of k_r over the region of propagation, between $r = r_t$ and R, must be an integral multiple of π:

$$(n * \alpha)\pi \simeq \int_{r_t}^{R} k_r dr \simeq \int_{r_t}^{R} \frac{\omega}{c}(\frac{S_l^2}{\omega^2})^{1/2} dr, \tag{1.54}$$

[4] developed by Jeffreys, Wentzel, Kramers and Brillouin.

where α contains the phase changes at the point of reflection of the modes. This last equation can be written as:

$$\frac{(n+\alpha)\pi}{\omega} \simeq F(\frac{\omega}{L}). \tag{1.55}$$

where

$$L = l(l+1) \tag{1.56}$$

and, assuming $w \equiv \omega/L$,

$$F(w) = \int_{r_t}^{R} (1 - \frac{c^2}{w^2 r^2})^{1/2} \frac{dr}{c}, \tag{1.57}$$

Observed solar frequencies satisfy Eq. (1.55), known as the *Duvall law* (Duvall 1982 [68]).

The Duvall law is not always satisfactory on the physical point of view (it ignores the fact that the oscillations are not purely acoustic, neglects effects of variatons of stellar surface with position and there is not a proper treatment of the near surface reflection), so a better description can be based on the asymptotic analysis of the oscillation equations, described in the set of Eq. (1.22). As already mentioned before, the observed modes are of high radial order (and high degree in the solar case), condition that allow us to be in the Cowling approximation. In this approximation, the order of the Equations (1.22) is reduced to two. Assuming $\chi = \mathrm{div}(\delta\mathbf{r})$, and $\Psi = c^2\rho^{1/2}\chi$, we can write the oscillations equation in its more general asymptotic form:

$$\frac{d^2\Psi}{dr^2} + K(r)\Psi = 0, \tag{1.58}$$

with

$$K = \frac{\omega^2}{c^2}[1 - \frac{\omega_c^2}{\omega^2} - \frac{S_l^2}{\omega^2}(1 - \frac{N^2}{\omega^2})] \tag{1.59}$$

where ω_c is the acoustical cut-off frequency, which rules the reflection of the acoustic waves at the surface. It is defined as:

$$\omega_c^2 = \frac{c^2}{4H^2}(1 - 2\frac{dH}{dr}),$$

with H the density scale height.

Applying the JWKB analysis to Equations (1.58) and (1.59) we obtain:

$$\omega \int_{r_1}^{r_2} [1 - \frac{\omega_c^2}{\omega^2} - \frac{S_l^2}{\omega^2}(1 - \frac{N^2}{\omega^2})]^{1/2} \frac{dr}{c} \simeq \pi(n - \frac{1}{2}) \tag{1.60}$$

where the region between r_1 and r_2 is characterized by positive values of $K(r)$.

Asymptotic theory of p-modes

In the asymptotic description of the p-modes, we may approximately neglect the term in N and, except near the surface, the term in ω_c. Near the surface we have that $S_l \ll \omega$ for small or moderate l, and may be neglected. Therefore the position of the upper turning point R_t is determined by $\omega \simeq \omega_c$. Physically it corresponds to the reflection of waves where the wavelengths becomes comparable to the local density scale height. ω_c approximally tends to be constant toward the stellar atmosphere. Modes with frequencies exceeding the atmospheric values are non totally trapped and tend to be strongly damped.

If we assume that $|N^2/\omega^2| \ll 1$, Eq. (1.60) can be written as:

$$\omega \int_{r_1}^{r_2} 1 - \frac{\omega_c^2}{\omega^2} - \frac{S_l^2}{\omega^2}^{1/2} dr \simeq (n - \frac{1}{2})\pi \tag{1.61}$$

where $r_1 \simeq r_t$ and $r_1 \simeq R_t$. Since $\omega_c/\omega/ll1$, except close to the upper turning point, we obtain a further semplification, the integral can be expand, so we find:

$$w \int_{r_t}^{R} (1 - \frac{S_l^2}{(\omega^2}})^{1/2} \frac{dr}{c} \simeq (n + \alpha(\omega))\pi, \tag{1.62}$$

see Christensen-Dalsgaard and Hernandez 1982 [51].

Recovering Eq. (1.55) and (1.57) the assumption on S_l ensures that the waves travel nearly vertically colose to the surface. For low-degree modes these relations are even more semplified, because, except for the region very close to the lower turning point, the integrand is nearly one. As a result we obtain:

$$F(w) \simeq \int_0^R \frac{dr}{c} - \frac{1}{w}\frac{\pi}{2}. \tag{1.63}$$

Furthermore, for low degree modes, $L \simeq l + 1/2$, and according to Tassoul 1980 [150], using Eq. (1.55), we derive:

$$\nu_{nl} \simeq (n + \frac{l}{2} + \frac{1}{4} + \alpha)\Delta\nu - (AL^2 - \beta)\frac{\Delta\nu^2}{\nu_{nl}}. \tag{1.64}$$

Neglecting the last term, Eq. (1.64) predicts a uniform spacing of modes of the same degree. This difference in frequency of modes of the same degree and consecutive order, represented by the quantity $\Delta\nu$, which is one of the most important asteroseismic observables. It is defined as:

$$\Delta\nu \approx \nu_{n+1,l} - \nu_{n,l} = [2\int_0^R \frac{dr}{c}]^{-1}, \tag{1.65}$$

and it is the inverse of twice the sound travel time between the centre and the surface of the star, providing thus informations about the mean properties of the stellar structure, as we will show in the next Section. $\Delta\nu$ is called *large separation*.

The other terms of Eq. (1.64) are:

$$A = \frac{1}{4\pi^2\Delta\nu}[\frac{c(R)}{R} - \int_0^R \frac{dc}{dr}\frac{dr}{r}], \tag{1.66}$$

α is a function of frequency, and it depends by the reflection properties near the surface, while δ is a small correction term predominantly related to the near-surface region. Eq. (1.64) predicts a degeneracy between frequencies of modes with degree of the same parity, defined as:

$$\delta_{nl} \equiv \nu_{nl} - \nu_{n-1,l+2} \simeq -(4l + 6)\frac{\Delta\nu}{4\pi^2\nu_{nl}}\int_0^R \frac{dc}{dr}\frac{dr}{r}. \tag{1.67}$$

Even this quantity has a valuable diagnostic potential, in fact, according to the relation:

$$c_s^2 \simeq \frac{\Gamma_1 k_B T}{\mu m_u}. \tag{1.68}$$

we note that the core sound speed is reduced as the mean molecular weight of the matter, μ, increases because of the conversion of hydrogen to helium, as the star evolves. As a result, δ_{nl} is reduced in turn, providing a measure of the evolutionary state of the star.

Both of these patterns are clearly observed in solar data, and they are the clearest indicators for the detection of solar-like oscillations. In Section 1.4.4 we will show how these quantities are powerful indicators of stellar properties.

Asymptotic theory of g-modes

As already mentioned, g-modes are trapped in the stellar radiative interior, behaving as evanescent in the convective region. Their propagation is thus limitated by two turning points, the lower one, r_1 close to the centre of the star and the upper one, r_2, close to the boundary of the convection zone. According to Tassoul 1980 [150], the frequencies of low-degree high-order g-modes are defined by:

$$\omega = \frac{L \int_{r_1}^{r_2} N \frac{dr}{r}}{\pi(n + \frac{l}{2} + \alpha_g)},$$

which indicates that the spacing is inversely proportional to the degree.

In the limit of $\omega \ll N$, also g-modes are equally spaced, just like p-modes, not in frequency but in period:

$$\Pi_{nl} = \frac{\Pi_0}{\sqrt{l(l+1)}}(n + \epsilon). \tag{1.69}$$

In Equation (1.69), ϵ is a small constant, and Π_0 is defined as:

$$\Pi_0 = 2\pi^2 (\int \frac{N}{r} dr)^{-1}, \tag{1.70}$$

where N is the bouyancy frequency, and the integral is computed over the cavity in which the g-modes propagate.

The period spacing depends on the degree, leading to a more complex structure of the spectrum than in the case of the acoustic modes. Actually, it is too difficult so far to disentangle the period spacings, due to the rotational splitting effects, because of lack of identification of l and n. It has thus not yet been possible to exploit the period spacings seismically for main-sequence stars, as was done for the White Dwarfs (Winget et al. 1991 [155], 1994 [156]).

1.4.4 Diagnostics potentiality of Asteroseismology

To obtain useful informations on the stellar characteristics from the frequencies oscillation, it is necessary to be able to correlate the latter to the properties of the star. As already mentionded in the previous Section, the large frequency spacing, $\Delta\nu$, and small separations, $\delta\nu$, contain informations about fundamental stellar parameters. A convenient way to illustrate the details of the frequency spectrum is in terms of the so called *echelle diagram*. Graphically this corresponds to dividing the spectrum in segments of length equal to the mean large separation $\Delta\nu$, and stacking the segments. We express the frequency as:

$$\nu_{nl} = \nu_0 + k\langle\Delta\nu\rangle + \tilde{\nu}_{nl} \tag{1.71}$$

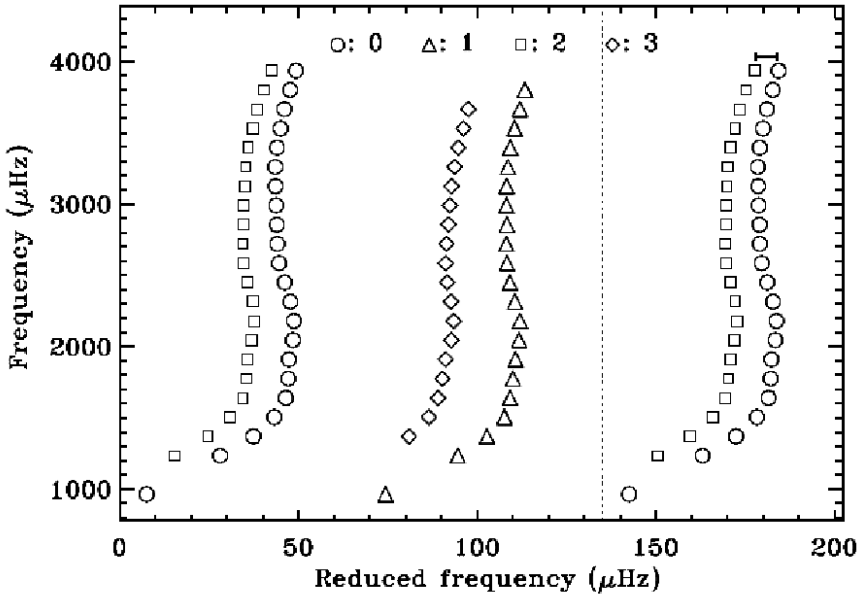

Figure 1.8: Echelle diagram for observed solar frequencies, the measured mean large separation of the Sun is $\Delta\nu_{\odot} = 135\mu Hz$. Circles, triangles, squares and diamonds represent modes of degree $l = 0$, 1, 2 and 3, respectively (taken from Christensen-Dalsgaard 2003 [42]).

where ν_0 is a arbitrary reference frequency, k is an integer, $\langle\Delta\nu\rangle$ is a suitable average of $\Delta\nu_{nl}$ and the reduced frequency $\tilde{\nu}_{nl}$ is between 0 and $\Delta\nu$. These frequencies plotted versus the reduced frequency lay on almost vertical lines, according to the value of the degree l.

Figure (1.8) shows, as an example, observed solar frequencies. According to the asymptotic predictions in Eq. (1.64), the result would be largely vertical sets of points, separated by the large and small separation, according to the values of (n, l). As shown there are significant departures from this behaviour; in particular, the curvature arises largely from the term in $\alpha = \alpha(\omega)$ in the asymptotic relation. This behaviour carries information about the helium content in the stellar envelope. Due to the factor $1/r$, the small separation is very sensitive to the sound-speed structure of the stellar core. From a physical point of view this is the result of the propagation regions of the modes. Non radial modes are reflected at the inner turning point r_t whereas the radial modes penetrate essentially to the centre. This property makes acoustic modes of low degree (so far the only degrees that are observable in distant stars with solar-like oscillations) particularly valuable as diagnostics of stellar cores.

Another powerful diagnostic tool is provided by the relation between the large and the small frequency separation. According to Kjeldsen and Bedding 1995 [99] the great separation can give indications on the stellar mass for Main Sequence stars or even near the Main Sequence, according to this scaling relation:

$$\Delta\nu \propto (\frac{M}{R^3})^{1/2} = \rho^{1/2}. \tag{1.72}$$

According to the discussion in Section 1.4.3, the small separation, is sensitive to the inner regions of a star, thanks to the dependence from the variation of the sound speed (see Eq.

(1.68)). This fact provides a clear indication on the evolutionary state of the star. After these considerations, if we plot in a diagram the great separation on the abscissa and the small separation on the ordinate, we obtain the so called *asteroseismic H-R diagram*. The potentialities of such a diagram are clear: the knowledge of the location of a star on this diagram should immediately provides its mass and its evolutionary state.

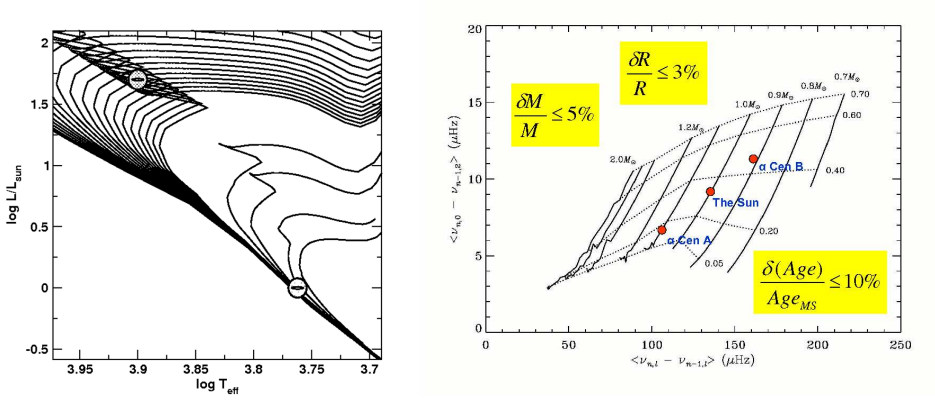

Figure 1.9: *Left:* Degeneracy of isochrones in the HR diagram, which makes difficult the age estimation for non evolved stars and for stars close to the turn-off point (Taken from Lebreton & Montalban 2009 [105]). *Right:* The Asteroseismic HR diagram ($< \Delta\nu >$, $< \delta\nu >$) resolve the degeneracy using the large and small frequency separations. The solid lines correspond to the evolutionary tracks for the indicated stellar masses, while the dotted lines follow the constant hydrogen abundance. The locations of the Sun, α Cen A and α Cen B are shown (taken from Kjeldsen et al. 2008 [98]).

Figure (1.9, right panel) shows an asteroseismic H-R diagram in comparison with the the classic Hertzsprung-Russell diagram (Figure 1.9, left panel). It appears quite clear that the evolutionary tracks of stars, defined as function of ($< \Delta\nu >$, $< \delta\nu >$), are free from the degeneracy of the age, which represents the most important problematic in the classical HR diagram. The exact position of the tracks in Figure (1.9) will depens on the detailed physical properties, including the chemical composition. However the stellar parameters can be estimate with some robustness. According to Kjeldsen et al. 2008 [98] with a resolution of 0.1 μHz for the observed frequencies, and a further information about the effective temperature with an accuracy of 150-200K and the heavy elements abundance known within a factor 2, the precision in the estimate of fundamental stellar parameters is:

- $\sim 5 - 10\%$ for the age of a main sequence star;
- $\sim 5\%$ for the mass of the star;
- $\sim 2 - 3\%$ for the radius of the star;
- $\sim 1\%$ for the mean density of the star.

This precision for asteroseismic estimation of stellar parameters is an incredible improvement compared with the other techniques. These results are valuable not only for stellar

astrophysics alone, but they yield precious informations in the characterization of extrasolar planets, nowadays one of the most important topics in astrophysics. In the next Chapter will be discussed the synergy between Asteroseismology and the search for exoplanets, also because at the present days there are a lot of observational projects, especially from space using, that exploit the asteroseismic inferences to improve the knowledge of planets' properties. Space missions like CoRoT or Kepler are searching for extrasolar planets using the transit method (see next Chapter). A planet transit potentially gives a very precise measure of the radius of the planet relative to its host star. However, additional observations are required to establish the actual size scale. Without applying Asteroseismology and without a distance measurement, the stellar radius has to be constrained by spectroscopy and photometry. In this case the determination of temperature has a precision of roughly 100 K (or 2%), and the absolute luminosity to approximately 40%. The accuracy in the radius is therefore roughly 20%. From the location in the classical HR diagram, the estimation of the mass is about 10% using stellar models. It is then clear that the results from asteroseismology is of significant help to constrain the actual stellar radius, using only the photometric transit data.

Helioseismic, and likely asteroseismic, inversion is another powerful investigative method, which, as the word itself suggests, inverts the theorical equations to find the interest quantities. In the solar case it has produce many results on the inner properties, like the variation of the sound speed with the radius, directly from the data (see 1.4.3). This kind of analysis is based on the assumption that the real Sun could be obtained applying small corrections on a reference model. A linear perturbation analysis provides the frequency differences between the observations and the model, $\omega_{nl}^{(obs)} - \omega_{nl}^{(0)}$. Figure (1.10) shows the resulting

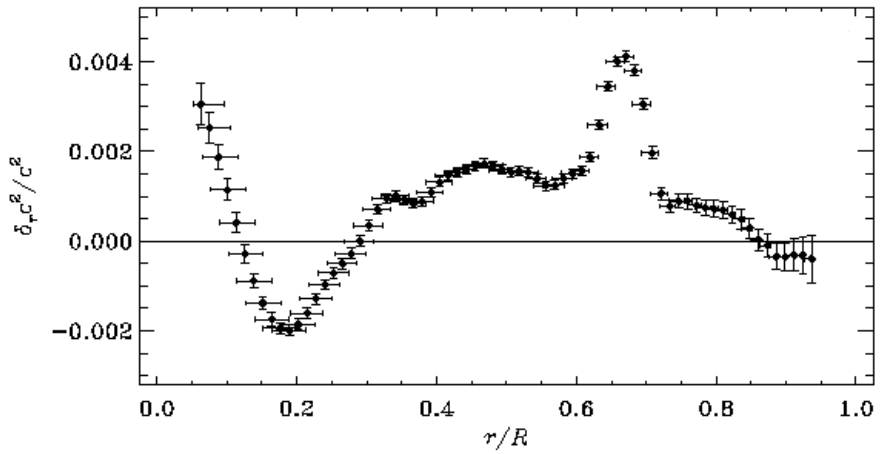

Figure 1.10: Corrections to a reference solar model, obteined by the inversion of the differences between the observed frequencies and the frequencies of the model (taken from Christensen-Dalsgaard 2003 [42]).

corrections obtained with this technique. The inversion is in terms of the variation $\delta_r c^2/c^2$. The bump at $r/R \simeq 0.65$ is likely due to a sort of mixing in the region beneath the convection zone, which is responsible, at the edge of the core for the negative values of the correction.

Generally the inverse problem is expressed in terms of pairs of coupled variables, like the sound speed and the density, (c^2, ρ), or (u, Γ_1), with u the ratio between the pressure and the density, and Γ_1 the adiabatic coefficient, but other structural parameters can be used, like (ρ, Y), with Y the helium abundance, which defines the frequency difference. Moreover, inversion can give us proof on the goodness of the solar models computated without the support of the observations, but only with the known solar physics. The results are quite encouraging. The problem concerning the helioseismic inversion is its possibility to introduce systematic errors in the results, in particular as showed in Basu and Christensen-Dalsgaard 1997 [13], taking into account the difference between the theoretical and the experimental equation of state, on the other hand it increase the error in the solutions.

Asteroseismic determinations of the stellar internal rotation could provide informations on the star formation processes. Since the rotation depends directly on the evolutionary history, it is possible to know the reasons that lead to the angular-momentum loss or the redistribution within the star. It is however important to combine the asteroseismic inferences with other informations coming from the observations to obtain good interpretations of the stellar evolution.

Finally, useful indications on the convective zone are provided by the modes lifetime, because the observed damping of the modes depends on the driving mechanism.

1.5 Pulsations in the Hertzsprung-Russell diagram

Figure (1.11) shows the distributions of all the stellar classes in the Hertzsprung-Russell diagram. The large number of pulsating classes indicates that the oscillations are highly spread in mass or evolutionary state, producing thus many different types of pulsation characteristics. In this Section we will focuse our attention on three types of pulsating classes, according to the targets of interest for this thesis.

1.5.1 Solar-type pulsators

In the early 60's there was the first detection of some kind of variability in our Sun, characterized by movements of small regions with a velocity of the order of 15 cm/s and a period of 5 minutes. At that time this phenomenon wasn't fully understood, but some years later, a deeper analysis established that the observed oscillations were the manifestation at the surface of resonant sound waves travelling across the solar interior. After this discovery a very large amount of efforts were accomplished to improve the knowledge of our star providing new techniques of observation and analysis, and giving birth to the Helioseismology. The improvements to solar modeling due to the results of this new science were unprecedent and it is clear that the same kind of investigation would have been necessary for other stars.

Solar-like oscillations are present in the Sun, solar-like stars and red giant stars, driven in all of these cases by the turbolent convection of the outer stellar envelope. Solar-like stars present similar features to the solar ones, as the quite low effective temperature (less than 7000 K) and a mass that doesn't exceed 1.7 solar masses. Their evolutionary state is in the phase of hydrogen burning or slightly more evolved and a convective envelope is present. Typical solar-like stars are K dwarfs, subgiants, and the G-F spectral type stars. Unfortunately the detectable oscillation modes in these stars are so few and with extremely low amplitudes compared to the solar ones, and their typical periods are about 10-20

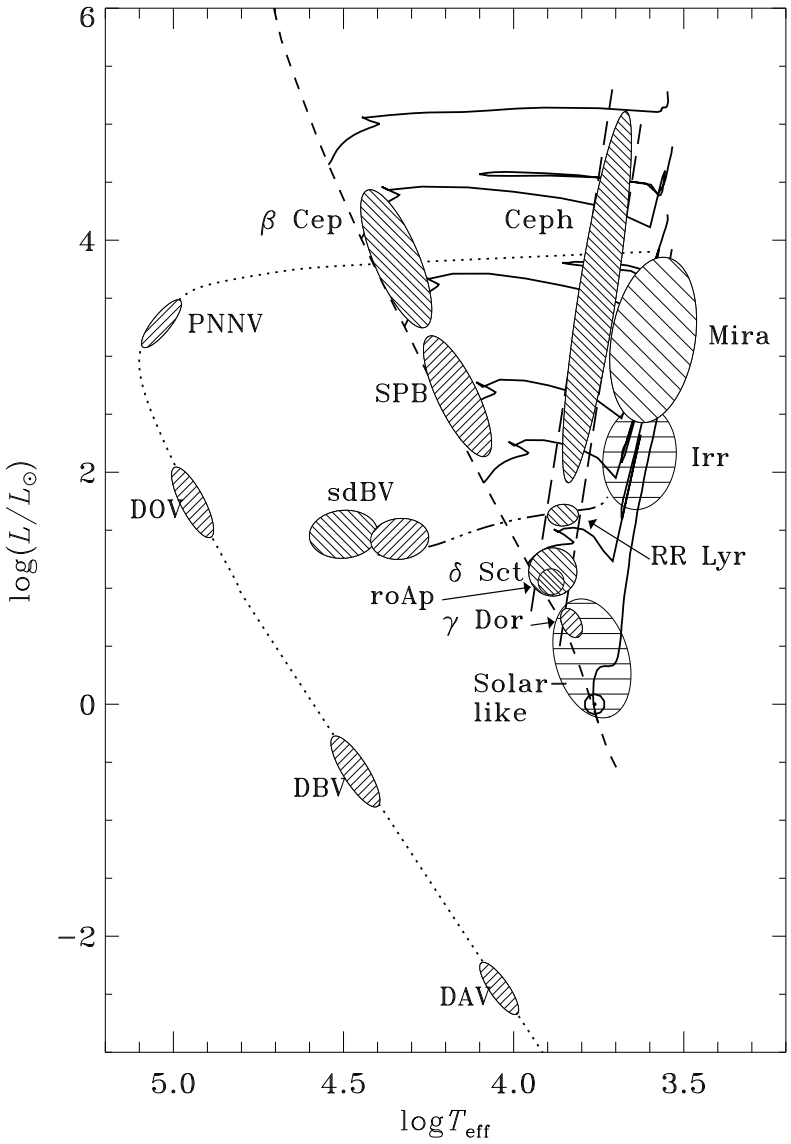

Figure 1.11: Distributions of all the stellar classes in the Hertzsprung-Russell diagram specifying the typical type of pulsation. Areas filled with horizontal lines define solar-like oscillations; areas filled with lines (from left to right) up to down indicates p-modes oscillators; areas filled with lines down to up indicates g-modes oscillators (taken from Christensen-Dalsgaard 2003 [42]).

minutes. Nevertheless the improvements of instruments and techniques both for ground-based and space-based observation have made possible their detection and identification. From the '90 more and more observational efforts were made to detect solar-like oscillations in other stars with ground-based instruments. Thanks to the technological improvements and the construction of high-resolution high-precision spectrographs, the first detections were obtained with the radial velocity technique (e.g. Bedding et al. 2004 [20], Leccia et al. 2007 [106], Bonanno et al. 2008 [28], Arentoft et al. 2008 [7], Bedding et al 2010a [21]). Figure (1.12) shows the location of some of those targets in the H-R diagram, bounded in the typical region of solar-like stars. Strong improvements are now obtained thanks to the

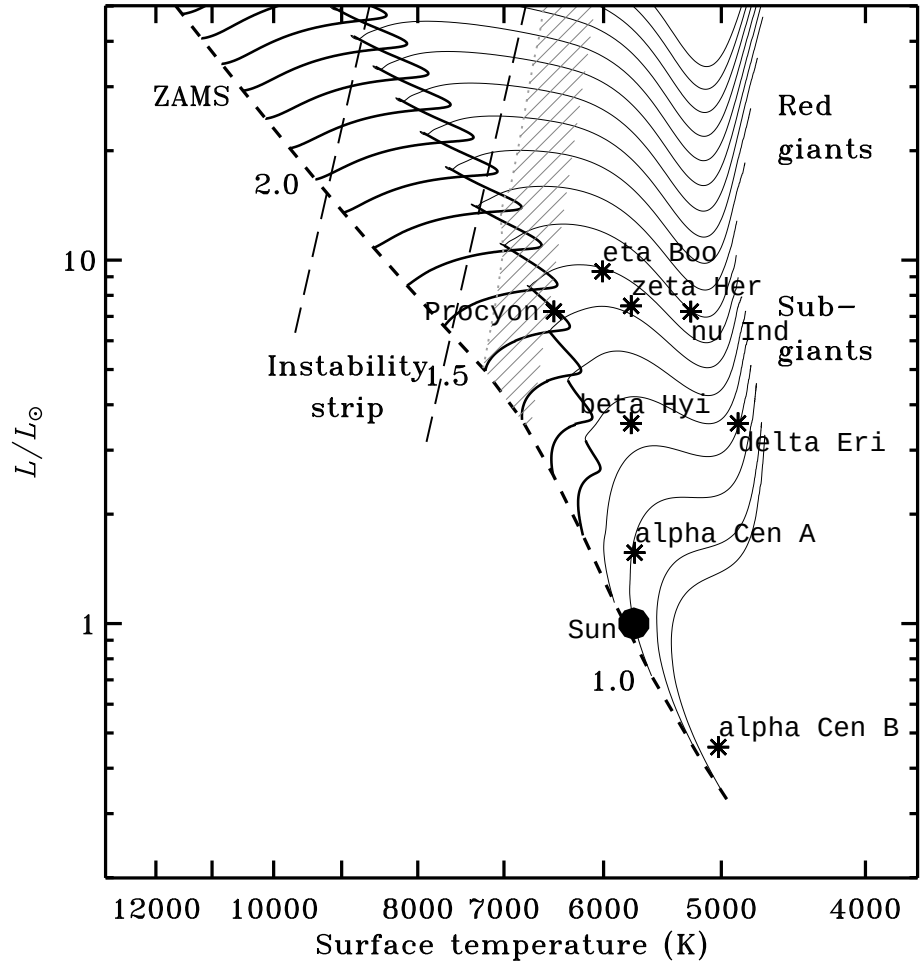

Figure 1.12: The solar-like pulsators belong to the region extending from the cool edge of the classical instability strip to the red giants branch in the Hertzsprung-Russell diagram (taken from Bedding and Kjeldsen 2003 [18]).

space mission CoRoT and Kepler, which are providing thousands photometric light curves of solar-like stars, that will allow to put firm contraints to the stellar parameters (see e.g. Deheuvels et al. 2010 [63], Chaplin et al. 2010, [37]).

Even in the case of red giants the first indications of solar-type oscillations were obtained on ground-based observations in radial velocity (e.g. Arcturus, Merline 1999 [116], Frandsen et al. 2002 [70]) which largely suffered from low signal-to-noise data sets and aliasing. In fact the typical pulsations of red giants show longer periods than the solar-like

stars (of the order of hours). The detection of solar-like oscillations in red giants has been well established by the space mission MOST (Barban et al. 2007 [10]), but significant improvement in quality and quantity of the observations came from the 150-day long observations with CoRoT, which provided clear detections of radial and non-radial oscillation modes in numerous stars (e.g. Kallinger et al. 2010 [94]; Mosser et al. 2010 [122]), mainly lying in the core-helium-burning evolutionary phase (Miglio et al. 2009 [119]). Most recently, the NASA Kepler Mission has demonstrated its great asteroseismic potential to observe solar-type oscillations in red giants (e.g. Bedding et al. 2010b [17]; Hekker et al. 2010 [85]; Stello et al. 2010 [146]).

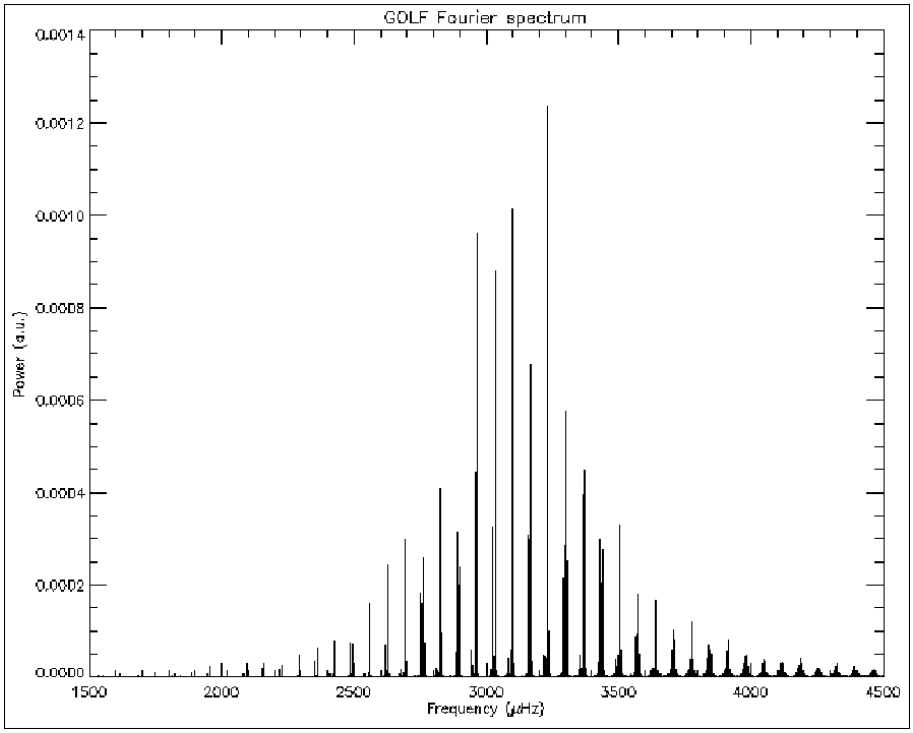

Figure 1.13: The power spectrum of the Sun, obtained with data from SOHO satellite.

Figure (1.13) shows the example of the solar power spectrum. As pointed out in Section 1.4.2, solar-like oscillations are characterized by a clear excess of power modulated by a Lorentian profile. This excess is generally centred at the frequency corresponding to the maximum power, ν_{max}. Its value is of about 3 mHz for the Sun, while for solar-like stars can be expressed through the acoustic cut-off frequency, ν_{ac} (see Brown et al. 1991 [33]). Scaling from the solar case, the frequency of maximum power of an arbitrary star provides indications about stellar parameters. According to Kjeldsen and Bedding 1995 [99], using $\nu_{max\odot}$=3.05 mHz and $T_{eff\odot}$ the solar values, the following relation is satisfied:

$$\nu_{max} = \frac{M/M_{\odot}}{(R/R_{\odot})^2\sqrt{T_{eff}/5777\mathrm{K}}}3.05\mathrm{mHz}. \tag{1.73}$$

According to the asymptotic theory, the frequencies of the power spectrum are defined by the asymptotic expression:

$$\nu_{n,l} = (n + \frac{l}{2} + \frac{1}{4} + \alpha)\Delta\nu \tag{1.74}$$

where $\Delta\nu$, the great separation defined in Eq. (1.65), corresponds to the almost regular spacing between the peaks, i.e. the modes, characterised by the same value of the degree and with a unitary difference in the radial orders. An interesting relation between the great separation and the main stellar parameters is provided in Kjeldsen and Bedding 1995 [99], according to whom:

$$\Delta\nu = (\frac{M}{M_\odot})^{1/2}(\frac{R}{R_\odot})^{-3/2}(\Delta\nu)_\odot \propto \rho^{1/2}, \tag{1.75}$$

where the solar value of $(\Delta\nu)_\odot$ is 134.92μHz, as in Toutain et al. 1992 [151]. Figure (1.14) shows the detail of the solar power excess: the large and also the small separations for a set of modes are clearly visible. Stello et al. [147], found a relation between the extension

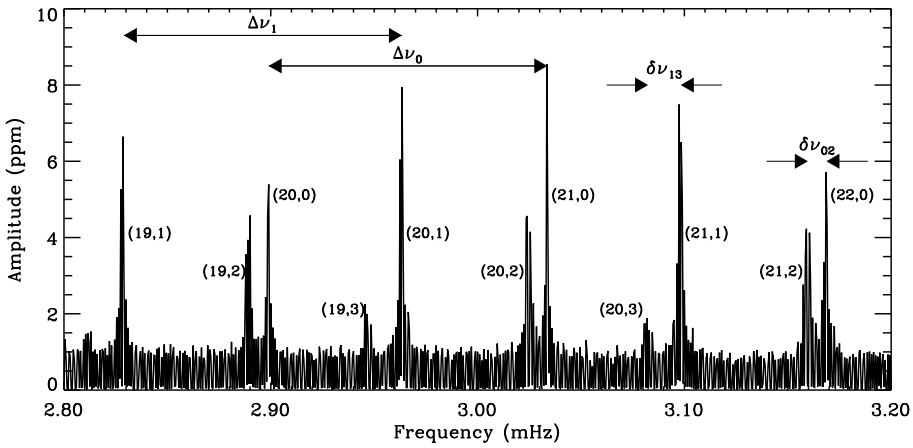

Figure 1.14: Detail of the solar amplitude spectrum, corresponding to the power excess. The small and great separations are indicated.

of the power envelope and the value of ν_{max} for solar-like stars:

$$\langle\Delta\nu\rangle \simeq (0.263 \pm 0.009)\nu_{max}^{0.772\pm0.005} \tag{1.76}$$

while Mosser et al. 2010 [122] present the same relation more suited to red giant stars:

$$\langle\Delta\nu\rangle \simeq (0.280 \pm 0.02)\nu_{max}^{0.75\pm0.01}. \tag{1.77}$$

Figure (1.15) shows the power spectra of four observed stars, the giant ξ Hydrae (Frandsen et al. 2002 [70], Procyon (Arentoft et al. 2008 [7]), α Centauri A (Bedding et al. 2004 [20]) and α Centauri B (Kjeldsen et al. 2005 [100]). The oscillation periods range from 3 - 4 hours for ξ Hydrae, 20 - 25 minutes for Procyon, 7 minutes for α Cen A and 4 minutes for α Cen B. These differences, and those in the detailed structure of the power spectra, reflect the differences in stellar properties and their evolutionary state.

The p modes *lifetime*, τ is defined by the relation with the observation time, T_{obs}:

$$\tau \propto \frac{1}{T_{obs}\sigma_{freq}^2} \tag{1.78}$$

where σ_{freq}^2 is the width of the mode peak in the power spectrum. A resolved mode for the lifetime creates in the power spectrum a series of peaks in which it spreads its power. Therefore the power is not collected in a single peak, and its computation is more difficult.

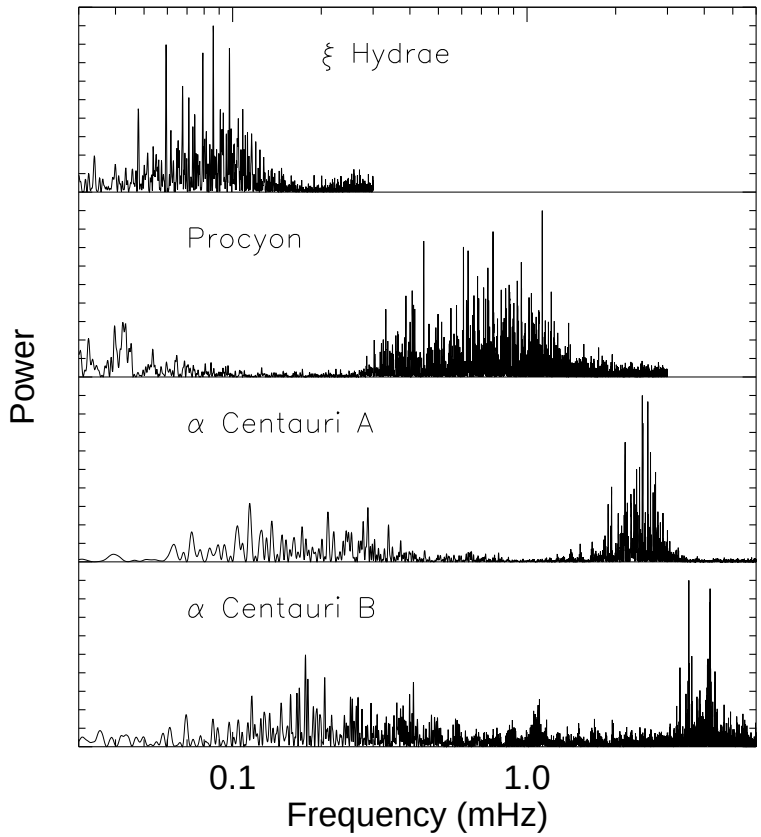

Figure 1.15: Power spectra of radial velocities time series for four observed stars in four different evolutionary phases. The more evolved in the upper part (ξ Hydrae) and the younger one in the lower part (α Cen B) (taken from Kjeldsen et al. 2008 [98]).

Another feature in the power spectrum likely due to the driving processes is the increasing of the line width toward the high frequencies, that let us to deduce that the damping rate is proportional to the frequency. Furthermore the height (H) of each mode is related to the linewidth (Γ) and the amplitude (A), according to Chaplin et al. 2005, by:

$$H = \frac{2A^2}{\pi\Gamma}, \qquad \text{where} \qquad \Gamma = \frac{1}{\pi\tau}. \tag{1.79}$$

Arentoft et al. 2008 [7] measured the amplitude envelope for all the stars observed at that time, with the radial velocities. Figure (1.16) shows the results on the oscillations amplitudes of these stars.

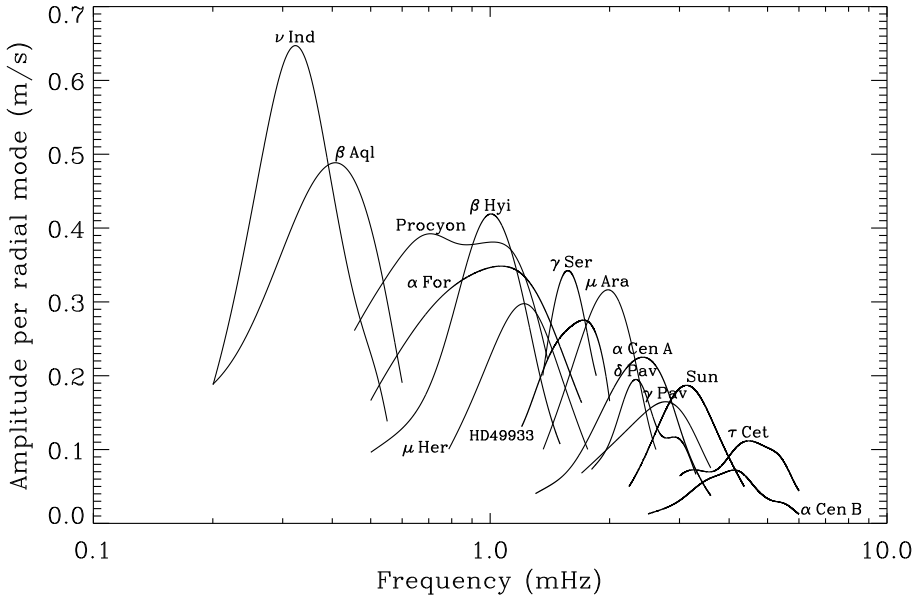

Figure 1.16: Amplitude envelope for the pulsators observed with the radial velocity technique (Arentoft et al. 2008 [7])

Figure (1.17) shows the plot of the cyclic frequency $\nu = \omega/2\pi$ as function of the degree l for a normal solar model. Depending on their values, are showed the locations of p- , g- and f-modes. The properties of solar-like oscillations are expected to change as the star evolves. Oscillation frequencies of a given harmonic degree should decrease as the star evolves and the radius increases and should be almost uniformly spaced by $\Delta\nu$. However, during the evolution of subgiants and red giants the radial modes the frequencies of some non-radial modes appear to be shifted from the regular spacing, and it seems that the frequencies of g- and p-modes are crossing. Actually this doesn't really happened, they get closer and closer but never meet, producing, instead, the so called *avoided crossings*. As the core contracts the radius expands, causing an increase of the local gravitational acceleration and therefore to the value of the buoyancy frequency. As a consequence g modes with high frequencies are allowed to propagate and can interact with p modes of similar frequency and same harmonic degree, giving rise to modes with mixed character, which behave as g modes in the interior and p modes in the outer envelope (Aizenmann et al. 1977 [4]).

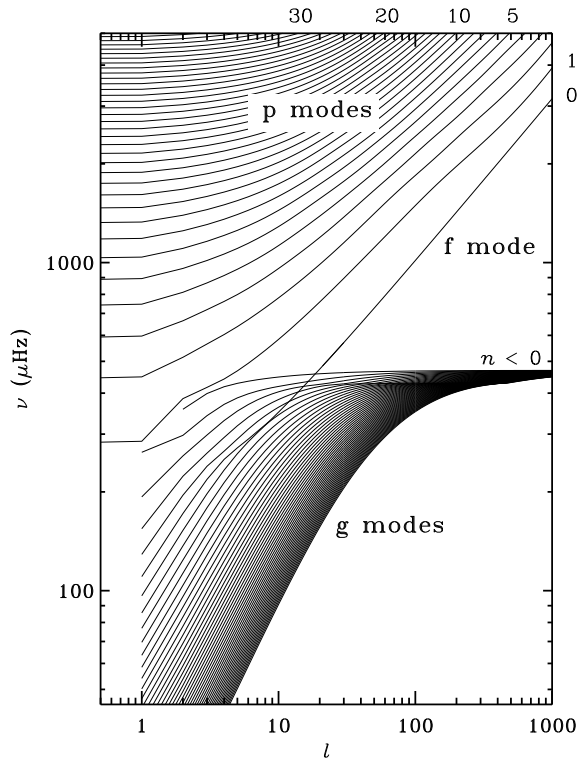

Figure 1.17: Cyclic frequencies $\nu = \omega/2\pi$ as function of the degree l. Values of the radial order n are indicated (taken from Christensen-Dalsgaard 2003 [42])(taken from Christensen-Dalsgaard 2003 [42]).

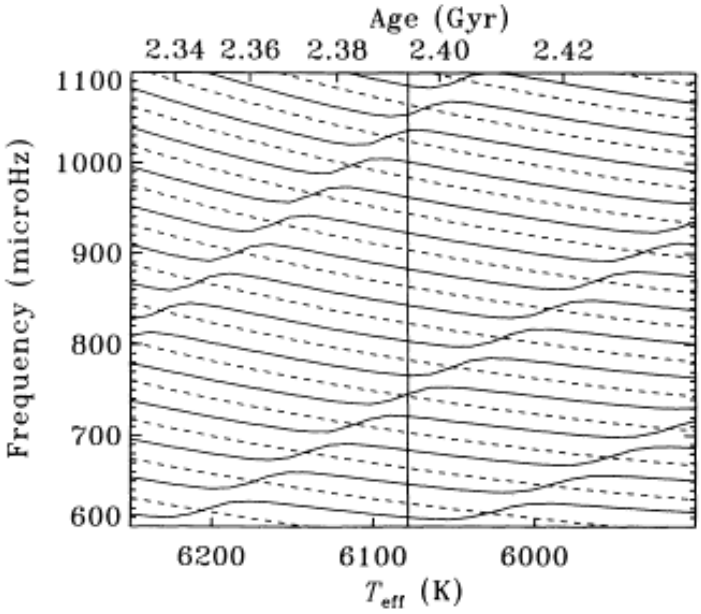

Figure 1.18: Evolution of adiabatic frequencies with the stellar age. Dashed lines correspond to degree $l = 0$, while the solid lines to the $l = 1$ modes (taken from Christensen-Dalsgaard 2003 [42])(taken from Christensen-Dalsgaard 2003 [42]).

Figure (1.18) shows the evolution of adiabatic frequencies with age, for a model of 1.6 $M_\odot$ star (See Christensen-Dalsgaard et al. 1995 [45]). The avoided crossings are present as well. The dashed lines indicates the modes with degree $l = 0$, i.e. radial modes, which behave as predicted by Eq. (1.74), and the decrease of the frequency with the age corresponds to the increasing of the stellar radius. It has to expect the same trend also for the non-radial modes with $l = 1$, the solid lines, but the effect of the increasing frequencies of the g-modes with the age give rise to the clearly visible variations in Figure (1.18). Also the modes with degree $l = 2, 3$ are undergone to the avoided crossings but the effect is much more weak.

We define the inertia E, a dimensionless parameter of the mode, as:

$$E \equiv \frac{\int_V \rho |\delta \mathbf{r}|^2 dV}{M |\delta \mathbf{r}|_s^2} \tag{1.80}$$

where V and M are the volume and the total mass of the star, $\delta\mathbf{r}$ is the displacement vector, and its square module, $|\delta\mathbf{r}|_s^2$ is evaluate over the stellar surface. The numerator of Eq. (1.80) is equivalent to the so called modal mass, M_{mode}, which relates the mode velocity at the surface, $|\mathbf{v}|_s$, and its total energy, $\mathcal{E}$:

$$\mathcal{E} = M_{mode} |\mathbf{v}|_s^2$$

The mode inertia is a function of the degree and the frequency, with an inverse dependence. Since the inertia is related to the quantity of stellar volume interested to the oscillation, its value for an high order mode, which has the lower turning point nearer to the surface, is smaller compared with a lower degree mode. A similar discussion, but in terms of the

eigenfunctions, can be made also for the frequency dependence. Computations showed that the decreasing of inertia due to the increase of the frequency is larger than the decrease due to the increase of l. Very low values of the inertia are found for high degree and high frequency g-modes which undergo the avoided crossings. The inertia parameter give useful indications on the surface amplitude of the stochastically excited modes, in fact according to Houdek et al. 1999 [88], for the amplitude A_{nl} of a mode we have that:

$$\frac{A_{nl}}{A_0(\delta_{nl})} \simeq [\frac{E_{nl}}{\bar{E}(\delta_{nl})}]^{-1/2} \tag{1.81}$$

where E_{nl} is the normalized inertia, and $A_0(\delta_{nl})$ and $\bar{E}(\delta_{nl})$ are obtained with interpolations with the radial modes.

There are basically two method to detect stellar oscillations, i.e. with intensity and velocity measurements. It is, therefore, useful to try to find a relation between luminosity and velocity amplitudes. Following the approach of Kjeldsen and Bedding 1995 [99] changes in temperature cause changes in luminosity, the fractional variation in the bolometric luminosity of a star, $(\delta L/L)_{bol}$, is then proportional to $\delta T/T$. Hypothesizing adiabatic oscillations, the fractional variation of the temperature is in turn due to the variation in density $\delta\rho/\rho$. Then we obtain:

$$(\frac{\delta L}{L})_{bol} \propto \frac{\delta\rho}{\rho}, \tag{1.82}$$

which means that the luminosity variations depend on the relative compression in the stellar atmosphere. According to Landau 1959 [102], for an adiabatic sound wave in a medium characterized by a sound speed c_s, we have:

$$\frac{\delta\rho}{\rho} = \frac{v}{c_s},$$

where v is the velocity of the fluid, which in the case of stellar oscillation is equal to the observed velocity amplitudes, v_{osc}. The square sound speed is proportional to the mean local temperature, assumed to be the effective temperature of the star. The final relation is then:

$$(\frac{\delta L}{L})_{bol} \propto \frac{v_{osc}}{\sqrt{T_{eff}}} \tag{1.83}$$

between luminosity and velocity amplitude for solar-like oscillations.
In Christensen-Dalsgaard et al. 1983 [48], a theoretical prediction of the amplitudes is given in the several regions of H-R diagram, but without a general law, even if the differences are quite small. A possible scaling relation from fundamental stellar parameters is provide in Kjeldsen and Bedding 1995 [99], according to whom the velocity amplitudes for Main Sequence and Red Giant stars are proportional to:

$$v_{osc} \propto \frac{L}{M}. \tag{1.84}$$

Since $M \propto gR^2$ and $L \propto R^2T_{eff}^4$, the final relation is of the type:

$$v_{osc} \propto \frac{T_{eff}^4}{g}. \tag{1.85}$$

Scaling from the solar values, v_{osc} can be, in good approssimation defined as:

$$v_{osc} = \frac{L/L_\odot}{M/M_\odot} v_{osc\odot} \quad [cm \cdot s^{-1}].$$

1.5.2 Subdwarf B stars

Subdwarf B stars were identified as pulsating class by Charpinet et al. 1996 [39] in theoretical way, and by Kilkenny et al. 1997 [96] and Billeres et al. 1997 [25] after the observational investigations. A lot of paper reviews present the characteristics of SdB stars, both on the theoretical and observational point of view. In particular we recall here two of the latest published: Kawaler 2010 [95] and Østensen 2010b [123], from which we take the most important informations for a brief description of these objects. Subdwarf B, also known as extreme horizontal branch (EHB) stars, belong to the population of faint blue stars, burning helium in their core. They are characterized by masses close to $0.5 M_{\odot}$ (Han et al. 2003 [82]) and their thin hydrogen envelopes doesn't allow the H-shell burning. After their lifetime in the EHB they pass directly to the White Dwarf cooling sequence. A full knowledge about the formation and evolution of these objects is still missing. In particular, researcher are studying which mechanisms are able to leave the star with such a thin hydrogen layer. Many scenarios were proposed: the binary mass exchange, the variation of the mass loss efficiency on the RGB, mass stripping by planetary companions. Observational evidence indicates the binary scenario to be the most probable. Thanks to the detection of pulsation of these stars, it would be possible to address question about the origin of SdB stars.

There are basically two pulsating classes belonging to the EHB stars: the EC14026 types, with $T_{eff} \sim 30,000 - 36,000$ K, show periods in the range of 100 - 600 s (Kilkenny et al. 1997 [96]), while the so called *Betsy* with $T_{eff} \sim 25,000 - 30,000$ K, show periods in the range of 45 minutes - 2 hours (Green et al. 2003 [77]). The former class pulsates with low-order, low degree p-modes, the latter in high order, relatively high degree ($l \geq 3$) g-modes. In both cases the oscillation mechanism is driven by for the opacity mechanism related to iron group elements (Charpinet et al. 1997 [38]). Intermediate pulsation characteristics (both p and g modes) were detected by Schuh et al. 2006 [137] for the SdB star HS0702+6043, demonstrating thus the existence of hybrid objects.

Several observational programs operate to provide data useful to answer to the questions about the formation of SdB stars, particularly focused on the binarity hypothesys. For instance, Green et al. 2008 [76] presented a survey of a substantial sample including most of known hot Subdwarfs. Figure (1.19) shows resulting distribution of these objects in the HR diagram, as well as their pulsational characteristics. Among other surveys from the ground we can cite the Whole Earth Telescope network (WET), the multicolor photometry of ULTRACAM at VLT or the observing programs carried on at the Mercator Telescope (La Palma). From space, very interesting results are coming from the satellite Kepler (see Østensen 2010a [126]). A small but extremely interesting observing program is EXOTIME (see next Chapter), aimed to search for planetary companion to EHB stars and the secular variation of the oscillation periods.

1.5.3 Hybrid γ Doradus and δ Scuti stars

The γ Doradus (Dor) and δ Scuti (Sct) stars show pulsations characterized by many simultaneous frequencies, making them particularly useful for asteroseismic studies. These stars are core hydrogen burning and they are characterized by higher masses than the Sun (1.2 - 2.5 $M_{\odot}$), they show convective cores, shallow convective envelopes in comparison to the Sun, and rapid rotation (Grigahcène et al. 2010a [79]). γ Dor stars pulsate in high order gravity modes, driven by convective blocking at the base of their envelope convection zone.

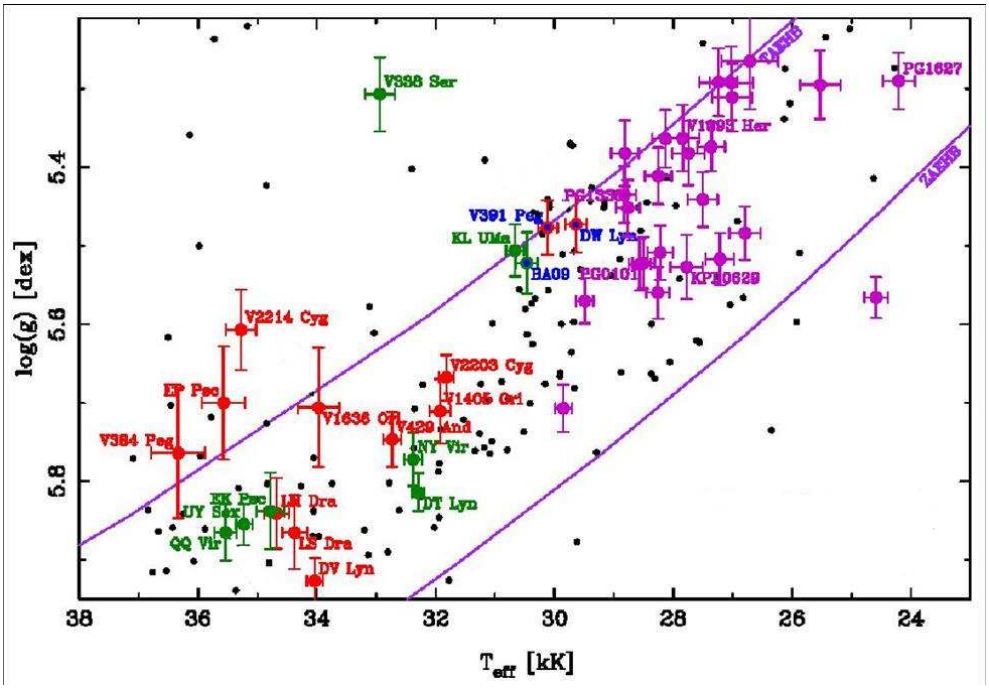

Figure 1.19: Section of the $T_{eff} - logg$ diagram showing the location of the EHB stars. Large symbols indicates objects observed through the survey presented by Green et al. 2008 [76]. Small symbols indicate stars not observed to pulsate. The green and red points locate short period pulsators, the former with published asteroseismic results, the latter, without. Finally, magenta points are the long period pulsators, while those with blue core are the hybrid pulsators (taken from Østensen 2010b [123]).

Typical periods of those modes are between 0.3 and 3 days. Furthermore, the g-modes reach the stellar surface with small amplitudes resulting in very difficult detection, particularly from the ground. δ (Sct) stars show low-order g- and p-modes with periods ranging from 0.014 and 0.333 days, driven by the κ mechanism operating in the He II ionization zone (Grigahcène et al. 2010a [79]). Handler and Shobbrook 2002 [83] considering the pulsation constant Q, showed the clearer distinction between the two classes: δ Sct stars have $Q < 0.055$ days whereas for γ Dor stars $Q > 0.24$ days. Since their discovery as pulsating stars (Balona et al. 1994 [9]), their position on the Hertzsprung-Russell diagram (see Figure (1.11)) suggested a possible relationship with the δ Sct group. The γ Dor in fact lie in a zone close to the cool border of the classical instability strip, partially overlapping with the δ Sct pulsators. This latter property led astronomers to investigate the possible existence of hybrid stars exhibiting both types of pulsations (Breger and Beichbuchner 1996, [32]). The susprising results of the first observations of γ Dor and δ Sct stars from the *Kepler* satellite (see next Chapter), show that almost all of these objects present hybrid characteristics in their pulsational behavior (Grigahcène et al. 2010a [79]). The existence of different types of pulsation modes in hybrid stars provides additional constraints on the stellar structure. Indeed, the g modes probe the stellar core, while the p modes probe the stellar envelope. The high-order g modes provide an additional advantage in terms of modelling, as the asymptotic approximation can be used, implying that the equations can be solved analytically (Smeyers & Moya 2007 [143]). In hybrid stars, this advantage can be extended to p modes pulsators. Furthermore, in the same region of the HR Diagram, where the δ Sct and γ Dor instability strips overlap, solar-like oscillations are also predicted to occur for δ Sct stars (Houdek et al. 1999 [88]). Up to now, no detections of solar-like oscillations in such hot stars have been reported, probably due to the detection limits imposed by ground-based measurements. Pereira et al. 2007 [134] also predict possible stochastic excitation as driving mechanism in γ Dor stars, but up to now, no evidence of that was found. Figure (1.20) shows the observational status of γ Doradus and δ Scuti stars, in which the hybrid objects are depicted toghether with the pure ones.

Grigahcène et al. 2010a [79] proposed a new observational scheme for the classification of γ Dor and δ Sct stars, on the ligh of the new discoveries from *Kepler*. In this classification they use not only the characteristic frequencies but also the amplitudes.

- δ Sct: most of the frequencies are ≥ 5 day^{-1}, and the lower frequencies are of relatively low amplitude;
- δ Sct/γ Dor hybrid: most of the frequencies are ≥ 5 day^{-1}, but there are some lower frequencies which are of comparable amplitude;
- γ Dor: most of the frequencies are ≤ 5 day^{-1}, and the higher frequencies are of relatively low amplitude;
- γ Dor/δ Sct hybrid: most of the frequencies are ≤ 5 day^{-1}, but there are some higher frequencies which are of comparable amplitude.

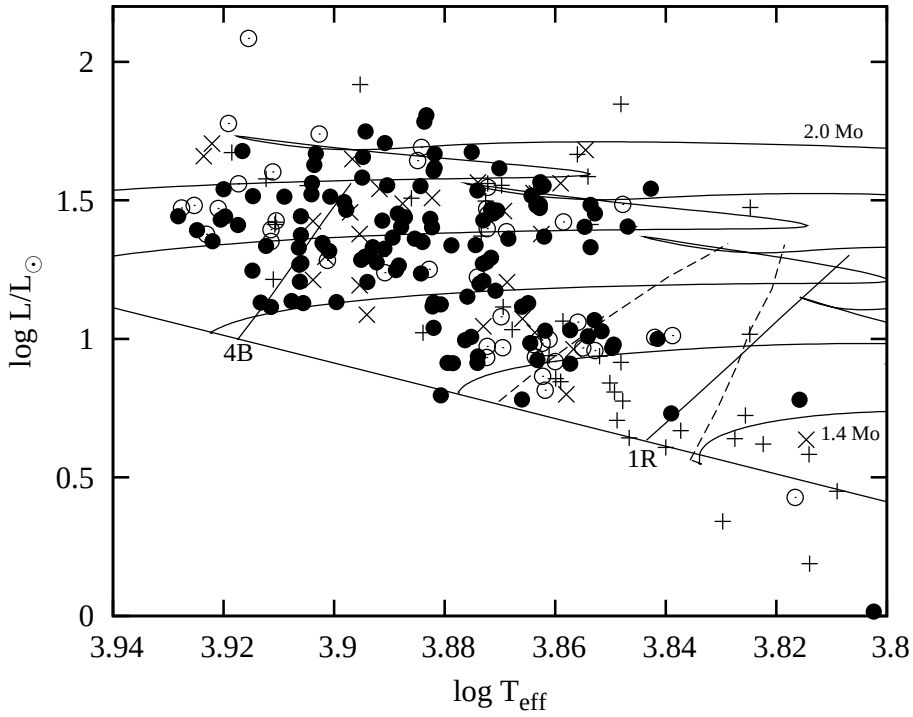

Figure 1.20: Classification of Kepler target stars in the theoretical HR diagram. The symbols rep- resent: δ Sct (•), δ Sct/γ Dor (⊙), γ Dor/δ Sct (×), γ Dor (+). The solid lines show the Zero-Age Main Sequence and the δ Sct instability strip delimited by the radial fundamental red edge (1R) and the 4th overtone radial blue edge (4B). The dashed lines are the red and blue edges of the γ Dor instability strip (Dupret et al. 2005 [67]). (Figure taken from Grigahcène et al. 2010b [80]).

Chapter 2

Asteroseismology and Exoplanets search

In this Chapter we consider the synergy between Asteroseismology and the search for Extrasolar planets, with particular attention on the observational point of view. After some considerations about the mutual support of these two research we present some facilities and the state of the art both for ground based observations (such as the HARPS spectrograph at ESO-La Silla [127], the SARG spctrograph at the ORM-La Palma [74], the EXOTIME project [138]) and for space based observations, which provide long and uninterrupted time series, making them particularly suited to perform Asteroseismology. Space satellites like CoRoT [8] and Kepler [29] are bright examples of the connection between Asteroseismology and the Exoplanets search. We present the mission profiles as well as the most important results obtained up to now, with particular attention to Kepler, since part of this thesis is based on Kepler data.

2.1 Asteroseismology and the search for Extrasolar planets

As already pointed out in the previous Chapter, the analysis of the oscillation frequencies allow us to constrain fundamental parameters of stars such as density, mass, radius, age, rotation period and chemical composition. These informations are crucial to understand the fundamental properties of exoplanet systems. During the last years it has been demonstrated that Asteroseismology is indeed a powerful tool to characterize and even to find planets, thanks to the informations obtainable from the host stars. Examples of this synergy can be found in the cases of the exoplanet discovery through the seismological observations of the stars μ Ara (Bouchy et al. 2005 [30]) and ι Hor (Laymand & Vauclair 2007 [104]).

The connections between Asteroseismology and the search for Extrasolar planets are several, and allow us to understand why there have been made so many efforts to build and project both ground-based instruments and space satellites. First of all the measured quantities are the same, i.e. the reflex motion of a star due to an orbiting planet or its luminosity variations due to the transit of the body across the stellar disk, causes the same small variations of stellar parameters as those due to the pulsations. It is therefore clear that the observations can be performed with the same instruments. Asteroseismology is then very important for exoplanet researchers, because the so called *stellar noise*, which affects the observations, is nothing but the oscillations of the star, and a better treatment of

it can help to discriminate between planetary and stellar sources of signal. Anyway, direct and precise informations about the planet properties are still far to be achieved without reliable values of the parent stars parameters. In fact both in the case of the transits and in radial velocities methods the achievable informations about radius and mass of the planet are always in function of stellar radius and mass. In order to search for Earth-like planets the knowledge of the planet density is mandatory, since it helps to discriminate rocky to gaseous planets. It is therefore clear that the measure of planetary mass and radius is fundamental for the characterization of the planet itself. The asteroseismic investigation to the planet candidates host stars is the only useful tool to quantify with an unprecedent accuracy the fundamental stellar parameters. Nowadays Asteroseismology yields these informations as demonstrated in, e.g., Mosser et al. 2010 [122] and Metcalfe et al. 2010 [117], which put firm constraints to stellar parameters using the asteroseismic observables and the support of theoretical models. The potential of this combination is now quite clear, and it is thought that it could bring us to obtain hints about the theories of planetary formation and migration.

Since in this Ph.D thesis will be focused to space missions which perform high precision photometry in order to search for planetary transits, we briefly discuss the main characteristics of a transit and why Asteroseismology is defined a fundamental tool for this kind of studies.

2.1.1 Planetary Transits

There are several techniques to detect Estrasolar planets, both with direct methods, such as the direct imaging, and indirect methods like radial velocities, microlensing, timing and transits. Since the detection of exoplanets is beyond the aim of the present thesis we avoid to describe these techniques, except for the last one, the planetary transits. Actually this is the method used both by Kepler and PLATO, main topics of this work.

The principle of the transits method is quite simple and it takes into account of the luminosity variations of a star that occur when a body, such as a planet, crosses its disk, repeating this effect at the orbital period of the planet (see Figure (2.1)). For a Sun - Jupiter system seen at 10 pc the change in the stellar luminosity is of the order of 2% (0.02 mag). The detection probability depends on the transit geometry and on the decreasing of the intensity produced by an object on the line of sight. A strict treatment of the problem would takes into accounto of the limb darkening effect on the stellar disk, which produces a decrease of the luminosity toward the edge due to the increasing atmospheric depth. Using the approximation of a uniform brightness of the stellar disk, the depth of the transit in flux units is:

$$\frac{\Delta L}{L_*} \simeq (\frac{R_p}{R_*})^2, \tag{2.1}$$

where L_* is the stellar luminosity while R_* and R_p are the radius of the star and of the planet respectively. Values of $\frac{\Delta L}{L_*}$ for Earth, Mars and Jupiter transiting the Sun are: 8.4×10^{-5}, 3×10^{-5}, 1.1×10^{-2}. If the radius of the star can be measured, then the radius of the planet can be estimated from this equation. The depth in magnitude is:

$$\delta M = -2.5 \log_{10}(1 - (\frac{R_p}{R_*})^2). \tag{2.2}$$

The duration of an extrasolar planet transit is of the order of 3 hours, depending on

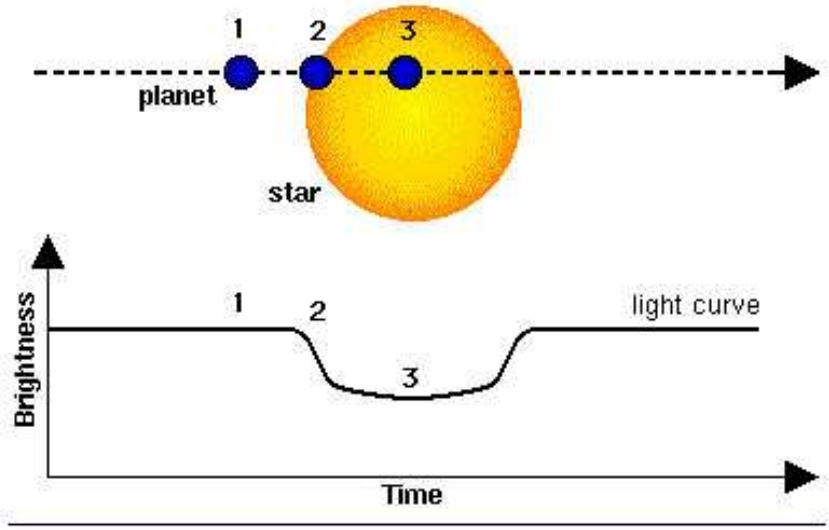

Figure 2.1: Light curve of a star during a planetary transit.

the orbital period and the radius of the star and of the planet. It is calculated as:

$$\tau = \frac{P}{\pi}(\frac{R_* \cos\delta + R_p}{a}) \simeq 13(\frac{M_*}{M_\odot})^{-1/2}(\frac{1}{1AU})^{1/2}(\frac{R_*}{R_\odot})[hours] \tag{2.3}$$

where δ is the latitude of the transit on the stellar disk, and it produces a value of 25 hr for Jupiter-like planet and 13 hr for a Earth-type planet. Figure (2.2) shows the geometry

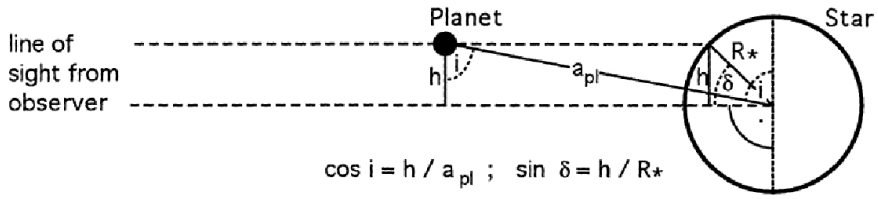

Figure 2.2: Geometry of a planetary transit.

of a transit and suggests that the orbital inclination is correlated with the latitude δ:

$$\cos i = \frac{R_* \sin\delta}{a}. \tag{2.4}$$

Using Eq. (2.4) we can define the minimum inclination where transits can occur ($\delta = \pi/2$):

$$i_{min} = \arccos\frac{R_*}{a}, \tag{2.5}$$

while the probability of observing transit for a randomly oriented system is:

$$p = \frac{R_*}{a} = \cos i_{min}. \tag{2.6}$$

The principal drawback of this method is the fact that it requires configurations in which the viewing direction lies in the orbital plane of the planet.

Since the last performances of measuring stellar radii with Asteroseismology has reached a relative accuracy of 2-3% (see Kjeldsen et al. 2008 [98]) it is clear that the combination of these two techniques has a great potential to obtain the planet radius. Knowing the mass of the planet it is possible to calculate de planet density that give us a fundamental information on its structure, i.e. if it is a gaseous or a rocky planet.

2.2 Ground-based observations

The detection of stellar oscillations can be performed both with spectroscopic and photometric techniques. In fact the three stellar parameters affected by the oscillations are the radial velocity, the equivalent width and the luminosity. Thus with the spectroscopic measurements, variations of the radial velocity and of the equivalent widths can be performed, particularly indicated in the search for solar-like oscillations. With photometric observations it is possible to obtain the variations of the luminosity of the star. The use of sophisticated instrumentations is necessary in this kind of search since, as already said, the variations are very small and also the time scales can be prohibitive for the observations.

The search for solar-like oscillations from the ground is restricted to spectroscopy, since the luminosity amplitudes are totally covered by the scintillation noise of the Earth atmosphere. However the spectroscopic campaigns have produced very encouraging results, with prospectives of improvement. This success has been driven thanks to the development of ultra-precise spectrographs built for the search for extrasolar planets (e.g. HARPS at ESO, La Silla (Chile), or SARG at TNG, Canary Islands). There are two main techniques to obtain high precision radial velocities measurements: the simultaneous thorium calibration and the iodine cell technique.

2.2.1 HARPS and the simultaneous thorium calibration

With this kind of technique, the instrument is feed by two optical fibers, one that leads to the spectrograph the light coming from a Thorium lamp and the second that brings the starlight. As a result it keeps stable and constant the slit illumination, and reduces the spectrograph instabilities. With such a technique, both the star and the lamp spectra are detected on the CCD in a unique exposure (*scramble* of the images). The great advantage is the simultaneous wavelength calibration, and the possibility to check if some displacements occur between the spectra. For this technique is mandatory a fixed set-up to eliminate possible variations of instrumental profile. The radial velocities are measured with the cross-correlation technique. In principle, simultaneous thorium method doesn't allow the same radial velocity precision obtainable with the iodine cell (see Section 2.2.2), but it has other advantages such as:

- the larger wavelength coverage, since the absorption features of the iodine range between 5000 and 6300 Å;
- the greater efficiency, since it doesn't need bright stars to get high signal to noise ratio as in the iodine cell technique;
- a more simple data analysis technique than the iodine cell, that require a complex set of algorithms.

Figure 2.3: HARPS, the High Accuracy Radial velocity Planet Searcher, is a fibre-fed high resolution echelle spectrograph for the measurement of radial velocities with the highest accuracy currently available.

The HARPS Spectrograph (Pepe et al. 2002 [127], see Figure (2.3)) is the most efficient and precise instrument performing this method. HARPS is fibre-fed by the Cassegrain focus of the 3.6m telescope at ESO - La Silla (Chile). It is contained in a vacuum vessel to avoid spectral drift due to temperature and air pressure variations. One of the two fibres collects the star light, while the second is used to either record simultaneously a Th-Ar reference spectrum or the background sky. The precision in the radial velocities measurement is lower than 1 m/s.

Among the results obtained by HARPS we stressed the unexpected discovery of a 14 earth mass planetary companion of the G3IV-V star μArae, see Figure (2.4, left panel), confirmed by Santos et al. 2004 [136], obtained with asteroseismic observations by Bouchy et al. 2005 [30]. Particular attention was dedicated to this target, and up to 43 p-mode oscillations (see Figure (2.4, right panel)) were identified with a further investigation on the origin of the metallicity excess in this planet-hosting star. Comparison with stellar structure models and interpretation are then presented in a related paper by Bazot et al. 2005 [16]).

Asteroseismology of binaries was also performed, e.g. the visual binary 70 Ophiuchi by Carrier and Eggenberger 2006 [35], obtaining radial velocity measurements with a standard deviation of about 1.39 m/s. The power spectrum of the time series clearly presents several peaks between 3 and 6 mHz, showing regularity with a large spacing of $\Delta\nu = 161.7 \pm 0.3$ μHz. Fourteen individual modes were identified. See Figure (2.5).

Bazot et al. 2007 [15] presented a new analysis of the G2V star α Cen A. They identified 34 p modes with angular degree in the frequency range 1.8-2.9 mHz and amplitude range 13-48 cm/s, in agreement with previous seismic studies. In particular they found an enhancement of the frequency scatter with the angular degree l that indicates, considering the high inclination axis of α Cen A, rotational splitting and explains the low values of previously suggested mode lifetimes. Finally, they derive new values for the small separations

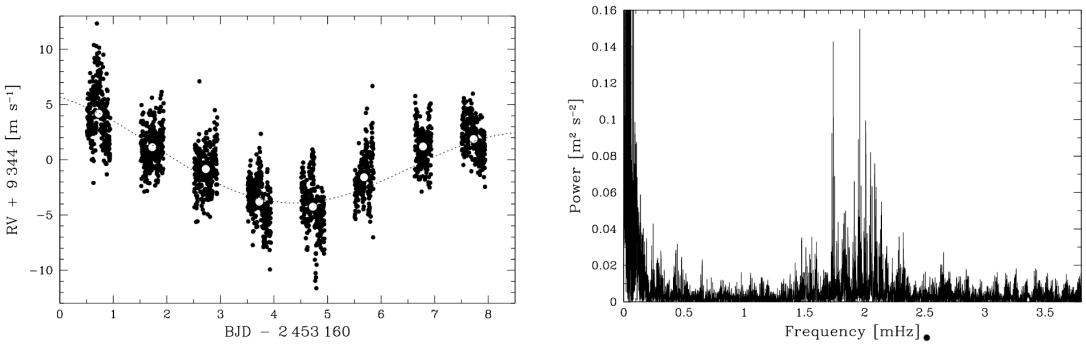

Figure 2.4: *Left panel:* time series of the radial velocities of the star μArae obtained with the HARPS spectrograph. The dotted curve correspond to the orbital fit of the low-mass-planetary companion, showing a period of about 8 days. *Right panel:* power spectrum of μArae, showing typical feature of solar-like oscillations (taken from Bouchy et al. 2005 [30]).

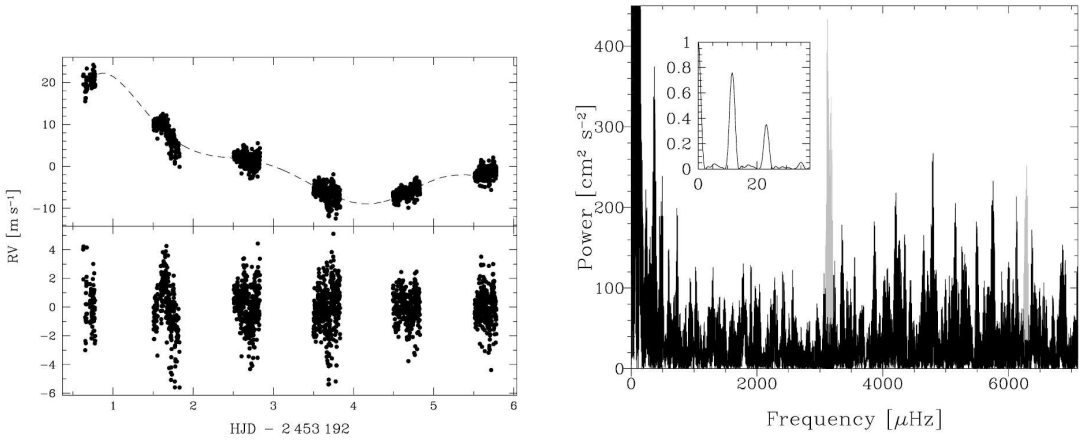

Figure 2.5: *Left panel:* time series of the radial velocities of the binary star 70 Ophiuchi, obtained with the HARPS spectrograph. In particular the lower panel shows the time series after the removal of the binary trend (dashed line on the upper panel). *Right panel:* The related power spectrum was 'cleaned' removing the two high peak in gray probably due to a technical problem (taken from Carrier and Eggenberger 2006 [35]).

that take the effect of rotational splitting into account.

During the Workshop about the Exoplanets, held in Porto (Portugal) in 2009 the Geneva University group claimed the detection of 32 new extrasolar planets, obtained thanks to the HARPS' survey. These planets range from around five times the size of Earth to around five times the size of Jupiter. A lot of planets were detected thanks to this instruments, but the most important one is the discovery of an Earth-mass planet in the GJ 581 planetary system, found by Mayor et al. 2009 [115]. The planet, in the famous system Gliese 581, is only about twice the mass of our Earth. The team also refined the orbit of the planet Gliese 581 d, first discovered in 2007, placing it well within the habitable

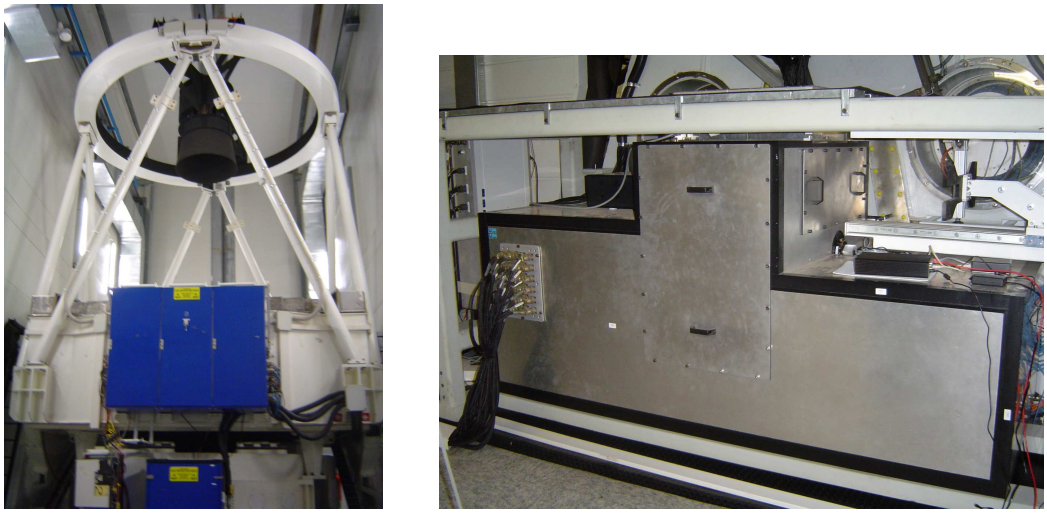

Figure 2.6: SARG, Spettrografo ad Alta Risoluzione Galileo, is a cross dispersed echelle spectrograph equipped with a Iodine cell, yielding accurate radial velocities measurements.

zone, where liquid water oceans could exist.

2.2.2 SARG and the Iodine cell technique

The principle of this method is based on the comparison of the lines positions between an high resolution spectrum of the interest object, and the corresponding spectrum obtained in rest conditions (i.e. in laboratory). In order to do that a gas absorption cell (mostly I_2) is located in the light path of the spectrograph and superimposes a dense reference spectrum in the same way. The resulting displacement between the lines provides indications on the radial motion of the target according to the Doppler shift theory. It is important to note that the spectrum obtain with cell technique cannot be use to find Equivalent Width of the lines or to glean information on temperature anymore, at least for the wavelength range occupied by the Iodine lines. The extraction of the radial velocities requires a sophisticated data modelling that includes the reconstruction of the shape of the spectrograph instrumental profile (e.g. the AUSTRAL code by Endl et al. 2000 [69]).

SARG (Gratton et al. 2001 [74]), see Figure (2.6), right panel) is a cross dispersed echelle spectrograph covering the wavelength range between (370 - 1000) nm. The maximum resolution attained is R=164,000. It is permanently mounted at the TNG (see Figure (2.6, left panel)) the Italian telescope at the Roque de los Muchachos, La Palma, Canary Islands. SARG is equipped with a Iodine cell, which superimposes its deep lines in the wavelength range between 5000 and 6000 Å.

Among the results obtained with SARG and its accurate determination of radial velocity (in the field of Asteroseismology and Exoplanet search) we find:

- Procyon A (F5 IV) was observed in two different runs with SARG in January 2001 and in January 2007, for nine nights in all. Using the iodine cell technique, and processing the spectra with the AUSTRAL code by Endl et al. (2000) [69], Claudi et al. 2005 [53] and Leccia et al. 2007 [106] were enable to reach very high precision measurements, allowing to detect solar-like oscillations for the former campaign. In particular, they identified 11 pulsation modes and their estimation of the large separation is in full

agreement with theory and other determinations from literature.

The observations performed in 2007 were collected in the framework of the global network which involved 11 observatories. Several studies of Procyon exist. They agreed on the location of the excess power (around 0.5 - 1.5 mHz), but they disagreed on the individual oscillation frequencies. This huge observational effort (almost continuous coverage for three weeks) was aimed to obtain a final and more reliable modes identification. The complete analysis of this set of data is presented in Arentoft et al. 2008 [7] and Bedding et al. 2010 [21]. Figure (2.7) shows the uncertainties in the time series for the partecipating telescopes. Dark blue points indicates the uncertainties obtained for SARG, showing one of the most low dispersions.

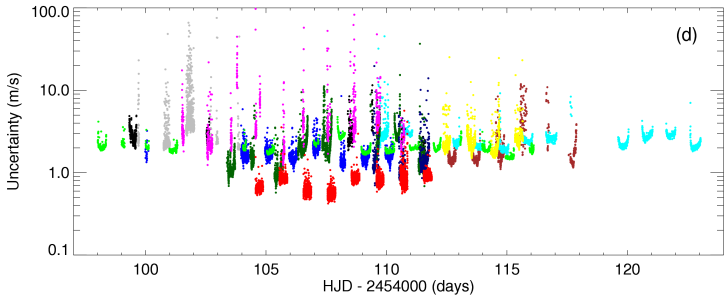

Figure 2.7: Comparison of the uncertainties calculated for the single telescopes partecipating to the global observing network for the star Procyon A (α CMi). SARG spectrograph is indicated by dark blue points (taken from Arentoft et al. 2008 [7]).

The resulting power spectra are shown in Figure (2.8). The excess of power for the solar-like oscillations is clearly visible for all of the telescopes, but even in this case SARG shows its particular instrumental stability (very low presence of red and white noise, taking into account that no filters were applied to the data). Bedding et al. 2010 [21] developed a new method for adjusting the weights in the time series that allowed to minimize the sidelobes in the power spectrum that arise from diurnal gaps. This technique allow them an unambiguous identification of 55 oscillation modes.

- The subgiant star μ Herculis (G5 IV) was observed with SARG in June 2006 for seven continuous nights. The clear detection of solar-like oscillation was presented by Bonanno et al. 2008 [28]. The rms scatter of the radial velocity time series is 2.53 m/s (see Figure (2.9)) and the uncertainties for the velocity measurements were estimated from residuals in the range 1 - 2 m/s. Figure (2.10) shows thw power spectrum of the solar-like oscillation detected in μHer. The calculated frequency spacing expected from asymptotic theory is $\Delta\nu \simeq 57\mu$Hz, in agreement with expectations. Modes identification was performed as well. Furthermore, they obtain a valuable confirmation that oscillations in solar-like stars really do have the amplitudes that scales as L/M by extrapolating from the Sun.

- In 2008 Benatti et al. [23] presented the intrinsic radial velocity limits obtained from the cited asteroseismological observations with the aim to calculate the mass upper limits for possible planetary companions of the targets. In this case the stellar noise (i.e. the oscillations) could cover the smaller radial velocity amplitudes due to the secondary body. It was shown that averaging consecutives radial velocity

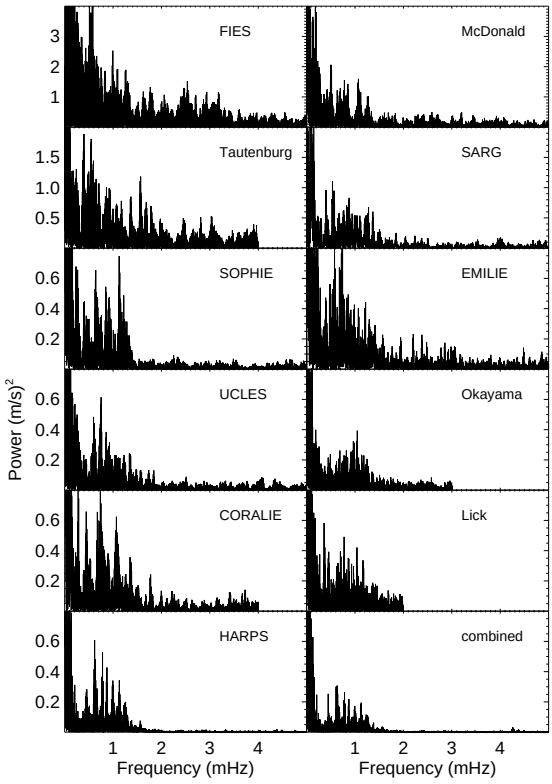

Figure 2.8: Plots of all the power spectra obtained from all the telescopes (taken from Arentoft et al. 2008 [7]).

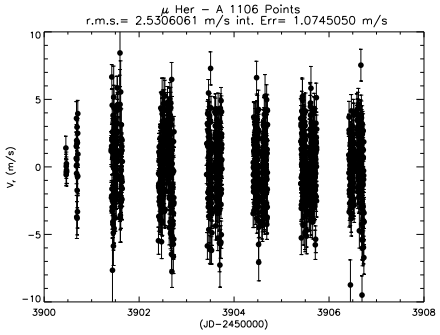

Figure 2.9: Radial velocity time series of the Subgiant μHer obtained with the SARG spectrograph (taken from Benatti 2007, master degree thesis [22]).

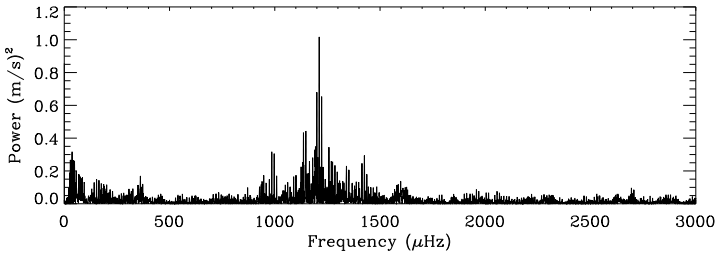

Figure 2.10: Power spectrum of μHer. The excess of power is clearly visible and centred at $\nu_{max} \sim 1200\mu$Hz (taken from Bonanno et al. 2008 [28]).

measurements it is possible to limit these effects (Santos et al. 2004 [136]). Averaging the exposures of each night they reduce the photon noise and limit the effect of the intrinsic stellar noise, like oscillations and granulations. The nightly averages show rms dispersion of ~ 0.2 m/s over one week, see Figure (2.11). Following the approach

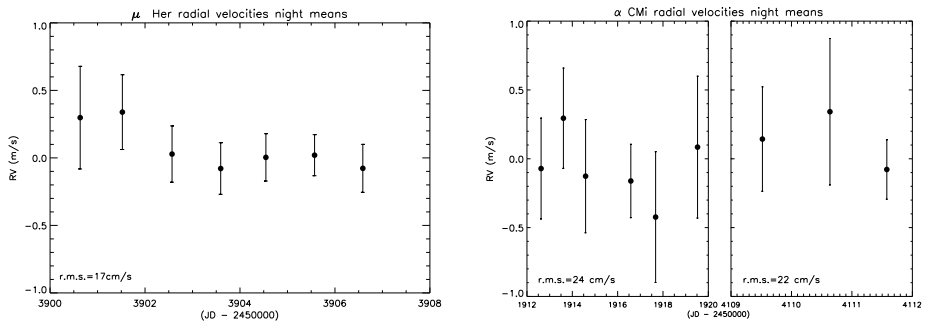

Figure 2.11: Radial velocities nightly means for the three sets of data (taken from Benatti et al. 2008 [23]).

of Desidera et al. (2003) [64], and using the MULO code by M. Barbieri, they obtained an estimate of the region in the mass-semimajor axis plane. Here the presence of the planetary companion is excluded by the available data, since its presence would have created a detectable excess of variability. Figure 2.12 shows the results obtained for μ Her and Procyon. It is the first time that a precision of the order of 20 cm/s is reported for a spectrograph working with the absorption gas cell technique. This demonstrates that a suitable observing strategy can push the intrinsic stellar limit of radial velocities measurements well below 1 m/s.

2.2.3 The EXOTIME Project

The EXOTIME project (EXOplanet search with the TIming MEthod) is a coordinated observing program aimed at the search for substellar companions around pulsating subdwarf B stars and the derivation of evolutionary timescales. The required observations span over a very long time (of the order of years), so this method is quite expensive in terms of observing time, but with the advantage to be sensitive to wide orbits and relatively low masses (down to $\sim$ M$_{Jup}$).

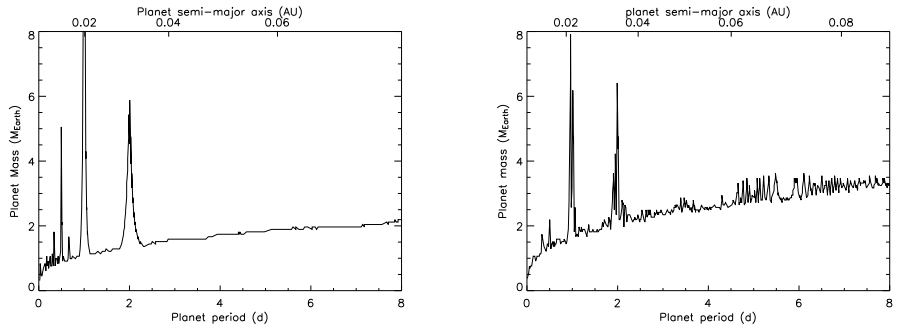

Figure 2.12: Projected mass upper limits for μ Her (left) and Procyon (right) (taken from Benatti et al. 2008 [23]).

Using the timing method it is possible to measure both the variations of the pulsation periods and the phase variations; the latter potentially allow us to detect the presence of substellar companions as in the case of V391 Peg b (Silvotti et al. 2007 [142]), the first planet discovered with this technique around a pulsating star. The discovery of V391 Peg b has raised the interest to investigate evolved planetary systems beyond the main sequence and beyond the red giant branch. The orbital distance of this planet, lower than 2 AU, suggests that this planet may have "survived" to the RG expansion of the parent star. Recently, two substellar companions have been detected orbiting the sdB eclipsing binary HW Vir (Lee et al. 2009 [107]), suggesting that substellar objects might be a relatively common phenomenon around sdB stars.

Further goals of EXOTIME are the characterization of the targets using asteroseismic methods and the measurement of the secular variation of the oscillation period (the so called P-dot, $\dot{P}$), giving a further example of the synergy between asteroseismology and the search for exoplanets, already known in the case of solar-like stars. Measuring $\dot{P}$ allows a precise determination of the evolutionary status of a star and can help the identification of the pulsation modes. As a final goal, EXOTIME wishes to improve our understanding of the formation and evolution of the sdB stars. The formation processes of sdB stars still represent an unclear topic in stellar evolution. Different scenarios have been proposed, both for single stars and binaries. The presence of a secondary body such as a planet, in particular for single stars, has been suggested to play a role in this process, enhancing the mass loss near the RGB tip (Soker 1998 [144]).

As in the case of the pulsar timing, the oscillation periods are used as a clock in order to detect all the possible variations in the travel time of the photons. These variations could be attributed to the secular variation of the oscillation period, $\dot{P}$, or to a wobble of the sdB location due to the presence of a perturbing body, such as a planet. These variations are easily detectable through the O-C diagram, in which the theoretical (*Calculated*) expectations of a particular quantity are compared with the *Observed* ones. Once one obtains a sufficient number of data, it is possible to compare the mean phase of a long monitoring period with the phases at different time steps. If changes occur in the pulsation period, they can be detected and identified according to the distribution of the points in the graph. When a pulsation period changes linearly in time, the O-C diagram shows a parabolic shape caused by the evolutionary timescale. The presence of a companion is revealed by a sinusoidal trend which means cyclically advanced or delayed timings of the

maxima (or minima), due to the motion around common barycentre.

The drawback of timing is the need of long-term monitoring, which imposes to collect data for many years. Anyway this technique is somewhat complementary to the radial velocity and transit methods, since these methods can hardly provide information on stars with small radii and hardly detect planets in wide orbits and relatively low masses (down to $\sim M_{Jup}$).

The targets of EXOTIME (see Table 2.1) were selected following different criteria. At first, known binaries and stars with an IR excess from the 2MASS data were excluded . It is also important the stability of the spectra in terms of phases and amplitudes, moreover the spectra should be not very rich of frequencies, ideally with only 2 or 3 main components. In fact a low number of frequencies allows to resolve the frequency spectrum even in short runs while, on the same time, it gives the opportunity to obtain independent O-C plots from each individual frequency. Finally the higher piority is give to bright targets, high pulsation amplitudes and high observability, considering that the available telescopes are mostly in the northern emisphere.

Object name	ref.	B mag	Main Period [s]	Amplitude [mma]
HS 0444+0458 (V1636 Ori)	a	15.2	∼137	∼11
HS 0702+6043 (DW Lyn)⋆	b	14.7	∼360	∼22
EC 09582-1137	c	15	∼136 ∼151	∼8 ∼7
PG 1325+101 (QQ Vir)	d	13.8	∼138	∼26
HS 2201+2610 (V391 Peg)⋆	e	14.3	∼350	∼10

Table 2.1: Targets of the EXOTIME program. References: (a) Østensen et al. 2001b [124]; (b) Dreizler et al. 2002 [66]; (c) Kilkenny et al. 2006 [97]; (d) Silvotti et al. 2002 [141]; (e) Østensen et al. 2001a [125]. ⋆ Hybrid pulsators.

Since 2008 the EXOTIME collaboration collected a large amount of data from several observing sites covering the longitude range between Eastern Europe to Western North America, equipped with telescopes having typical apertures of 1-2 meters (up to 4 m). The observations are performed in B filter and, according to the pulsation period of the target and the magnitude, the time sampling is set to obtain at least 5-6 points per cycle. Because of the different characteristics of the instruments, it is necessary to weight the incoming data in order to obtain a coherent data set. The list of the observations performed during the first two years of EXOTIME is available from a dedicated web site (*www.na.astro.it/∼silvotti/exotime/*). The web site provides informations on the target stars, observing instructions and scheduled observations, useful to optimize the planning of the observations, and the coverage of the targets.

The EXOTIME program carries on with its activity of collecting data for each target

star. Preliminary analysis of HS 0702+6043 and HS 0444+0458 are available in Schuh et al. 2010 [138], while an updated phase analysis including the new data on V391 Peg will be performed in the next months. The data set collected up to now on EC 09582-1137 is still too poor for its goals. In the next Chapters the contribution of our group to this project will be presented: the data collection, reduction and frequencies extraction of HS0207+6043, and then the preliminary analysis of PG1325+101 (QQ Vir) using part of the available data, also presented in Benatti et al 2010 [24].

2.3 Space-based observations

Only Space-based observations can provide uninterrupted photometric time series and thus avoid sidelobes in stellar oscillation power spectra. Photometric observations from the ground are performed for fainter stars that show higher pulsation amplitudes, such as Subdwarf B stars or even White Dwarfs. However the collection of data from a single site on the ground does't allow a continuous monitoring, producing data strongly affected by aliasing. Only with a world network this effect can be reduced, even if not always erased. The only way to obtain uninterrupted time series is to go to space.

2.3.1 MOST: Microvariability and Oscillations of STars

The Canadian *Microvariability & Oscillations of STars* space mission is the first satellite launched with the aim to search for stellar oscillations. MOST was launched on June 2003 and a full description is provided by Walker et al. (2003) [153]. It is a photometric microsatellite designed to perform ultra-high-precision photometry in order to detect low-degree acoustic oscillations (periods of minutes) with micromagnitude precision in solar-type stars and metal-poor subdwarfs. Other objectives are the detection of the light reflected from giant, short-period, extrasolar planets and the oscillations of roAp stars and the turbulent variability in the dense winds of Wolf-Rayet stars. Figure (2.13) shows a picture of MOST. The satellite is equipped with an optical Telescope with a collecting mirror with aperture of only 15 cm, feeding a CCD camera with twin frame-transfer devices side-by-side. One CCD is used for science measurements; the other is read out every second to track guide stars for satellite attitude control. The Instrument contains a single broadband filter which selects light in the wavelength range 350 - 700 nm. The camera is equipped with an array of Fabry microlenses which project a large stable image of the Telescope pupil illuminated by target starlight, which is key to the photometric precision of MOST. For low cost and high reliability, the Instrument has no moving parts - the structure automatically maintains the same focus across a wide range of temperatures, and exposure times are controlled by rapid frame transfer of the CCDs. The CCDs are cooled by a passive radiator system. The Instrument is housed in a suitcase-sized microsatellite ($65 \times 65 \times 30$ cm; mass ~ 60 kg) powered by solar panels and oriented by a system of miniature reaction wheels and magneto- torquers. The attitude control system should keep the Telescope pointing within 10 arcseconds of the desired target 99% of the time. This is an improvement of two orders of magnitude over previous micro-satellite pointing capability. MOST was injected into a low-Earth polar orbit (period ~ 100 min) in a Sun-synchronous mode. It will have a Continuous Viewing Zone (CVZ) spanning declinations from about -19 to +36 degrees, in which a selected target star will remain observable for up to 60 days without interruption.

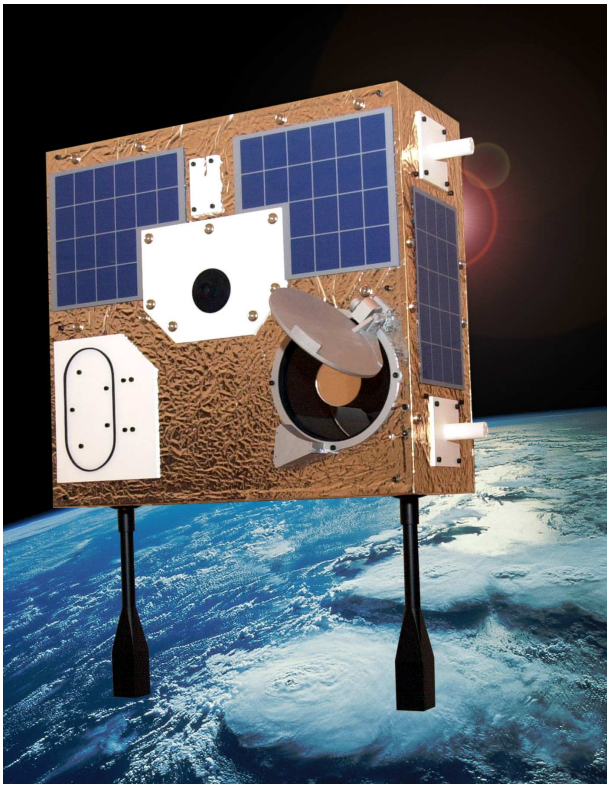

Figure 2.13: Model of the micro-satellite MOST.

MOST observations have significantly detected solar-like oscillations in red giants (Barban et al. 2007 [10]; Kallinger et al. 2008 [93]), clarified the pulsational properties of B stars, discovering the new type of variables slowly pulsating B supergiants (SPBsg) (e.g. Saio et al. 2006 [135]). Miller-Ricci et al. 2008 [120] measured transit times for the HD 209458 planetary system. Furthermore the deviations from a constant orbital period indicate the presence of additional planets in the system still undetected. Before the era of CoRoT and Kepler the MOST data sets of represent unprecedented time coverage with nearly continuous observations.

The most famous and controversal result of MOST was anyway the claim of the null detection of solar-like oscillations in Procyon (Matthews et al. 2004 [114]). According to Matthews et al. 2004 [114], the hump in the power spectrum of the ground-based detections (e.g. in Martic et al. 1999 [111]) was only an artefact, as result of the daily gaps. That conclusions have been questioned by Bedding et al. 2005 [19], that addressed the lack of detection to the high level of instrumental noise of MOST. Furthermore, Bedding et al. 2005 [19] demonstrate, via simulations, that the signal due to the daily gaps, or to any other noise source, cannot turn into a excess of power. Finally they found indeed, after a deeper analysis, a distribution of peaks in the MOST amplitude spectrum, consistent with the presence of oscillations at the expected level of Procyon. This guess was then confirmed at that time by Regulo and Roca Cortés 2005 [131], and now the presence of solar-like oscillations in Procyon find full confirm with the results of global network presented by Arentoft et al. 2008 [7] and Bedding et al. 2010 [21].

A new release of Procyon data was presented in 2008 by Guenther et al. [81], showing an

amplitude spectrum with some evidence for p-mode signal: excess power centred near 1000 μHz and an autocorrelation signal near 55 μHz, but the analysis of the echelle diagram still doesn't show regularly spaced frequencies aligned in common l-valued ridges. This study was also supported by three-dimensional numerical models of convection by the Yale group. These models show that, unlike in the Sun, Procyon's granulation signal in luminosity has a peak coinciding with the expected frequency region for p-modes near 1000 μHz. The direct comparison of the two simultaneous data sets will almost certainly reveal even more insights into the nature of Sun-like stars.

2.3.2 CoRoT: Convection Rotation and planetary Transits

The ESA-COROT mission (Baglin et al 2000 [8]) is led by the French National Space Agency, CNES. It is a 27 cm aperture space telescope (see Figure (2.14)) designed to perform high-precision photometry for nearby stars, searching for stellar oscillations and planetary transits. The spacecraft was launched on 27 December 2006 from the Baikonur Cosmodrome in Kazakhstan, Russia.

Three observing programs are expected to be pursue:

- Focused on the internal hydrodynamic processes of stars in the main sequence evolution stage and around it, the seismology central program studies in details the variations of the luminous flux emitted by a small number (50) of stars brighter than magnitude 9. The associated observing runs last 150 days, which provides a resolution of 0.1 μHz in the Fourier space. This frequency resolution is necessary to discriminate a significant number of modes, to reveal the frequency splittings and to rebuild the line profiles.

- The purpose of the exploratory program is to observe a wide variety of stars (from B to K spectral types) up to magnitude 9, where the Hertzsprung & Russel (HR) diagram is scanned. This will be accomplished by inserting a 20-day observing run between two long runs of the central program. With this shorter time window, the resolution on the frequencies falls to 0.6 μHz, but it is sufficient to produce statistical data about the excitation of the oscillating modes, as a function of mass, age, rotation speed and metallicity.

- The planet finding program consists in observing, in a systematic way, fields of 12 000 stars. The observing runs of 150 days allow to detect with complete confidence telluric planets with a revolution period lower than 50 days (transit repeated). The short observing runs will be an opportunity to harvest many hot Jupiters, making statistics consolidated.

As already mentioned, CoRoT is discovering planets using the method of the transits. According to existence hypotheses, the Corot mission is supposed to discover, in addition to a large number of giants (hot Jupiters), a few tens of rocky planets (exoEarths). Potential rings or satellites could also be detected around giant extrasolar planets. The chromatric analysis of the Corot light curves, thanks to a dispersion device (prism) mounted in front of the exoplanet channel CCDs, will make it possible to precise the different families of detected events (transits, stellar activity, eclipsing binaries...).

About 120,000 stars, with magnitude between 12 and 15.5, will be surveyed during the 5.5 years (after the extension of 3 further years) of mission lifetime.

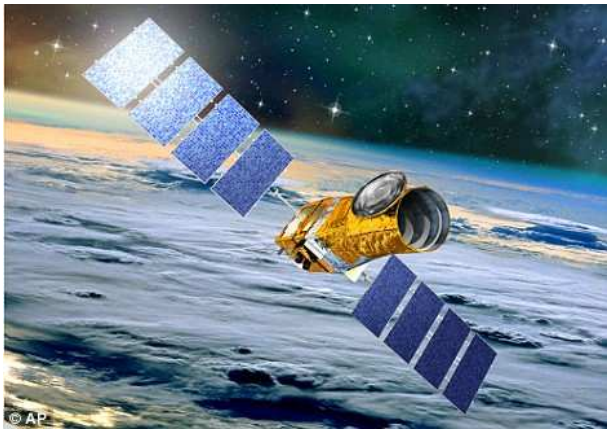

Figure 2.14: Model of the satellite ESA-CoRoT.

The detectors are 4 CCD's 2048 × 2048 wide, (EEV, 13.5-μm thinned, back illuminated), installed in the focal box, working in the visible. For the seismology mission, the image spot for a star is spread out on about 400 pixels, with an exposure time of 1 second. A prism is installed before the exoplanet field, allowing to get a coloured image of the star. It will enable to distinguish between stellar activities and a planetary transit, for the brightest stars. The afocal telescope is at first constituted of two parabolic mirrors allowing to decrease 3 times the equivalent entry pupil diameter, then 6 dioptric lens allowing to have a 1.2 m focal length. The field of view is a square of $2.8° \times 2.8°$, half for the seismology mission, the other half for the exoplanet mission.

COROT is in a circular polar orbit around the Earth at an altitude of 896 km. The telescope is pointed to observe within a cone of 10° from the perpendicular to the orbit. This ensures there is no Earth occultations to hinder the observations.

Up to now CoRoT detected 17 extrasolar planets. In 2007 COROT-1b and COROT-2b were found to be Hot Jupiters. Barge et al. 2008 [12] report the detection of the first planet discovered by CoRoT (orbiting with a period of 1.5 days), characterizing it with the help of follow-up observations, estimating radius and mass of the planet 1.49 ± 0.08 R_{Jup} and 1.03 ± 0.12 M_{Jup}, showing thus a particularly low mean density of 0.38 ± 0.05 g/cm^3. The discovery and characterization of COROT 2-b, orbiting with a period of 1.743 days, was reported by Alonso 2008 [6] and Bouchy 2008 [31]. They found a radius of 1.465 ± 0.029 R_{Jup} and a mass of 3.31 ± 0.16 M_{Jup}, corresponding to a density of 1.31 ± 0.04 g/cm^3. The large radius of CoRoT-Exo-2b cannot be explained by current models of evolution of irradiated planets.

In February 2009, COROT-7b was announced (Léger et al. 2009 [108], Rouan et al. 2010 rouan10). It is the smallest exoplanet to have its diameter confirmed at 1.7 Earth's diameter. The measured mass is 4.8 $M_\oplus$, and thus of its density which is equal to that of Earth, suggesting a similar composition dominated by silicates. The orbital period was found to be $0.85359 \pm 3 \times 10^{-5}$ day. Lastly, it is shown that a second planet, of only twice the mass of CoRoT-7b, is found on a slightly larger orbit, but still extremely close to the star.

On the point of view of asteroseismological analysis CoRoT provides high precision photometric light curves, that allow to detect stellar oscillations for several stellar classes. A study of the solar-like star HD 49385 and the spectroscopic characterization was performed

by Deheuvels et al. 2010 [63]. The seismic analysis of the star leads to a clear identification of the modes for degrees $l = 0, 1, 2$. Around the maximum of the signal ($\nu_{max} \simeq 1013\mu$Hz). Significant peaks are found outside the identified ridges and are fitted. They are attributed to mixed modes.

CoRoT is providing also useful data for the study of the pulsational behavior of red-giant stars (e.g. De Ridder et al. 2009 [61]) and thanks to the asteroseismic observable Kallinger et al. 2010 [94] and Mosser et al. 2010 [122] obtain very strong constraints to the stellar fundamental parameters of a sample of red giant stars in the CoRoT seismo-field.

2.3.3 Kepler

A very large amount of extrasolar planets have been discovered so far, more than 500. Most of them are giant planets, with masses of the order of Jupiter or Neptune. The challenge now is to find terrestrial planets, especially those in the habitable zone of their stars where liquid water and possibly life might exist. The NASA-Kepler Mission (Borucky et al. 2009 [29]), is designed to survey our region of the Milky Way to discover hundreds of Earth-size and smaller planets in or near the habitable zone and determine how many of the billions of stars in our galaxy have such planets. Results from this mission will allow us to place our solar system within the continuum of planetary systems in the Galaxy.

The scientific objective of the Kepler Mission is to explore the structure and diversity of planetary systems. This is achieved by surveying a large sample of stars (see a picture of the field of view in Figure (2.15)) to:

- Determine the percentage of terrestrial and larger planets there are in or near the habitable zone of a wide variety of stars;
- Determine the distribution of sizes and shapes of the orbits of these planets;
- Estimate how many planets there are in multiple-star systems;
- Determine the variety of orbit sizes and planet reflectivities, sizes, masses and densities of short-period giant planets;
- Identify additional members of each discovered planetary system using other techniques;
- Determine the properties of those stars that harbor planetary systems.

For a planet to transit, as seen from our solar system, the orbit must be lined up edgewise to us. The probability for an orbit to be properly aligned is equal to the diameter of the star divided by the diameter of the orbit. This is 0.5% for a planet in an Earth-like orbit about a solar-like star. (For the giant planets discovered in four-day orbits, the alignment probability is more like 10%.) In order to detect many planets one can not just look at a few stars for transits or even a few hundred. One must look at thousands of stars, even if Earth-like planets are common. If they are rare, then one needs to look at many thousands to find even a few. Kepler looks at 100,000 stars so that if Earths are rare, a null or near null result would still be significant. If Earth-size planets are common then Kepler should detect hundreds of them.

The Kepler instrument is a specially designed 0.95-meter diameter telescope called a photometer or light meter (see Figure (2.16)). It has a very large field of view for an astronomical telescope (105 square degrees), in order to observe the necessary large

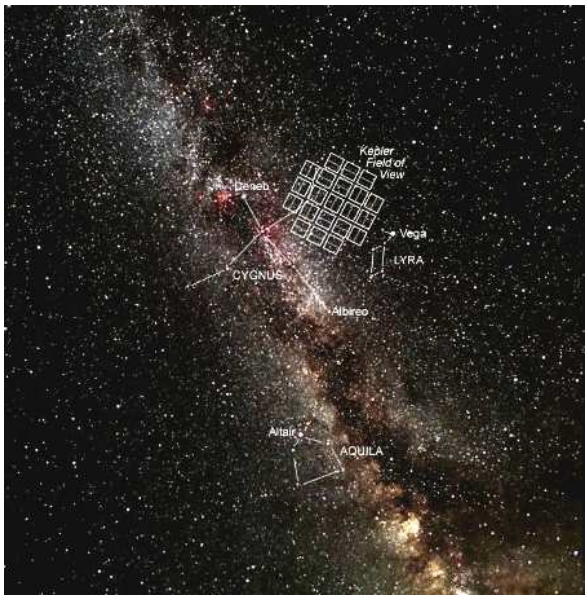

Figure 2.15: Field of view of the NASA-Kepler satellite.

number of stars. It stares at the same star field for the entire mission and continuously and simultaneously monitors the brightnesses of more than 100,000 stars for the life of the mission, 3.5 years.

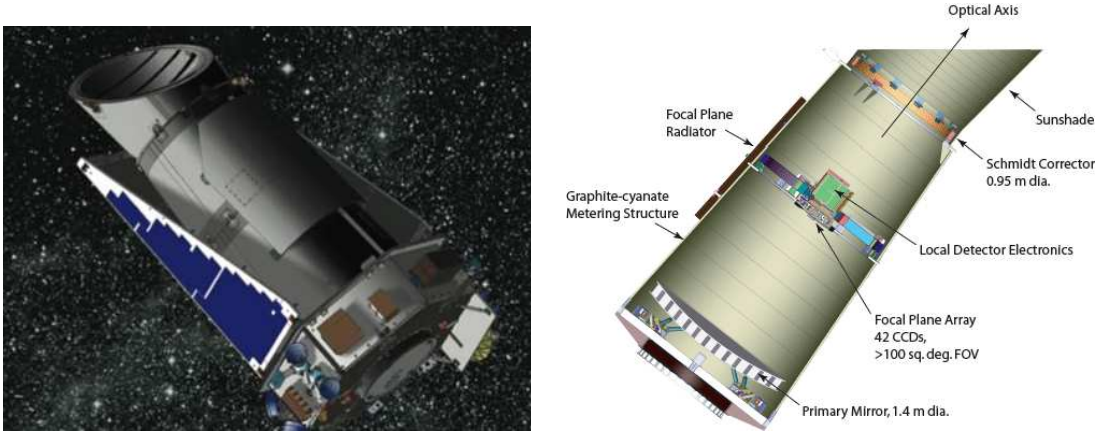

Figure 2.16: *Left panel:* Model of the Kepler satellite. *Right panel:* Optics of the telescope.

The diameter of the telescope needs to be large enough to reduce the noise from photon counting statistics, so that it can measure the small change in brightness of an Earth-like transit. The design of the entire system is such that the combine differential photometric precision over a 6.5 hour integration is less than 20 ppm (one-sigma) for a 12th magnitude solar-like star including an assumed stellar variability of 10 ppm. This is a conservative, worse-case assumption of a grazing transit. A central transit of the Earth crossing the Sun lasts 13 hours. And about 75% of the stars older than 1 Gyr are less variable then the Sun on the time scale of a transit. The photometer must be spacebased to obtain the photometric

precision needed to reliably see an Earth-like transit and to avoid interruptions caused by day-night cycles, seasonal cycles and atmospheric perturbations, such as, extinction associated with ground-based observing. Extending the mission beyond three and one half years provides for improving the signal to noise by combining more transits to permit detection of smaller planets; finding planets in orbits with larger periods; finding planets around stars that are noisier either due to being fainter or having more variability.

Based on the mission described above, including conservative assumptions about detection criteria, stellar variability, taking into account only orbits with 4 transits in 3.5 years, etc., and assuming that planets are common around other stars like our Sun, then we expect to detect:

- From transits of terrestrial planets in one year orbits:
  - About 50 planets if most are the same size as Earth ($\sim$1.0 $R_\oplus$) and none larger;
  - About 185 planets if most have a size of $\sim$1.3 $R_\oplus$;
  - About 640 planets if most have a size of $\sim$2.2 $R_\oplus$;
  - About 12% with two or more planets per system.

- From modulation of the reflected light from giant inner planets:
  - About 870 planets with periods less than one week.

- From transits of giant planets:
  - About 135 inner-orbit planet detections;
  - Densities for 35 inner-orbit planets
  - About 30 outer-orbit planet detections.

  Detection of the short-period giant planets should occur within the first several months of the mission. The sample size of stars for this mission is large enough to capture the richness of the unexpected. Should no detection be made, a null result would still be very significant.

Up to now Kepler has found 9 confirmed planets and over 700 planet candidates (source: official website). No ground-based follow up observations have been performed so far to confirm or reject the transiting planet interpretation. In particular five candidate exoplanetary systems were found through different methods, discussed by (Steffen et al. 2010 [145]) as well as false-positive rejection methods.

The requirements for planet transit detection also make the Kepler mission very suited for Asteroseismology. The photometric precision is similar to that required by Asteroseismology and the large field of view ensures a huge number of interesting targets (solar-like and other types of pulsators) to be available. Furthermore, the two different cadences of observations allow to detect both short scale (p-modes) and long scale periodicities (g-modes). The sampling is of about one minute for the short cadence data and about 30 minutes for long cadence.

Now, after the first two years of operations, Kepler data demonstrate that the early prospects were really promising: the extraction of individual oscillation frequencies, amplitudes, phases and mode life-times can be used to interact with theoretical stellar models to measure accurate stellar parameters (mass, radius, age, luminosity, effective temperature, rotation) and to test the details of the physics of the stellar interiors.

The *Kepler Asteroseismic Science Consortium* (KASC) collects 13 Working Groups, each dedicated to a particular pulsating class. Their activities are self-organized in order to handle the raw data incoming from the satellite, to perform the seismic anaysis of the targets and to write papers. The KASC WG are:

- WG1: Solar-like p-mode Oscillations;
- WG2: Oscillations in Clusters;
- WG3: Beta Cephei Stars;
- WG4: Delta Scuti stars;
- WG5: roAp stars;
- WG6: Slowly Pulsating B-stars;
- WG7: Cepheids;
- WG8: Red Giants;
- WG9: Pulsations in binary and multiple stars;
- WG10: Gamma Doradus stars;
- WG11: Compact pulsators;
- WG12: Miras and Semiregulars;
- WG13: RR Lyrae stars.

The KASC WGs produced so far a lot papers with preliminary or full analysis of the most interesting targets. Three solar-like stars were first analysed by Chaplin et al. 2010 [37], after the first 33 days of observations, showing clear evidence of solar-like oscillations (see Figure(2.17)) and frequency spacings. A deeper investigation of one of them, supported by the comparison of several theoretical models, was report by Metcalfe et al. 2010 [117].

Bedding et al. 2010 [17] and Huber et al. 2010 [91] presented the analysis of the pulsational behavior of red giant stars, while Østensen et al. 2010 [126] reported first results on compact pulsators. A first characterization of the variable behaviour of the large sample of A-F stars is then in preparation by Uytterhoeven et al., a coordinated work between WG4 (δ Sct) and WG10 (γ Dor).

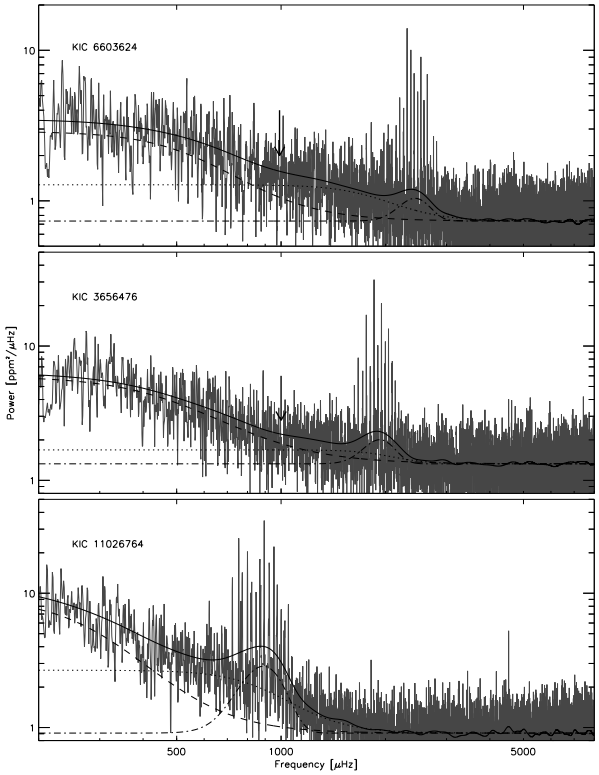

Figure 2.17: Power spectra of the three Kepler targets analysed by Chaplin et al. 2010 [37] (plotted on a logarithmic scale). A series of fits were calculated in order to estimate: smoothed power spectra (continuous black lines); power envelope due to oscillations (dot-dashed); faculae (dotted) and granulation (dashed). Finally the arrows indicate a change in the slope of the background due to the facular components.

Chapter 3

PLATO: a feasibility study

Part of this thesis is focused on the preliminary study of PLATO satellite [36], the next generation planet-finder. This is the reason why we dedicated a few Sections of this Chapter to introduce the main features of this mission, namely the science case, the scientific requirements, the stellar sample and the payload. After that we discuss about our analysis of simulated images in order to evaluate the quality of the preliminary optical design. We also deal with the problem of the stellar crowding in the simulated fields, by evaluating the contaminating flux due to the brighter sources. Finally we present a tool useful to check if the stellar oscillations can be actually observed by PLATO, and to evaluate the impact of the stellar noise on the detection of a planetary transit.

3.1 PLATO - PLAnetary Transits and Oscillations of stars

The PLATO mission (Catala et al. 2008 [36]) was proposed in 2007 as a medium class candidate in response to the first call for missions of the European Space Agency *Cosmic Vision 2015-2025* program. The proposal was submitted by Dr. Claude Catala (Observatoire de Paris) on behalf of a large consortium of more than 150 scientists from laboratories all across Europe. Following favorable reviews by ESA's scientific advisory bodies, PLATO was selected in 2007 as one of the missions for which an assessment study has been carried out in 2008 and 2009 by ESA, supported by the PLATO Study Science Team (PSST). Its scientific objectives are to detect and characterize transiting exoplanetary systems of all kinds (including both the exoplanets and their host stars), in particular small, telluric planets in their habitable zones. PLATO will perform a detailed seismic analysis of the planet host stars, allowing a precise determination of their radii, masses and ages, from which the radii, masses and ages of the exoplanets will be derived. This will provide a complete characterization of the exoplanetary systems, including their evolutionary status, and enabling us to deduce the nature of the planetary bodies (e.g. ocean or rocky planets etc). These objects will be prized targets for future more detailed characterization, including the search for biomarkers in their atmospheres.

3.1.1 Science case

PLATO is the next generation planetary transit space mission; its objective is to characterize exoplanets and their host stars in the solar neighbourhood. While it builds on the heritage from CoRoT and Kepler, the major breakthrough to be achieved by PLATO will

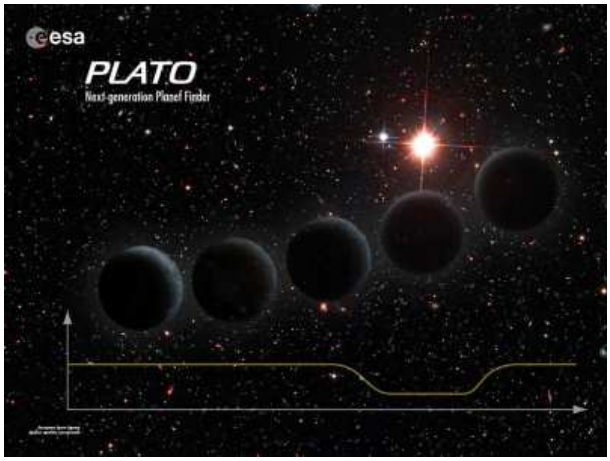

Figure 3.1: PLATO Mission.

come from its strong focus on bright targets, typically with $m_V \leq 11$. The PLATO targets will also include a large number of very bright and nearby stars, with $m_V \leq 8$. The prime science goals of PLATO are:

- the detection and characterization of exoplanetary systems of all kinds, including both the planets and their host stars, reaching down to small, terrestrial planets in the habitable zone;
- the identification of suitable targets for future, more detailed characterization, including a spectroscopic search for biomarkers in nearby habitable exoplanets.

These ambitious goals will be reached by ultra-high precision, long (few years), uninterrupted photometric monitoring in the visible band of very large samples of (pre-selected, low activity) bright stars, which can only be done from space. The resulting high quality light curves will be used on the one hand to detect planetary transits, as well as to measure their characteristics, and on the other hand to provide a seismic analysis of the host stars of the detected planets, from which precise measurements of their radii, masses, and ages will be derived. For the brightest targets, planets are also expected to be detectable through the modulation of stellar light reflected on the planet surface, and/or through the astrometric wobble induced on the star by the planet orbital motion. The PLATO space-based data will be complemented by ground-based follow-up observations, in particular very precise radial velocity monitoring, which will be used to confirm the planetary nature of the detected events and to measure the planet masses. The full set of parameters of the systems with detected exoplanets will thus be measured, including all characteristics of the host stars and their orbits, radii, masses, and ages of the planets. Measurements of the radii and masses will be used to derive the planet mean densities and therefore will give insight on their internal structure and composition. The orbital parameters, together with the precise knowledge of all characteristics of the host star, will enable us to estimate the temperature and radiation environment of the planets. Finally, the knowledge of the age of the exoplanetary systems will allow us to put them in an evolutionary perspective.

PLATO will address the basic question of the existence, distribution, evolutionary state, and characteristics of exoplanets in the solar neighbourhood. Answers to these questions are essential to understand how planetary systems, including our own, are formed and

evolve, and also as a first and necessary step to understand whether life can exist elsewhere in the Universe, and locate potential sites for life. Since the discovery of the first exoplanet in 1995, this field has seen a remarkable development, with about 400 exoplanets known as of the end of October 2009. Most of these objects are giant planets in close-in orbits, but continuous progress in the precision of radial velocity observations is now enabling the detection of *super-Earths*, with masses just a few times that of the Earth. Exoplanet discovery has been recently boosted with the launch of the CoRoT satellite in December 2006, followed by that of Kepler in March 2009. The discovery of CoRoT-7b, the very first small telluric, rocky planet with measured radius and mass, and therefore with a known density, has opened up a new era, in which the CoRoT extended mission and Kepler are now playing a major role. Both CoRoT and Kepler target rather faint stars, up to $m_V = 15$ and beyond. Their ground-based follow-up, in particular in radial velocity monitoring, is made difficult by this relative faintness. As a consequence, ground confirmation and mass measurements are restricted to the largest of the CoRoT and Kepler planets, which severely impacts the scientific return of these two missions. While it is possible today with CoRoT, and soon with NASA's Kepler mission, detect the passage of a planet the size of our own world, it is impossible to confirm the presence of such an object found by either spacecraft with the required precision. Moreover, even in cases where radial velocities can be measured to the required precision to confirm the planetary nature of the detected event and measure the planet-to-star mass ratio, our knowledge of the faint host stars is still too poor to allow us to derive estimates of the planet radii, masses and ages to a sufficient accuracy to significantly constrain their structure and state of evolution. The main goal of PLATO is to alleviate these severe difficulties by focusing on bright stars, typically 3 to 4 magnitudes brighter than CoRoT and Kepler, and also by including in its target list a large sample of very bright ($m_V \leq 8$) and nearby stars. This will bring three decisive advantages:

1. the ground-based follow-up observations will be greatly facilitated, and the required precision will be reached to confirm small, terrestrial planets in the habitable zone and to determine their masses;

2. the host stars of the detected planets will be studied in detail, in particular via seismic analysis using the PLATO data themselves; seismic analysis, i.e. the measurement of stellar oscillations, will be used to probe the internal structure of these stars, and determine their radii, masses, and ages in a precise and reliable way;

3. the detection of exoplanets orbiting very bright and nearby stars will allow us to identify the best targets for subsequent detailed follow-up observations, both from space (e.g. JWST) and from the ground (e.g. E-ELT), including in particular spectroscopy of their surfaces and atmospheres, in the search for biomarkers.

The scientific goals of PLATO will then be:

- The detection of extra-solar planetary systems of all kinds, including small, terrestrial planets in the habitable zone of solar-type stars. The understanding of how planetary systems form, evolve in time and eventually harbour suitable conditions on the planet surface for life to develop requires a detailed study of each of the mentioned stages, for the different types of low-mass planets. It is thus extremely important to pave the planet physical parameter space, from giant planets down to Earth twins, in a statistically significant way. Although challenged by transit probability and by

the difficulty of the radial velocity follow-up, PLATO will follow a sufficiently large number of bright stars to achieve this goal. As a by-product, PLATO will also consolidate with actually confirmed planets the occurrence frequency of potentially habitable worlds around solar-type stars.

- A precise characterization of the basic physical parameters of the detected exoplanets and the host stars: radius, mass, age. While the actual principles of the determination of the parameters of both planets and stars have been carried out for gaseous giant transiting planets, they have been verified for the first time for a super-Earth with CoRoT. PLATO will mark the beginning of detailed science on exoplanets. The perspective of 'true' comparative planetology, i.e. when one begins to compare different planetary systems with a precision in the determination of physical parameters of order 1-2%, coupled with age determinations with a precision of about 200-300 million years, will allow (for the first time) evolutionary sequences for planets to be put together. In order to achieve this, the basic requirements are light curves measured with very high photometric precision, with a high cadence and a very high duty cycle. Further it is necessary to measure very large numbers of bright stars, in order to have enough transiting planets of different types, ages and stellar primaries, with full physical parameter characterization. PLATO will reach these goals taking the results to an unprecedented level.

- The identification of suitable targets for future, more detailed characterization. In the past few years we have seen the first attempts to determine the atmospheric constitution of exoplanets. By determining the difference of the star spectra taken before/after and during the transit, a spectrum of the planet can be derived. While systematic effects in the data and the luminosity difference between the star and planet make this extraordinarily difficult to achieve, these studies have led to the first analysis of the planetary atmospheric constitution and height structure which can be compared directly with models.

3.1.2 Payload definition

The PLATO mission was subject to three independent studies, two by industrial contractors and one by the PLATO PayLoad Consortium (PPLC). All three studies have been running in parallel and were completed simultaneously at the end of summer, 2009. They results from these studies differ significantly from one another, but have in common optical designs with very wide fields-of-view, and overall large collecting areas. Wide fields-of-view are required to obtain large samples of bright stars, while large collecting areas are necessary to reach the desired photometric precision. In all three concepts, this is achieved by using a collection of small, optically fast, wide-field telescopes, each with its own CCD-based focal plane. The light and centroid curves from each individual telescope unit are transmitted to the ground at the required cadence, where they are co-added to reach the desired precision. In concept A, the chosen solution has 12 reflective telescopes with a field-of-view of about 1800 deg^2, and a total collecting area for each observed star of 0.15 m^2, while concept B is using 54 refractive telescopes with a field-of-view of 625 deg^2, and a total collecting area for each observed star of 0.29 m^2. Concept C proposes a different arrangement with 42 refractive telescopes. In the two first solutions, all telescopes are pointed in the same direction and are covering the same field. Concept C instead has the telescopes grouped in 4 sections, each section having its line of sight offset from the next one by one-half of

the field-of-view. This overlapping line-of-sight arrangement results in a total surveyed field of about 1800 deg^2, each star being observed either by 10, 20, or 40 telescopes, with a resulting collecting area of 0.12, 0.24, or 0.48 m^2, depending on the star's position in the field (See Figure (3.2)). All three designs are shown to be compliant with the science

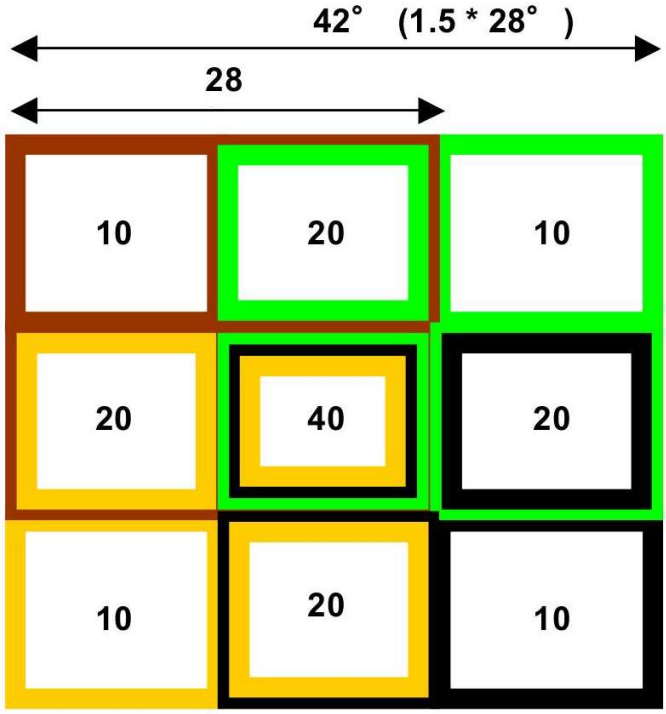

Figure 3.2: PLATO field of view according to the Optical Concept C.

requirements, and to be feasible. The reliability of the PLATO concept is supported by the fact that three viable optical solutions have been found, which can be traded off against one another before the start of the definition phase.

Concept C was developed by the Optical Group of the INAF - Astronomical Observatory of Padua (P.I. Prof. R. Ragazzoni). They realized the so called Telescope Optical Unit (TOU), which represents the single optical element of the configuration of 42 telescopes, divided in 40 *normal* telescopes and two *fast* telescopes, dedicated to the observations of brighter sources. The study of the TOUs includes the optical and mechanical designs, the analysis of suitable glasses, the straylight analysis and the study of baffling solutions, the thermo-mechanical analysis. There is no difference in the TOU design for normal and fast telescopes, but the latter will include broadband filters that will be studied in a subsequent phase. The TOU optical design consists of 6 lenses with 2 aspheric surfaces of radiation hardened glasses. The Entrance Pupil Diameter is 120 mm and the f number is 2.06 at 700 nm. A simulated image of how the TOU would appear is presented in Figure (3.3), while Figure (3.4) shows the configuration of the payload with the ensemble of 42 single telescopes.

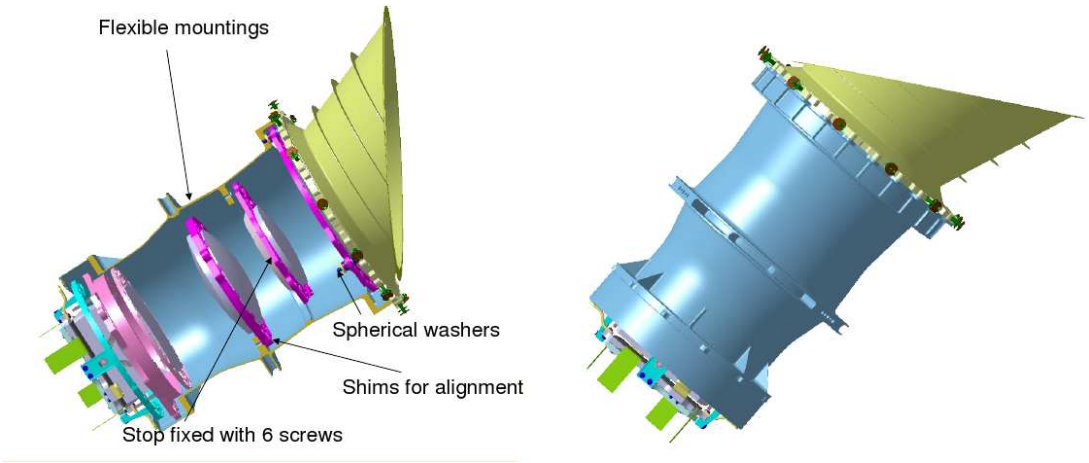

Figure 3.3: *Left panel:* mounting of the optical elements of a single Telescope Optical Unit. *Right panel:* telescope tube of TOU.

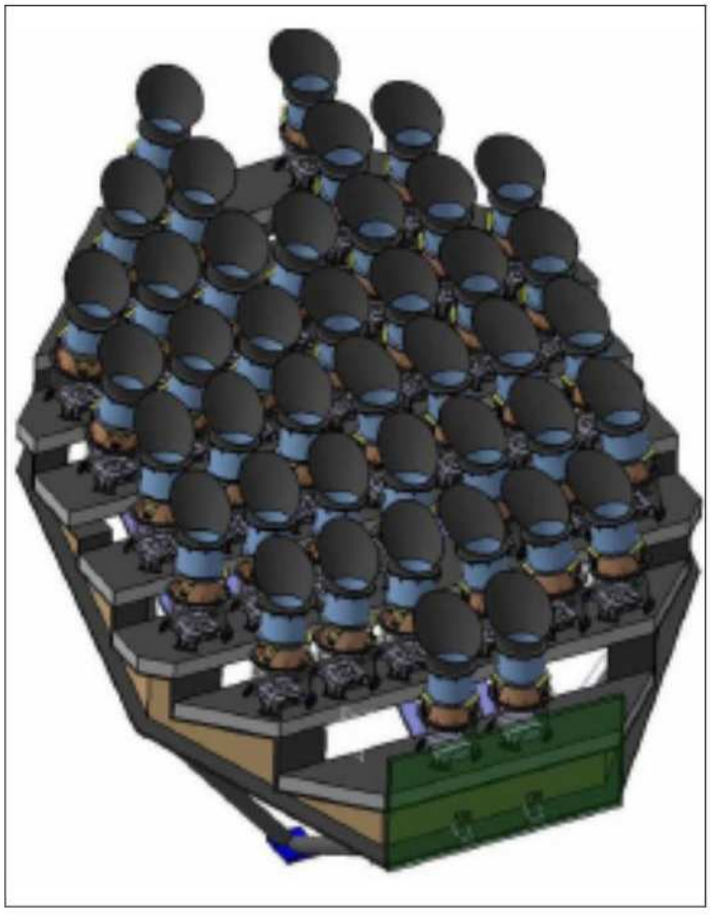

Figure 3.4: PLATO payload according to the Optical Concept C.

3.1.3 Scientific requirements

Required noise levels and monitoring durations

The depth of a planetary transit is given by the ratio of the areas of the planet and its transited star, which is of the order of $\Delta Fstar$ / $Fstar \sim 10^4$ in the case of Sun-Earth analogs, while transit durations are typically of the order of 12 hours. In order to detect such transits at more than 4σ, a dimensioning requirement, it is necessary to obtain a photometric noise level lower than about 2.5×10^5 in 12 hours, i.e. about 80 part per million [ppm] in one hour. This is the minimum requirement for the detection of an Earth-like planet in front of a solar-like star. However, the measurement of several points across the transits will be necessary, implying lower levels of noise. In practice, a minimum of 8 to 9 points across the transit are necessary to characterize its shape, in particular the ingress and the egress parts. The requirements are therefore a photometric noise level below 27 ppm in one hour, for the highest priority star sample of the mission. Recent results from CoRoT have shown that detecting, measuring and identifying oscillation modes in solar- type stars requires a noise level in amplitude Fourier space below about 1.6 ppm per $(\mu\text{Hz})^{1/2}$ (Michel et al. 2008 [118], Deheuvels et al. 2010 [63], Garcia et al. 2009 [71]), which is equivalent to 2.5 ppm in 5 days, or 1 ppm in 1 month, and which translates approximately into a noise level of 27 ppm in 1 hr, i.e. similar to that for the detection and characterization of Earth-like transits. The duration of the observations needs to be longer than 2 (goal 3) years, so that at least 2 (goal 3) consecutive transits for Sun-Earth analogs can be detected. For the seismic analysis of the target stars, the total monitoring time must be sufficient to yield a relative precision of 10^4 for the measurement of individual mode frequencies, which is needed to perform the inversion of the oscillation spectra. For solar-type stars, this comes down to an absolute precision of 0.2 to 0.1 μHz, which translates into a minimum monitoring time of 5 months for a reasonable S/N of 10 in the power spectrum.

Stellar samples and photometric noise level

Five complementary stellar samples were defined as targets of the PLATO mission.

1. Given the probability to detect planet transits, estimated to be about 0.1% (geometric probability x fraction of stars with planets), at least 20,000 cool dwarfs and subgiants need to be surveyed for a sufficient amount of time to detect long period orbits, i.e. typically for 2 to 3 years. This number of surveyed stars implies an expected number of telluric planets in the habitable zone of the order of 20, considered as the objective for PLATO. This would represent a very significant improvement compared to Kepler, considering in addition that such exoplanetary systems detected by PLATO would also be fully characterized. Additionally it is expect to detect many transits of larger planets around these stars. Therefore, more than 20,000 dwarfs and subgiants later than spectral type F5, with a noise level below 27 ppm in 1 hr, must be observed with the required duty cycle for more than 2 years. This sample, with m_V typically between 8 and 11 is considered as the highest priority objective.

2. Some of the targets can be observed at a noise level enabling the detection of small exoplanets, significantly below 80 ppm in 1 hr (Earth-size). This strategy defines a second, more numerous, star sample, for which planet detection and seismic analysis

can potentially be achieved in different phases of the mission. These objects will typically be between 11 and 13 in m_V.

3. The search for planetary transits around very bright and nearby stars presents a specific interest, as these sources will become privileged targets for further ground- and space-based observations. We therefore request the monitoring of a large number of very bright stars with the goal of detecting a few telluric planets in their habitable zone. Hence, more than 1,000 dwarfs and subgiants later than spectral type F5 and brighter than $m_V = 8$ must be monitored with a noise level below 27 ppm in 1 hr, with the required duty cycle for more than 2 years.

4. The detection of an even larger number of short period planets around such very bright stars will also be used as input for further instruments aimed at characterizing the planetary atmospheres. Hence, more than 3,000 dwarfs and subgiants later than spectral type F5 and brighter than $m_V = 8$ must be monitored with a noise level below 27 ppm in 1 hr, with the required duty cycle for more than 5 months.

5. Finally, the observation of very large number of stars with the required precision to detect telluric planets around solar-type stars, i.e. 80 ppm in 1 hr, but without seismic analysis. They will be more than 250,000 dwarfs and subgiants later than spectral type F5, with a noise level below 80 ppm in 1 hr, with $m_V = 8$ typically between 8 and 13-14, must be observed with the required duty cycle for more than 2 years.

Duration of monitoring and time sampling

The total duration of the monitoring of the first and second fields must be longer than 2 years. The step and stare phase at the end of the mission must have a duration of at least 1 year. During this phase, previously monitored fields, as well as additional fields, will be surveyed for at least 2 months and up to 5 months each. In addition, further visits of the previously surveyed fields will be organized in an optimized way to study long period exoplanets (several years), and will possibly occur at any time during the step and stare phase. The duration Δt of a transit of a planet with semi-major axis a and orbital period P in front of a star with radius R_{star} is given by:

$$\Delta t = \frac{P R_{star}}{a/\pi}. \tag{3.1}$$

For true Earth analogs $\Delta t = 13$ hours. Planets in the habitable zone, however, will cause transits lasting between five hours (around M stars) and 15 hours (for F stars), for equatorial transits. Because individual transits have durations longer than 2 hours, a time sampling of about 10 to 15 minutes is in principle sufficient to detect all types of transits, as well as to measure transit durations and periods. However, a higher time resolution is needed in order to accurately time ingress and egress of the planet transits for which the S/N in the light curve will be sufficient. The accurate timing will allow the detection of third bodies, which cause offsets in transit times of a few seconds to about a minute, and will allow to solve ambiguities among possible transit configurations through the determination of ingress and egress time of the planet. In practice, a time sampling of about 50 sec will be necessary to analyze in such detail the detected transits. The needed time sampling for the asteroseismology objectives can be derived directly from the frequency

interval needed to explore, which is from 0.02 to 10 mHz. In order to reach 10 mHz, the time sampling must correspond to at least twice this frequency, i.e. of the order of 50 sec.

Overall duty cycle

The probability that N transits of the same planet are observed is given by $p_N = {d_f}^N$, where d_f is the fractional duty cycle of the instrument. In order to achieve an 80% probability that all transits of a three-transit sequence are observed, a duty cycle of 93% is needed, ignoring gaps that are much shorter than individual transits. The requirement for planet-finding is therefore that gaps which are longer than a few tens of minutes do not occur over more than 7% of the time, with a loss by gaps as small as 5% being desirable. A similar requirement is also imposed for seismology. Gaps in the data produce sidelobes in the power spectrum, which make mode identification ambiguous. Periodic gaps in the data must be minimized, as they will produce the most severe sidelobes in the power spectra. It can be shown that periodic outages representing 5% of the total time produce aliases with a power of about 1.5% of that of the real signal. Such sidelobes are just acceptable, as they will remain within the noise for most of the stars observed. It is therefore required that periodic data gaps are below 5%. Non-periodic interruptions have a less problematic influence on the power spectrum, and can therefore be tolerated at a higher level, provided the time lost is compensated by a longer elapsed time for the observation. Random gaps in the data representing a total of 10% of the monitoring time yield sidelobes with a power lower than 1% of that of the real signal, which will be adequate for this mission. The requirement on random data gaps is therefore that they do not exceed 10% of the elapsed time.

3.1.4 Mission Scenario

The current mission scenario is to launch PLATO using a Soyuz 2-1b launcher, which will inject the spacecraft in a direct transfer orbit around the Sun-Earth second Lagrange point, L2, with a transfer orbit inclination of 5.3 degrees. The orbit, selected for maximising spacecraft mass (less delta-v required and hence less propellant) is a large amplitude libration orbit with 500.000 km and 400.000 km axes. L2 was chosen for its stable ambient environment in terms of temperature, radiation, possibility to have eclipse-free orbits and un-obstructed view of large parts of the sky (Sun, Earth, moon are all located in a relatively small solid angle). The mission is foreseen to have a nominal lifetime of 6 years, which is divided into three different phases. The first two phases are used for long-duration observations, each observation focusing on a particular part of the sky which is expected to contain a high density of cool dwarfs. These sky fields are assumed to be around ecliptic longitude and latitude of 210° and -60° respectively, which is close to the galactic plane. The duration of each of these observations is several years, in order to repeatedly observe transits with orbital periods similar to the Earth. This is necessary to reduce the likelihood of flagging false transits because there can be other reasons for detection of changes in the stars brightness, either naturally occurring in the star, the stellar environment (e.g. background objects), or artificially induced in the spacecraft payload. The last phase will be a step & stare phase where several different fields with interesting scientific targets will be monitored for a period of several months each. The exact duration of each phase will be consolidated in the following phase, should PLATO be selected. The long-duration periods will be between 2-3 years with the possibility to have one long-duration observation of 3

years and the second of 2 years. The step&stare-phase will be at least one year long.

3.1.5 PLATO Consortia

Two Consortia were created to organize and perform the feasibility study of PLATO: the PLATO Payload Consortium and the PLATO Science Preparation Management. A general Council was also created to allow a connection between the two groups.

The **PLATO Consortium Council** is composed by:
C. Aerts (Belgium)
C. Catala, M. Deleuil (France)
J. Christensen-Dalsgaard (Denmark)
M. Mas, H. Deeg (Spain)
G. Piotto, S. Desidera (Italy)
D. Pollacco, A. Smith (UK)
H. Rauer, A. Hatzes (Germany)
S. Udry, W. Benz (Switzerland)
W. Weiss (Austria)
I. Roxburgh (ESA/PSST)

PPLC : PLATO Payload Consortium:
PI: C. Catala, Co-Pi: M. Deleuil.

- System group
  Marseille: M. Deleuil (co-PI), P. Levacher (project manager), L. Hill ; Meudon: C. Catala (PI), G. Epstein (system engineer), R. Samadi, Ph. Plasson, A. Semery, C. Cara (CEA/Saclay)

- Telescopes
  Padova: R. Ragazzoni; Catania: I. Pagano

- Data processing
  Berlin: H. Rauer; Meudon: R. Samadi; Padova: A. Baruffolo; Leuven: C. Aerts

- Focal planes
  MSSL: D. Walton; Madrid: M. Mas

- Ground data centre
  Lindau: L. Gizon; Orsay: T. Appourchaux

PSPM: PLATO Science Preparation Management
The PSPM, coordinated by Heike Rauer (Institut für Planetenforschung - DLR) will take responsibility for organizing the European and international community around the scientific preparation of the mission. These activities, which are needed for an optimized scientific exploitation of the PLATO data, include the following elements:

- Exoplanet Science: Don Pollacco - Queens Univ. of Belfast
  The development of methods and algorithms for exoplanet science, such as algorithms for transit detection, planet parameters determination, light curve filtering by the characterization of stellar intrinsic 'noise', identification of false positives, etc.

- Stellar Science: Marie-Jo Goupil - Obs.de Paris
  The development of methods and algorithms related to the stellar physics programme, such as oscillation mode inversion techniques, production of grids of stellar evolution models involving new physical ingredients (rotation, internal waves, magnetic fields), etc.

- Target/Field Characterization: Giampaolo Piotto - Univ. of Padova
  The provision of all necessary data and information for the construction of the PLATO input catalogue.

- Follow-up Coordination: Stèphane Udry - Obs. de Genève
  The identification of the required follow-up facilities, including a world-wide effort obtaining in particular radial velocity observations to determine planet masses; preparation of the organization and coordination of follow-up observations.

- End-to-end simulations: Wolfgang Zima - Univ. of Leuven
  The development of the end-to-end PLATO data simulator, including realistic modelling of the stellar fields and of the expected behaviour of the targets and instrument.

- Additional Science: Werner Weiss - University of Vienna
  The coordination of additional science activities within PMC and the general community.

3.2 Simulations

3.2.1 Modelling space-based high precision photometry

According to the Work Packages defined by the PLATO Scientific council, the first step is the production of simulated images and their reduction in order to obtain simulated light curves. Once we have had these images we peroformed photometric analysis using our IDL procedures written on purpose. In order to understand which kind of data we handled, we briefly described how they were created.

The images were modeled thanks to a code developed by the Stellar Oscillations Group at the Aahrus University (Denmark, see De Ridder et al. 2006 [60]) and furhter adapted for the PLATO mission by Zima et al. 2010 [158]. The need of such a code during the feasibility study is to evaluate and to analyse all of the possible noise sources that affect space-based instruments like stray light and satellite pointing movements.

The formalism that has been used for this simulator was also used for other space mission such as MOST, CoRoT and Kepler, in order to:

- perform in advance an end-to-end analysis of the time series;

- verify the instrument design;

- optimize the observing strategy;

- design, test and verify the on-board and on-ground analysis software;

- optimize the target selection (both for space-based and ground-based observations);

- compute time series to learn more about the final expected time series;

- verify the scientific feasibility of an observing proposal (given the target, the duty cycle and the instrumental set up).

The formalism is divided into two main components: the former models time series of CCD images affected by all the instrumental effects, while the latter models stellar light curves of stochastically oscillating stars free from instrumental deterioration.

Time-series of CCD images

The modeling of CCD images of a space-based instrument has to take into account of a series of noise sources, that in this formalism are investigate and analysed. These contributions are mainly due to the noise from the sky, from the CCD and from the satellite itself.

The field of view image $I(x, y)$, where (x, y) are the pixel coordinates can be expressed as the sum of scaled point-spread functions (F_{PSF}) centred around the stellar coordinates (x_i, y_i), obtained with catalogues. It can be thus modeled as follow:

$$I(x, y) = \sum_i a_i F_{PSF}(x - x_i, y - y_i). \tag{3.2}$$

The normalized (F_{PSF}) was provided by the optical group of PLATO and includes all of the optical features. In Equation (3.2), a_i is a scaling coefficient that let the photon flux F_{phot} to be conserved. This flux is defined as:

$$F_{phot} = F_0 \times 10^{-0.4m} TA, \tag{3.3}$$

where F_0 is the photon flux per second for a star with $m = 0$, A is the effective collecting area and T is the effective transmission efficiency through the optical system and the detector. The fluxes are then evaluated with the exposure time and converted to ADUs, with an additional modeling that takes into account the quantum efficiency and the gain of the detector. The contribution from the sky background is due to the zodiacal light, faint unresolved stars, cosmic rays and so on. To model the first two components the formalism add a constant light flux to every pixel (useful also to produce possible stray light). The number of the collisions of high energy cosmic particles against the CCD per second and per pixel is found from a Poisson distribution around a mean value that varies randomly by 10% from image to image. The cosmic hits are randomly distributed over the entire CCD. Another important effect is the saturation of the pixels, when the full-well capacity is exceeded after an exposure and the extra-charge will flow to the neighbouring pixels in the readout direction to the first non saturated pixel.

The combination between the sensitivity variability of the detector and the pointing movements can produce significant photometric variations. It is therefore mandatory to simulate a flat-field image, in order to define sensivity variations not only on a pixel to pixel scale but also intra-pixel and over a larger parts of the CCD. The pixel to pixel variations are modelled with a random flat-field image I_{ran}, and the resulting flat-field image I_{FF} is given by:

$$I_{FF}(x, y) = \sum_{i=0}^{N} a_i I_{ran,i}(x, y) \tag{3.4}$$

where a_i is the amplitude of random image $I_{ran,i}$. It is important to note that even within the individual pixel the sensitivity is not constant but this effect cannot be removed only

with the flat-field calibration. To solve this problem the flat-field is constructed at high pixel resolution with white noise added to the sensitivity of the individual sub-pixels. The final high-resolution flat field is combined at a later stage with the stellar field-image in such a way that the satellite pointing variations causes the stars to move 'on top of' the flat-field map introducing the flat-field variations in the scientific data.

ACS jitter

In a space instrument perturbations are due to solar wind, magnetic fields or gravity gradient effects. But also the internal torques from thrusters, satellite spin and momentum or reaction wheels can produce slow motions of the optical axis of the telescope. The spacecraft movement, known as Attitude Control System (ACS) jitter, affects the photometric precision, therefore it is another important contribution to taking into account and to model. It is assumed that the ACS actuators act to correct a deviation exponentially on a time scale τ_{cor}, so that for a deviation Y_{yaw} at the time t_i is:

$$Y_{yaw}(t_i) = Y_{yaw}(t_{i-1})e^{-\Delta\tau/\tau_{cor}} + \epsilon(t_i) \tag{3.5}$$

where the time step $\Delta t = t_i - t_{i-1}$ is smaller than the correction time scale τ_{cor} and $\epsilon(t_i)$ is a normally distributed random variable that scales with $\sqrt{\delta}t$. In the end the data will be low-pass filtered with a smoothing function to model the acceleration limit of the satellite due to the inertia of the whole spacecraft.

CCD readout effects

In space instruments is preferable to avoid mounting of moving parts which are easily breakable. The shutter is one of these sensitive components, therefore the detectors are generally fast frame transfer, so that the CCD continuously detects photons, or they have a very fast readout. This can produce the star trailing in the readout direction, visible as vertical lines (as Figure (3.5)), adding supplementary structures in the sky backgroung. The investigation of this additional source of noise through this algorithm let us to define how fast the readout or the frame transfer should be in order to avoid excessive contamination of the data.

Also the charge-transfer efficiency (CTE) is an important parameter to take into account. It depends on the number n of crossed pixel, and for a fraction ϵ of charge that is not transferred, it is equal to a total fraction of charge of $1 - (1 - \epsilon)^n$ that leads to a smearing of the image.

3.3 Analysis of the simulated images

In order to test the photometric quality of the simulations obtained with the previously described code, a series of IDL procedures have been written and applied to the simulated images files provided by our collaborators (Dr. T. Arentoft and Dr. W. Zima). First of all two possible stellar fields have been tested, Carina and Hipparcos (provided by Dr. M. Barbieri) at different plate scales.

Different scenarios have been simulated and then automatically reduced with the mask photometry algorithm. For each given position of the PSF (at the centre or at a certain degrees far from it) and of the optical design, sets of 200 and 100 images were produced,

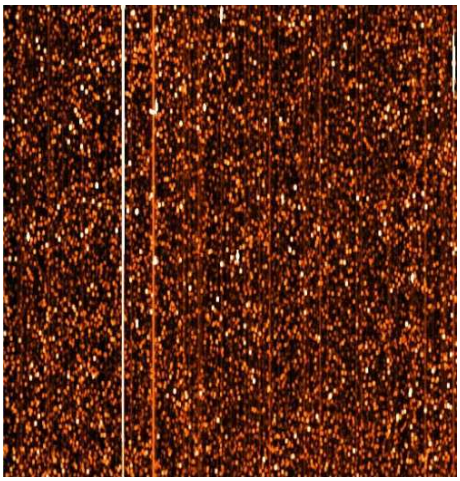

Figure 3.5: An example of the simulated image with the star trailing effect (from De Ridder et al. 2006 [60]).

with fields of 150 × 150 pixels in the three cases with pixel scale of 12.5, 15 and 20 arcsec/pix, at a pixel resolution of 64 subpixels per pixel. It was used an existing ACS jitter signal, scaled to give a jitter signal of a few sub-pixels. At the beginning only a single telescope is simulated, and the flux level is scaled such that a V=11 star with 20 telescopes would give 27 ppm/hr, as required. The exposure time is fixed at 20 seconds with 1.6 seconds as readout time, while the readout noise is assumed to be 15 e-. A small sky-signal was added (5e- per pixel per second) and subtracted again during the reduction. At the end of the simulation process for each image, the image was rebinned to normal pixel resolution (i.e. no subpixels spacing). Figures (3.6) and (3.7) show the simulated fields (sub-images of 150 × 150 pixels) where the size and colour of the symbols are defined according the magnitude of the stars.

The better way to evaluate the quality of an image is to measure the signal-to-noise ratio dipersion. The optimal scatter, given by the photon noise (we called ϵ_{opt}), is calculated as:

$$\epsilon_{opt} = \frac{\sqrt{F_i}}{F_i} \tag{3.6}$$

with F_i the simulated input flux, while the measured scatter is defined as:

$$\epsilon_{rel} = \frac{\sigma_{F_o}}{F_i} \tag{3.7}$$

with F_o the output flux. All is then converted in parts per million (ppm).

Figures (3.8) and (3.9) show the first results of the evaluation procedures for the Hipparcos field in the two optical designs, with plate scale of 12 and 15 arcsec/pixel. In the left panels is shown the dispersion of the signal to noise ratio compared to that obtained by the photon noise (straight line), In the right panels we can see the histogram that gives the distribution of the stars in bins of magnitude, in order to define the luminosity function of that particular field.

The same has been done in the case of the Carina field, including also the simulations with the PSF for a design of a plate scale of 20 arcsec/pixel. Figure (3.10) shows the SNR dispersion, while Figure (3.11) shows the histograms of magnitude.

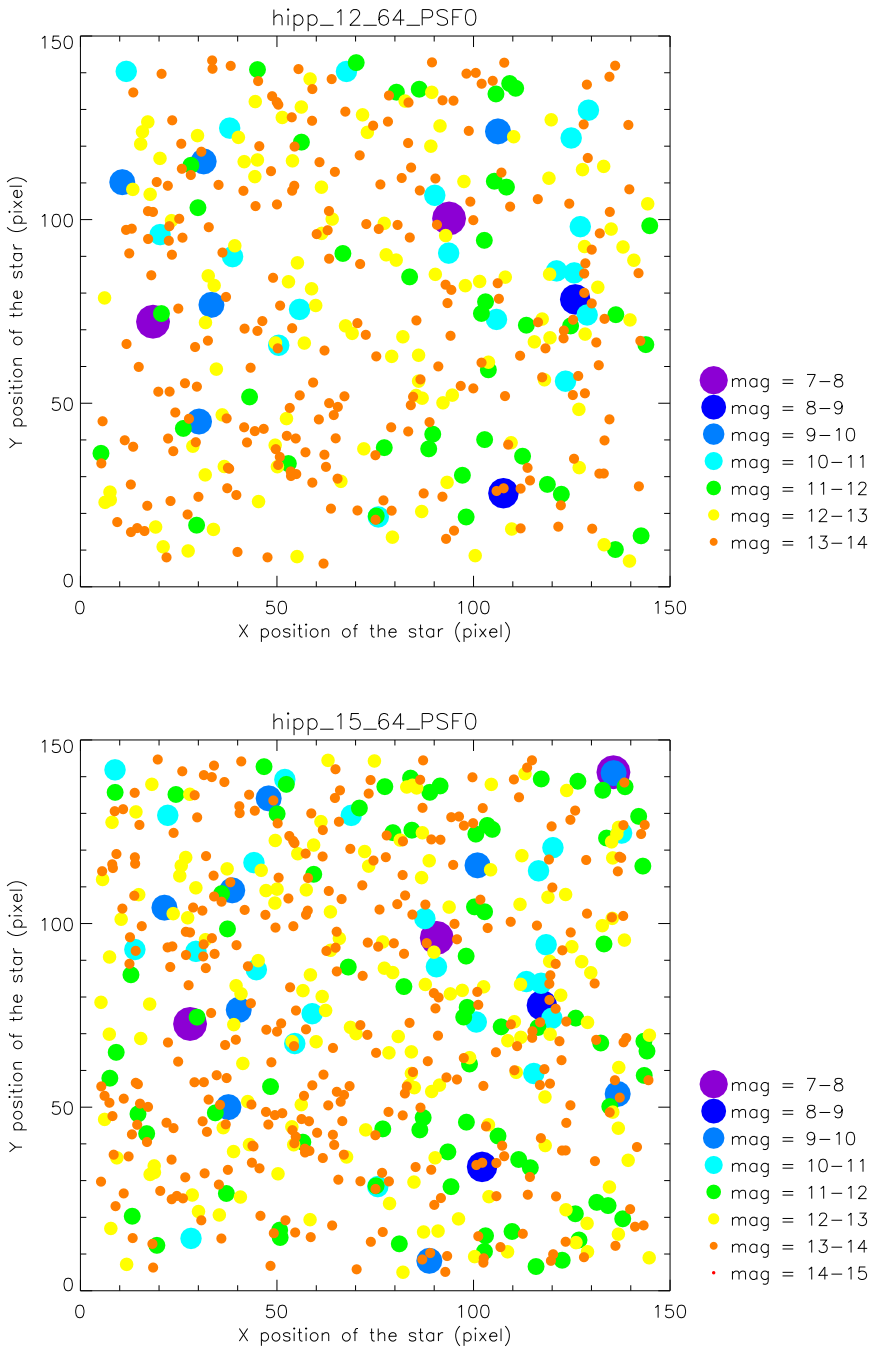

Figure 3.6: Distribution of the position of the stars in the Hipparcos field on a grid of 150 × 150 pixels of the detector. In the left panel is plotted the field observed with a plate scale of 12.5 arcsec/pixel, while in the right panel is plotted the field observed with a plate scale of 15 arcsec/pixel.

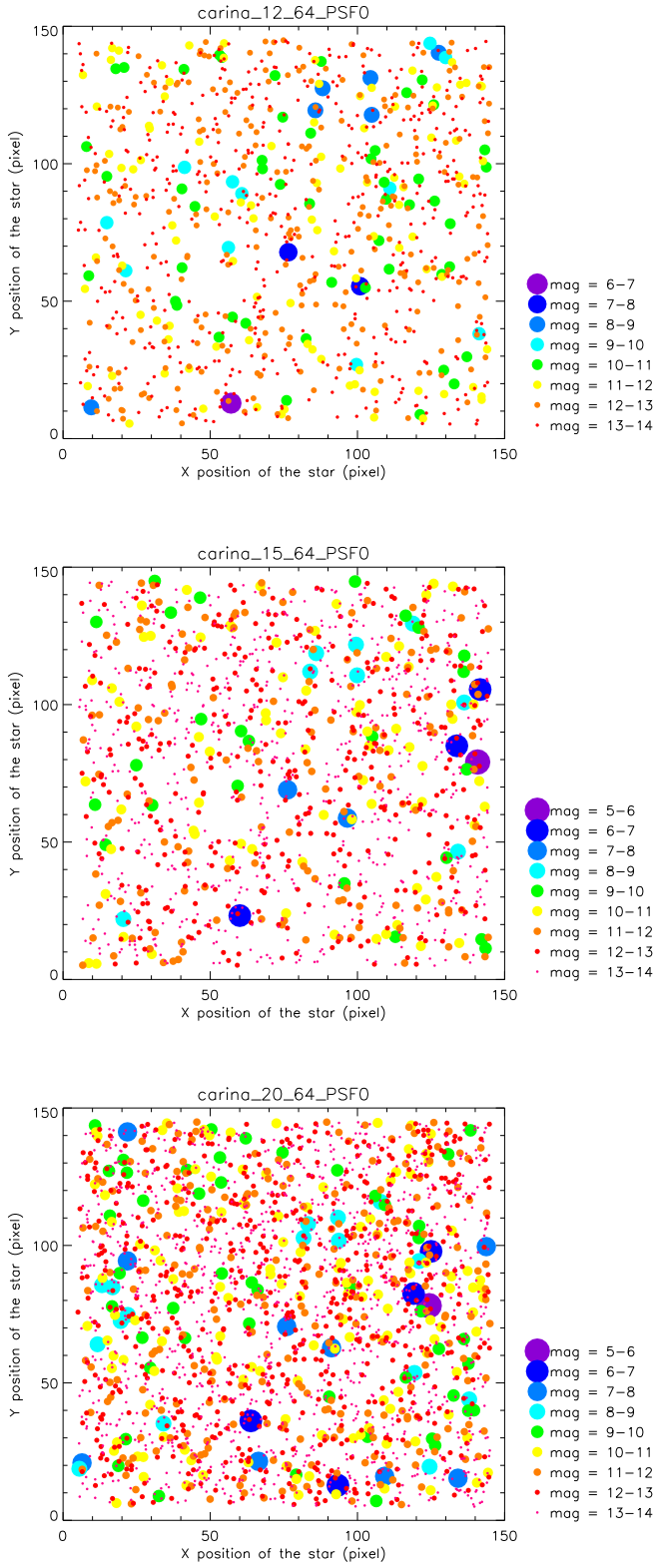

Figure 3.7: Distribution of the position of the stars in the Carina field on a grid of 150 × 150 pixels of the detector. In the left upper panel is plotted the field observed with a plate scale of 12.5 arcsec/pixel, while in the right upper panel is plotted the field observed with a plate scale of 15 arcsec/pixel. In the lower panel is plotted the field observed with a plate scale of 20 arcsec/pixel.

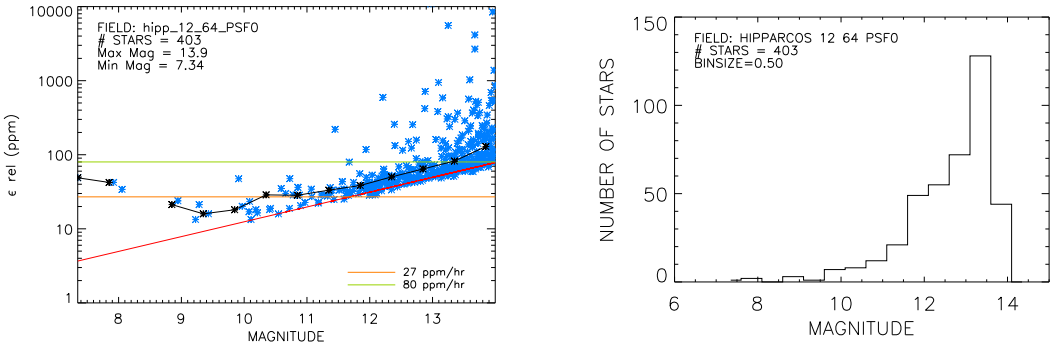

Figure 3.8: Plots of the SNR dispersion versus the input magnitude and the distribution of the number of stars with the magnitude for the optical design which use the plate scale of 12 arcsec/pixel for stars in the Hipparcos field. The red line indicates the limit of the photon noise, while the orange and the green ones set the required noise limits at 27 ppm/hr (for Asteroseismology) and 80 ppm/hr (for Exoplanet search). The black asterisks linked by the black line show the median of the relative error at each step of magnitude (0.5).

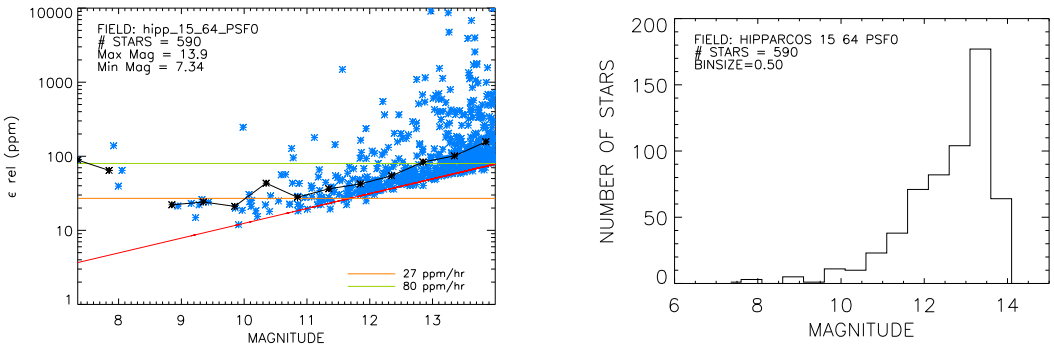

Figure 3.9: Plots of the SNR dispersion versus the input magnitude and the distribution of the number of stars with the magnitude bins for the optical design which use the plate scale of 15 arcsec/pixel for stars in the Hipparcos field.

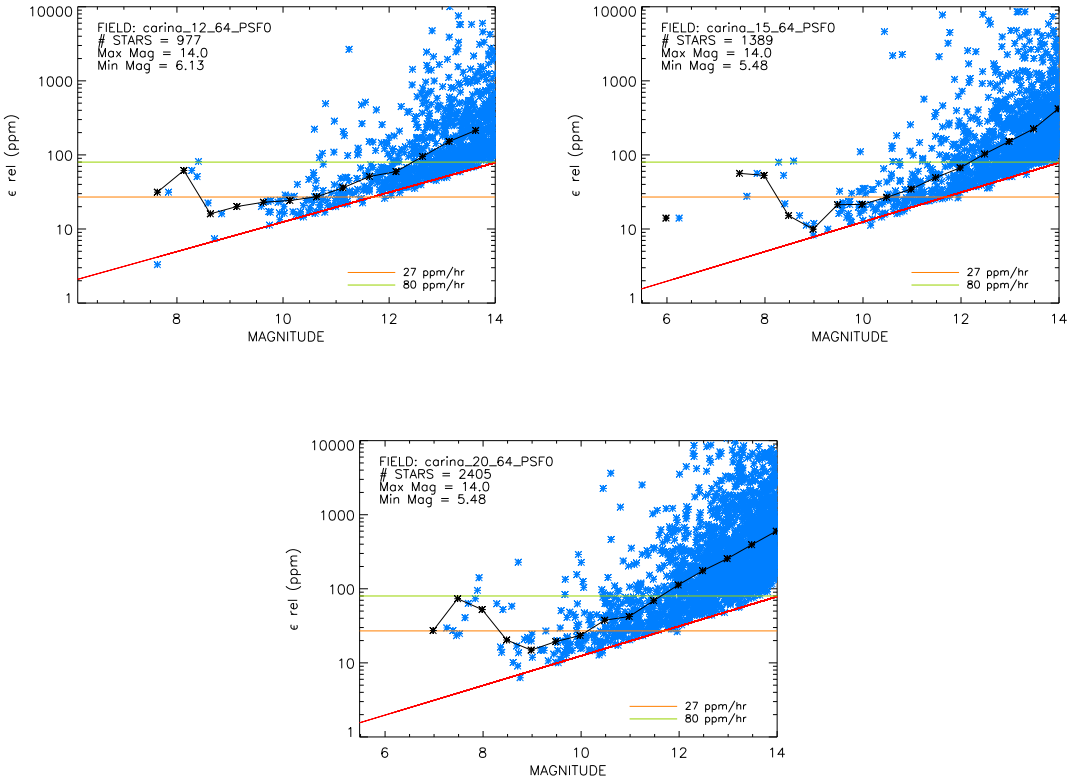

Figure 3.10: Plots of the SNR dispersion versus the input magnitude for the three different optical designs for stars in the Carina field. The red line indicates the limit of the photon noise, while the orange and the green ones set the required noise limits at 27 ppm/hr (for Asteroseismology) and 80 ppm/hr (for Exoplanet search). The black asterisks linked by the black line show the median of the relative error at each step of magnitude (0.5).

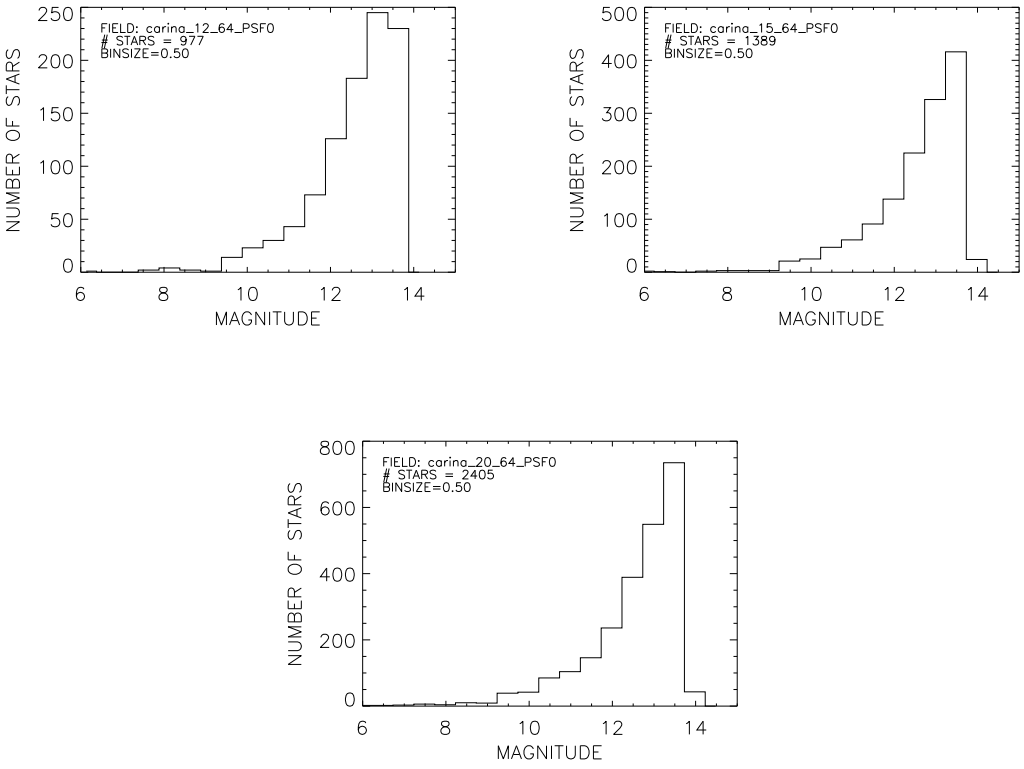

Figure 3.11: Luminosity functions of the Carina field for the three optical designs.

As a final test of this first part we made a comparison between the mean r.m.s. in every bins of magnitude for the Carina field in the three different optical designs. Figure (3.12) shows this. As we can see, it seems that the 12, 15 and 20 arcsec/pixel simulations does not produce very different results. After a first look of these plots it is easy to see

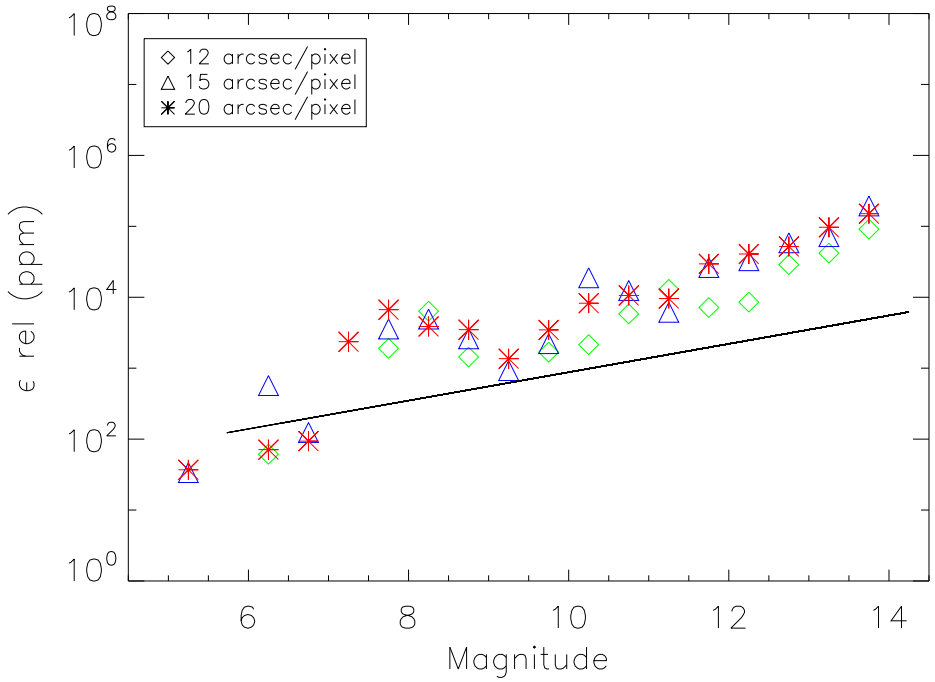

Figure 3.12: Comparison between the mean r.m.s. in every bins of magnitude for the Carina field in the three different optical designs. The straight line is the theoretical curve defined by the photon noise.

the problem of confusion, i.e. the contaminating sources add a pollution that is set to 1/3 of the photon noise. This is the most important problem, and a correction is required to avoid the wrong determination of the photometric measurements.

After this first series of simulations it has been decided to focus our attention on a single optical design (in particular that with 15 arcsec/pixel plate scale), and to evaluate the images produced using a combination of PSFs. In order to obtain simulated images that resemble as close as possible the real ones, a bigger number of PSF has been used, ranging between the centre and at the edges of the images. These PSFs were also monochromatic, with a step of 25 nm without any transmission/efficiency correction. Since the introduced ACS jitter produces a quasi-periodic variation in the resulting light curve, which probably affects the measured relative error ϵ_{rel}, the second set of simulation is performed without this additional source of noise.

The images provided by Dr. W. Zima are simulated using the Carina field only, integrating the PSF with a black body radiator of 6000K, with three different star concentration, dense, medium and sparse. The available images are performed with several combinations of PSFs, but we decided to focus our analysis on the following configurations:

- simulations and aperture photometry of the dense field with the central PSF;

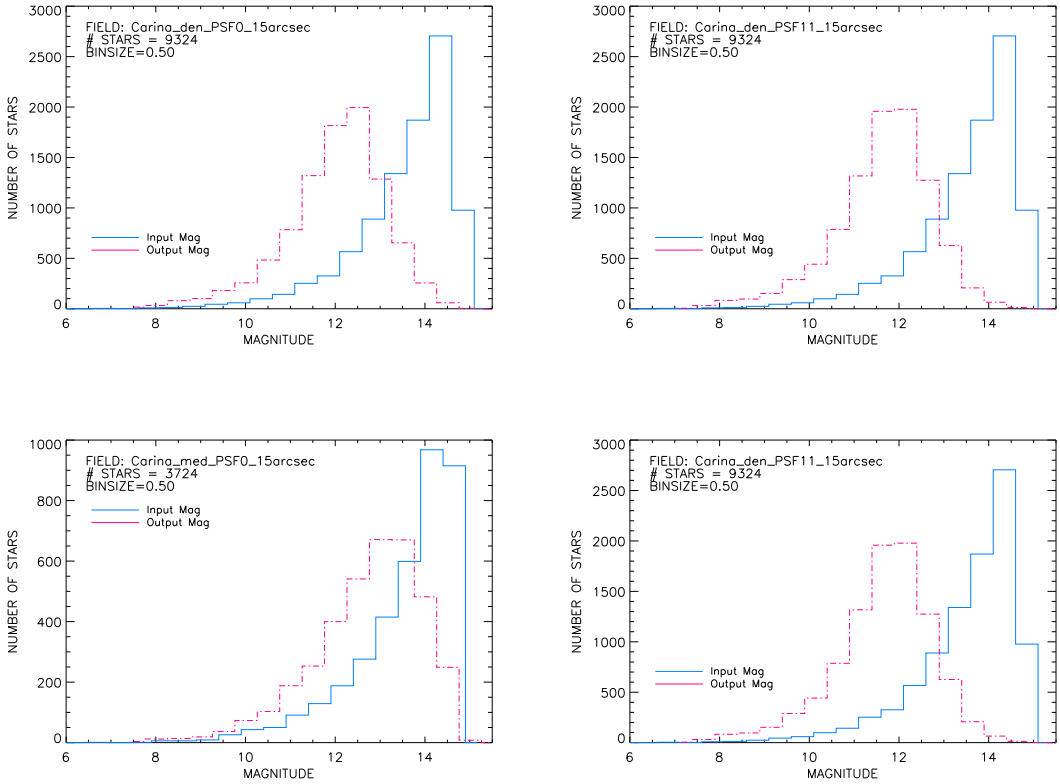

Figure 3.13: Luminosity functions for the new sets of simulations. The blue lines indicates the histogram of the input catalog magnitudes, while the pink one represents the output magnitudes resulting from the data reduction technique (aperture photometry).

- simulations and aperture photometry of the dense field with the near edge PSF (at 11 degrees far from the centre, i.e. 50 mm from the optical axis);
- simulations and aperture photometry of the medium field with the central PSF;
- simulations and aperture photometry of the medium field with the near edge PSF (at 11 degrees far from the centre);

The implementation of the procedures and the informations provided from this set of simulations allow us to go deep into the analysis, for example to evaluate differences between the luminosity function of the input catalog and the one obtained with the aperture photometry algorithm proposed for the data reduction. This algorithm selects the pixels around the sub-pixel position of the target star, such that the 90% of the stellar flux to fall into the mask (T. Arentoft, private communication). As Figure (3.13) shows the computed magnitudes are systematically brighter than the input ones, as a result of the contamination from other sources like stars and background or instrumental effects or even the reduction algorithm.

Since the sparse field has no statistical meaning we were focused on the other two fields.

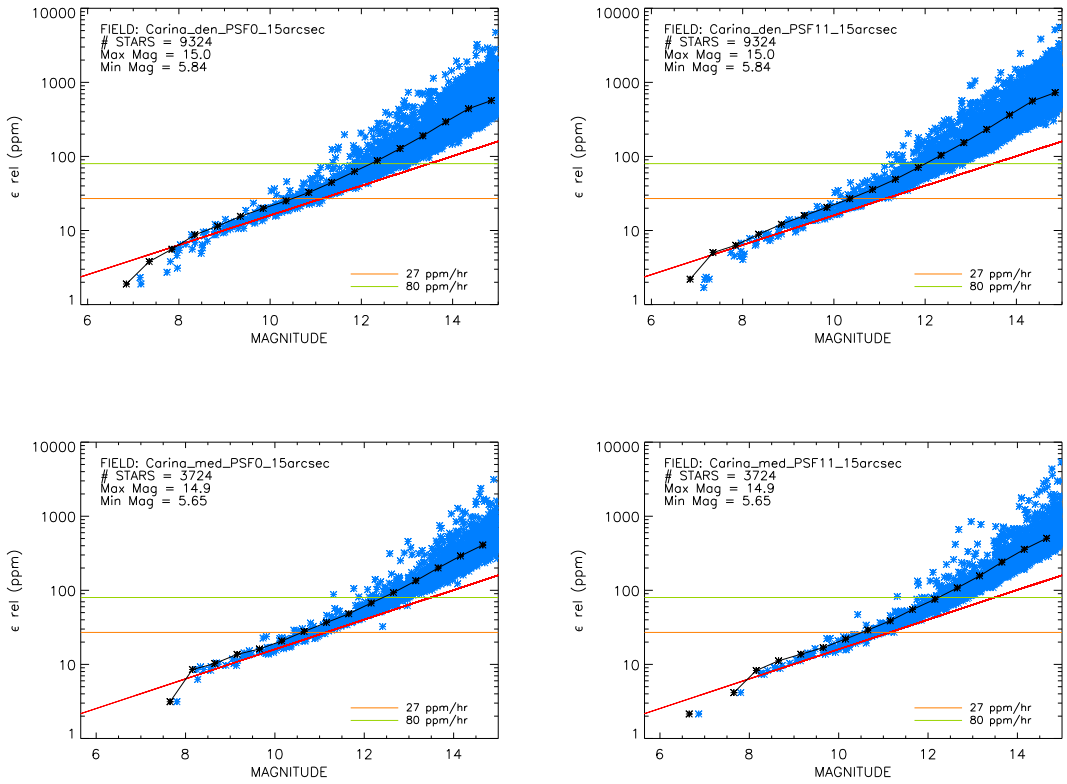

Figure 3.14: The red line indicates the limit of the photon noise, while the orange and the green ones set the required noise limits at 27 ppm/hr (for Asteroseismology) and 80 ppm/hr (for Exoplanet search). The black asterisks linked by the black line show the median of the relative error at each step of magnitude (0.5). These values are always obtained with the aperture photometry algorithm.

As already done for the previous simulations we evaluate the signal to noise dispersion to obtain the noise budget (that we also call *relative error*, see Figure (3.14)).

In order to test the last design studied by the Optical Group (Dr. R. Ragazzoni and collaborators, INAF, Astronomical Observatory of Padova), a new set of simulations was then provided by Dr. Zima, adding also a new method for the data reduction, i.e. employing weighted mask photometry. This new algorithm was defined by Dr. R. Samadi and it gives much more weight to the central pixel of the PSF defined as follow (private communication):

$$Weighted \quad Mask = B \int_{\Delta x, \Delta y} PSF \tag{3.8}$$

where B is the normalization factor, the PSF is the theorical one, as provided by the Optical Group, binned in a sub-pixel grid defined by Δx and Δy.

As Figure (3.15) shows, the introduction of the weighted mask produce an improvement in the computation of the photometry, since the output luminosity function is closer to the theorical one than in the aperture photometry case. The choice of the weighted mask photometry is then required. We also compare the input magnitudes and the output magnitudes. Figure (3.16) shows this comparison, and as a reference we added the line of

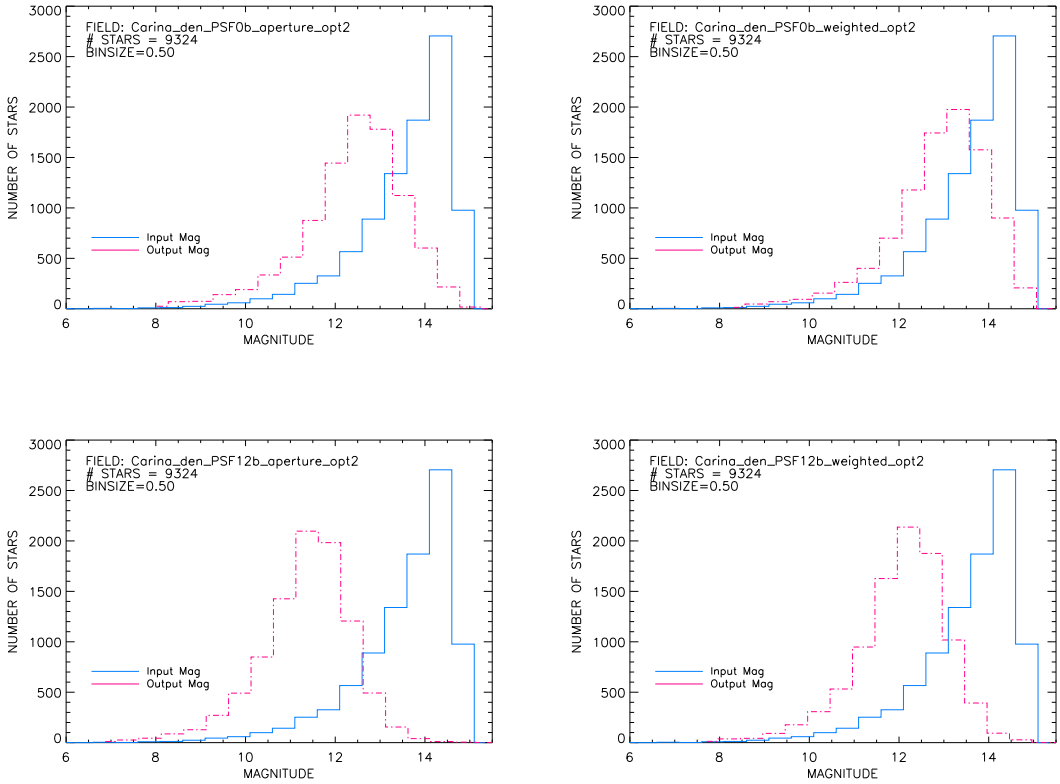

Figure 3.15: Comparison between the two different methods for data reduction: the aperture photometry (left panels) and the weighted mask photometry (right panels). We only report the case of the dense field with the configuration of the central PSF and the 12 degree PSF.

the 1:1 ratio.

All of the simulations have been analysed with the same previous procedures, and they produced the plots shown in Figure (3.17).

Figure (3.18) shows some examples of light curves obtained with the dense field simulations and a central PSF.

Another interesting result is to evaluate how many stars show a particular r.m.s. in their light curve. Figure (3.19) shows the histogram of these occurrences. The bulk at low r.m.s. is an index of the saturated pixels.

Thanks to this analysis we had the possibility to ensure that the amount of the simulated noise won't compromise the detection of stellar oscillations and planetary transits. Our evaluation of the signal-to-noise ratio in terms of the relative error, ϵ_{rel}, shows that in the best case the scientific requirements are fulfilled by stars with magnitude $m_V < 11$ and $m_V < 13$ respectively. This is an encouraging result for PLATO, since its scientific goals are particularly focused tor bright stars. Furthermore this kind of analysis can be a useful test for the development of the optical design.

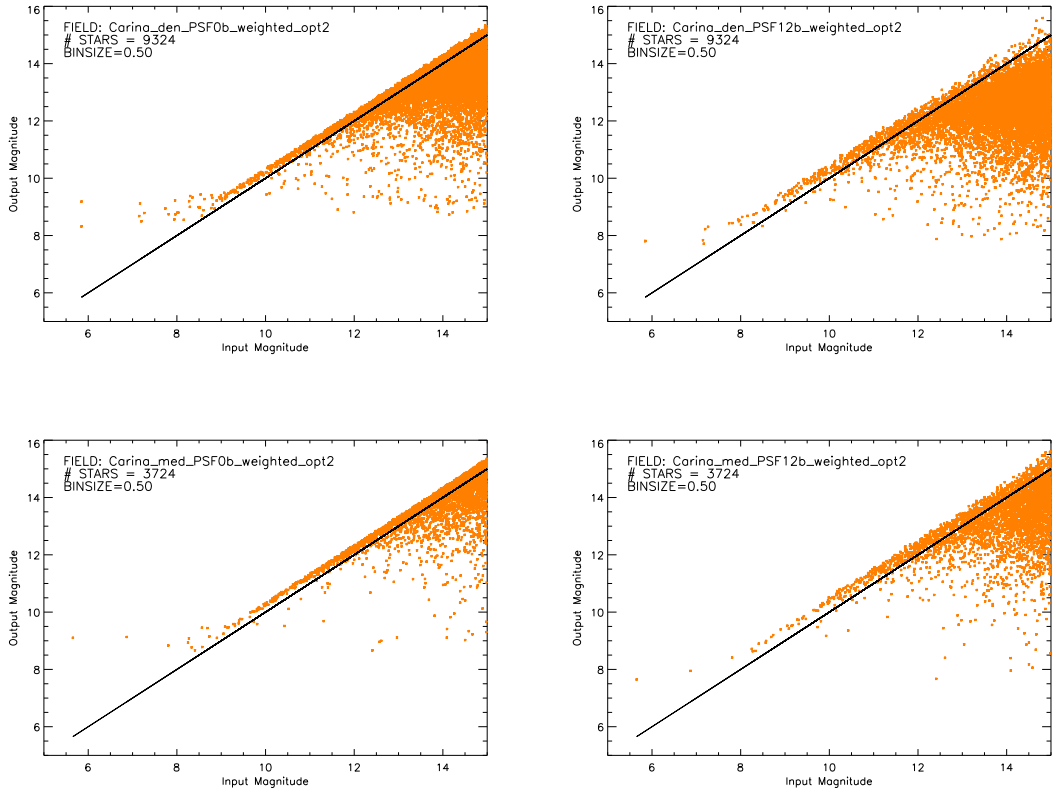

Figure 3.16: Plots of the input magnitude catalog versus the computed magnitude. The black line defines the 1 to 1 ratio.

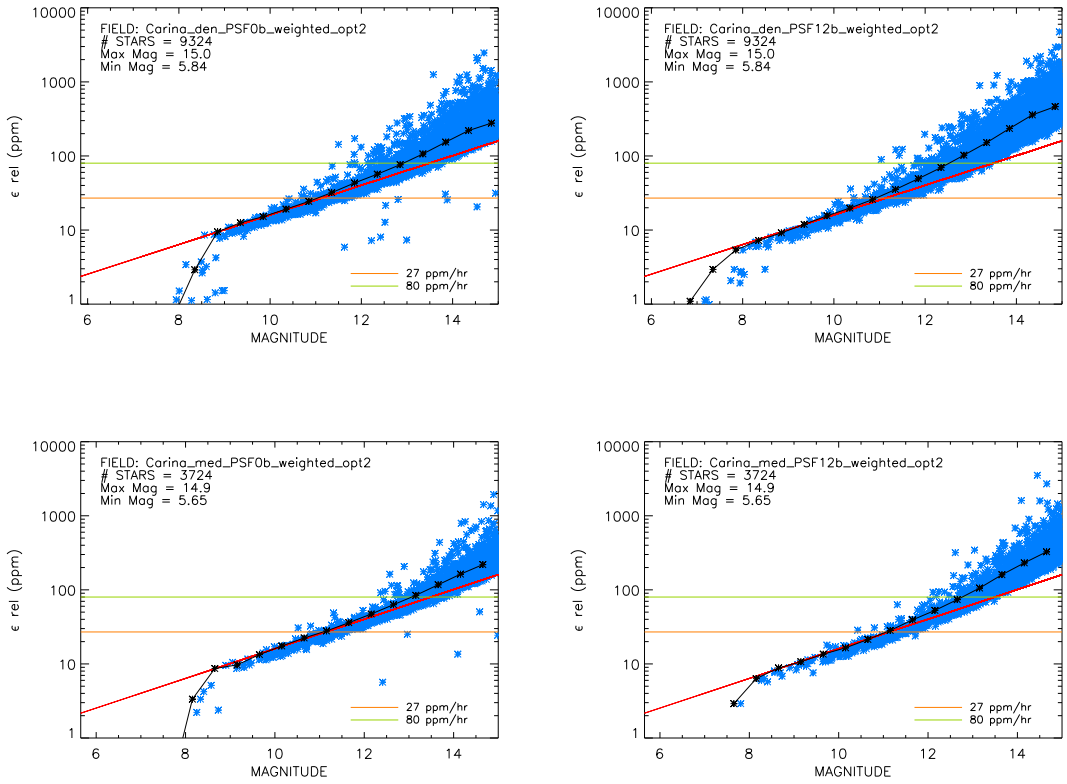

Figure 3.17: Plot of the relative error versus magnitude in the case of 15 arcsec/pixel optical design. The four panels shows the cases of a central PSF and a PSF at 12 degrees (from the centre) for the dense and medium field, as indicated. The red line indicates the limit of the photon noise, while the orange and the green ones set the required noise limits at 27 ppm/hr (for Asteroseismology) and 80 ppm/hr (for Exoplanet search). The black asterisks linked by the black line show the median of the relative error at each step of magnitude (0.5).

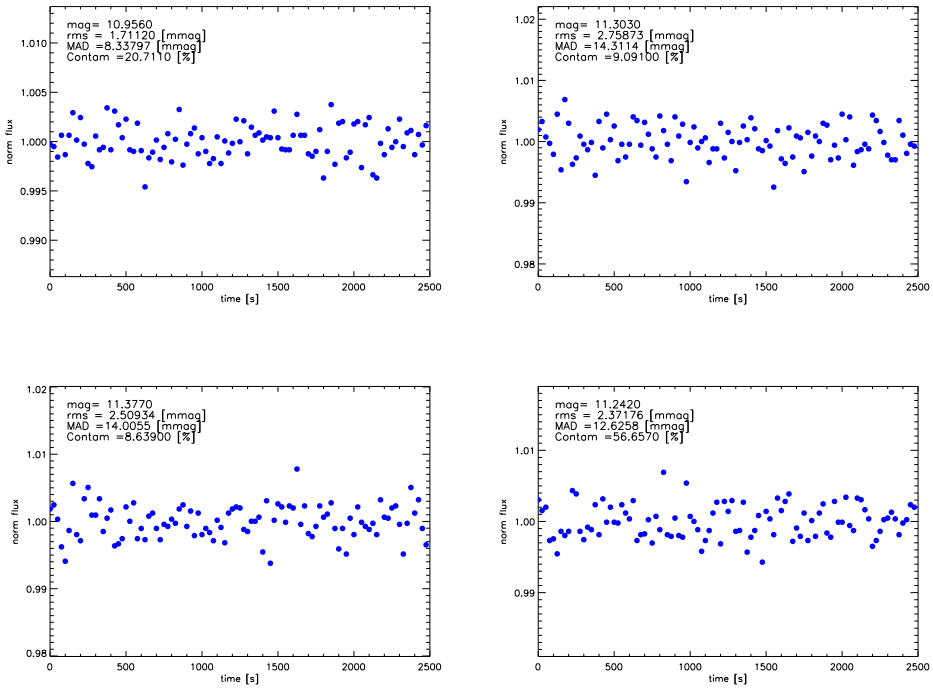

Figure 3.18: Light curves of 30 minutes four stars in the dense Carina field.

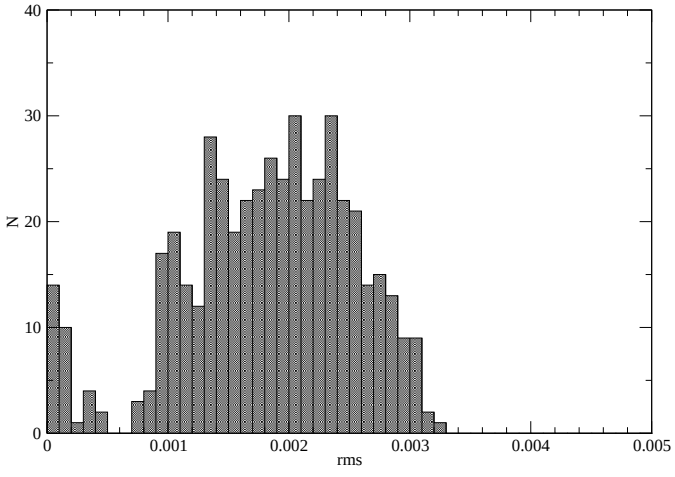

Figure 3.19: Number of stars binned in light curve r.m.s.

3.3.1 Introduction of the jitter noise

The pointing variations of the satellite, known as *jitter*, is another important source of noise in the scientific images, resulting as a smearing of the stellar images on the detector. We were not provided with the simulations obtained with the introduction of this noise, but we report how they were obtained and the main differences in comparison with the previous simulations noise free.

First of all a model of PLATO jitter was obtained using the ISO satellite, and with the introduction of the required pointing accuracy of 0.2 arcsec, a time series of noise jitter was simulated. The resulting displacement of a pixel is of 1.3%, that means less than one sub-pixel in our simulations (W. Zima, private communication). The roll of the satellite contributes in the worst case with a displacement of 0.75% of a pixel. If we combine all the three jitter components, the produced shift is about 2 sub-pixels.

The produced simulations after the jitter introduction shows that the most noise affected stars are the fainter ones, the same stars that are affeected also by the contamination of the brighter sources.

3.4 Defocus and the problem of crowding

At the beginning of the feasibility study for PLATO it was chosen to defocate the telescopes in order to avoid the pixels saturation due to the brighter stars of the field. As we saw in the previous Section the topic of the confusion due to the crowding represents a very critical problem, therefore after the analysis of the simulations that we shown before, it was decided to abandon the idea of the defocus because it would add further confusion in the images, with the risk of the non-identification of the single sources.

Since we were assigned to this task we performed some preliminary calculations before the rising of this complication, so we show them as completeness. The concept of the defocus is quite simple: since the photon flux emitted by the brighter sources is very high, it can exceed the full well capacity of the detector and thus saurate the pixels. It is therefore required to spread the incoming light into a specific area of pixels and not into a single point, through the defocusing of the optical system.

The amount of the defocus depends on the detector that we use and on the magnitude range that we want to explore. The source signal on each CCD pixel (assuming an uniform PSF) is defined as:

$$F = \frac{f_0 S \Delta\lambda \eta t_{exp} 10^{-0.4 m_V}}{N_{pix}} \tag{3.9}$$

where f_0 is the incoming flux from a star with visual magnitude $m_V = 0$ ($1000\ s^{-1}\mathring{A}^{-1}cm^{-1}$), S is the collecting area ($113\ cm^2$ for one telescope), $\Delta\lambda$ is the bandpass of the instrument (5500 Å), η is the total throughput of the instruments that we vary in order to evaluate the performances at different wavelengths and magnitudes, as well as the exposing time t_{exp}. In the end, N_{pix} is the number of pixels occupied by the PSF. Table (3.1) shows the variations of the quantum efficiency and of the optical transmission used to evaluate the parameter η (P. Levacher, private communication). The samples for PLATO and their corresponding exposure times [1]) are:

- *s1*: magnitude range = 8 - 11, exposure time = 20 s;

[1] these are the old requirements, used during the evaluation of the defocus, the updated values are in the Section (3.1.1

Wavelength (Å)	4500	5000	6000	7000	8000	9000	10000
Q.E.	0.55	0.64	0.76	0.84	0.88	0.64	0.1
O. T.	0.66	0.84	0.85	0.88	0.91	0.94	0.94

Table 3.1: Values of the quantum efficiency and of the optical transmission as function of the wavelength, used for the evaluation of the defocus.

- *s2*: magnitude range = 11 - 14, exposure time = 300 s (not suitable for defocusing, too faint);
- *s3*: magnitude range = 4 - 8, exposure time= 4 s.

Another important parameter in this evaluation is the full well capacity, that is 616 ke-.

The flux F_{spread} that we want to spread in N_{pix}^2 pixels is defined as the full well capacity multiplied for the percentage of how much we can fill with charge only one pixel to avoid the saturation. This percentage was fixed at 75%. The number of pixels is then calculated as:

$$N_{pix} = \frac{f_0 S \Delta\lambda \eta t_{exp} 10^{-0.4 m_V}}{F_{spread}}. \tag{3.10}$$

Figure (3.20), shows the obtained values for different stellar magnitudes for the brighter stellar samples. Since the horizontal dashed lines represent the dimensions of the PSF (7 pixel^2) we can see that the defocus is required when are observed stars with visual magnitudes brighter than 7 for the case of sample 3, while the need of the defocusing is less important in the case of sample 1 apart for the brighter edge of magnitudes.

Figure (3.21) shows how appear the three simulated fields with dense, medium and sparse stellar concentration using the second optical design. It is clear that for the statistical and scientific reasons the most interesting field is the dense one, near the galactic plane, therefore the situation dominated by crowding. In this condition the major risk is to perform an erroneous measurement of the stellar flux and thus of the magnitude, leading to a strong overestimation of the stellar magnitude in comparison with the input one (see again Figure (3.15)). In order to evaluate, in first approximation, the amount of flux that affect the real flux of a single star measured through a weighted photometry mask we proceed as follow.

The mask used to perform the photometry and thus to obtain the flux from each star in the image has a radius of 3 pixels, while the radius of the PSF is 1.5 pixels. This means that if 2 stars are closer than 3 pixels on the CCD then they affect each other. We then evaluate how many stars and how much of their flux can pollute the flux of a specific target. As Figure (3.22) shows, the PSF is defined as the area of the detector that contains the 90% of the stellar flux, while the remaining 10% is supposed to be confined within the mask. We stress that we use the approximation of a non-weighted mask, so our results should slightly overestimate the contaminating flux. With an IDL procedure we evaluated the percentage of contamination due to the surrounding sources $S_{\star,i}$ for each star $S_\star$. So we take the fraction of the input flux of $S_{\star,i}$, according to the distance between their centroids and the centroid of the star $S_\star$ and the position of each $S_{\star,i}$ relative to the mask. Figure (3.23) shows the results of this analysis. The dense and medium, as well as the sparse field show a very strong pollution, in particular for stars with fainter magnitudes.

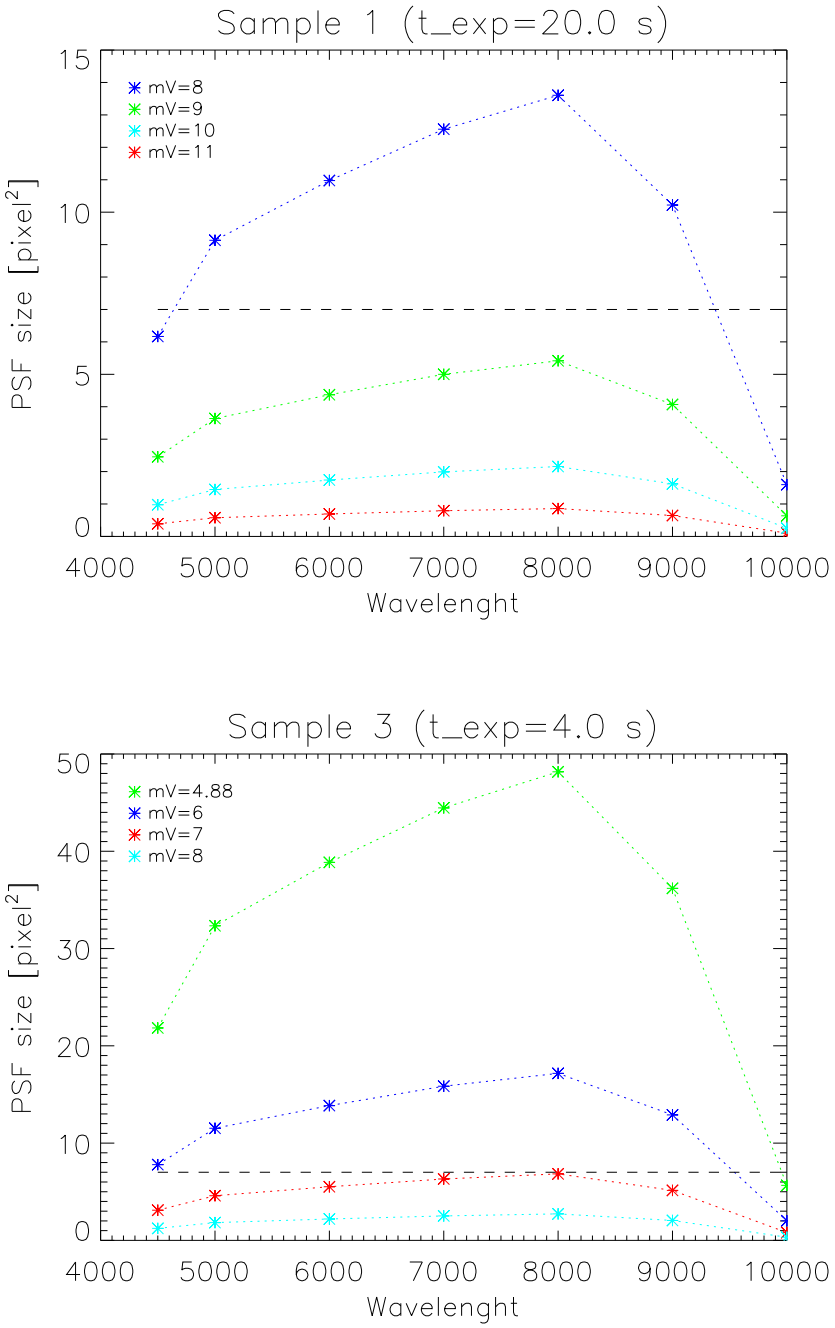

Figure 3.20: Plot of the total area in pixels required to span the stellar flux and to avoid the saturation at different wavelengths at the defined exposing times. We studied the two bright stellar sample of PLATO giving as reference four different magnitudes. the visual magnitude 4.88 is the brighter star included in the simulations that we analysed. The horizontal dashed line defines the dimensions of the PSF.

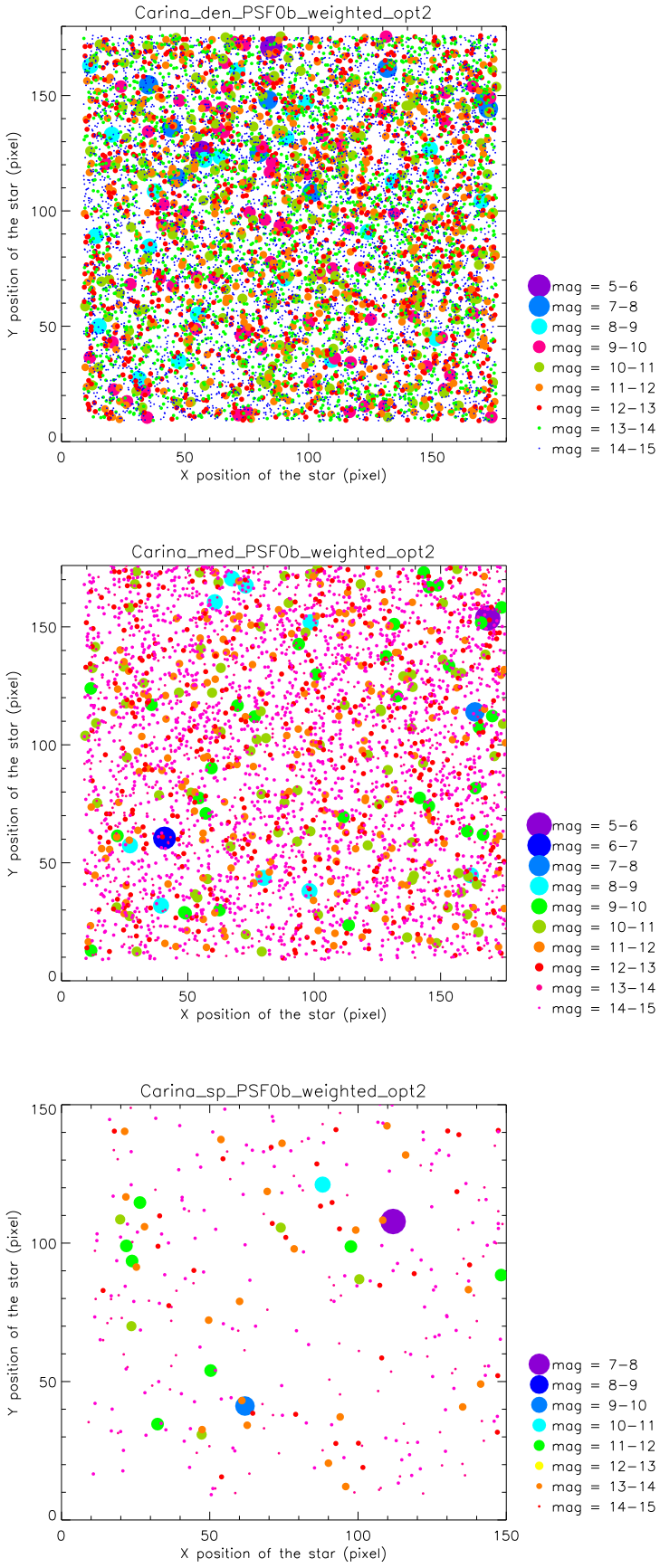

Figure 3.21: View of the three simulated fields: *a*) the dense Carina field (9324 stars); *b*) the medium Carina field (3724 stars); *c*) the sparse Carina field (969 stars).

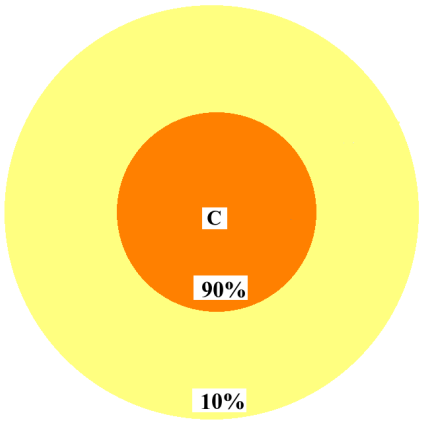

Figure 3.22: Image that represents the dimension of the PSF (inner circle) and of the mask (outer circle). The central point C is the centroid of the star.

3.5 Evaluation of noise

Among the tasks to be performed by the PLATO Science Consortium was the evaluation of the impact of the simulated noise on the detections of planetary transits and stellar pulsations. We foucused our attention on the oscillations, trying to find a reliable method to estimate this contribution. We were provided by the simulated noise of more than 14,000 stars, already analysed in the previous Sections. We stress that for time series of *noise* we indicate the light curves affected by all the possible instrumental noise (sky background, stray light, readout noise of the detector, photon noise, ...) and not the contribution due to stellar activity. We are also able to compute stellar theoretical models with the code ASTEC (Christensen-Dalsgaard 2008a [44]) and to calculate the corresponding oscillation frequencies using ADIPLS (Christensen-Dalsgaard 2008b [43]). A description of these codes will be reported in Chapter 5. We decided to compute a stellar model for a typical target of PLATO, a solar-like star, with stellar parameters similar to our Sun. Using the associated theoretical frequencies and inferring oscillation amplitudes using the parameters resulting from ADIPLS, we were allowed to simulate a time series with the same temporal sampling of the simulated light curves of noise. The comparison between the stellar oscillation and noise spectra provides a direct indication on the noise impact on the simulated pulsations.

As first step we compute a stellar model of our target having the characteristics listed in Table (3.2):

Mass	1.1 $M_{\odot}$
Age	5.54424 Gyr
Radius	1.138 $R_{\odot}$
Effective temperature	5871.1 K
Luminosity	1.380 $L_{\odot}$
Central Hydrogen abundance	0.225
Heavy elements abundance	0.020

Table 3.2: Parameters of the computed stellar theoretical model.

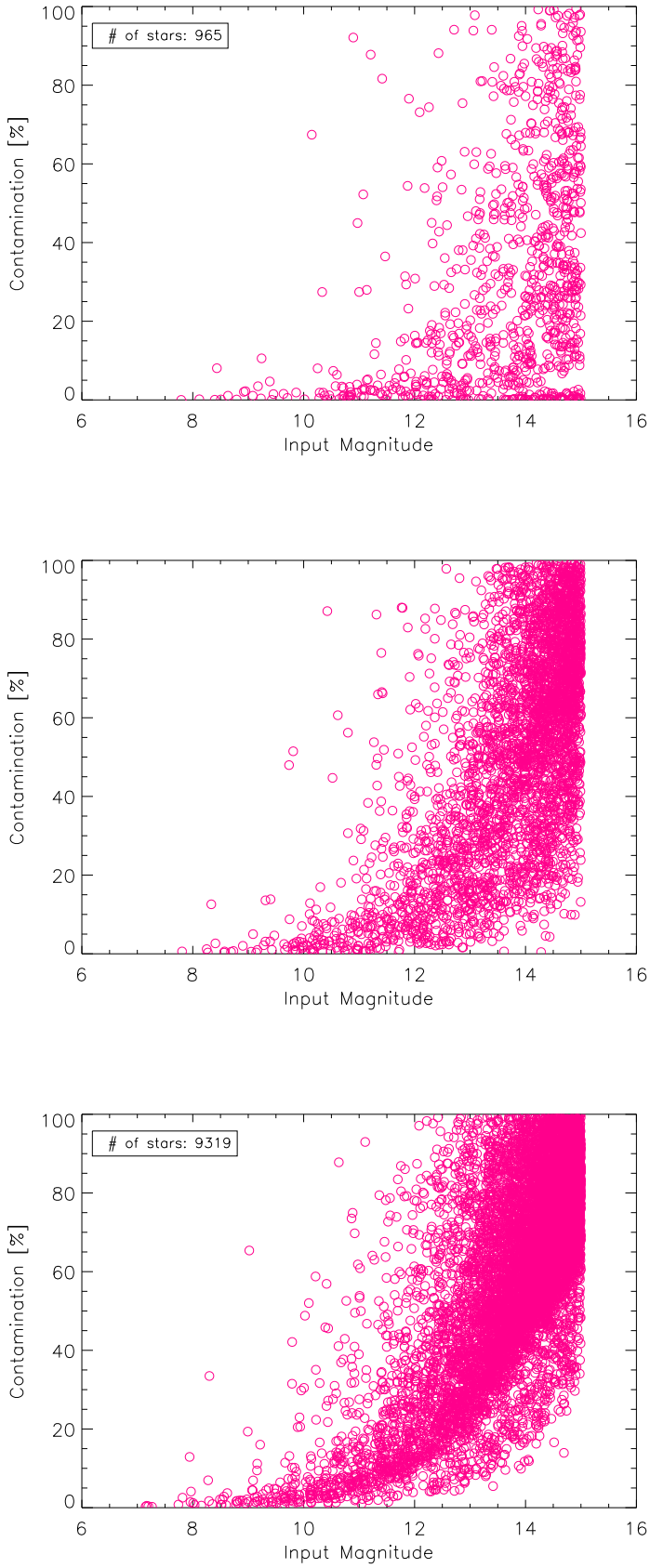

Figure 3.23: Plot of the magnitude versus the percentage of contamination for the sparse (upper panel), medium (medium panel) and dense (lower panel) fields.

The theoretical frequencies are listed in the third column of Table (3.3), while a raw estimate of their amplitudes is given in the fifth column, as a result of the proportionality relation (Christensen-Dalsgaard and Houdek 2010 [50]):

$$\langle A^2 \rangle^{1/2} \propto E^{-1/2}, \tag{3.11}$$

being E the energy of the mode listed in the fourth column of Table (3.3). The modes are also labelled with the angular degree l (first column) and the radial order n (second column).

Each mode present in Table (3.3) can be described by a periodic function like:

$$f(t) \approx A \cos(2\pi\nu t_k + \phi). \tag{3.12}$$

According to the superposition principle, the time series resulting from the oscillations of our targets should be equal to the sum of the single contributions of each mode. So we simulated an observation of our target with the same temporal cadence (25 seconds) as the available time series of noise, Figure (3.24). Note that both the noise and the stellar time

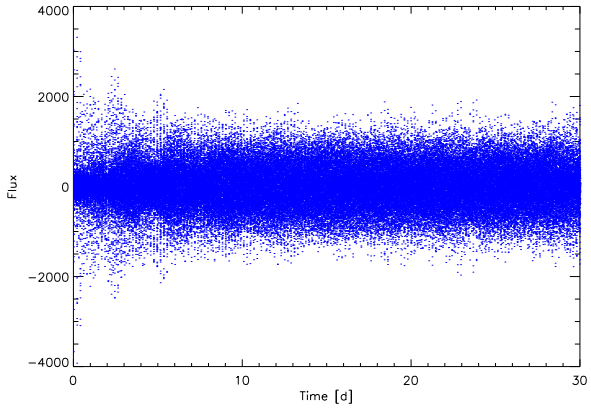

Figure 3.24: Simulated time series for 30 days of observation of the target star.

series are regularly sampled every 25 seconds, so in the amplitude spectra we don't expect to observe spurious peaks due to an unevenly sample. However we point out that since the available time series of noise is simulated for only 60 minutes, we created a synthetic time series by replicating the original one until we reach a total length of 30 days. Finally, in order to take into account of the ontribution of all the 40 normal telescopes we divide the flux by the square root of 40.

Figure (3.25) shows both the amplitude spectra of the simulated stellar time series and the simulated noise. We remind that the amplitudes of the stellar signal are only a raw estimate. For this reason they were divided by a constant factor in order to obtain typical values for amplitudes of solar like stars.

Figure (3.26) shows the amplitude spectrum of the time series obtained through the sum of the simulated stellar signal and the simulated the noise. Two important peaks at about 5000 μHz and $\sim$ 2500μHz are clearly visible in the spectrum of pure noise. Apparently our procedure shouldn't be able to create spurious peaks in the spectrum. We hypothesize that the algorithm used to simulate the instrumental noise can introduced some artefacts in the time series. However we expect a flat spectrum from a pure noise source like the one

l	n	ν [μHz]	E dimensionless	A dimensionless
0	15	1919.1313	1.3168662e-09	27556.825
0	16	2034.8403	9.0554422e-10	33231.134
0	17	2150.3972	6.7951816e-10	38361.843
0	18	2267.0362	5.3705551e-10	43150.955
0	19	2384.2392	4.3507937e-10	47941.957
0	20	2501.6708	3.5536903e-10	53046.925
0	21	2619.3220	2.9680201e-10	58045.236
0	22	2737.0080	2.5368260e-10	62784.821
0	23	2855.2277	2.2052671e-10	67339.425
0	24	2973.7697	1.9371797e-10	71848.060
0	25	3092.5550	1.6970853e-10	76762.333
0	26	3211.5514	1.4894792e-10	81937.514
0	27	3330.5470	1.3062432e-10	87495.956
0	28	3449.8044	1.1416291e-10	93591.731
0	29	3569.1210	9.9278211e-11	100362.86
0	30	3688.5354	8.5270707e-11	108292.92
0	31	3808.0280	7.2447502e-11	117486.59
0	32	3927.4351	6.0484809e-11	128581.01
0	33	4046.8571	4.9341923e-11	142361.31
0	34	4166.0001	3.8883972e-11	160366.88
0	35	4284.6279	2.8687587e-11	186703.73
1	15	1973.0692	1.0916405e-09	30266.360
1	16	2088.9558	7.7996181e-10	35806.620
1	17	2205.3652	6.0477147e-10	40663.462
1	18	2322.4492	4.8414831e-10	45447.583
1	19	2440.1328	3.9350849e-10	50410.725
1	20	2557.6951	3.2525630e-10	55448.160
1	21	2675.4399	2.7401103e-10	60410.993
1	22	2793.4690	2.3689644e-10	64971.177
1	23	2911.8317	2.0695762e-10	69511.921
1	24	3030.7105	1.8151857e-10	74223.165
1	25	3149.6862	1.5924135e-10	79245.036
1	26	3268.9048	1.3939521e-10	84698.571
1	27	3388.2844	1.2224562e-10	90444.747
1	28	3507.7680	1.0649690e-10	96901.725
1	29	3627.4374	9.2098748e-11	104201.30
1	30	3747.0166	7.8784306e-11	112662.70
1	31	3866.6195	6.6355036e-11	122761.75
1	32	3986.0852	5.4931425e-11	134924.11
1	33	4105.3395	4.4131758e-11	150530.46
1	34	4224.2809	3.3882295e-11	171796.22
2	15	2026.2980	9.2551246e-10	32870.693
2	16	2142.1686	6.8923591e-10	38090.445
2	17	2259.1440	5.4329417e-10	42902.488
2	18	2376.6671	4.3940587e-10	47705.348
2	19	2494.4803	3.5834746e-10	52826.013
2	20	2612.4440	2.9893808e-10	57837.482
2	21	2730.4109	2.5502841e-10	62618.941
2	22	2848.8853	2.2159023e-10	67177.632
2	23	2967.6344	1.9458278e-10	71688.221
2	24	3086.6509	1.7042896e-10	76599.918
2	25	3205.8543	1.4957622e-10	81765.242
2	26	3325.0696	1.3110309e-10	87336.047
2	27	3444.5606	1.1458785e-10	93418.032
2	28	3564.1090	9.9637722e-11	100181.63
2	29	3683.7804	8.5588710e-11	108091.55
2	30	3803.5132	7.2744987e-11	117246.12
2	31	3923.1582	6.0753168e-11	128296.72
2	32	4042.7987	4.9607268e-11	141980.06
2	33	4162.1331	3.9142932e-11	159835.53
2	34	4280.9488	2.8957280e-11	185832.26

Table 3.3: Parameters of the computed stellar theoretical model. $l = 3$ modes were also available, but since they are not observable from photometric data, we exclude them, as well as low-order modes (n less than ~ 15).

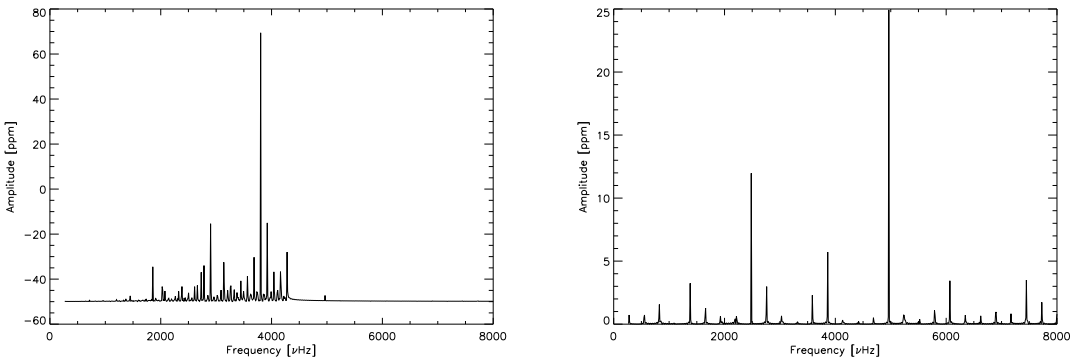

Figure 3.25: *Left panel:* Amplitude spectrum of the simulated stellar signal and, *Right panel:* amplitude spectrum of the simulated noise.

we analysed, and it is quite clear that the spurious peaks are due to effects, not present in a real case. Figure (3.26) shows the amplitude spectrum resulting from the sum of the two time series.

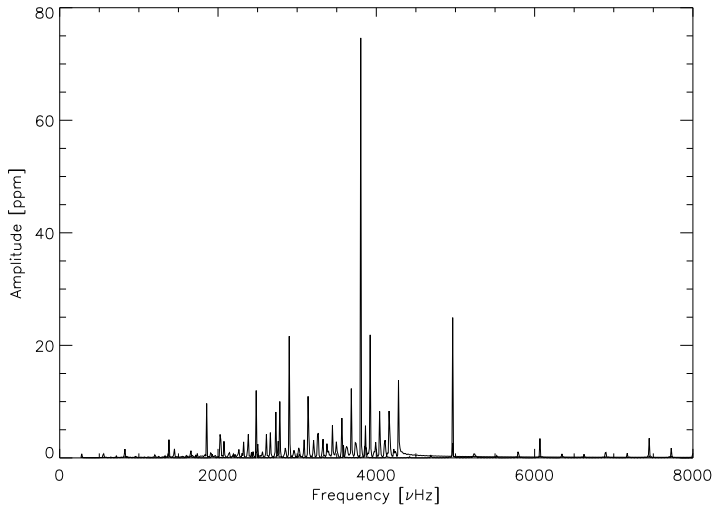

Figure 3.26: Amplitude spectrum of the time series obtained through the sum of the simulated stellar signal and the simulated noise.

It is important to note that the jitter noise is not present, and in principle the regular sampling of the light curves makes the spectra more clean than in the case of a real observation. Nevertheless the *instrumental* noise doesn't seem to affect in a serious way the possible detection of solar-like oscillations.

3.6 Conclusion

In the present Chapter we described our contribution to a preliminary study of the ESA-PLATO satellite. The simulations analysed here provided all the sources of noise, except

for the jitter satellite, that could affect the scientific outcomes. Our aim was to ensure that this amount of noise won't compromise the detection of stellar oscillations and planetary transits. Our evaluation of the signal-to-noise ratio in terms of the relative error, ϵ_{rel}, shows that this is possible for stars with magnitude $m_V < 11$ and $m_V < 13$ respectively. This is an encouraging result since the main goals of PLATO are expected to be reach in particular for bright stars, and it represents a good test for the development of the optical design.

During the analysis the problem of the high stellar crowding of the simulated fields rised up, involving strong contaminating flux caused by the brighter stars. In particular we found a shift toward the brighter magnitudes in the luminosity function of the field. The order of magnitude of this shift depends on the data reduction strategy used to compute the output flux of the simulated images: it scales of ~ 2 in the case of aperture photometry, ~ 1 in the case of weighted masks photometry. The contaminating flux due to the neighbour sources for each star was evaluated, according to the dimensions of the Point Spread Function and the specified encircled energy. As expected, fainter stars are the most affected by crowding effect, even for the less concentrated simulated field.

Thanks to the creation of a simulated time series for a typical target of PLATO we were also able to evaluate the impact of the simulated noise on the detection of stellar oscillations. Even if the spectrum of the pure noise seems affected by some kind of artifacts (actually not present in real data), according to our evaluations the instrumental noise doesn't seem to affect in a serious way the detection of solar-like oscillation as well as planetary transit.

Chapter 4

Seismic analysis

In the next Sections we present our procedure for the analysis of time series. In order to obtain a reliable tool for asteroseismic analysis of photometric light curves, several sets of real data have been utilized. Two types of images were processed and analysed to accomplish this treatment, both form the ground and from space. In the former case we analyse some Kepler light curves in order to study the hybrid γ Doradus and δ Scuti stars as part of the coordinated work of the KASC Working Group 10. In the latter we handled the data of Subdwarfs B stars coming from a series of observing runs at the telescope located at Mount Ekar (Asiago) in the framework of the EXOTIME project. Since these data were collected by our group, data collection and reduction are also described.

4.1 Observation and detection of oscillation modes

The observation of stars involve the observation in integrated light, i.e. of the whole disk. A high resolution imaging was obtained only for the Sun, and the number of detected modes in the solar disk run from $l = 0$ to $l > 1000$ (it depends on the quantity of the resolution elements). For the other stars the oscillation signals over the whole disk are defined as the average on the solar surface, so the presence of high degree modes signal is strongly weakened. This is the reason for what the observation of other stars than the Sun provides the detection of only low degree and high order modes. By the way these kind of modes travel deep into the stars, and they are useful instruments to investigate the inner stellar zones.

Photometric observations measure the light intensity over the visible surface of the star. During the pulsation the number of emitted photons varies, even if of a very small quantity, and the measure of this variation, allows to know the properties of the oscillations. Using a polar coordinates system (r, θ, ϕ), choosing the coordinate axis pointing to the observer, allowed for a sperically symmetric star, the integration of the intensity depends on a quantity called *spatial response function* for the intensity, $S_l^{(I)}$:

$$S_l^{(I)} = 2\sqrt{2l+1} \int_0^{\pi/2} P_l(\cos\theta) \cos\theta \sin\theta d\theta \tag{4.1}$$

with P_l a Legendre polynomial. Eq. (4.1) represents an ideal case, because the stellar rotation implies the existence of a preferred axis, and it must be completed with the integration on the angular coordinate ϕ. Eq. (4.1) also assumes that the brightness of

the disk is uniform, i.e without the effect of the limb-darkening, which depends on the wavelength. In this case, more similar to the reality, Eq. (4.1) becomes:

$$S_l^{(I_\lambda)} = 2\sqrt{2l+1}\int_0^{\pi/2} W(\lambda,\theta)P_l(\cos\theta)\cos\theta\sin\theta d\theta, \tag{4.2}$$

where $W(\lambda,\theta)$ takes into account the limb-darkening.

With spectroscopic observations, the oscillations can be detected by the measure of the radial velocity variations, sensitive only along the line of sight. Even in this case it depends on a spatial response function for the velocity, $S_l^{(V)}$, which, in ideal case of uniform brightness and with the axis pointed at the observer, is defined as:

$$S_l^{(V)} = 2\sqrt{2l+1}\int_0^{\pi/2} P_l(\cos\theta)\cos^2\theta\sin\theta d\theta. \tag{4.3}$$

The term $\cos\theta$ is added as a projection factor, because the Doppler shift is measured only in the radial direction. In the real case Eq. (4.3) includes the function $W(\lambda,\theta)$, to taking into account of the variation in the light profile for the limb-darkening.

Both intensity and velocity measurements are thus dependent on the coordinate θ, but in different ways, thus the ratio between the amplitudes of the modes, obtained with the two different methods can give useful informations in the identification of the modes. This test is however limitated by the fact that the amplitudes ratio is dependent on the wavelength value through the optical depth of the stellar atmosphere from which the radiation originates.

4.2 Analysis of the time series

Using the programming language IDL we developed a series of procedures which treat time series starting from the raw data to the computation of the power spectrum and the subsequent analysis. To accomplish and test this tasks we worked with photometric time series, obtained from the ground using the observations that we performed at the Asiago-Ekar Telescope, and from space with the Kepler satellite.

In order to measure frequency amplitudes it is a common convention to turn the flux, generally expressed as number of photons, to part per million (ppm). This could be very important in the framework of large consortia such as in the KASC or in the EXOTIME program because the amplitudes should be compared among numerous data sets. The conversion to ppm is:

$$Flux[ppm] = 10^6 \cdot (flux_{input}/fit - 1) \tag{4.4}$$

where fit is the polynomial function that we used to describe any possible trend of the time series like the small instrumental drifts or the variation in the airmass during the night. Finally, the subtraction of 1 indicate that the time series is averaged to zero. After this procedure we obtaine a time series like the one showed in Figure (4.1). Also the correction of the temporal data can be useful, in our case, we initialise the time at $t(k) - t(0)$ where $k = 1, ..., N$ for N data points.

The distribution of the data points can be assessed by simple statistical analysis. This could be very useful to suggest any problem in the data such as the presence of extreme outliers responsibles for wrong interpretation in the spectral analysis. Following Warner 1998 [154] we start calculating the histogram of the values, searching for a normal distribution

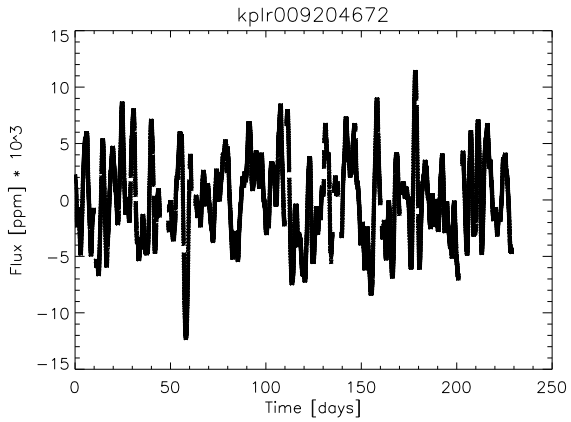

Figure 4.1: Time series of a variable star (Hybrid γ Dor and δ Sct in the Kepler field). The initial Baricentric Julian Date was set to zero, subtracting the time t_0 of the first datum.

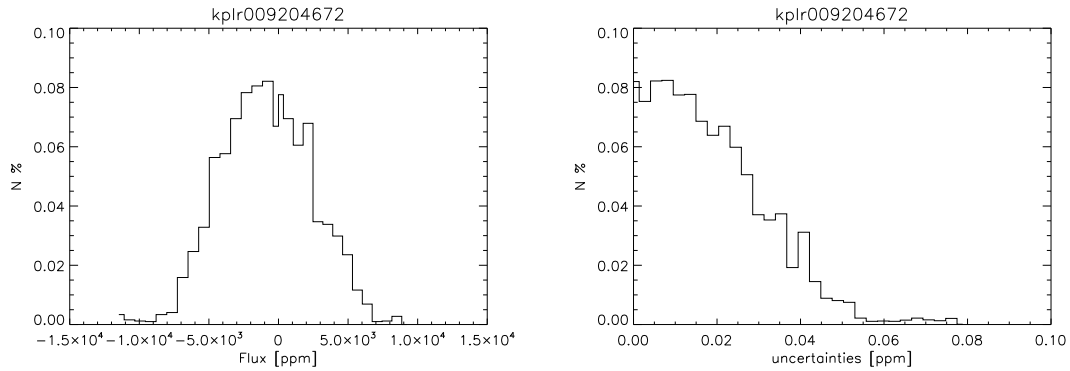

Figure 4.2: Histogram of values (left) and uncertainties (right) of the time series in Figure (4.1).

centred, in this case, at the mean value (i.e. zero). Also the distribution in the uncertanties should be normal as index of random errors, avoiding the presence of systematic trends in the uncertainties (See Figure (4.2)).

Another diagnostic for data distribution is the variance: a time series with large variance can be non periodic or characterized by two or more periodicities, highly probable in light curves of variable stars. Indeed the measured variances in our data are quite large. The stationariety of the time series is referred to the characteristics of the driving process and can be assessed calculating the homogeneity of the variance as function of time. So we diveded the time series into several bins and measured the variance for each of these segments. If the variance of the time series is not stable across the bins, this could be due to one or more extreme outliers that enlarge the variance. The removal of the bad points is a possible solutions to this problem. Since the homogeneity is not always satisfied in our data, a useful way to proceed is to take the logarithm of the time series and compute the variance for it. Figure (4.3) shows the logarithm of the same light curve and the plot of the variance calculated for 20 temporal bins. In this case the variance is quite stable except for the times around the 50th day, but, as it is clear from the time series plot, we

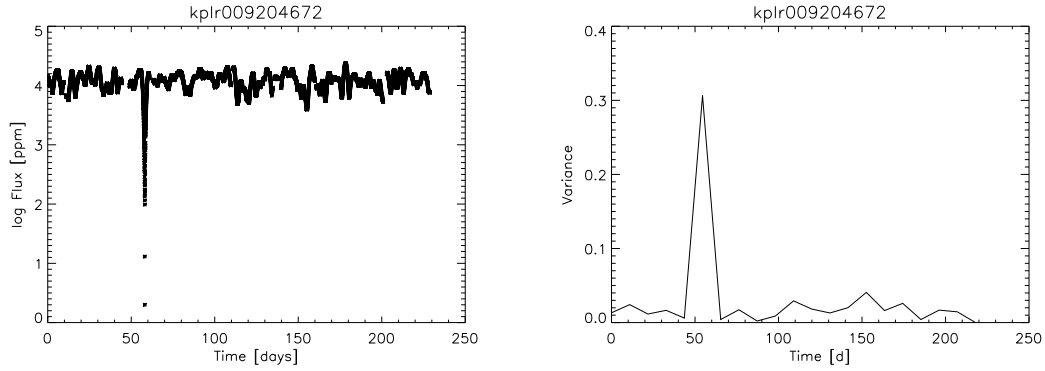

Figure 4.3: *Left panel*: Logarithm of the light curve shown in Figure (4.1). *Right panel*: Evaluation of the stability of the variance for the logarithm of the time series.

find few outliers there.

Finally, the evaluation of the autocorrelation reveals the presence of pattern in the time series. So we calculate the autocorrelation coefficients between the value of the time series at time $t(k)$ and its value at time $t(k-1)$, through the IDL routine `A_CORRELATE`. The plot shows no significant sources of pattern in the data, since it is almost close to zero except for the abscissa equal to zero. Now that we have took a look on the light curve and to its

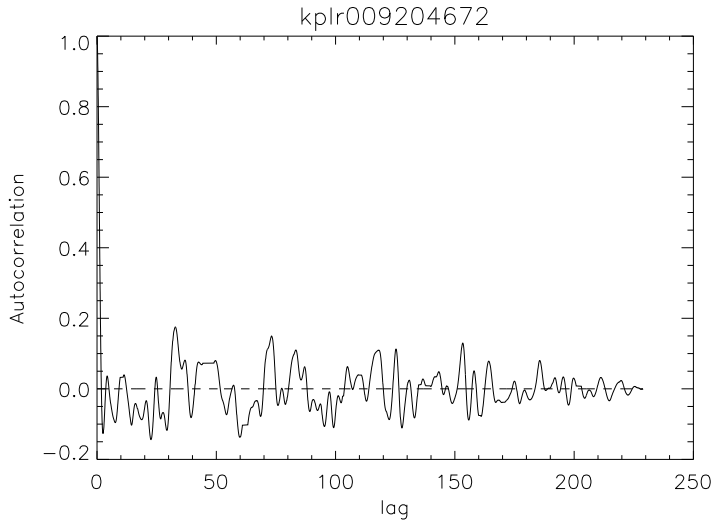

Figure 4.4: Autocorrelation of the analysed time series.

characteristics, we can start to analyse its periodical contributions.

4.3 Frequency analysis

The observed oscillations can be treated as harmonic oscillating signals, that allow us to analyse them with the Fourier theory. In the first part of this Section we present a trace of analysis of this kind of signals, starting from the simplest case.

- **Single oscillation.** The simple harmonic oscillating signal is of the type:

$$v(t) = a_0 \cos(\omega_0 t - \delta_0), \tag{4.5}$$

where ω_0 is the angular frequency. The oscillation period is $\Pi = 2\pi/\omega_0$. When such a signal is observed in a period of time between $t = 0$ and $t = T$, the Fourier transform of Eq. (4.5) is:

$$\tilde{v}(\omega) = \int_0^T v(t) e^{i\omega t} dt$$

Figure (4.5) shows the power spectrum of this oscillation, i.e. power of the signal

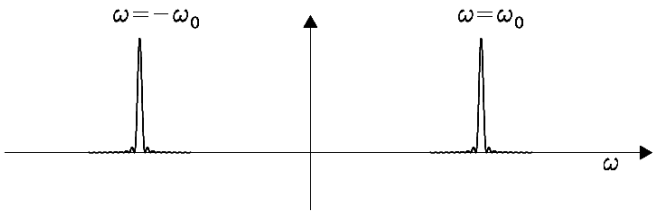

Figure 4.5: Power spectrum of a single harmonic oscillation.

plotted against the frequency. Its analytical form is:

$$P(\omega) = |\tilde{v}(\omega)| \simeq \frac{1}{4} T^2 a_0^2 \mathrm{sinc}^2[\frac{T}{2}(\omega - \omega_0)].$$

This is a semplification, because a real power spectrum is affected by noise and fluctations of the amplitudes. The width of a peak in the power spectrum, $\delta\omega$, provides indications on the accuracy in the frequencies determinations. Therefore it is very important to be able to obtain an high resolution of the peaks, usually closely spaced. Since $\delta\omega \simeq 2\pi/T$, where T is the time of observation, the right degree of accuracy is reached if the time of the observation is quite large.

- **Several simultaneous oscillations.** In this case the oscillation signal is the sum of a certain number of signals:

$$v(t) = a_1 \cos(\omega_1 t - \delta_1) + a_2 \cos(\omega_2 t - \delta_2) + a_3 \cos(\omega_3 t - \delta_3)... \tag{4.6}$$

The observations show that such a spectrum is composed by a great quantity of non-resolved frequencies, and so the modes aren't well separated. Semplifying using only two signals, the expression of the power spectrum contains the separated contributions of the two spectra, and a term due to their interference. The computed width of the peaks has almost the double value of the same quantity in the previous case of a single detection. Figure (4.6) shows, as an example, the importance to avail of a long time of observation to get a good frequency resolution. The Figure refers to a simulations with an increasing observation times from 3 hours to 600.

- **Oscillations affected by gaps.** From a single ground-based site is obviously impossible to obtain uninterrupted time series greater than 10-12 hours. This observation time doesn't suffice to the necessary frequency resolution, and the only way to get it is the combination of the data of the different days. The matching of two observations,

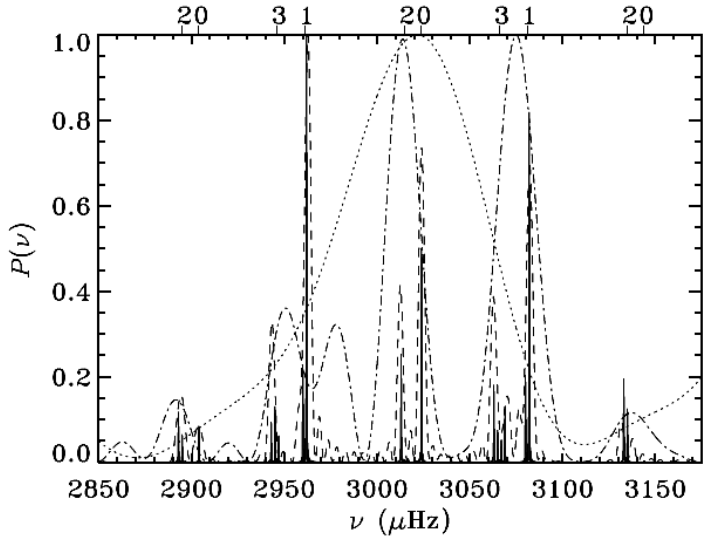

Figure 4.6: Power spectra of simulated time series. For 600 hours of uninterrupted observations the modes are completely resolved. For 60 hours the splitting due to rotational effects cannot be observed but the modes are quite resolved. For 10 hours some modes merge. For 3 hours the spectrum is dominated by the interference and there is no way to distinguish any modes.

one made in a time between $t = 0$ and $t = T$, the other from $t = \tau$ and $t = \tau + T$, is provided by the sum of two integrals, and its Fourier transform is:

$$\tilde{v}(\omega) = \int_0^T v(t)e^{i\omega t}dt + \int_\tau^{\tau+T} v(t)e^{i\omega t}dt \tag{4.7}$$

The corresponding power spectrum is:

$$P(\omega) = T^2 a_0^2 \cos^2[\frac{\tau}{2}(\omega - \omega_0)]\mathrm{sinc}^2[\frac{T}{2}(\omega - \omega_0)] \tag{4.8}$$

that is the spectrum of a single day modulated by $\cos^2[\tau/2(\omega-\omega_0)]$. The combination of different days smooths the fine structure that raises when $\tau > T$, but never completely removes it, leaving two peaks separated from the main peak by $\delta\omega = 2\pi/\tau$. Figure (4.7) shows the case of $\tau = 3T$. A function, called *window function* $w(t)$, describes the effects of the gaps on the observations, and its value ranges between 0 and 1, according to the conditions:

$$w(t) = \begin{cases} 1 & \text{during the periods with data} \\ 0 & \text{during the gaps} \end{cases} \tag{4.9}$$

If $v_0(t)$ is the basic signal, the observed signal, $v(t)$, is then defined as:

$$v(t) = w(t)v_0(t)$$

and its Fourier transform in frequency domain is the convolution of the single transforms:

$$\tilde{v}(\omega) = (\tilde{w} * \tilde{v_0})(\omega) = \int \tilde{w}(\omega - \omega')\tilde{v_0}(\omega')d\omega'. \tag{4.10}$$

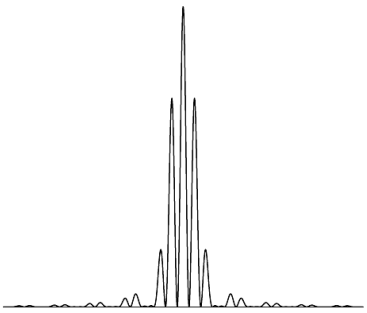

Figure 4.7: Power spectrum of a time series with time gap of $\tau = 3T$.

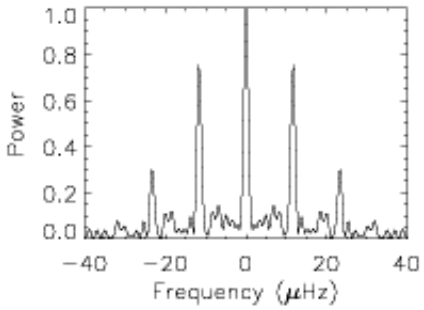

Figure 4.8: Example of a spectral window.

The transform of the window function, $\tilde{w}(\omega)$, defines the *spectral window*.

Figure (4.8) shows the amplitude spectrum of the window function, which is characterised by the main peak (centred in $\nu = 0$ and with a width equal to the inverse of the total observation time), and a series of secondary peaks which compose the so called side-lobes structure. In practice it describes the interference due to the gaps. A further phenomenon, called *aliasing*, is caused by the interference among the frequencies. We can conclude that the discontinuity in the observations can provoke serious alterations in the data, like the rise of false peaks in the power spectrum.

- **Other affecting factors.**
  The main factor that affects the oscillation signal is the pulsation damping. In this case Eq. (4.5) is rewritten as:

$$v(t) = a_0 \cos(\omega_0 t - \delta_0) e^{-\eta t}$$

being η the damping rate. The power spectrum in the ideal case of an infinite time series is:

$$P(\omega) = \frac{1}{4} \frac{a_0^2}{(\omega - \omega')^2 + \eta^2}$$

which correspond to a Lorentian profile with HWHM equal to η. For the real case, with a time of observation T, the peak earns the intermediate form between the Lorentian profile and the sinc^2 function. In the other borderline case of small observation time it tends to the latter. In the case of the Sun, the combination of the stochastic nature of the oscillation driving with the exponential decay, provides a Lorential profile.

Another factor to taking into account is the noise from the Earth and stellar atmospheres, assumed as a random variable oscillation. It, added to the stellar signals, can affects their amplitudes and phases. The noise influence can be reduced increasing the time of observation.

4.3.1 Real data with the Discrete Fourier Transform

As previously shown, with real data we are not able to obtain observations lasting for an infinite period of time and our sampling can't be continuous and equally spaced. Therefore we are not allowed to use the classical definition of the Fourier transform, $F(\nu)$, for a function $f(t)$ variable with the time, defined as:

$$F(\nu) = \int_{-\infty}^{+\infty} f(t) e^{i2\pi\nu t} dt, \tag{4.11}$$

which represents a complex number [1] and consists of a series of delta functions at particular frequencies. In the case of a real data which represent a discrete sampling, $f(t_k)$, we introduce the Discrete Fourier Transform (DFT) as shown in Deeming 1975 [62].

$$F_N(\nu) \equiv \sum_{k=1}^{N} f(t_k) e^{i2\pi\nu t_k}. \tag{4.12}$$

[1] The integral in Eq. (4.11) exists only if the function $f(t)$ is absolutely integrable, i.e. if $\int \mid f(t) \mid dt$ exists. Thus periodic functions are excluded from this definition because they are not absolutely integrable.

Using the same notation we can define the corresponding window function as follow:

$$w_N(t) \equiv \frac{1}{N}\sum_{k=1}^{N}\delta(t-t_k), \tag{4.13}$$

as well as the spectral window:

$$W_N(\nu) \equiv \frac{1}{N}\sum_{k=1}^{N}e^{2\pi\nu t_k}. \tag{4.14}$$

As seen in the previous Section the DFT is the result of the convolution between the full Transform $F(\nu)$ with the spectral window:

$$\frac{F_N}{N} = (F \otimes W_N)(\nu). \tag{4.15}$$

If $F(\nu)$ is a δ-function at frequency ν_1, then $F_N(\nu)/N$ will have the same behavior as the spectral window $W_N(\nu)$. Comparison between F_N/N and $W_N(\nu)$ near the frequency ν_1 helps to conclude if ν_1 is real or not. Whenever $F(\nu)$ is a sum of m δ-functions then $F_N(\nu)/N$ is the sum of m spectral windows centred at different frequencies. Because of this fact we expect to observe interference among the peaks, producing the already mentioned phenomenon of aliasing.

There are many softwares or codes that provide tools for the analysis of time series, such as Period04 (Lenz & Breger 2004 [109]) and SigSpec (Reegen 2007 [130]). Nevertheless the development of a personal code gives the possibility to intervene directly on the code or modify some part of the computations depending on the possible cases. Even in this case we used the programming language IDL for the development of a series of procedures for power spectrum analysis. A description of these procedures is provided in this Section, while a schematic view of the process' sequence can be found in Appendix A.

The procedure that we used to perform the frequency analysis is based on the algorithm defined in the paper of Deeming (in 1975 [62]) which proposed the use of the Discrete Fourier Transform (DFT) for finite and unevenly time series. The DFT for the time series described by the function $x = f(t_k)$ and shown in Figure (4.9, *Left panel*) is defined as:

$$F_N(\nu) = \sum_{k=1}^{N} f(t_k)e^{i2\pi\nu t_k}. \tag{4.16}$$

where N is the number of data points, each collected at the time t_k. According to Deeming we can calculate the normalized power P_N as:

$$P_N = \frac{|F_N|^2}{N^2} = \frac{(\sum_{k=1}^{N} x\cos(2\pi\nu t_k))^2 + (\sum_{k=1}^{N} x\sin(2\pi\nu t_k))^2}{N^2}. \tag{4.17}$$

Since the calculated power corresponds to

$$P_N(\nu) = \frac{A^2}{4} \tag{4.18}$$

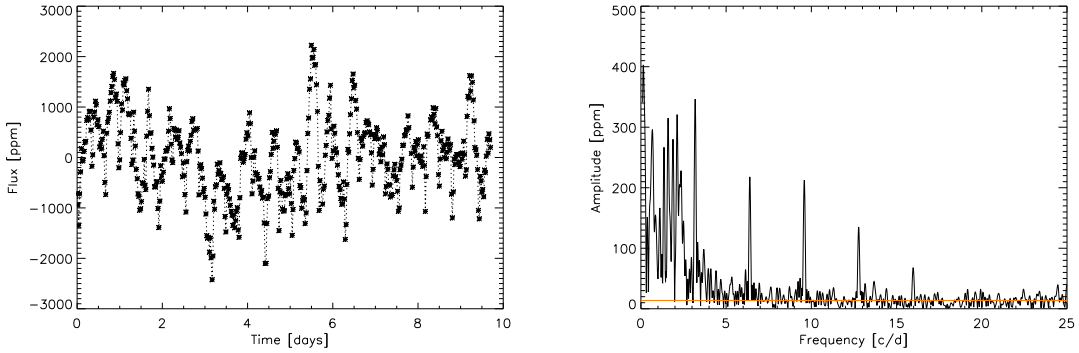

Figure 4.9: *Left panel*: Light curve for a Kepler target (namely a hybrid γ Dor/δ Sct star). *Right panel*: Amplitude spectrum of the time series in left panel. The horizontal line indicates the level of the white noise of the spectrum.

the amplitude spectrum of the time series in Figure (4.1) is shown in Figure (4.9), with the addition of the white noise level, defined by the median of the power at the high frequencies. Finally, the phase is given by:

$$\phi = \arctan \frac{F_{N_i}(\nu_i)}{F_{N_r}(\nu_i)} \tag{4.19}$$

In order to avoid that the sampled signal is ambiguously represented, we need to fix the Nyquist frequency, generally indicated as the upper frequency limit. According to the Sampling Theorem by Nyquist and Shannon the Nyquist frequency is equal to half of the sampling frequency, but only in the case of evenly time series. With real data we can use two different approaches:

- if the data are approximately even, such as the observations provided by a satellite with high duty cycle, the Nyquist frequencies can be computed as follows:

$$\nu_{nyq} = \frac{1}{2 \cdot median(t_{k+1} - t_k)}; \tag{4.20}$$

- if the data are characterized by remarkable gaps, such as the daily interruption in ground based observations or the merging of independent time series, a conservative value of the Nyquist frequencies is given by:

$$\nu_{nyq} = \frac{1}{2\Delta t}. \tag{4.21}$$

where Δt is the largest temporal interruption.

The power or amplitude spectrum of a periodic phenomenon is not free from sources of noise, which can be of several types. The temporal distribution of the data (that in a real case won't be perfectly even), the finite number of the measurements over the interval [0,T] and the presence of simultaneous beatings are responsible for the rising of spurious peaks in the power spectrum. All of these peaks (real or false) can interfer with the other ones, giving rise to the phenomenon of aliasing. As already pointed out in previous Sections, the distribution of the data is described by the window function ($w_N(t)$) and by

its Fourier Transform, the so called spectral window ($W_N(\nu)$). Figure (4.10) shows the spectral window of the time series shown in Figure (4.9, Left panel), characterized by the peak at $\nu = 0$ having a width equal to the inverse of the total time of the observations (T^{-1}, corresponding to the width of a *sinc* function and comparable to the resolution of the spectrum, see below). These data are the results of the long term, uninterrupted and almost even monitoring of Kepler, therefore significative secondary peaks due to the daily aliases (at multiples of ± 1 cycles per day $[c/d]$ or multiples of ± 11.57 μHz) or other due to peculiarities of the data spacing to are not present. Some Kepler instrumental effects are known and tabulated ($\nu \sim 32d^{-1}$, $\sim 400d^{-1}$, $\sim 430d^{-1}$, $\sim 690d^{-1}$), but in this case they don't affect the spectral window.

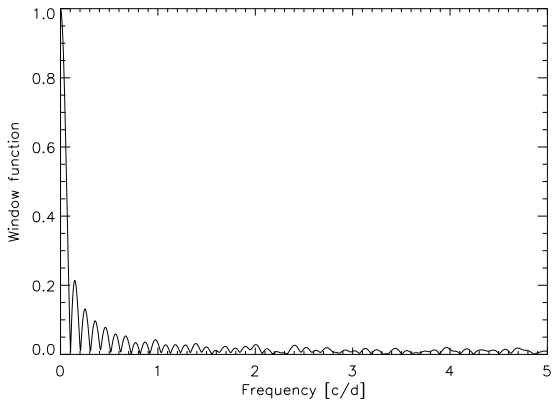

Figure 4.10: Spectral window corresponding to the time series shown in Figure (4.9).

In order to show how the temporal distribution of the data can affect a time series we computes the amplitude spectrum of the main component of our time series, defined as a sinusoidal function having the frequency of the highest peak in the power spectrum (recognizable at $\nu = 0.1405d^{-1}$), its amplitude and its phase. Figure (4.11) shows the comparison between the spectrum of this time series and the same one but evenly spaced. We add two further simulated time series as well, in order to evaluate the behaviour of the amplitude spectra increasing the number of data points. As shown in the plot, the more the number of points is high, the more the function becomes a *delta* function, centred at the value of ν_{max}.

As briefly mentioned above, a rough estimate of the frequency resolution in a power spectrum is the width of the main peak of a *sinc* function. Similarly we can say that two different frequencies, ν_i and ν_k can be well resolved if $T \gg 1/|\nu_i - \nu_k|$. Whenever this relation is not satisfied, peaks in the periodogram can interfere and obstruct the identification of the frequencies. According to Loumos & Deeming [110] a more accurate expression of the minimum separation of two different frequencies is:

$$\frac{1}{T} < |\nu_i - \nu_k| < \frac{1.5}{T}. \tag{4.22}$$

They also define as $2.5/T$ the minimum distance between two peaks that don't undergo interference, since the first sidelobe of one *sinc* function no longer interferes with the main peak of the other *sinc* function.

Once we have calculated the amplitude spectrum, we can proceed to extract the oscillation frequencies of the target, using a technique known as *prewhitening*. Since our time

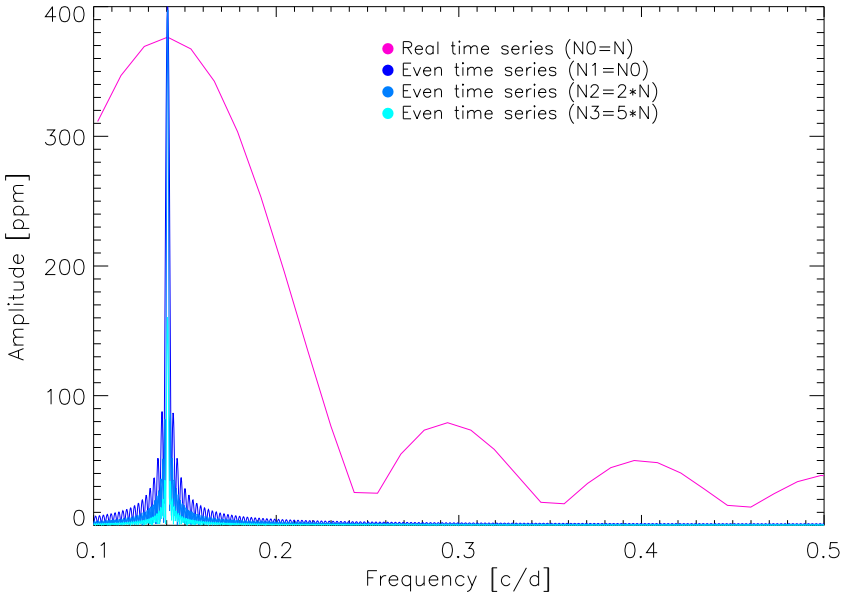

Figure 4.11: Amplitude spectrum of the time series in Fig. (4.9) described only by the main component ($\nu = 0.1405d^{-1}$). In the plot is represented the same time series but with different sampling and different number of data point. The real time series is the one affected by peculiarities in the sampling, responsible for the rising of spurious peaks.

series is equal to the sum of all the periodic components of the analysed signal, we can identify the most powerful peak in the spectrum and describe it as a periodic function as in Barbieri et al. 1977 ([11]) :

$$f(t) = \langle B \rangle + \sum_{i=1}^{N} [4P_N(\nu_i)]^{1/2} \cdot \cos(2\pi\nu_i t - \arctan(\frac{F_{N_i}(\nu_i)}{F_{N_r}(\nu_i)})) \tag{4.23}$$

where $\langle B \rangle$ is the mean value of the time series and $F_{N_r}(\nu_i)$ and $F_{N_i}(\nu_i)$ are the real and imaginary part of F_N. We adopted the IDL least-squares `MPFIT` package[2], implemented from the Levenberg-Marquardt algorithm, in order to optimize amplitude and phase (the frequency remains generally fixed) and to minimize a merit function of the type:

$$\chi^2 = \sum_{i=1}^{N} w_i(y_i - y(t_i; a_1, a_2, ..., a_k))^2 \tag{4.24}$$

where w_i are the weights of each point of the time series and $a_1, a_2, ..., a_k$ are the coefficients of the fitting function to optimize. The starting values of these coefficient are set as the extracted frequency, amplitude and phase from the periodogram. When we have obtained the best fitting function we subtract this function to the time series and then we compute a new power spectrum which is characterized by a new highest peak. We try to fit again the time series with Eq. (4.23), using the new frequency, amplitude and phase. Then we repeat the procedure subtracting the fitting function to the residual time series and compute a

[2]http://www.physics.wisc.edu/∼craigm/idl/idl.html

new power spectrum. This iterative procedure is stopped once the highest peak in the power spectrum has a signal to noise ratio less than 3 times the white noise, defined as the median power at high frequencies, or in a part of the power spectrum free from stellar oscillation modes.

Once we have defined the best values of frequencies, amplitudes and phases we can also assign their uncertainties. As pointed out by Aerts et al. 2010 [2] there are some conditions to satisfy, at least as first approximation. These conditions are:

- the times of the measurements (t_k) and the reference time (t_0) should be error free; this situation is generally satisfied when the ratio of the integration time to the oscillation periods (i.e. the *temporal resolution*) is less than 1%;
- the white noise should be uncorrelated, with average equal to zero and constant variance, σ_N^2 , in time;
- there should not be interference between true frequencies and noise peaks, even if this condition is seldom satisfied.

If these conditions are satisfied we can define the values of the uncertainties as follow:

$$\sigma_\nu = \frac{\sqrt{6}\sigma_N}{\pi\sqrt{N}AT}, \qquad \sigma_A = \frac{\sqrt{2}}{\sqrt{N}}\sigma_N, \qquad \sigma_\phi = \frac{\sigma_N}{\pi\sqrt{2N}A} \tag{4.25}$$

where T is the total time of the observations and A is the amplitude (see Bloomfield 1976, [26]; Cuypers 1987, [59]; Montgomery & O'Donoghue 1999, [121]). If the errors estimates of the single measurements are not available, it is common to use, instead of σ_N^2, the standard deviation of the residuals after the prewhitening process.

The time series of the residuals can be analysed in order to investigate the noise properties of the measurements. We follow the approach of Butler et al. 2004 [34] and Leccia et al. 2007 [106], and we analise the ratio $|r_i/\sigma_i|$, where r_i are the residuals and σ_i the uncertainties in the measurements. Since the uncertainties available for Kepler time series are too low (of the order of $\sim 0.01\%$) we decided, to be conservative, to use the r.m.s. of the light curve as σ. Figure (4.12) shows the cumulative histogram of $|r_i/\sigma|$ compared with a gaussian distribution. It shows a departure from the normal behaviour for data points characterised by $|r_i/\sigma| > 1.6$, and extreme outliers for $|r_i/\sigma| > 2.5$. The ratio between the observed points and the corresponding ones along the Gaussian trend provides the fraction, f, of data to be considered as 'good', namely the ones close to the unity (see Figure (4.13)). According to Butler et al. 2004 [34], the quantity f is useful to determine the weights to apply to the weighted amplitude spectrum as:

$$w_i = \frac{1}{\sigma_i^2 f}. \tag{4.26}$$

The weighted spectrum is a very important issue in the frequen case in which the time series is represented by the merging of two or more sets of data. What can happens is that the time series is composed by data taken with different instruments (as usually happens with ground-based observing networks), or with large temporal gaps, so the weighting of different measurements is a crucial task in order to obtain a reliable analysis. There are several approaches to this problem. One is the approach of Butler et al. 2004 [34], mentioned above. The method that we used in the framework of the EXOTIME project (see Section 2.2.3) consists first of all on the extraction of all the possible frequencies in

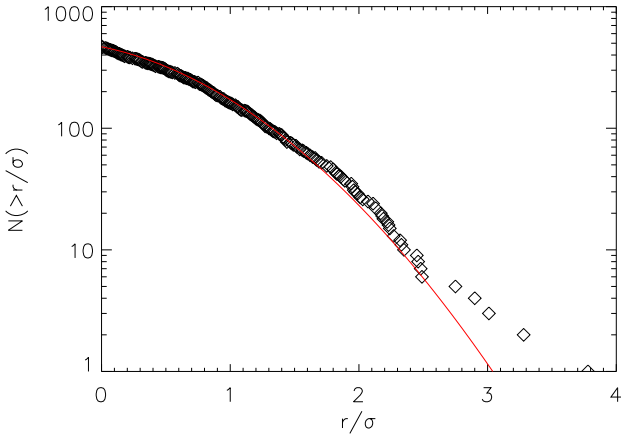

Figure 4.12: Cumulative histogram of $|r_i/\sigma|$ for Kepler data of the target KIC001573064 obtained in the first observation quarter Q0. The distribution of the red diamonds follows the normal one (solid line) up to a value $|r_i/\sigma| < 1.6$.

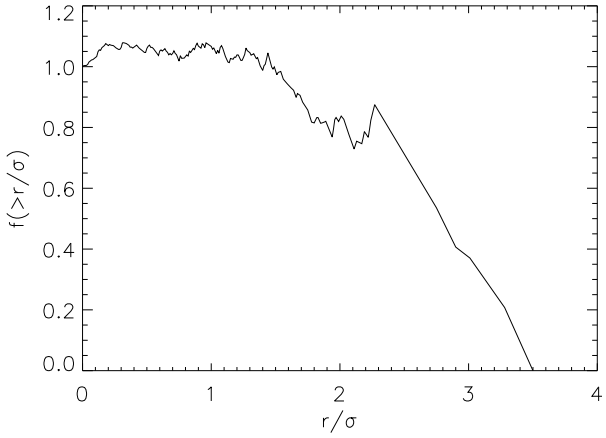

Figure 4.13: The ratio between the observed and the expected histograms, indicating the fraction of 'good' data points.

an unweighted power spectrum. Then we assign the weight for each datum as the inverse of the standard deviation of the residual time series, computed over a range of about 100 points centred in that particular point (see Silvotti et al. 2006 [140]).

After this process in which we assign the weights w_k for each datum of the time series we are able to compute a weighted power spectrum, rewriting Eq. (4.17) as:

$$P_N = \frac{|F_N|^2}{N^2} = \frac{(\sum_{k=1}^{N} w_k x \cos(2\pi\nu t_k))^2 + (\sum_{k=1}^{N} w_k x \sin(2\pi\nu t_k))^2}{N^2}. \quad (4.27)$$

4.4 Frequency analysis of Hybrid stars in the Kepler field

We applied our tools in the framework of a project defined for the KASC Working Group 10 (dedicated to the study of γ Doradus stars). This is only a part of a huge work for the classification and comprehension of the seismic characteristics of a large sample of A-F spectral type pulsators. As already shown in Section 1.5.3, thanks to the first observations provided by Kepler, stars like γ Doradus (hereafter γ Dor) and δ Scuti (hereafter δ Sct) showed hybrids behavior between the two classes. A paper by K. Uytterhoeven and the WG10 is in preparation with the aim to analyse the seismic characteristics and try to characterize the very large sample of A-F stars in the Kepler field of view. The total sample is composed by almost 800 stars, some of them are observed with both the observing modes available, namely the long and short cadence. The former case is suited to detects long periodicities (g-modes), having a time resolution of about 30 minutes, while the latter detects frequencies of shorter timescales (p-modes), having a one minute sampling.

Our contribution in this work consisted in the extraction of the frequencies for 20 stars of the sample, 10 observed with the long cadence and 10 with the short cadence. After the conversion of the flux to part per million and the correction of the trend due to the instrumental drifts, we apply the statistical analysis tool to each star. An example of the analysis for one of these objects was already provided in Section 4.2. We then proceed to perform the extraction of the frequencies, taking as an example the light curve in Figure (4.1). The amplitude spectrum of this time series, obtained with the Deeming's algorithm is shown in Figure (4.14), where also the modes with $SNR > 4$ are indicated. From this spectrum we extracted 36 frequencies, listed in Table (4.1) with their amplitude and phase and the formal uncertainties defined in Eq. (4.25).

Figure (4.15) shows the residual time series and amplitude spectrum. Figure (4.16) shows in red the fitting function for the analysed time series obtained from the sinusoidal fit calculated as the sum of all the extracted frequencies.

According to the Kepler Input Catalog, this star is labelled as γ Dor, and its global parameters are defined in Table (4.2). However a quick look to the amplitude spectrum clearly shows that several pulsation g-modes typical for γ Dor stars are present, but all the components with frequency $\nu > 3$ [c/d] are all due to p-modes pulsations, typical for δ Sct stars, showing thus a hybrid behavior.

4.5 Analysis for Solar-like oscillations

The frequency analysis explained so far can be generally applied to all the pulsating stars. As already described in Chapter 1, solar-like oscillations show particular features, suited to be investigated with further analysis, taking advantage of the asymptotic regime. First of all the presence of a 'hump' in the frequency spectrum modulated by a Lorentian function

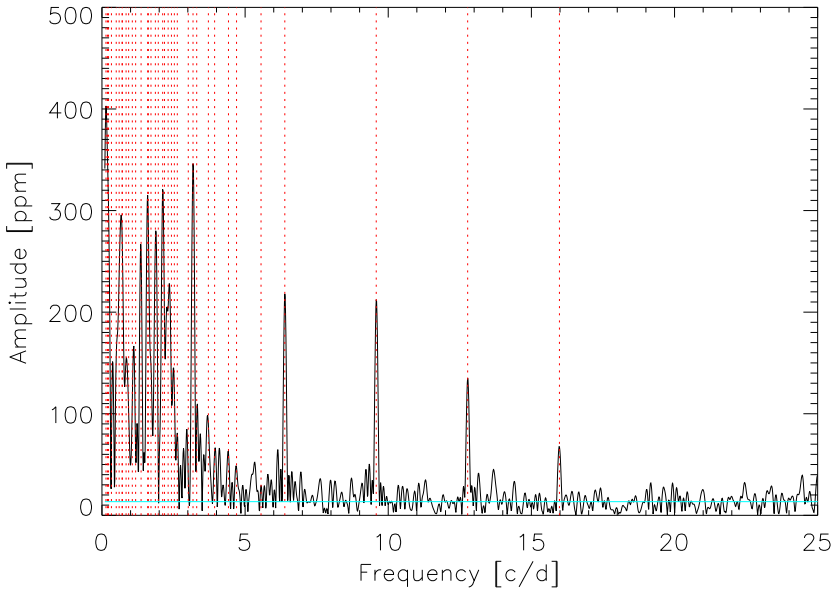

Figure 4.14: Amplitude spectrum of the labelled γ Dor star KIC001573064, using the long cadence time series.

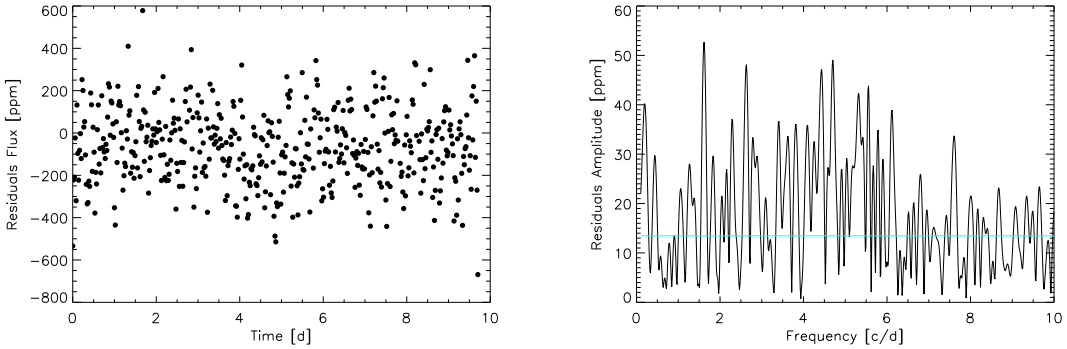

Figure 4.15: Time series and amplitude spectrum of the residuals after the prewhitening process.

#	Frequency ν [c/d]	$\delta\nu$ [c/d]	Amplitude A [ppm]	δA [ppm]	Phase ϕ [rad]	$\delta\phi$ [rad]
1	0.1405166	0.0000715	403.0021469	0.5071381	-0.3444051	0.0000962
2	3.1807845	0.0000826	348.7093960	0.5071381	2.7460748	0.0001112
3	2.1205230	0.0000882	326.5478149	0.5071381	1.9415751	0.0001187
4	1.5967794	0.0000929	310.1767091	0.5071381	3.0210462	0.0001250
5	0.7025829	0.0000925	311.3689262	0.5071381	1.5857665	0.0001245
6	1.8650383	0.0000993	290.0537607	0.5071381	-1.7053410	0.0001336
7	1.3668432	0.0001146	251.5134650	0.5071381	2.8069136	0.0001541
8	2.3121366	0.0001194	241.4233113	0.5071381	1.1938663	0.0001606
9	0.2299362	0.0001200	240.1172940	0.5071381	-1.4776286	0.0001614
10	6.3871176	0.0001356	212.5679031	0.5071381	1.5687779	0.0001824
11	9.5806763	0.0001429	201.6539431	0.5071381	0.7653168	0.0001922
12	0.6003890	0.0001585	181.8360444	0.5071381	-2.9821537	0.0002132
13	2.5292986	0.0002102	137.0667755	0.5071381	-0.8335943	0.0002828
14	2.1843942	0.0002177	132.3408037	0.5071381	-1.4204627	0.0002929
15	12.7742351	0.0002255	127.7817813	0.5071381	0.0159082	0.0003034
16	0.8430995	0.0002361	122.0240105	0.5071381	1.9587582	0.0003177
17	0.4981952	0.0002419	119.1357419	0.5071381	-1.3743069	0.0003254
18	3.0147195	0.0002514	114.6103404	0.5071381	1.4441830	0.0003382
19	1.7117475	0.0002559	112.6050414	0.5071381	1.1772134	0.0003442
20	1.0602615	0.0002605	110.6055903	0.5071381	-0.1410340	0.0003505
21	0.9325192	0.0002947	97.7734583	0.5071381	-2.0230849	0.0003965
22	3.7173024	0.0002902	99.2789575	0.5071381	-0.7645612	0.0003905
23	2.4271047	0.0003213	89.6781920	0.5071381	-2.3839997	0.0004323
24	0.3321301	0.0003700	77.8824166	0.5071381	0.0033890	0.0004977
25	3.3085269	0.0004061	70.9583780	0.5071381	-2.9490924	0.0005463
26	15.9805681	0.0004223	68.2377422	0.5071381	-1.1284151	0.0005681
27	1.1752296	0.0004802	60.0028272	0.5071381	2.0061483	0.0006460
28	3.9344644	0.0004801	60.0243136	0.5071381	-2.5410986	0.0006458
29	1.9672322	0.0004998	57.6487624	0.5071381	0.5076527	0.0006724
30	0.7153572	0.0005296	54.4138165	0.5071381	-0.1403503	0.0007124
31	1.6223279	0.0005468	52.6961365	0.5071381	-2.8956825	0.0007356
32	4.7009185	0.0005857	49.1949034	0.5071381	-1.2964869	0.0007880
33	2.6314924	0.0005839	49.3491672	0.5071381	-2.5839614	0.0007855
34	5.5567923	0.0006691	43.0662625	0.5071381	-2.5432950	0.0009001
35	0.1916135	0.0006673	43.1830041	0.5071381	-2.3500321	0.0008977
36	4.4198853	0.0006867	41.9636364	0.5071381	0.7080268	0.0009237

Table 4.1: Result of the frequencies extraction for the target KIC001573064, with the corresponding amplitude and phase and computation of the uncertainties.

Magnitude	$R/R_\odot$	T_{eff}	$\log g$	$[Fe/H]$
12.764	10.682	4633	2.537	-0.037

Table 4.2: Stellar global parameters for KIC001573064.

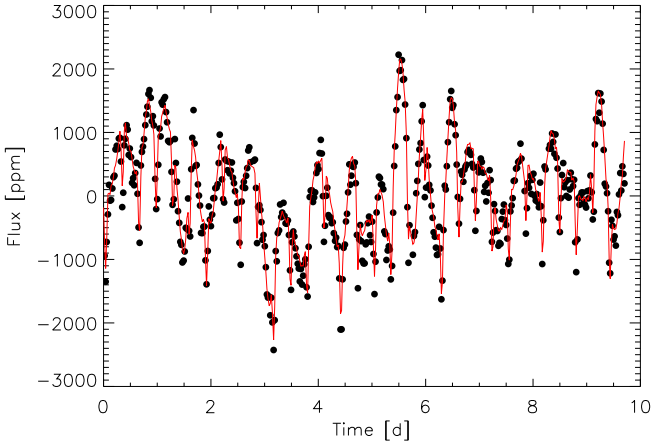

Figure 4.16: The analysed time series is overlapped by the sinusoidal fit obtained with the sum of all the extracted components.

is the clearer evidence of solar-like oscillations detection. The magnification of this part of the spectrum, generally known as power excess, reveals a regular frequency pattern which is another typical feature of this kind of pulsators, as shown in Figure (1.14) for the solar case. This periodicity in the frequencies is nothing but the large separation $\Delta\nu$. The most important technique used to evaluate this quantity consists in the computation of the so called *comb-response function* (CR). It is similar to the computation of the power spectrum of the power spectrum ($PS \otimes PS$), but preferable in comparison to the latter because it is less affected by possible gaps in the data. According to Kjeldsen et al. 1995 [101] this function is defined as:

$$\begin{aligned} CR(\Delta\nu) \quad = \quad & PS(\nu_{max} - \frac{1}{2}\Delta\nu)PS(\nu_{max} + \frac{1}{2}\Delta\nu)PS(\nu_{max} - \Delta\nu) \\ & PS(\nu_{max} + \Delta\nu)[PS(\nu_{max} - \frac{3}{2}\Delta\nu)PS(\nu_{max} + \frac{3}{2}\Delta\nu) \\ & PS(\nu_{max} - 2\Delta\nu)PS(\nu_{max} + 2\Delta\nu)]^{0.5}. \end{aligned} \tag{4.28}$$

In Eq. (4.28) the quantity PS is the power spectrum of the oscillations frequencies, ν_{max} the frequency corresponding to the higher value of the power and $\Delta\nu$ is defined in a range of possible values of the large separation. The presence of a high peak, centred in a particular value of $\Delta\nu$, indicates the existence of a regular series of peaks in the spectrum, centred in ν_{max} with a spacing of $\frac{1}{2}\Delta\nu$. Figure (4.17) shows the comb response function for the data collected for the star μ Herculis in Bonanno et al. 2008 [28]. The largest value of the function corresponds to a large separation equal to 56 μHz, in agreement with the theoretical predictions.

Once the large frequency separation is known, it is possible to create the echelle diagram (presented in Section 1.4.4) that allow a simple illustration of the properties of the frequency spectrum. Since modes with the same angular degree lay in vertical lines, the echelle diagram is useful also for their identification.

The frequency spectrum is not only affected by stellar oscillations, in fact other stellar phenomena produce significant signatures useful to extract further informations about the effects taking place at the stellar surface. The most important components, aside from

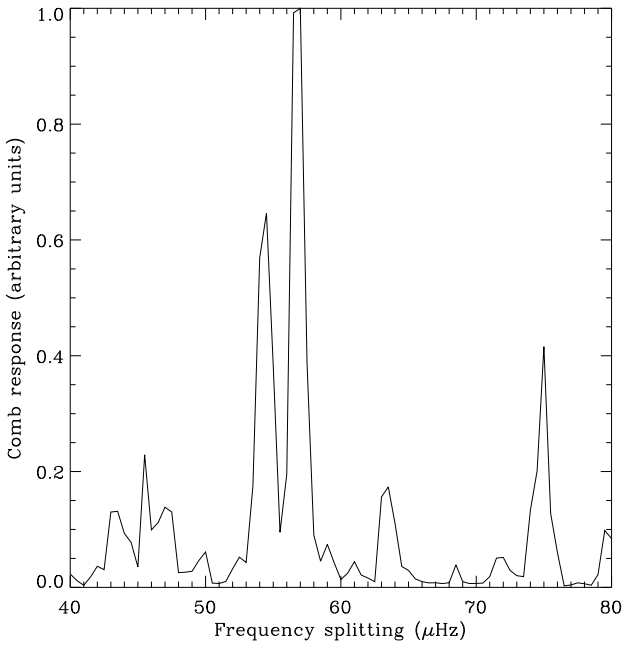

Figure 4.17: Plot of the comb-response function from data collected for the subgiant star μHer (Bonanno et al. 2008 [28]).

the white noise already discussed in Section 4.3.1, are the stellar activity and granulation, rising in a frequency range lower than the one for solar-like oscillations. These 'background' components were modelled by Harvey 1985 [84] for the solar case. Aigrain et al. 2004 [3], by using the same type of model represented the background as a sum of N power laws, representing separate phenomena, of the type:

$$P(\nu) = \sum_{i=1}^{N} P_i = \sum_{i=1}^{N} \frac{A_i}{1 + (B_i \nu)^{C_i}}, \tag{4.29}$$

where A_i and B_i are the amplitude and characteristic timescales of the i-th component, while C_i is the slope of the power law. Figure (4.18) reports the same image shown in Aigrain et al. [3], in which they fit the background of the power spectrum obtained through a simulated time series containing stellar micro-variability such as granulation and activity signatures. The thick black line results from the funtion defined in Eq. (4.29) as the sum of the three components (including white noise), represented by dashed lines.

4.5.1 Some results from Kepler

The first detections of solar-like oscillations using Kepler data were reported by Chaplin et al. 2010 [37] for three solar-like stars. Since we were provided by the power density spectra of these objects and we had the possibility to follow the discussion about the analysis conducted for the paper, we attempt to create the previously discussed procedures (written in IDL language) in order to extract informations about these targets, having the opportunity to compare them with the ones obtained by Chaplin et al. [37]. In the following we discuss the results of our 'exercise'.

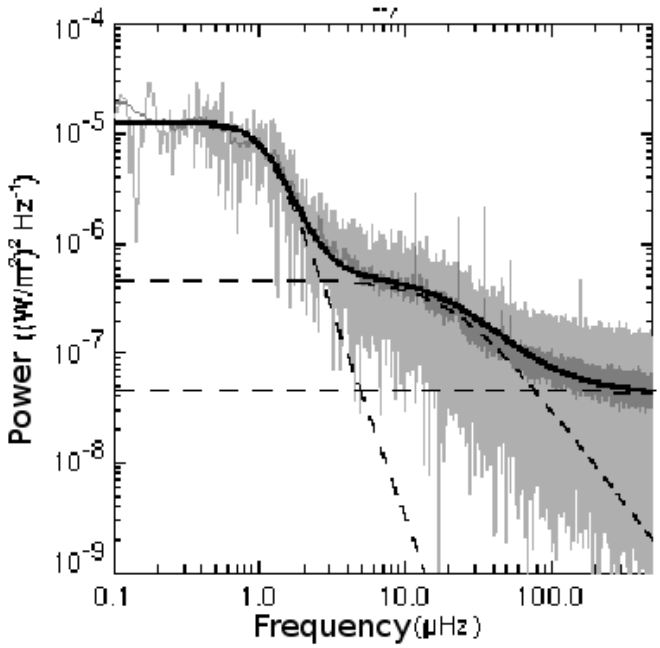

Figure 4.18: Power spectrum of a simulated light curve containing stellar micro-variability showed in Aigrain et al. 2004 [3]. The thick black line indicate the multi-component power law used to model the background, resulting by the sum of the single components indicated by the dashed lines (activity, granulation and white noise).

The targets at issue are three solar-like stars, KIC11026764, KIC3656476 and KIC-6603624, observed by Kepler during its first month of science operations, with short sampling cadence (about one minute), suited to detect the short-timescale of solar-like oscillations. Table (4.3) summarizes the main parameters of these stars according to the Kepler Input Catalog (KIC). At first, as a preliminary analysis we computed a smooth

KIC-ID	RA	DEC	Kepler Magnitude	$T_{eff}[K]$	$R/R_\odot$	$M/M_\odot$
3656476	19 36 48.79	+38 42 56.8	9.516	5666	1.31	1.04
6603624	19 24 11.21	+42 03 09.7	9.087	5790	1.18	1.05
11026764	19 21 24.65	+48 30 53.2	9.303	5760	2.10	1.10

Table 4.3: Stellar global parameters found in the Kepler Input Catalog for the three stars KIC11026764, KIC3656476 and KIC6603624.

for each power spectrum, by using a boxcar, that highlight the characteristic features of the spectra, in partcular the clear presence of the power excess centred at $\nu_{max} \sim 954\mu$Hz for KIC11026764, $\nu_{max} \sim 1854\mu$Hz for KIC3656476 and $\nu_{max} \sim 2308\mu$Hz for KIC6603624. Figure (4.19) shows the power density spectra for the three stars, overlapped by the resulting smoothing function (light blue lines), the white noise (green line) and the power level of 4σ (red line).

After that, following the example of Aigrain et al. 2004 [3] as well as of Chaplin et al. 2010 [37] we evaluate the several components of the power spectra background. In

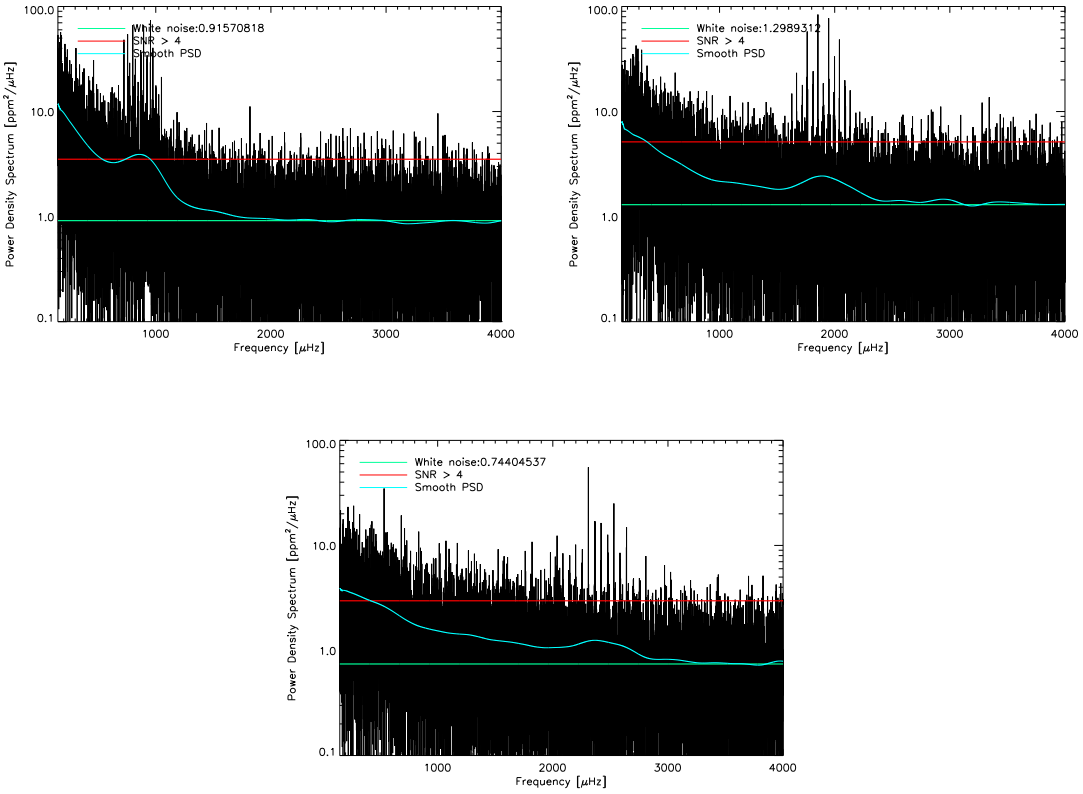

Figure 4.19: Power spectra modelled by a smooth function for: *Left upper panel*: KIC11026764; *Right upper panel*: KIC3656476; *Lower panel* KIC6603624.

order to have the possibility to compare the background model obtained using Eq. (4.29), we recomputed the same smoothing function avoiding the frequency range of the excess of power. Then we adopted the IDL `MPFIT` package[3] as in Mathur et al. 2010 [113]. This procedure performs a least-squares fit between the smoothed spectrum and a specific function. In this case we adopted the formulation in Hekker et al. 2010 [86] for the modelling of stellar granulation and activity:

$$B(\nu) = \frac{p_{gran}}{1 + (\tau_{gran}\nu)^a} + \frac{p_{act}}{1 + (\tau_{act}\nu)^2} + b, \tag{4.30}$$

where p_{gran} and p_{act} correspond to the power level for granulation and activity signals, while τ_{gran} and τ_{act} are the time-scales for these two phenomena, described by two different power laws (a and 2 respectively). Finally, b is the offset due to the white noise of the spectrum. We computed the model function with a set of guess values starting to the ones used by Hekker et al. 2010 [86], so p_{act} is equal to the maximum value of a binned power spectrum and $p_{gran} = p_{act} \times 10^{-1}$, $\tau_{act} = 100,000$, $\tau_{act} = 1,000$, and b as defined in Section 4.3.1. The procedure runs until a best-fit between the smoothed background and the model function is reached. Figure (4.20) shows the results obtained with this procedure for the three stars. The power spectra (in grey) are overlapped by every single background components defined by the dashed lines (from the top of the plots: activity, granulation and white noise) and by their sum, defined by the thick black line. The results produced with this fit are listed in Table (4.4).

KIC-ID	Power activity $[ppm^2/\mu\text{Hz}]$	Power granulation $[ppm^2/\mu\text{Hz}]$	Granulation power law	White noise $[ppm^2/\mu\text{Hz}]$
3656476	5.24	0.30	3.6	1.26
6603624	2.76	0.18	3.6	0.68
11026764	9.25	1.50	3.6	0.83

Table 4.4: Results of the background fitting performed for the three solar-like stars observed with Kepler.

Now we are interested to analyse the excess of power of the targets. We tryed at first to verify the relation presented by Hekker et al. 2010 [86], according to whom the width of the power envelope can be directly scaled from the solar values. In particular they divide the power spectrum into windows of variable width (w) centred at a particular frequency ($\nu_{central}$). Approximating the central frequency to the frequency of the maximum power, ν_{max}, they obtained:

$$w = \frac{\nu_{central}}{\nu_{max\odot}} w_\odot, \tag{4.31}$$

being $w_\odot = 2000\mu$Hz the extension of the solar power excess. We measured the central frequency as the value of the maximum power obtained by using the smoothed power spectrum shown in Figure (4.19) and calculated the extension of the power excess through Eq. (4.31). Actually, according to our procedure this relation is verified, as shown in Figure (4.21). Only for the target KIC11026764 this estimate results narrower than the expectation. The extension of the power envelope is indicated by the two vertical arrows, according to the relation, above the smoothed power spectrum. For KIC11026764 this

[3] http://www.physics.wisc.edu/∼craigm/idl/idl.html

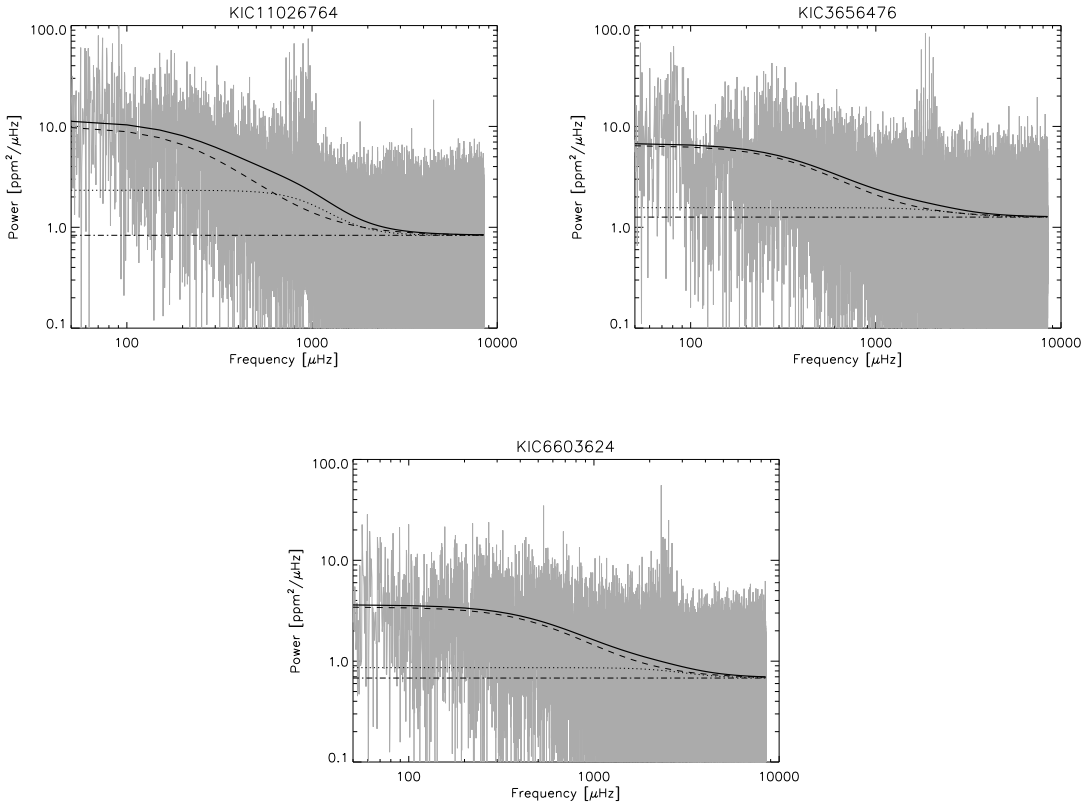

Figure 4.20: Evaluation of the background components for the three power spectra of the targets of Kepler: *Left upper panel*: KIC11026764; *Right upper panel*: KIC3656476; *Lower panel* KIC6603624. The power spectra are in grey, the background fitting is defined by the thick black line, while the single components are defined by the dashed lines.

width is resulted to be 662.6 μHz, for KIC3656476 $w = 1416.6\mu$Hz and for KIC6603624 $w = 1773.5\mu$Hz.

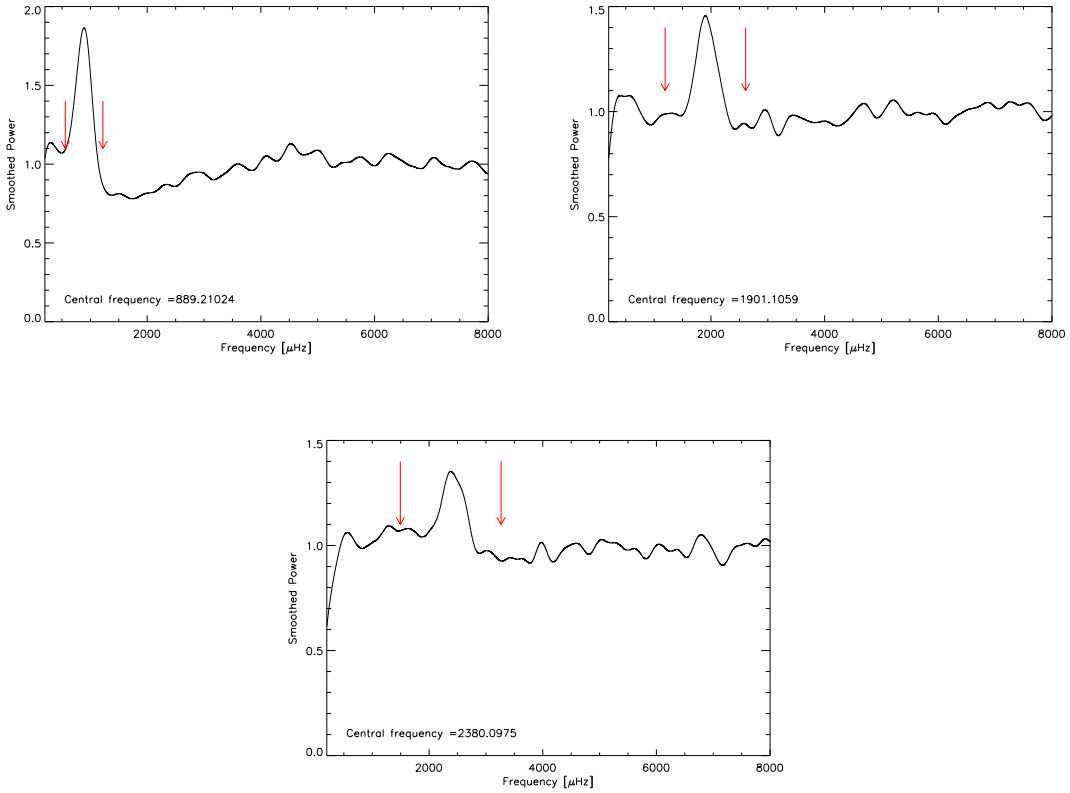

Figure 4.21: Smoothed power density spectra for *Left upper panel*: KIC11026764; *Right upper panel*: KIC3656476; *Lower panel* KIC6603624. The arrows define the range of the automatic determination of the power excess, using the value of ν_{max}.

A further step is the evaluation of the comb response function in order to search for the most probable value of the large separation, $\Delta\nu$. For each possible ν_{max} (determined by taking all the peaks inside the power envelope with Signal to Noise Ratio larger than 4) we applied Eq. (4.28) for the three spectra. In particular the computations were made by using three different sets of trial values of large separation, i.e. by sampling $\Delta\nu$ with a chosen frequency difference of 1, 0.5, 0.25 μHz. The results of each computation is listed in Table (4.5), compared with the theoretical values ($\Delta\nu_{th}$, obtained with the data available from KIC) and the ones measured by Chaplin et al. 2010 [37] ($\Delta\nu_{obs}$). For KIC11026764 and KIC6603624, the agreement is quite good, while for the star KIC3656476 the values are slightly different. However the uncertainties are quite large, and an optimization in the calculation is required. Figure (4.22) shows the value of the comb response functions for the stars KIC11026764 and KIC6603624 evaluated for the measured ν_{max}.

Finally we attempted to find oscillation modes by using our procedure for the frequency extraction. In particular we selected the frequency range suited to search for solar-like oscillation modes by using the automatic determination of the power excess through the already mentioned procedure. Figure (4.23) shows the time series obtained from the first month of Kepler observations and the relative power spectrum in which we marked the

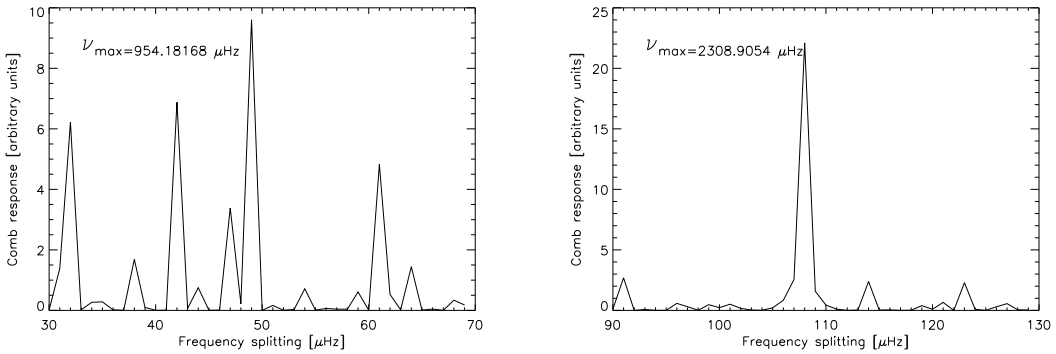

Figure 4.22: Plots of the comb response function for two target: *Left panel:* KIC11026764, *Right panel:* KIC6603624.

	KIC11026764	KIC3656476	KIC6603624
$\Delta\nu_{th}$	46.49 μHz	91.75 μHz	107.84 μHz
$\Delta\nu_{obs}$	50.8 μHz	94.1 μHz	110.2 μHz
$\langle\Delta\nu\rangle_1$	48.39 $\pm$ 10 μHz	98.8 $\pm$ 11 μHz	110.6 $\pm$ 11 μHz
$\langle\Delta\nu\rangle_{0.5}$	49.4 $\pm$ 10 μHz	98.9 $\pm$ 11 μHz	111.1 $\pm$ 11 μHz
$\langle\Delta\nu\rangle_{0.25}$	49.6 $\pm$ 11 μHz	99.9 $\pm$ 11 μHz	110.6 $\pm$ 11 μHz

Table 4.5: Theoretical and observed values of the large separations for the three solar-like targets of Kepler and their determination using the Comb Response function for three different sets of trial values.

frequencies extracted through our procedure.

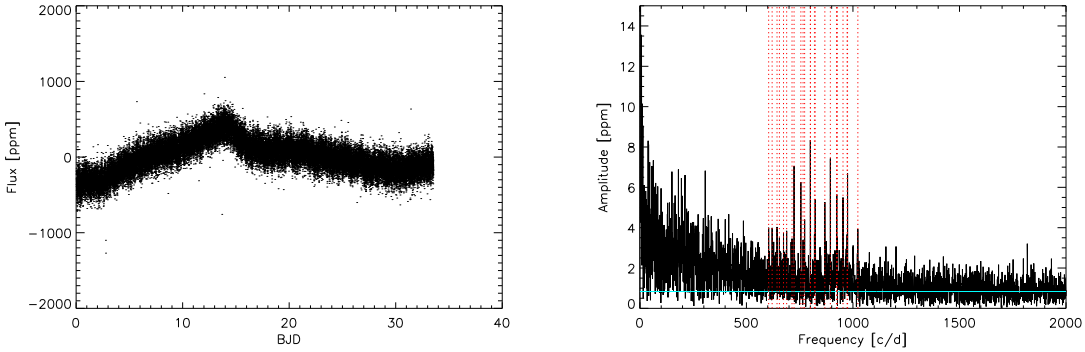

Figure 4.23: Time series of 33.5 days of Kepler data for the star KIC11026764 (*Left panel*) and the corresponding power spectrum and extracted frequencies (*Right panel*).

In order to identify the angular degree of these modes we created an echelle diagram with the resulting frequencies. As already discussed in Chapter 1, the frequencies in the echelle diagram are defined as:

$$\nu_{nl} = \nu_0 + k\Delta\nu + \tilde{\nu}_{nl} \tag{4.32}$$

with ν_0 a reference frequency, k an integer and $\tilde{\nu}_{nl}$ ranging between 0 and $\Delta\nu$. Figure (4.24) shows the echelle diagram for the star KIC11026764. Small triangles represent all the extracted frequencies, which show some disagreements if compared with the echelle diagram presented by Chaplin et al. 2010 [37]. We decided therefore to mark only the ones identified in the paper. Different symbols define different values of l: diamonds for $l = 0$, asterisks for $l = 1$ and plus for $l = 2$. One of the modes with $l = 1$ shows departure

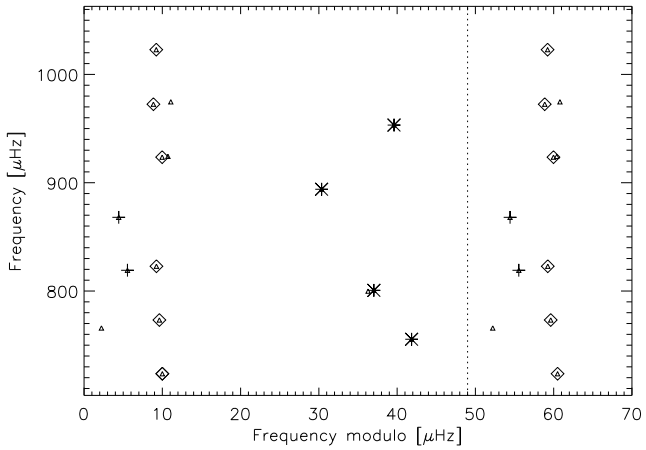

Figure 4.24: Echelle diagram of the extracted frequencies for the target KIC11026764.

from the vertical line, as the asymptotic theory foreseens. This is due to the presence of avoided crossings (Aizenmann et al. 1977 [4], see also Section 1.5.1), clear indicators of stars

significantly evolved, in which the internal g-modes increase their frequencies and interact with the frequencies of p-modes. Table (4.6) shows the results of frequency extraction procedure together with the value of the angular degree l, deduced thanks to the echelle diagram.

l	Frequency [μHz]
0	723.61928
0	773.24312
0	822.86696
0	923.59595
0	972.47913
0	1022.8437
1	755.46742
1	800.64733
1	893.96977
1	953.22212
2	819.16369
2	868.04687

Table 4.6: List of the frequencies extracted for the star KIC11026764 and the corresponding angular degree.

According to the scaling laws (e.g. Eq. (1.72)) we can derive the mean density of these stars. According to our determination of the large separation we calculated $\langle\rho\rangle = 0.2 g/cm^3$ for KIC11026764, $\langle\rho\rangle = 0.73 g/cm^3$ for KIC3656476 and $\langle\rho\rangle = 0.94 g/cm^3$ for KIC6603624. Thanks to this relation together with accurate determination of stellar radius (for instance with interferometry) it is possible to deduce the mass of the stars only with the informations taken from the oscillation frequencies. Further estimation of stellar parameters will be presented in the next Chapter.

4.6 Data analysis for EXOTIME

4.6.1 Photometry of HS0702+6043

In 2008-2009 we performed several observations in the framework of the EXOTIME project (described in Chapter 2). The targets of our observations are listed in Table (4.7). Following the indications of the EXOTIME website, our observing strategy was the same of the other groups and it was also based on the informations in Table (4.7). First of all these targets are faint objects but the constraints on the sampling forced us to use an integration time as smaller as possible. As a result we used a filter to observe these stars at their maximum emission wavelength. Since the readout time of the AFOSC CCD was too high to obtain the required sampling, we decided to read only a part of the frame (with the technique called *windowing*) to decrease it, but at the same time to get an image which includes several comparison stars in order to perform the so called *differential photometry*. In fact the search for stellar oscillations doesn't need of an absolute measure of the stellar flux but only its relative variations, so it is extremely important to have knowledge of systematic effects caused by seeing and airmass variations or the crossing of thin clouds during the exposures. The only way to do this is to include other stable sources than the target, and

TARGET	Coordinates	B mag	Pulsation period [s]	Frequency [μHz]	Amplitude [mmag]	ref.
HS0702+6043	α: 07 07 09.81	14.7	363	2754	21.7	[137]
	δ: +60 38 50.1		383	2606	4.6	[137]
			3600	283	3.7	[137]
PG1219+534	α: 12 21 29.1	12.4	148.7	6721.5	2.9	[129]
	δ: +53 04 37		143.6	6961.4	6.4	[129]
			133.5	7490.8	4.5	[129]
			128.0	7807.8	6.1	[129]
PG1325+101	α: 13 27 48.6	13.45	156.5	6389.0	1.29	[140]
	δ: +09 54 51		137.8	7255.5	27.12	[140]
			134.5	7431.1	1.12	[140]

Table 4.7: Target stars of the EXOTIME sample observed in Asiago. The values on pulsation periods, frequencies and pulsation amplitudes are reported from: [137] = Schuh et al. 2006, [129] = Ridder et al. 2009, [140] = Silvotti et al. 2006.

to detect every possible variations, and use them as reference during the analysis. Thanks to this shrewdness it would be possible to set limits on the noise levels, the instrumental stability and therefore the intrinsic accuracy of variability. This is briefly the principle of the differential photometry. This technique doesn't need of photometric weather that represents a very important advantage and allows to use unuseful nights for the absolute photometry. Figure (4.25) shows one frame of the field for HS0702+6043, taken during the run of February 2009. The locations of the target and of the four comparison stars are indicated.

The images have been treated using the Image Reduction and Analysis Facility IRAF, applying the standard calibrations (bias and flat field) and following a standard reduction procedure defined for the EXOTIME project. In the following points are reported the main steps of the performed reduction and data processing:

- creation of the masterbias and masterflat images and correction of the scientific frames;
- searching for the stellar sources and their pixel coordinates within the frames through the IRAF task *daofind*;
- alignment of all the images using the defined coordinates reference;
- choosing the reference stars suited for differential photometry using the following constraints: stars close to the target, stars with the same color of the target, isolated stars, bright stars. Another requirement is to choose a star quite far from the edges of the images, sets by the possible drift of the instrument during the observations or the trimming of the images during the data reduction phase;
- obtaining the aperture photometry using the task `digiphot` > `apphot` > `phot` for a series of apertures with radii between 3 to 11 pixels, obtaining 9 time series for each source in each frame.

As outcome we obtain for each image and for each aperture useful informations, e.g. the stellar flux, the total flux (from the star and from the background) and the instrumental

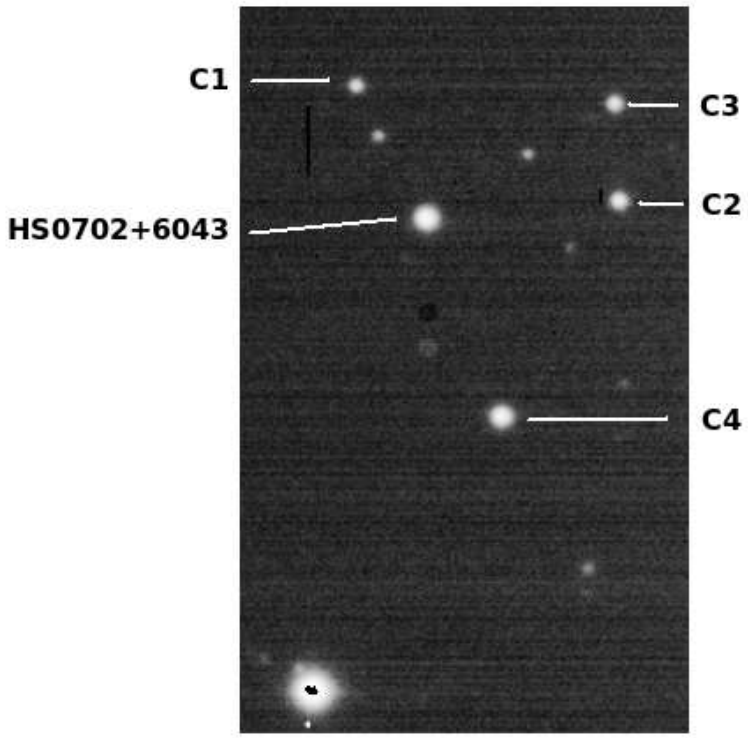

Figure 4.25: In this frame are located the target and the comparison stars in the case of HS0702+6043 taken the 2009 February 27th. It is also possible to see the saturation of the brightest star (bottom left) and the presence of a CCD defect which produces a dark circle and a ghost just below of it.

magnitude both for our target and the comparison objects. Figures (4.26) and (4.27) show the light curves obtained at four different aperture radii (3, 5, 8, 11 pixels) both as raw curve (the former, where it is also shown the airmass fitting) and the corrected and normalized curves (the latter, where the fluxes are summed to integer number just to show all of them). These curves were obtained with the processing of February 27th 2009 observation night (see in the Appendix Bfor a complete list of the observations). At first sight it is very clear the presence of some kind of common flux variation during the night, clearly dued by changing in the weather or in the sky background, as well as the airmass. In order to be sure that none of the comparison stars is a variable, we computed a power spectrum for each target in the frames. The results don't show any periodicity for the comparison stars, so we can deduce that they aren't subject to any variability, or, at least, it can be totally neglected in comparison to the one of the target star.

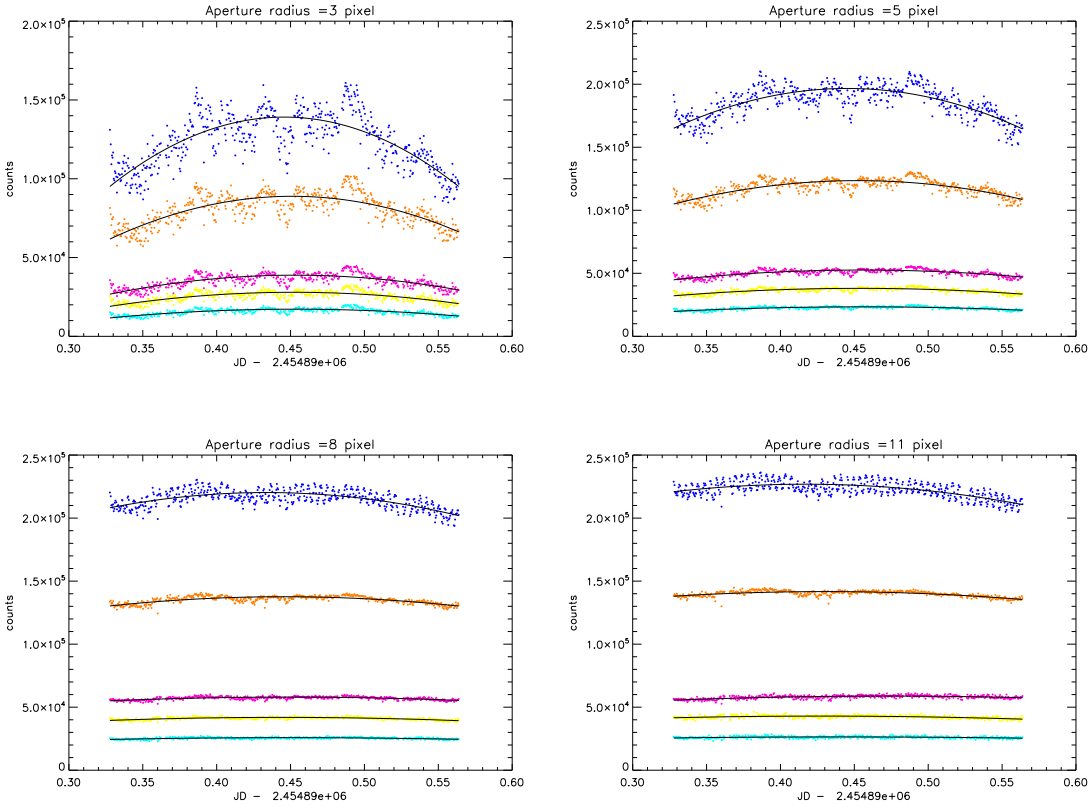

Figure 4.26: Light curves of HS0702+6043 (Target) and of the four comparison stars at 3, 5, 8, 11 pixels of aperture radius.

The important step is to choose which aperture is more suited to obtain the best light curve to perform the analysis of the power spectrum. According to the standard EXOTIME method we calculated the dispersion of the light curves for each aperture and chose the one with the small sigma, suited for the analysis. By the way we decided to perform a more deep analysis because each star has its own suited aperture radius. To perform some checks, following the works of Howell 1989 & 1992 ([89], [90]) and Stetson 1990 [148]. After this further study we saw that the differences were very small between the two different approach. We present in the following our results, using as reference the data of the 2009

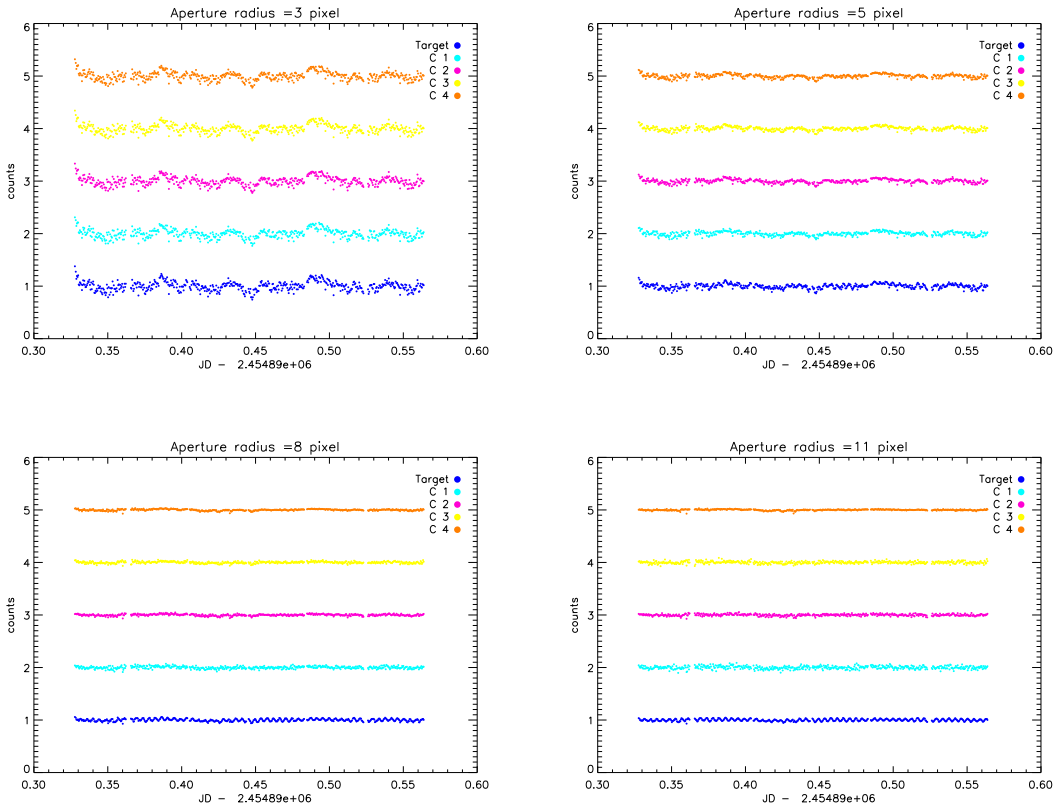

Figure 4.27: Same plots of Fig. (4.26) but the curves are corrected for airmass and normalized to their mean value.

February 27th for the star HS0702+6043.

First of all we were interested in the signal to noise ratio of our observations. For a perfect device, or in first approssimation in the case of bright stars and thus high counts above the noise, the SNR is defined as:

$$\frac{S}{N} = \frac{N_\star}{\sqrt{N_\star}} = \sqrt{N_\star} \tag{4.33}$$

where $N_\star$ is the number of counts from the source. In the real case of a CCD the standard equation for the SNR involved also the counts from the sky background (N_S), the dark level (N_D) and the read noise (N_R), and takes into account also of the number of pixels used in measuring aperture (n_{pix}). The SNR is thus as follow:

$$\frac{S}{N} = \frac{N_\star}{\sqrt{N_\star + n_{pix}(N_S + N_D + N_R^2)}}. \tag{4.34}$$

When we observe the Point Spread Function of a light source detected by an optical device we find that the maximum of the SNR is located at the centre and decreases in every direction toward the wings that cover much more area than the core, and most of this area is noisy. The SNR of the source is approximately given by the SNR at a radius equivalent to the Half Width at Half Maximum of the PSF. It is important to choose the right aperture radius to measure the flux because the too small of an apreture doesn't allow for enough signal, while a too large aperture includes too much noise. Figure (4.28, Left panel) shows the plot of the signal to noise ratio versus the considered aperture radius for each star. Together with the SNR the evaluation of the photometric precision give

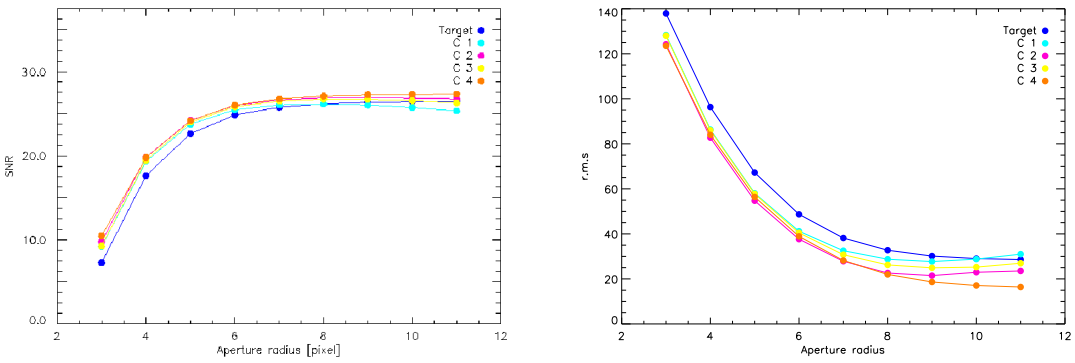

Figure 4.28: *Left panel*: SNR plotted versus the considered aperture radius for each star. *Right panel*: Rms of each light curve plotted versus the aperture radius.

us further informations about the best choice of the aperture radius. Figure (4.28, Right panel) shows the mean r.m.s. (millimag) of the light curve for each aperture. The best precision is reached toward higher radii, at least for the brighter stars (the target and the comparison star C4), while it is possible to note the presence of a minimum of the fainter star curves (C1, C2, C3).

The same kind of graph can be done using the measured instrumental magnitude. Figure (4.29, Left panel) shows the trends of the instrumental magnitude with the increasing of the aperture radius from 3 to 11 pixels. As we can see each star follows the same trend

that reach a flat shape toward greater radii. The only known magnitude is that of the target. The comparison between Table (4.7) and Figure (4.29, Left panel) shows that differential photometry doesn't provide absolute measurements of the stellar parameter, but as we will see in the following this aspect is not so important. The measure of the

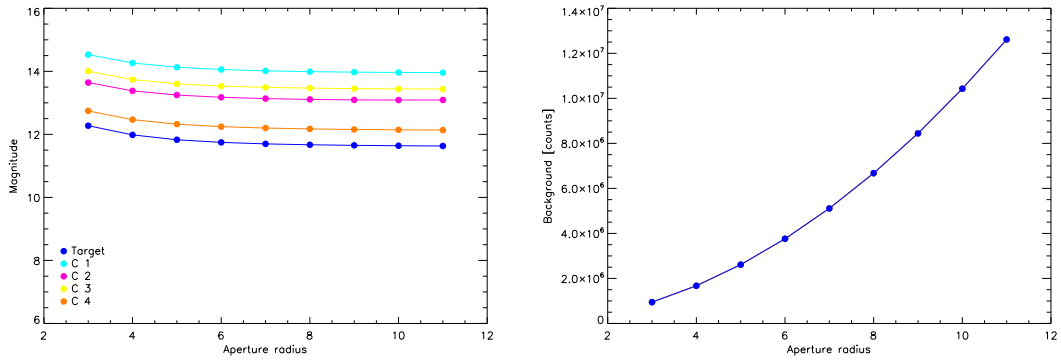

Figure 4.29: *Left panel*: Output magnitude of each light curve plotted versus the aperture radius. *Right panel*: Background of each light curve plotted versus the aperture radius.

sky background that will be subtracted to the entire flux within the aperture is another interesting parameter. Figure (4.29, Right panel).

Finally we can also compute the growth curves, i.e. to see how the flux of the star behaves by changing the aperture radius (Figure (4.30)). As pointed out in Howell 1989

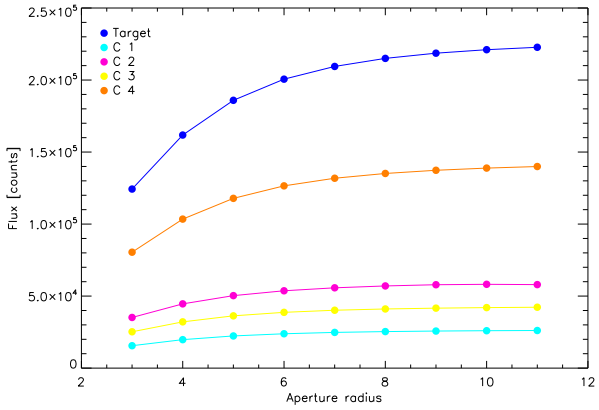

Figure 4.30: Growth curves computed for each light curve.

([89]) using a model of the brightest source in the frame it is possible to compare it to the other stars to check if there are some imperfection in their growth curves. As we can see in the plot shown by Figure (4.30) all of the source follow the same trend of the target (which is the brighter star), so we can exclude any problems about a bad flux extraction.

Previous Figures show that the values of the plotted parameters tend to not vary toward the last 3 values of aperture radius. The choice of the best aperture done with σ corresponds to the aperture radius equal to 9 pixels, as clearly appears also in Figure (4.28, Right panel). We decides then to use the data corresponding to that aperture.

We applied the frequency extraction described before to one of the light curves of HS0702+6043 that we obtained in order to test the procedure. In this case we can compare our results with the analysis performed by Schuh et al. 2006 [137]. Figure (4.31) shows the time series that we are going to analyse. We apply the Deeming algorithm to this light

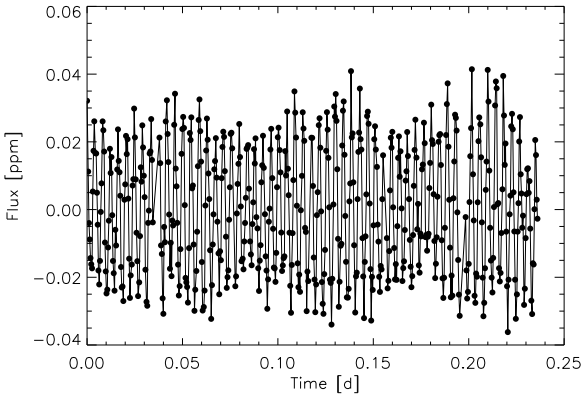

Figure 4.31: Light curve of HS0702+6043 observed in Mt. Ekar in 2009.

curve and obtain the amplitude spectrum. With the prewhitening procedure stopped at $SNR \geq 3$ we obtain three periodical components. The frequencies of these components are listed in Table (4.8) with their uncertainties, calculated as the formal errors of the sinusoidal fit (see Eq (4.25)). The comparison with the frequencies obtained by Schuh et al. [137], is good, at least for the two main periodicities. The long-term variability results from g-mode pulsations that places this target among hybrid stars, with both pressure and gravity modes, as pointed out by Schuh et al. [137]. Also the amplitudes are comparable, since different filters were used. Figure (4.32, Left panel) shows the amplitude spectrum

	This thesis	Schuh et al. 2006
f_1	ν=(2754 ± 0.02) μHz A=(24.6 ± 0.02) ppt	ν=(2754 ± 9) μHz A=(21.7 ± 5) mmi
f_2	(2607 ± 0.09) μHz A=(5.2 ± 0.02) ppt	(2606 ± 9) μHz A=(4.6 ± 5) mmi
f_3	(327 ± 0.2) μHz A=(1.8 ± 0.02) ppt	(283 ± 9) μHz A=(3.7 ± 5) mmi

Table 4.8: Frequencies obtained for HS0702+6043

obtained with the DFT, specifying the three extracted components and the white noise, while Figure (4.32, Right panel) shows the fitting function to the time series. The result of the subtraction of the fitting function to the light curve give us the time series of the residuals, characterised by a dispersion of the order of about 0.02 ppm, as shown in Figure (4.33).

4.6.2 PG 1325+101: preliminary analysis

At the present time the available measurements for this target doesn't allow us to obtain a reliable analysis, but they are enough to perform a preliminary check on the stability of

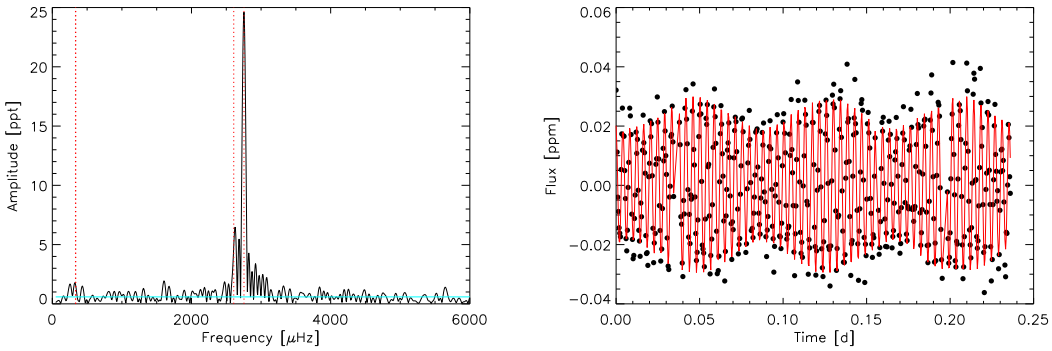

Figure 4.32: Amplitude spectrum obtained for the light curve of HS0702+6043. The red dotted vertical lines indicate the extracted frequencies while the blue horizontal line locate the level of the noise. The time series is now described through the function obtained with the sinusoidal fitting.

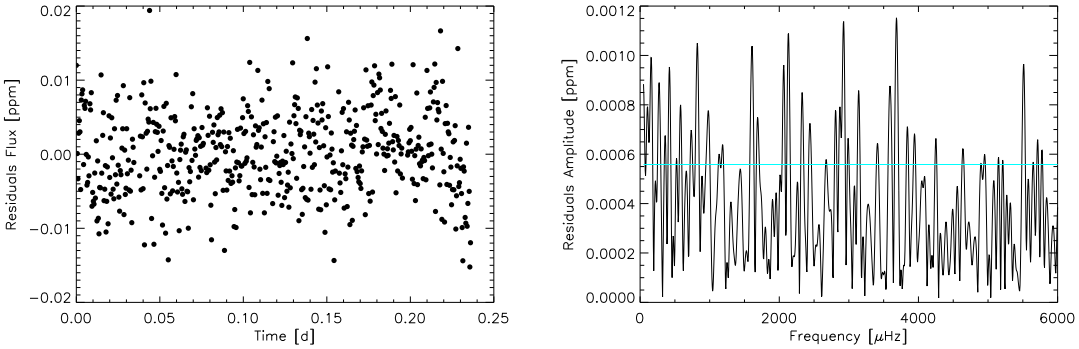

Figure 4.33: Light curve and amplitude spectrum of the residuals.

the oscillations. This verification is required since many of the sdB stars show amplitude variations (and sometimes phase variations) on various time scales from years to days.

As a first step we can exclude the presence of a cooler stellar companion, studying the Spectral Energy Distribution. Figure 4.34 shows the comparison between a black body

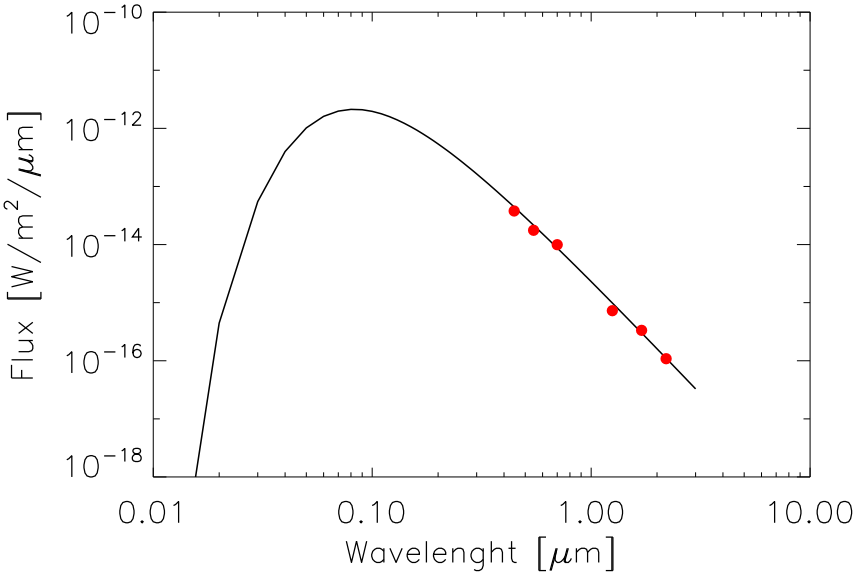

Figure 4.34: Spectral Energy Distribution of PG 1325+101. The filled red circles are 2MASS JHK and BVR magnitudes from the literature. There is no evidence for a cool stellar companion to the sdB.

(which provides a good approximation of the energy distribution of a sdB star) and the 2MASS JHK and BVR magnitudes. The plot doesn't show any infrared excess.

After this check we can start to analyse the incoming data set for this target. Generally the data are reduced directly by the observers, but since the outputs can be expressed in different ways, it is very important to turn them into a standard format. The time series are then barycentrically corrected and the differential photometric flux is expressed in mmi (milli-modulation intensity units, 1 mmi=0.1 per thousand). Then we calculate the uncertainty for each data point (following the approach of Silvotti et al. 2006) in order to fix the weights to the different data sets. The available data are shown in Table (4.9) and they sample the seasons 2008 and 2009 from January to June.

The pulsation frequencies of PG 1325+101 are well known from Silvotti et al. 2006 and Baran et al. 2010. We can thus fix the frequencies in order to calculate the mean phase of the whole data set using the software Period04 (Lenz and Breger 2005): this represents the *Calculated* value in the O-C diagram. We repeat the procedure also for the single runs, measuring the *Observed* values. The phase differences are then turned into time-lag and plotted against the observations periods. At this stage of the analysis we prefer to perform the calculations using only the main pulsation frequency (at 7255.5 μHz, with an amplitude of about 27 mma), in order to avoid confusion on the sinusoidal fit and on the estimate of the phase with P04 for the runs with poor frequency resolution.

We have calculated the O-C diagram mantaining separated the two years, since we

Date	Telescope	Filter	Length
2008/03/01	1.5m-Loiano	B	5.4 h
2008/03/13	1m-Piszkéstetõ	B	4.8 h
2008/02-05	1.2 Mercator + Suhora & Baker	V	95.5 h
2008/06/04,06	1.6m-Moletai	B	3 h
2009/01/28-31	1m-LOAO	B	9 h
2009/02/25-27	1.2m-MONET	B	11.7 h
2009/03/18	1.2m-MONET	B	1.7 h
2009/03/20-22	2.2m-Calar Alto	B	11.5 h
2009/03/25-28 2009/03/30-31	1m-LOAO	B	23.8 h
2009/04/22	1.2m-Loiano	B	2.9 h
2009/04/29	2.2m-Calar Alto	B	2.9 h
2009/05/06	2.2m-Calar Alto	B	3.9 h
2009/05/25-27	1m-LOAO	B	14 h

Table 4.9: Available data for PG 1325+101.

don't have enough data to link them. Furthermore we have the possibility to use a long run (3 months) performed in visual band for another project on the same star (Baran et al. 2010). From Figure (4.35) we see that the O-C diagram of the V band monitoring shows a good phase coherence over this time scale. The uncertainies are the formal errors of the sinusoidal fit, according to Montgomery and O'Donoghue 1999.

More difficulties are noticed when we calculate the O-C for the B-band data, probably related to a poor coverage. Figure (4.36) shows preliminary results for the three B-band runs of 2008. Considering that the second point has a very large error bar, the phase appears still rather stable. However, things are more complicate when we join B and V data and we are still working to understand what is the reason of these difficulties.

Similar problems are found also with the data of 2009 and preliminary results are under analysis. The present coverage in B band is not yet enough to ensure a unique solution, even over a single season. New data will help to converge towards a unique solution joining together the data of the different seasons with an improved measurement of the pulsation periods.

4.7 Conclusions and future work

In this Section we discussed the development of personal procedures aimed to perform time series analysis. Sometime the treatment of several type of data requires adjustments of the procedures not always possible with general public softwares. The creation and the implementation of these codes lasted for all the three years of PhD, but especially in the last months with the increasing commitments in the framework of the Kepler mission.

We had the opportunity to test the procedures both with ground- and space-based observations, and to verify our results with literature. They show quite good agreements with the results obtained by other research teams, motivating improvements in the accuracy of the outcomes.

We plan further implementations to the procedures, especially for the solar-like oscil-

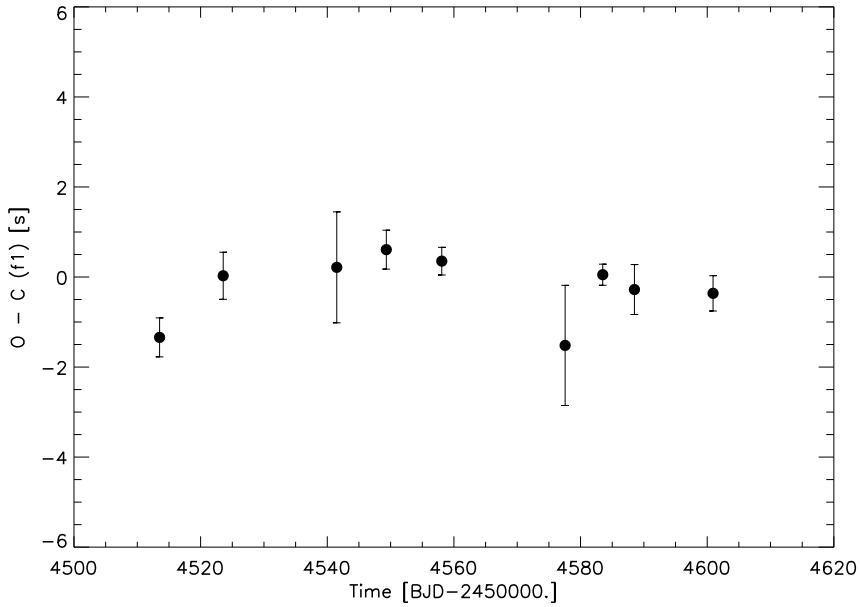

Figure 4.35: O-C diagram of the main frequency (f1) of PG 1325+101 for the V band run.

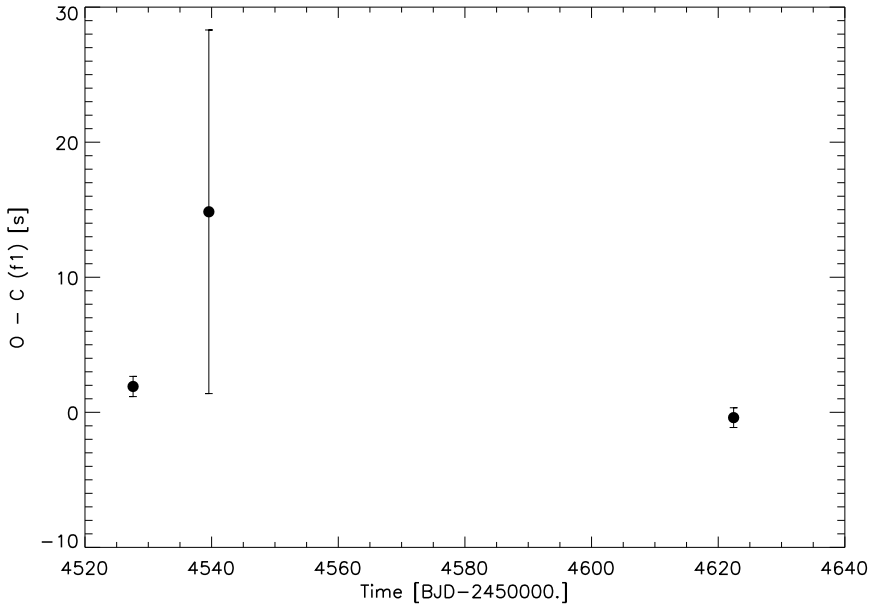

Figure 4.36: O-C diagram of the main frequency (f1) of PG 1325+101 for season 2008 (without V band run).

lation analysis, including for instance, techniques for the mode identifications. The work on the hybrid γ Doradus and δ Scuti stars is providing interesting developments for these targets, and the existing collaboration with the Working Group 11 of KASC will produce valuable results about the topics partially introduced here. Finally our commitment in the framework of the EXOTIME project also requires further efforts to conclude the analysis of the target PG1325+101.

Chapter 5

Modelling Solar-like stars with Asteroseismology

The possibility to work with unprecedent precision data, such the ones that would come from PLATO would allow us to improve our knowledge on many critical issues of stellar physics. During the preparation of a space mission with such a great potential it is clearly required to plan how to analyse the data in order to obtain the best science products as possible. A great lesson comes from the high performances of the NASA-Kepler satellite, launched in March 2009, with the aim to search for extrasolar planets and to perform Asteroseismology for a sample of thousands of targets which spans through several pulsation classes in the H-R diagram.

Thanks to the Kepler time series it is possible to obtain many informations of the stellar structure which help to improve the precision in the extraction of fundamental stellar parameters using theoretical models. Thanks to the collaboration with the Centro de Astrofisica da Universidade do Porto (Portugal) it was possible to use Kepler data in order to model a small sample of solar-type stars with the main goal to search for the best candidate to be a solar-twin. The first step is the computation of stellar evolution models using the code ASTEC, for stars already observed by Kepler, taking as input the stellar parameters available from the Kepler Input Catalog and from literature (e.g. heavy element abundance). Using these models as input data for the adiabatic oscillations code ADIPLS, we computed the relative theoretical frequencies, having therefore the possibility to compare, through a chi-square test, the observations made by Kepler with theoretical predictions. Thanks to this work we had the possibility to put some constraints on fundamental stellar parameters, and characterize the targets of interest.

5.1 Stellar modelling using the ASTEC code

5.1.1 ASTEC code

The Aarhus STellar Evolution Code (*ASTEC*) is the result of a long development, started in the in 70's, with the aim to provide an improved equilibrium model for investigation of solar stability (see Christensen-Dalsgaard 1974 [47]). With the increasing quality of helioseismic data the code was further developed, to allow for more realistic physics (like the inclusion of diffusion and settling). Thanks to those features it was possible to extract the so called Model S of the Sun (Christensen-Dalsgaard et al. 1996 [46]), which has found extensive

use as reference for helioseismic investigations and which at the time provided reasonably up-to-date representations of the physics of the solar interior. In parallel, extensions have been made to the code to consider the evolution of stars other than the Sun (including the treatment of convective cores and core overshoot, attempts to model red-giant evolution and the inclusion of helium burning). For use in asteroseismic fitting a new feature is the integration of the computation of adiabatic oscillations for specified models as part of the code. Basic physics of this code is fully described in Christensen-Dalsgaard 2008a [44].

A large number of input parameters and flags has to be defined in order to start the computation. They are provided in an input file, while the model mass and trial mass, heavy elements abundance and the number of timesteps nt are present in the command used to run the code. Among the inputs there is also a *trial model*, used as reference for the computation of the model of interest. In order to obtain a reliable output it is important that the trial and the model mass don't differ too much.

When the computations start, the initial ZAMS model is assumed to be static and with a prescribed chemical composition. The number N of the so called 'mesh points' inside the star is kept fixed during the evolution, but their distribution varies according to the changes in the structure of the model. In particular, a dense distribution of points is present near the boundaries of convection zones. Having computed model at timestep t^{s+1} the next timestep is determined from the change in the model between timesteps t^s and t^{s+1} ; this involves a complex algorithm aimed to limit the variations in, e.g., $\log_{10} p$, $\log_{10} T$ and X at fixed m, where m is the mass interior to the point considered. The algorithm ensures very short temporal steps in case of rapid evolutionary phases. In typical simple calculations, assuming ^{3}He to be in nuclear equilibrium, roughly 35 (100) timesteps are needed to reach the end of central hydrogen burning in models without (with) a convective core, and 100 (200) steps to reach the base of the red-giant branch. Calculations with more complex physics or requiring higher numerical precision obviously require a substantially higher number of timesteps. Evolution up the red giant branch can be obtained with a large number of timesteps.

When computing models of the present Sun it is important to adjust the input parameters such as to obtain a model that precisely matches the observed solar radius, luminosity and ratio Z_s/X_s between the abundances of heavy elements and hydrogen, at the present age of the Sun. This is achieved by adjusting the initial hydrogen and heavy-element abundances X_0 and Z_0 as well as the mixing-length parameter α_{ML} (or another parameter characterizing the treatment of convection). In ASTEC the iteration to determine these parameters is carried out automatically, making the computation of solar models, and the exploration of the consequences of modifications to the input physics.

The outcomes of the computations are stored in several output files. A summary file lists global properties of the models in the evolution sequence, whereas output of detailed models, on the full mesh of the calculation, can be obtained in three different forms: the `emdl` files, including the variables used in the calculation, as well as a complete listing of the input parameters, to provide full documentation of the calculation; the `amdl` files which provide the variables needed for the Aarhus adiabatic pulsation code (see Section 5.2.1); and the `gong` files, giving an extensive set of variables for use in further investigations of the models or plotting.

Output global parameters, provided by default, for each timestep of the computations are Mass, Age, Radius, Effective Temperature, Luminosity and Central Hydrogen abundance. Parameters of the stellar centre are also provided, such as the temperature, pressure

or Helium abundance. Finally, for each mesh point the code computes the stellar radius ($\log r_\star$), the temperature ($\log T_\star$), the luminosity ($\log L_\star$), the Hydrogen (X) and other elements abundance.

5.1.2 The stellar sample

The aim of this work is to obtain reliable stellar theoretical models with the help of Asteroseismology for a small number of solar-like stars in the Kepler sample. In particular we search for best candidate 'solar twin'. For all the target stars the *Kepler Input Catalog* (KIC, see Latham et al. 2005 [103]) provides values of the effective temperature, radius, metallicity, $\log g$, magnitudes and other stellar fundamental parameters. Most of them were estimated using atmospherical models or statistical distributions, and in some case from ground-based observations. Anyway this catalog provides stellar values with significant uncertainties, e.g. 200 K for the effective temperature or 0.5 *dex* for the metallicity or the logarithm of the surface gravity. The description of the algorithms used for the stellar classification in the KIC are reported in a document by T. Brown available at the KIC webpage[1]. This document report also the description of known systematic errors in the parameters evaluation, responsibles for the high values of the uncertainties in the stellar parameters.

We started from a list of 99 targets already observed with Kepler, released by the chairs of WG 1 (the KASC Working Group dedicated to solar-like pulsators), and indicated as interesting targets. We selected our small sample of stars such that their parameters are as similar as possible to the solar ones. In particular our selection criterium is based on the value of the effective temperature (from KIC) and the computed mean large separation, available from the data release webpage as computed by the Octave[2] pipeline (Hekker et al. 2009 [86]). Figure (5.1) shows the distribution of the solar-like stars, presented in the above mentioned list, in a (T_{eff},$\Delta\nu$) diagram.

We are interest to find a small sample of stars (four or five targets) with temperature and large separation (indicator of the stellar mass) as close as possible to the solar ones. We slowly enlarged our range in T_{eff} and $\Delta\nu$ until we found five stars falling within a grid centred in the corresponding solar values. The result is that the grid collects all the objects with an effective temperature and large separation which differ from the solar values by 2% and 40% respectively. The global parameters (available from KIC and Octave) for the selected stars are summarized in Table (5.1), while Table (5.2) shows the few informations available from literature. Finally Figure (5.2) shows as an example the light curves available for two stars of the sample (KIC3427720 and KIC8379927), obtained in three months of observations with Kepler.

5.1.3 Computation of models

We started to compute a grid of evolutionary tracks with large steps of incrementation for the input parameters, trying to obtain models spanning largerly in the HR diagram, able thus to be suited for each star of our sample. The stellar input parameters for the computations are shown in Table (5.3). The assumptions taken into account are the spherical

[1] http://www.cfa.harvard.edu/kepler/kic/kicindex.html

[2] The Octave pipeline, created for the automatic analysis of Kepler data and fully described in Hekker et al. 2009 [86], by using only the time series data as input is able to obtain accurate frequencies and oscillation parameters such as the mean large separation, the peak of the maximum amplitude.

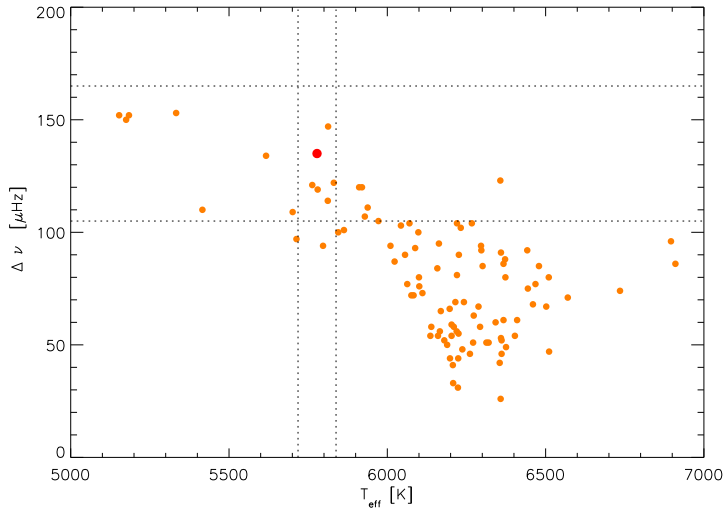

Figure 5.1: Sample of solar-type stars (small circles) already observed by Kepler, plotted in an Effective Temperature vs Large Separation diagram and compared with the Sun (larger circle at the centre of the grid). The dotted lines contains the region of the diagram in which the stars depart from the Solar parameters of 2% in Temperature and 40% in large separation.

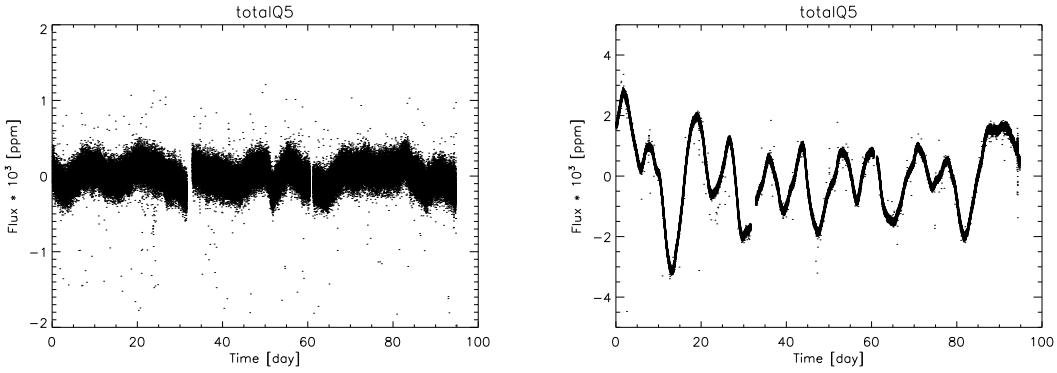

Figure 5.2: Light curves for two stars of our small sample (KIC3427720 in the left panel, KIC8379927 in the right panel), observed for three months in the Quarter number 5 (Q5), the fifth period of observations of Kepler, each subdivided in 3 months.

Kepler ID	T_{eff} $[K]$	$\log g$	Metallicity	$R/R_{\odot}$	$\Delta\nu$ $[\mu Hz]$	ν_{max} $[\mu Hz]$
7106245	5812 ± 200	4.316 ± 0.5	-0.325 ± 0.5	1.2	114	1954.0
10644253	5831 ± 200	4.283 ± 0.5	-0.152 ± 0.5	1.257	122	2862.0
3427720	5780 ± 200	4.440 ± 0.5	-0.374 ± 0.5	1.034	119	2815.0
8379927	5763 ± 200	4.238 ± 0.5	-0.097 ± 0.5	1.326	121	2906.0
10124866	5813 ± 200	4.200 ± 0.5	-0.135 ± 0.5	1.323	147	3553.0

Table 5.1: Global parameter of the selected targets from KIC and Octave.

Kepler ID	Age	T_{eff} $[K]$	Metallicity	$R/R_{\odot}$	Spectral Type
7106245	-	-	-	-	F2
10644253	-	-	-	-	-
3427720		6440[1]	-	-	F5
8379927	5.4	5956	-0.11	-	G0
10124866	9.8[2]	5821[2]	-0.31[2]	1.23[3]	G0

Table 5.2: Global parameter of the selected targets from literature. References: 1 The Tycho-2 Spectral Type Catalog (Wright et al. 2003 [157]); 2. Geneva-Copenhagen Survey (Holmberg et al. 2009 [87]); 3. Allende Prieto and Lambert 1999 [5]

symmetry, the absence of rotation and magnetic fields. For other features like trial models, technical aspects of the computations and the input physics, we mostly used the default parameters of ASTEC, so the OPAL equation of state tables (Rogers et al. 1996 [133]), OPAL opacities (Iglesias and Rogers 1996 [92]) and the standard mixing length theory (Böhm-Vitense 1958 [27]) were used. We set the Hydrogen abundance equal to the solar mixture given in Grevesse and Noels 1993 [78], namely $X = 0.733$. Figure (5.3) shows some of the grids computed in this first step. The legends in the plots defines the mixing-length parameter and the value of the heavy elements abundance used in that particular series of computations. Finally, we indicate the position of the Sun as well as the values of stellar radii, as a reference in comparison to the models.

Parameters	Values
$M/M_{\odot}$	0.95 - 1.30 (with steps of 0.5)
Z	0.01 - 0.03 (with steps of 0.005)
Y	0.24 - 0.27 (with steps of 0.01)
Mixing Length Parameter (α_{ML})	1.6 - 2.0 (with steps of 0.1)

Table 5.3: Input parameters for the first computed large grid of stellar models.

The output files of ASTEC summarize for each time steps (defined by the parameter nt) the computed values of effective temperature, luminosity, radius, and so on, providing then the evolutionary sequence for each star. It is important to note that for each time step we compute a full theoretical model of the star, showing not only the global parameters but also the internal structure of the star. By using an IDL procedure we read these files and select the time steps, and thus the models, that simultaneously represent the global parameters of a particular target, within the already mentioned uncertainties of the KIC. Just to clarify we report the evolutionary calculation steps suited to represent the targets KIC10124866 (Table (5.4)) and KIC8379927 (Table (5.5)), according to the values given in Table (5.1).

After the selection we are provided by a set of evolutionary models for each star of the sample, or at least we know which are the most suited input parameters. The next step is to focus our attention to the single stars by producing denser grids, with the aim to approach to the best model for each of them. As in the previous example, we show few sets of evolutionary tracks for the two targets KIC10124866 and KIC8379927, Figures

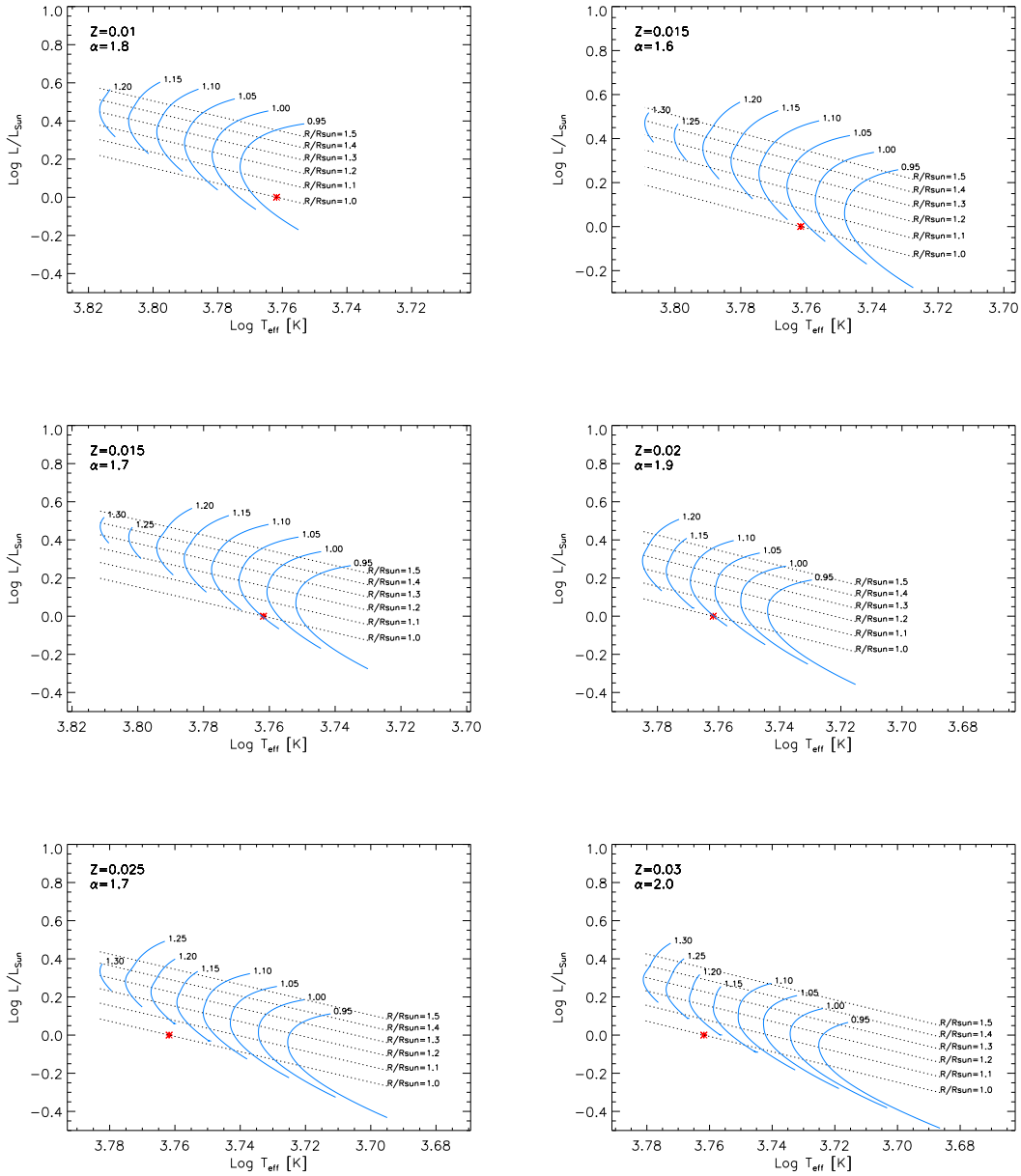

Figure 5.3: A few examples of the computed grids with the input parameters given in Table (5.3). The reference values of the stellar radius are defined by the diagonal dotted lines, whilw the asterisk represents the Sun as reference.

nt	$M/M_\odot$	Age [Gyr]	$R[cm]$	T_{eff} $[K]$	$L/L_\odot$	X
15	1.100	4.63880	7.81870×10^{10}	5777.9	1.262	3.22450×10^{-1}
16	1.100	4.84880	7.88346×10^{10}	5781.6	1.287	3.00986×10^{-1}
17	1.100	5.04500	7.94628×10^{10}	5784.7	1.310	2.80656×10^{-1}
18	1.100	5.22872	8.00735×10^{10}	5787.4	1.333	2.61402×10^{-1}
19	1.100	5.40118	8.06676×10^{10}	5789.6	1.355	2.43165×10^{-1}
20	1.100	5.56346	8.12459×10^{10}	5791.4	1.376	2.25885×10^{-1}

Table 5.4: Part of the calculation steps of ASTEC providing, within the available uncertainties, the global parameters of the star KIC10124866 for $Z = 0.02$ and $\alpha_{ML} = 1.7$. The column labelled with 'nt' defines the timesteps of the calculations from the ZAMS.

nt	$M/M_\odot$	Age [Gyr]	$R[cm]$	T_{eff} $[K]$	$L/L_\odot$	X_c
30	1.200	2.63658	7.71411×10^{10}	5757.7	1.212	4.97523×10^{-1}
31	1.200	2.94903	7.78987×10^{10}	5765.8	1.243	4.66810×10^{-1}
32	1.200	3.23742	7.86326×10^{10}	5772.9	1.272	4.37645×10^{-1}
33	1.200	3.50330	7.93403×10^{10}	5778.9	1.301	4.09961×10^{-1}
34	1.200	3.74825	8.00200×10^{10}	5783.9	1.328	3.83699×10^{-1}
35	1.200	3.97389	8.06712×10^{10}	5788.1	1.353	3.58800×10^{-1}
36	1.200	4.18183	8.12935×10^{10}	5791.6	1.378	3.35207×10^{-1}
37	1.200	4.37367	8.18871×10^{10}	5794.3	1.400	3.12862×10^{-1}

Table 5.5: Part of the calculation steps of ASTEC providing, within the available uncertainties, the global parameters KIC8379927 for $Z = 0.03$ and $\alpha_{ML} = 1.9$. The column labelled with 'nt' defines the timesteps of the calculations from the ZAMS.

(5.4) and (5.5), that we obtained with the input parameters provided in Table (5.6), as the previous models selection suggested. Even in this case we locate the Sun (red asterisk) as well as the position of the target according to the global parameters of KIC. Note that the KIC doesn't provide the stellar luminosity, so, to place the star in the HR diagram, we calculated it by using the formula $4\pi R^2\sigma T_{eff}^4$, where R and T_{eff} are the radius and effective temperature of the star, while σ is the Stefan-Boltzmann constant.

The global parameters of the star KIC3427720 were not satisfied by any of the previous models. Therefore we computed some preliminary models changing some input data, such as the mass and the mixing-length parameter. We found a better agreement between our models and the KIC parameters for lower values both for the mass and for α_{ML}. The input parameters for this new grid are then listed in Table (5.7). An example of a good model is presented in Table (5.8). Finally, the grid of theoretical models (with $Z = 0.009$ and $\alpha_{ML} = 1.5$) obtained for this star is shown in Figure (5.6), with the same notations of the previous ones.

At this stage we have a set of models able to reproduce the global parameters for each star of our sample. Tables (5.1) and (5.2) show several disagreements between the KIC parameters and the stellar parameters provided by literature. This fact leads to a further difficulty to search for a reliable stellar modelling. However, as already mentioned, values from KIC show quite high uncertainties, so we cannot exclude any possible result. In the next Sections the comparison between theoretical and observed frequencies will represent a more stringent criterium to discriminate among the possible models.

KIC10124866: Parameters	Values
$M/M_{\odot}$	1.0 - 1.1 (with steps of 0.2)
Z	0.01 - 0.03 (with steps of 0.005)
Y	0.24 - 0.27 (with steps of 0.01)
Mixing Length Parameter (α_{ML})	1.7 - 1.9 (with steps of 0.05)
KIC8379927: Parameters	**Values**
$M/M_{\odot}$	1.20 - 1.27 (with steps of 0.1), 1.30
Z	0.02 - 0.032 (with steps of 0.002)
Y	0.24 - 0.27 (with steps of 0.01)
Mixing Length Parameter (α_{ML})	1.8 - 2.0 (with steps of 0.02)

Table 5.6: Input parameters for the denser grids of stellar models computed for KIC10124866 and KIC8379927.

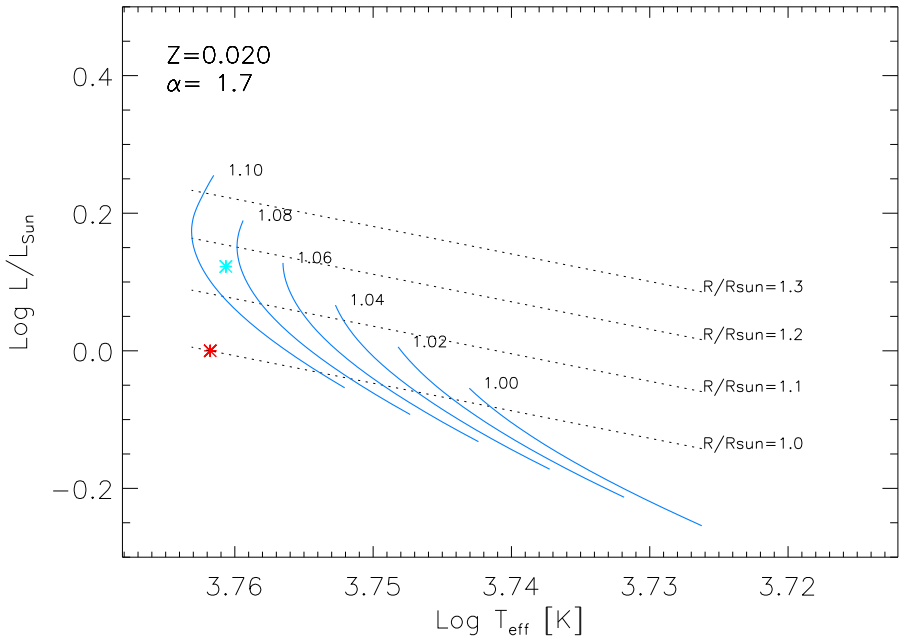

Figure 5.4: Denser grid of evolutionary tracks for the target KIC10124866 (heavy element abundance and the mixing-length parameter are defined in the plot). The red asterisk represent the Sun, whereas the light blue asterisk places the target according to the KIC parameters. Even in this case the reference for stellar radius is defined by the diagonal dotted lines.

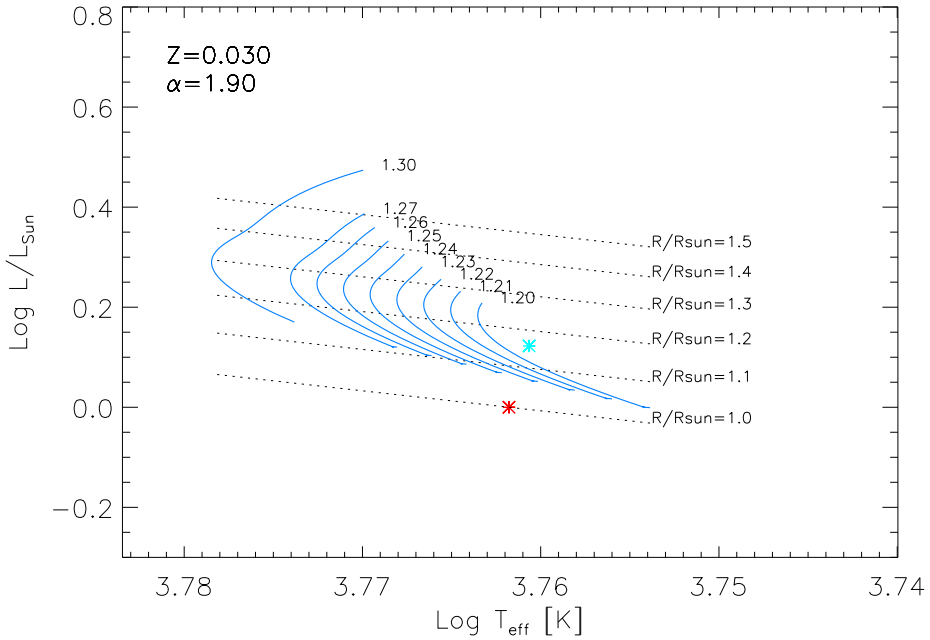

Figure 5.5: Denser grid of evolutionary tracks for the target KIC10124866 (heavy element abundance and the mixing-length parameter are defined in the plot). The red asterisk represent the Sun, whereas the light blue asterisk places the target according to the KIC parameters. Even in this case the reference for stellar radius is defined by the diagonal dotted lines.

KIC3427720: Parameters	Values
$M/M_{\odot}$	0.90 - 0.94 (with steps of 0.005)
Z	0.01 - 0.035 (with steps of 0.005)
Y	0.24 - 0.27 (with steps of 0.005)
Mixing Length Parameter (α_{ML})	1.2 - 2.0 (with steps of 0.05)

Table 5.7: Input parameters for the denser grid of models computed for the target KIC3427720.

nt	$M/M_\odot$	Age [Gyr]	$R[cm]$	T_{eff} $[K]$	$L/L_\odot$	X
20	0.920	7.19570	7.03210×10^{10}	5749.6	1.001	2.28719×10^{-1}
21	0.920	7.41737	7.09337×10^{10}	5754.2	1.022	2.12352×10^{-1}
22	0.920	7.62893	7.15451×10^{10}	5758.4	1.043	1.96827×10^{-1}
23	0.920	7.83120	7.21558×10^{10}	5762.2	1.063	1.82089×10^{-1}
24	0.920	8.02479	7.27655×10^{10}	5765.6	1.084	1.68079×10^{-1}
25	0.920	8.21002	7.33736×10^{10}	5768.7	1.105	1.54743×10^{-1}
26	0.920	8.38696	7.39784×10^{10}	5771.4	1.125	1.42029×10^{-1}
27	0.920	8.55539	7.45768×10^{10}	5773.7	1.145	1.29891×10^{-1}
28	0.920	8.71493	7.51645×10^{10}	5775.6	1.165	1.18294×10^{-1}
29	0.920	8.86508	7.57368×10^{10}	5777.1	1.184	1.07209×10^{-1}
30	0.920	9.00545	7.62889×10^{10}	5778.2	1.202	9.66233×10^{-2}

Table 5.8: Part of the calculation steps of ASTEC providing, within the available uncertainties, the global parameters of the star KIC3427720. Since the first large grid didn't fit the observed (or calculated) parametes it was necessary to compute a second grid with a lower mass and α_{ML} range (see Table (5.7)).

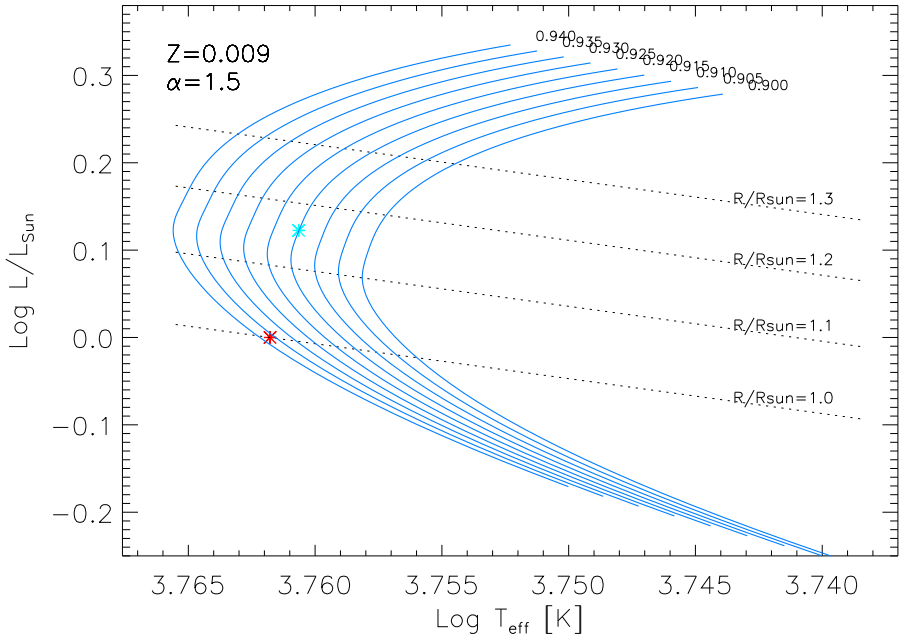

Figure 5.6: Denser grid of evolutionary tracks for the target KIC3427720 (heavy element abundance and the mixing-length parameter are defined in the plot). The red asterisk represent the Sun, whereas the light blue asterisk places the target according to the KIC parameters. Even in this case the reference for stellar radius is defined by the diagonal dotted lines.

5.2 Theoretical frequencies from ADIPLS code

5.2.1 ADIPLS code

The code *ADIPLS* (Aarhus adiabatic oscillation package) was developed since 1978 to create an efficient tool for the computation of adiabatic oscillation frequencies and eigenfunctions for stellar models, emphasizing also the accuracy of the results. An equilibrium model is provided to the code in the form of `amdl` files, generated by ASTEC. They consist of a minimal set of variables for computing adiabatic oscillations. These variables are required at each mesh point in the model, and they are defined as follow:

$$x = r/R, \tag{5.1}$$

$$A_1 = q/x^3, \qquad \text{where } q = m/M, \tag{5.2}$$

$$A_2 = V_g \equiv -\frac{1}{\Gamma_1}\frac{d\ln p}{d\ln r} = \frac{Gm\rho}{\Gamma_1 pr}, \tag{5.3}$$

$$A_3 = \Gamma_1, \tag{5.4}$$

$$A_4 = A \equiv -\frac{1}{\Gamma_1}\frac{d\ln p}{d\ln r} - \frac{d\ln \rho}{d\ln r}, \tag{5.5}$$

$$A_5 = U \equiv \frac{4\pi\rho r^3}{m} \tag{5.6}$$

The programme is controlled by a large number of control parameters that, just like ASTEC, they can be set through an input file, offering considerable flexibility in the choice of integration method as well as ability to determine all frequencies of a given model, in a given range of degree and frequency. Among the input parameters it is possible to set the range of the calculated frequencies or modes degree l or to discriminate between p- or g-modes. Previously computed frequencies can also be selected to be as trial models for the new computation. A detailed formulation of the basic equations and methods applied is provided by Christensen-Dalsgaard 2008b [43].

The output files can be found in different forms: frequency, wavenumbers and the values of the mode energy are given in a short summary file, but an extensive set of mode parameters can be also found. The latter provides also the mode eigenfunctions.

5.2.2 Computation of frequencies

Among the output files of ASTEC we found the ones which are suited to be used by the ADIPLS code. Thanks to those files ADIPLS can read the informations about the stellar parameters of the previous computation and exploit them for the evaluation of theoretical frequencies of a particular model. Even in this case the code requires a series of input parameters. Since the default values of these parameters are set with the aim to search for p-modes oscillations, even in this case we decided to use them.

Our procedure was to take as reference one of the models that simultaneously represent the KIC parameters, characterized by a fixed age, and select 10 or 15 models which precede and follow it in the evolutionary sequence. In the following we will show that this arbitrary selection is strictly dependent by the setting of temporal step of the computations. The calculation of theoretical oscillation frequencies is then performed for all of these selected models, in order to map the frequency values for the same staar in a particular temporal range. After the computations, by using an IDL procedure, we read the output files, yielding the frequencies, the angular degree and the radial order, and calculate the large

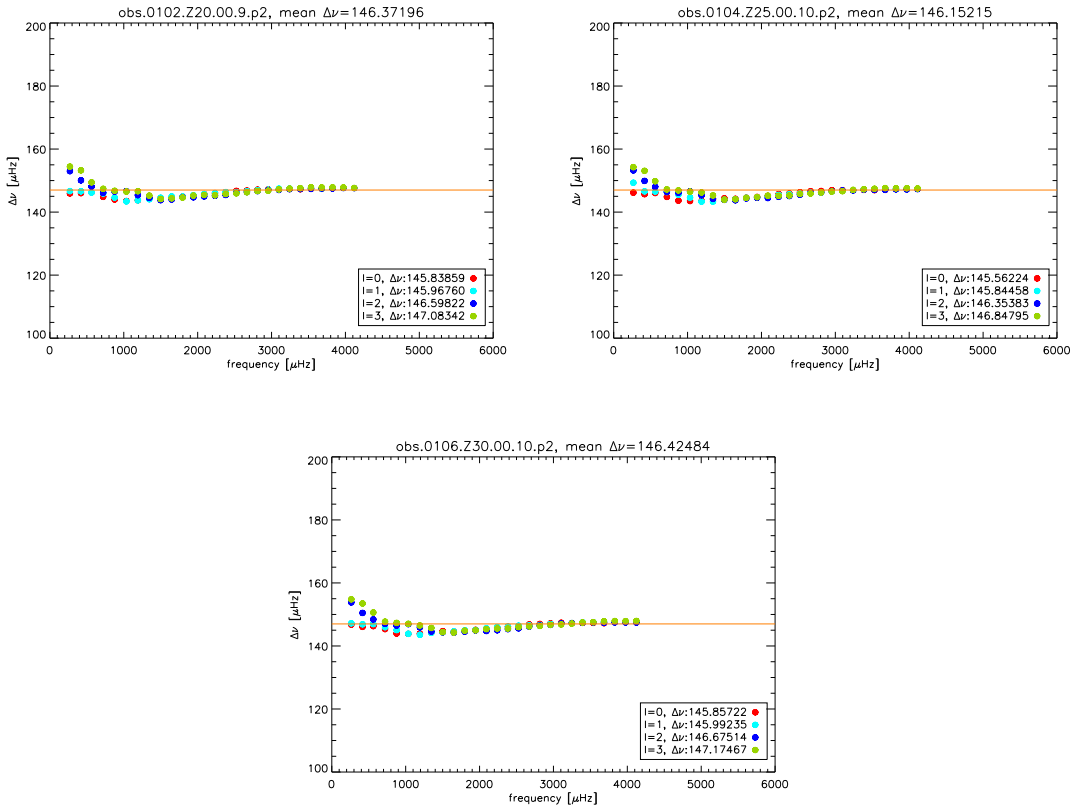

Figure 5.7: *Left upper panel*: $\alpha = 1.7$, $Z = 0.02$, $M = 1.02 M_{\odot}$, age = 4.00 Gyr; *Right upper panel*: $\alpha = 1.75$, $Z = 0.025$, $M = 1.04 M_{\odot}$, age = 4.74 Gyr; *Lower panel*: $\alpha = 1.75$, $Z = 0.03$, $M = 1.06 M_{\odot}$, age = 4.91 Gyr.

frequency separation for each couple ($\nu_{n,l}$, $\nu_{n,l-1}$) of theoretical modes with the same l and the mean value of the same quantity. We then proceed to compare the theoretical large separation with the mean $\Delta\nu$ obtained from the Kepler data and the Octave pipeline. Since the large separation varies with the stellar evolutionary state, this procedure, even if not accurate, works like a 'filter' that can help to identify which models are able to represent the observed frequencies of the investigated star.

Figures (5.7), (5.8) and (5.9) show this comparison for the target stars considered up to now. Colours indicate different groups of modes, characterized by l equal to 0 (red dots), 1 (light blue dots), 2 (dark blue dots) and even for $l = 3$ (green dots), invisible to photometric time series. The horizontal line defines the value of the observed mean $\Delta\nu$ (values from Table (5.1)), while the theoretical mean large separations for groups of modes with the same angular degree are reported in the legend of the plots. Finally the theoretical mean large separation is located at the top of each plot. However a deeper investigation is required, so we proceed to compare the theoretical frequencies for each model with the identified frequencies from Kepler, obtained thanks to the data exchange facility called *Catbasket*[3].

[3]The Catbasket is a tool used by members of the KASC WG1 who can upload and store the results of frequency analysis for individual stars. It is located and maintained in Birmingham and is accessible through a web interface.

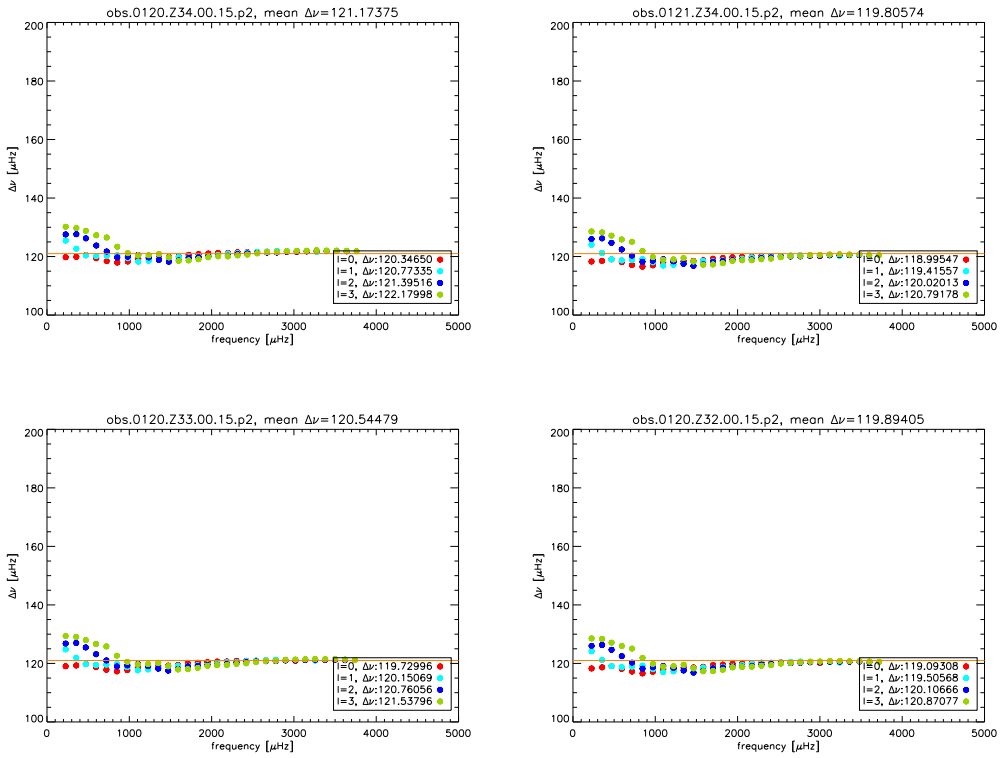

Figure 5.8: *Left upper panel*: $\alpha = 1.9$, $Z = 0.034$, $M = 1.20 M_{\odot}$, Age = 4.80 Gyr; *Right upper panel*: $\alpha = 1.9$, $Z = 0.034$, $M = 1.21 M_{\odot}$, age = 4.61 Gyr; *Left lower panel*: $\alpha = 1.9$, $Z = 0.033$, $M = 1.20 M_{\odot}$, age = 4.67 Gyr; *Right lower panel*: $\alpha = 1.9$, $Z = 0.032$, $M = 1.20 M_{\odot}$, age = 4.55 Gyr.

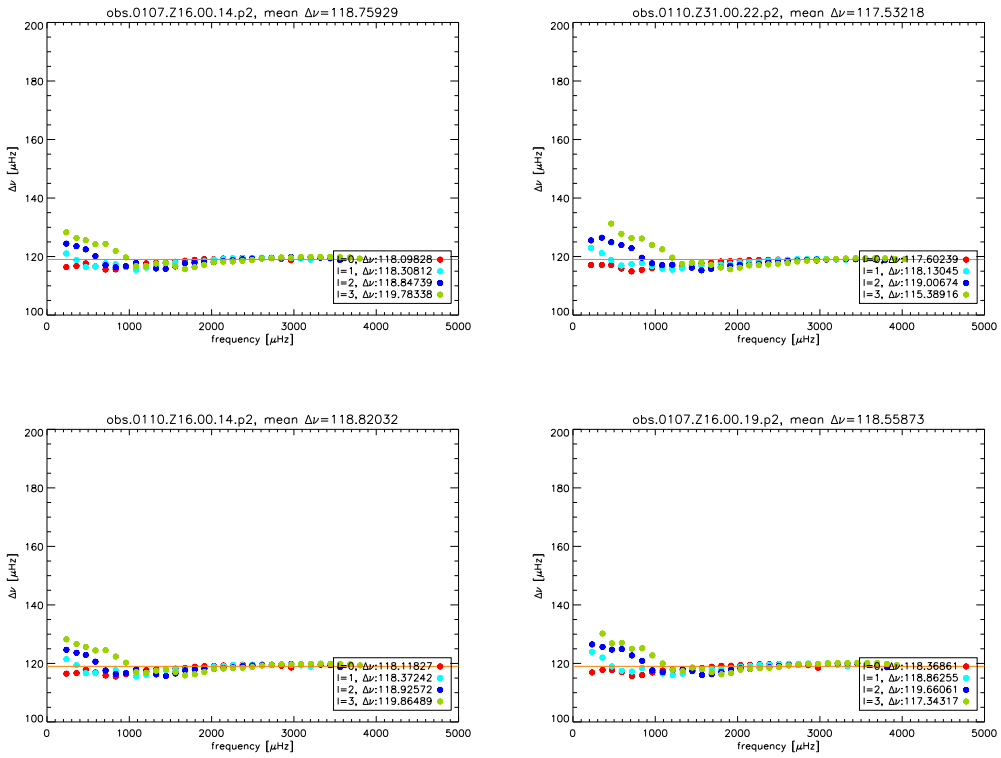

Figure 5.9: *Left upper panel*: $\alpha = 1.5$, $Z = 0.016$, $M = 1.07 M_{\odot}$, age = 4.24 Gyr; *Right upper panel*: $\alpha = 1.6$, $Z = 0.031$, $M = 1.1 M_{\odot}$, age = 8.19 Gyr; *Left lower panel*: $\alpha = 1.7$, $Z = 0.016$, $M = 1.1 M_{\odot}$, age = 3.76 Gyr; *Right lower panel*: $\alpha = 1.8$, $Z = 0.016$, $M = 1.07 M_{\odot}$, age = 5.16 Gyr.

5.2.3 Comparison with real data

The input data available so far are summarized as follow:

- a set of theoretical stellar models for each star of our small sample;
- a set of theoretical oscillation frequencies for each model mentioned above;
- a set of observed oscillation frequencies for only 3 stars of the five selected in the sample, obtained from the Catbasket facility.

By using these informations, the next step is to search for the stellar model whose corresponding theoretical frequencies are as similar as possible to the available observed ones. We accomplished this task with an IDL procedure that performs a chi-square minimization test for the goodness of the fit for every set of computed frequencies (i.e. for each model selected in the Section 5.2.2), through:

$$\chi^2 = \frac{1}{N}\sum_{n,l}\left(\frac{{\nu_l}^{model}(n)) - {\nu_l}^{obs}(n)}{\sigma({\nu_l}^{obs}(n))}\right)^2 \tag{5.7}$$

where N is the total number of modes included, ${\nu_l}^{obs}(n)$ and ${\nu_l}^{model}(n)$ are the observed frequencies, and the model frequencies, respectively, for each spherical degree l and the radial order n, whereas σ represents the uncertainty in the observed frequencies.

The results of the chi-square test are examined in order to search for the lowest value of the parameter in Eq. (5.7) corresponding to the best model of the investigated target, and therefore able to reproduce with good precision the observed frequencies. In the next Section we present the results for the single stars in our sample.

5.3 Results

We computed stellar models and frequencies for the targets KIC3427720, KIC10124866, KIC8379927, KIC10644253 and KIC7106245. Unfortunately no attempts of mode identification were performed up to now for the two latter stars. This is the reason why we focus out attention to the other three stars. Since the frequency spectra of all the stars in the sample show very weak oscillation features, in some cases the mode identification is severely disturbed, leading to ambiguous results. Our attempts to search for the best models of the single stars are described in the separate Sections 5.3.1, 5.3.2 and 5.3.3.

5.3.1 KIC3427720

The amplitude spectrum of the star KIC3427720, extracted through our tool from three months of Kepler light curve, is shown in Figure (5.10). The frequency range of the solar-like excess should be centred at $\nu_{max} \sim 2815\mu$Hz. Table (5.9) shows, in the first four columns, the available observed frequencies for this star, picked up by the Catbasket facility and obtained with the Octave pipeline ([86]), labelled with 'obs'. The angular degree l was not identified and we have the information about the radial order n for only 6 oscillation modes. The most probable reason for a bad or missing identification is that the typical lorentian envelope can be hardly recognized in the amplitude spectrum of this star, generating possible confusion in the detection of peaks due to stellar signal. Since these stars are very similar to the Sun, their oscillation amplitudes are tiny in comparison to the

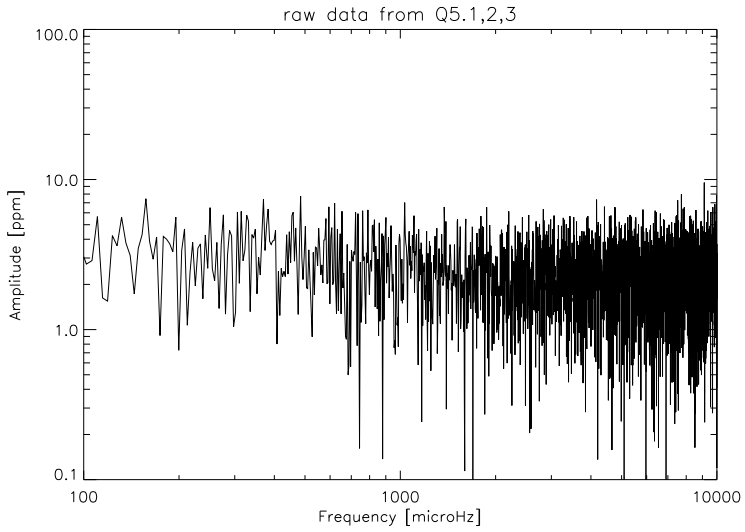

Figure 5.10: Amplitude spectrum for the star KIC3427720, obtained collecting three months of Kepler operations.

one observed in the Subgiant or Giant stars. This can lead to an erroneous identification of the oscillation modes, and only with a long-term monitoring it will be possible to enhance the signal to noise ratio and clearly distinguish real modes above the noise.

We attempted to compare the frequencies assuming alternated values of the angular degree. We found immediately that the theoretical models that better represent the apparently solar parameters of this star shown above(in terms of effective temperature, luminosity and radius), didn't match the observed frequencies at all. So we tried to compared them with theoretical frequencies produced by models with higher mass. In this passage we did not compute new models, just using the same dense grids of the other targets. The results from the chi-square test were improved, in particular if we assume the unknown value of l equal to 0, even if the value of χ^2 is still quite large. The theoretical frequencies corresponding to the lower value of χ^2 are listed in Table (5.9) as well, labelled with 'th'. The corresponding model for these theoretical frequencies provides the following

l_{obs}	n_{obs}	ν_{obs}	$\sigma_{\nu_{obs}}$	l_{th}	n_{th}	ν_{th}
-	20	2501.018799	0.283613	0	20	2495.5443
-	22	2741.559082	0.472374	0	22	2731.3559
-	23	2862.303955	0.295808	0	23	2849.5668
-	24	2981.268799	0.222963	0	24	2968.0434
-	25	3102.708008	0.281295	0	25	3086.9276
-	30	3650.520264	0.243205	0	30	3683.3078

Table 5.9: Observed and theoretical oscillation frequencies for the star KIC3427720. The model was obtained using as input M=1.1 $M_\odot$, α_{ML}=1.7, Z=0.016.

stellar parameters: Mass=1.1 $M_\odot$, Radius=7.905 $\times$ 10^{10} cm, age = 3.758 Gyr, Effective Temperature=5929 K; Luminosity=1.43 $L_\odot$, $X_c = 3.44 \times 10^{10}$.

In conclusion, this star was particular difficult to model because of the erroneous informations provided by the KIC, further confirmed by the estimates of T_{eff} found in literature. Anyway reliable values for this target are strongly required to improve its modelling. Fur-

thermore, only 6 modes were partially identified so far, providing an ambiguous comparison between the theoretical and observed frequencies.

5.3.2 KIC10124866

Figure (5.11) shows the amplitude spectrum of the Q1 (the first month of Kepler scientific operations) data for the star KIC10124866. The available observed frequencies for

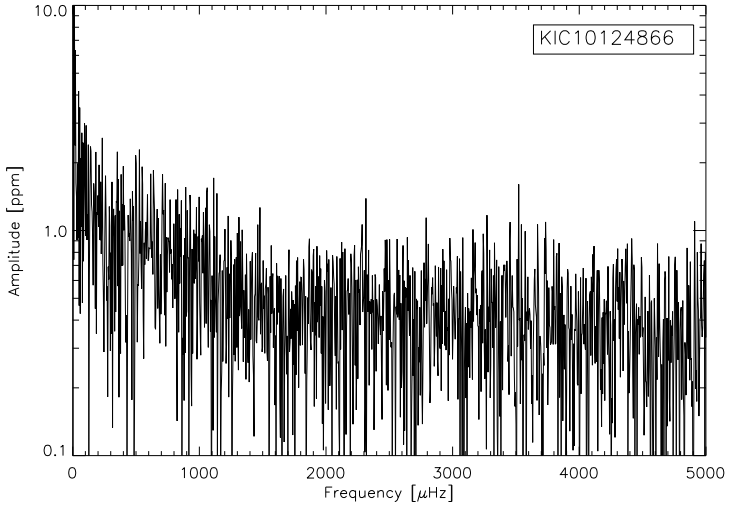

Figure 5.11: Amplitude spectrum for the star KIC10124866 for the Q1 period of observation.

KIC10124866 were obtained using the Bayesian approach described in Gaulme et al. 2009 [72]. However this method doesn't seem to work perfectly for this star. Indeed Table (5.10) shows too low values of the radial order n, rising doubts about the goodness of the fit. Actually only the high order oscillation modes can be detected for distant stars, We think that even in this case a possible reason is the very low signal to noise ratio in the frequency spectrum, even if the hump of solar-like oscillations can be partially recognized in Figure (5.11). Nevertheless we tried to compare these frequencies with the theoretical ones, assuming realistic values for the radial order but our results provided extremely high values of the chi-square, so an improvement of the modelling is required, as well as a reliable identification of the pulsation modes.

5.3.3 KIC8379927

The star KIC8379927 was found to be already observed by other groups and several values of global parameters are also available and listed in Table (5.11). The amplitude spectrum of this target is shown in Figure (5.12), extracted from three months of observations with Kepler. Even in this case the solar-like oscillation modes are hardly recognizable above the noise, but a set of identified pulsation frequencies is available for this star, performed by using a standard maximum likelihood approach. With this method the probability of peaks in the power spectrum being due solely to noise is evaluated, and those peaks that have only a small probability of being due to noise are tagged as modes. In the first 4 columns of Table (5.13) we listed these frequencies, found to be very useful for our purposes. As

l_{obs}	n_{obs}	ν_{obs}	$\sigma_{\nu_{obs}}$	l_{obs}	n_{obs}	ν_{obs}	$\sigma_{\nu_{obs}}$
0	1	2592.90	0.4	1	8	3669.80	1.
0	2	2724.70	0.3	1	9	3819.40	0.6
0	3	2866.10	0.2	1	10	3965.70	0.2
0	4	3000.60	0.3	1	11	4082.90	0.4
0	5	3187.90	0.8	1	12	4271.20	0.9
0	6	3304.50	0.5	1	13	4417.80	0.5
0	7	3486.10	0.3	1	14	4531.20	1.
0	8	3599.80	1.2	2	1	2592.90	0.7
0	9	3728.00	0.5	2	2	2726.40	0.5
0	10	3907.20	1.	2	3	2865.00	0.8
0	11	4071.50	0.1	2	4	2999.30	0.3
0	12	4181.30	0.5	2	5	3185.70	1.6
0	13	4302.70	0.4	2	6	3306.60	0.7
0	14	4464.50	4.2	2	7	3488.60	1.4
1	1	2642.20	0.3	2	8	3598.50	2.2
1	2	2791.50	0.2	2	9	3721.30	1.1
1	3	2922.70	1.	2	10	3907.20	1.0
1	4	3055.40	0.2	2	11	4069.30	0.2
1	5	3228.10	0.7	2	12	4183.20	0.7
1	6	3375.00	0.3	2	13	4300.80	0.4
1	7	3522.20	0.4	2	14	4463.30	4.4

Table 5.10: Observed and theoretical oscillation frequencies for the star KIC10124866. The model was obtained using as input M=1.1 $M_{\odot}$, α_{ML}=1.7, Z=0.016.

Parameter	KIC	A.P. & L. 1999	S 2003	M 2006	G-C 2009
T_{eff} [K]	5763 ± 200	6165.9	6110	5875 ± 51	5956.6
[Fe/H] [dex]	-0.097 ± 0.5	0.05	-	-	-0.11
Radius [$R_{\odot}$]	1.326	1.288	-	1.468 ± 0.041	-
$\log g$ [dex]	4.238	4.31	-	-	-
Mass [$M_{\odot}$]	-	1.23	-	-	-
Age [Gy]	-	-	-	-	5.4

Table 5.11: Summary of the available values of stellar parameters for the target KIC8379927 both from KIC and literature. References: KIC: Latham et al. 2005 [103]; A.P. & L. 1999: allende Prieto and Lambert 1999 [5]; S 2003: Suchkov et al. 2003 [149]; M 2006: Masana et al. 2006 [112]; G-C 2009: Holmberg et al. 2009 [87]

KIC8379927: Parameters	Values
$M/M_{\odot}$	1.20 - 1.23 (with steps of 0.01)
Z	0.03 - 0.034 (with steps of 0.001)
Trial mass	1.15 - 1.30 (with steps of 0.05)
Mixing Length Parameter (α_{ML})	1.9

Table 5.12: Input parameters for the denser grid of models computed for the target KIC8379927.

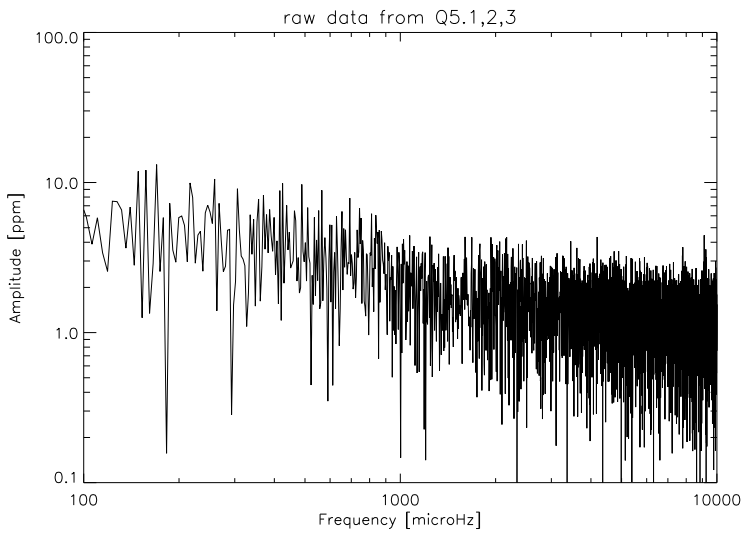

Figure 5.12: Amplitude spectrum for the star KIC8379927 for the Q5 period of observation (three months).

already said, a dense grid of models for this target was computed by using the input data shown in Table (5.6). We applied our procedure for the chi-square test and selected as best model the one with $M = 1.2M_{\odot}$, $\alpha = 1.9$, $Z = 0.032$, having a chi-square value of 39. Since slightly changes in the age of the model can deviate the computed frequencies resulting in a strong worsening of the chi-square test, we computed a further grid in order to improve this result. Using different values of trial mass the distribution of the time steps is different, allowing the investigation of different ages of the model and, of course, a better evaluation of the stellar parameters (see the input parameters in Table (5.12)). Actually, we slightly improve our value of the chi-square, having $\chi^2 = 35.59$ (see Figure (5.13)). Table (5.13) show both the observed frequencies and the theoretical oscillation modes for this best model. The corresponding model provides the stellar parameters listed in Table

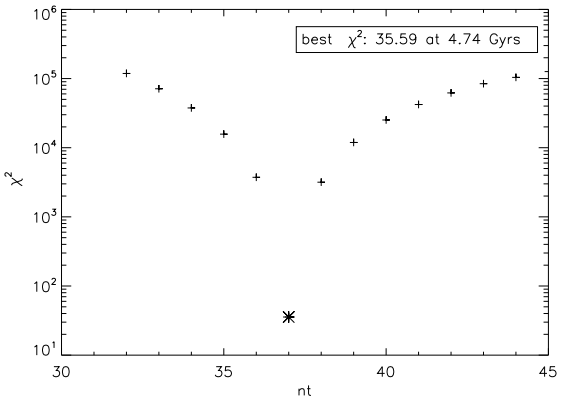

Figure 5.13: Values of the chi-square test for the time steps of the best model with $M = 1.2M_{\odot}$. Y-axis is in logarithmic scale, due to the high difference between the lowest and the other values. The lowest value is 35.59.

l_{obs}	n_{obs}	ν_{obs}	$\sigma_{\nu_{obs}}$	l_{th}	n_{th}	ν_{th}
0	19	2443.53	1.18	0	19	2441.7955
0	20	2563.44	0.48	0	20	2561.5652
0	21	2682.49	0.8	0	21	2681.5666
0	22	2803.83	0.65	0	22	2801.8061
0	23	2925.06	0.38	0	23	2922.1929
0	24	3045.68	0.58	0	24	3043.1286
0	25	3163.10	0.63	0	25	3164.3338
0	26	3280.04	0.38	0	26	3285.7027
1	19	2499.16	1.03	1	19	2499.0446
1	20	2620.63	0.56	1	20	2619.1948
1	21	2739.95	0.62	1	21	2739.2104
1	22	2860.24	0.58	1	22	2859.4979
1	23	2981.08	0.41	1	23	2980.0911
1	24	3103.03	0.68	1	24	3101.0002
1	25	3224.23	0.75	1	25	3222.3535
1	26	3344.31	0.38	1	26	3343.8014
2	18	2433.00	1.63	2	18	2433.4223
2	19	2554.64	0.52	2	19	2553.5502
2	20	2685.08	1.52	2	20	2673.9386
2	21	2795.25	0.93	2	21	2794.4698
2	22	2921.21	0.58	2	22	2915.1088
2	23	3034.62	0.57	2	23	3036.2523
2	24	3155.25	0.51	2	24	3157.6025
2	25	3272.63	0.38	2	25	3279.1263

Table 5.13: Observed and theoretical frequencies for the star KIC8379927.

(5.14).

$M/M_{\odot}$	Age [Gyr]	R [cm]	$\log g$	T_{eff} [K]	$L/L_{\odot}$
1.200	4.74	8.037×10^{10}	4.39	5696.5	1.260

Table 5.14: Stellar parameters obtained with the stellar modelling of the solar-like star KIC8379927 and validated by the comparison with the observed frequencies.

It is immediately clear that the stellar mass for the best model indicates that this star is not properly a solar-twin, being 1.2 solar masses. In order to seek another type of model more similar to a solar one, we examined all the models with a chi-square value lower than 100. Three of them are similar to the one with 1.2 solar masses, but there is one model, showing a chi-square value of 59, having a lower mass, 1.1 $M_{\odot}$, with lower value of the mixing length parameter (i.e. $\alpha_{ML} = 1.6$), Effective temperature of 5726 K, age of 4.1 Gyrs and a heavy element abundance $Z = 0.02$. In order to perform a deep investigation we thought to compute an extremely dense grid for this star, in order to evaluate the χ^2 around the age of this model, even if this procedure is very time consuming on the computational point of view. We set the input parameters of the time steps package of ASTEC in order to compute very dense temporal modelling: about 1500 stellar models were computed. In this way the time step for each computed model is forced to be ~ 0.03 Gyr. In this case we computed theoretical frequencies for more than 100 models around the age of the best one previously found. Figure (5.14) shows the values of the chi-square test for each of them. The lowest χ^2 is 52.7 for the time step 1317, corresponding to a model with an age equal to 4.167 Gyrs. Other parameters obtained in this case are listed

in Table (5.15). This result is clearly not satisfactory, because the χ^2 value is higher than

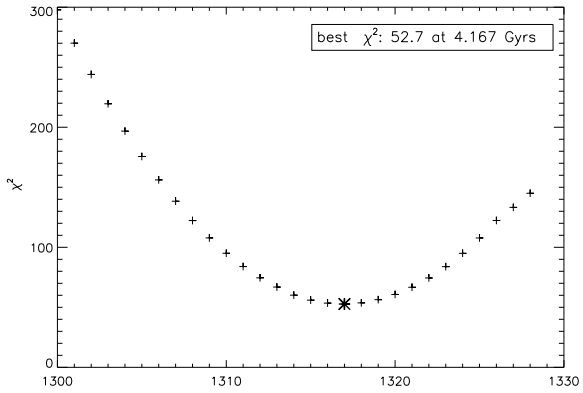

Figure 5.14: Values of the chi-square test for the time steps of the model with $M = 1.1 M_{\odot}$.

$M/M_{\odot}$	Age [Gyr]	R [cm]	T_{eff} [K]	$L/L_{\odot}$
1.1	4.16	7.788×10^{10}	5725.8	1.208

Table 5.15: Stellar parameters obtained from the model with $M = 1.1 M_{\odot}$ for the star KIC8379927.

the previous best model. We further computed a denser grid of models around it without improvements in the value of the chi-square test.

In conclusion, as best result for KIC8379927 we take the one shown in Table (5.14), with a mass equal 1.2 $M_{\odot}$. Figure (5.15) shows the evolutionary track covered by our best model, whose position is indicated by the asterisk. Figure (5.16) shows the theoretical large separation of the best model calculated in the range of the observed frequencies.

Finally, Figure (5.17) shows the echelle diagram (see Section 1.4.4) for the theoretical frequencies (thin squares), superimposed with the same diagram for the observed ones (thick diamonds). Because the frequencies are equally spaced we expect to observe a series of vertical lines (Grec et al. 1983 [75]). Anyway, since they are not precisely equally spaced the echelle diagram shows a sort of curvature in the lines. The value of the angular degree for each group of modes are directly defined in the plot. The dotted vertical line indicates the value of the frequency modulo, namely the large separation, used in the calculations. The comparison between theoretical and observed frequencies shows a quite good agreement, in particular for modes with $l = 1$.

5.4 Results and conclusions

In the previous Sections we reported the attempts to model a few solar-like stars in the Kepler field of view. Disagreement between KIC parameters and the corresponding ones from literature made the stellar modelling more difficult. In particular for KIC3427720 and KIC10124866 the comparison with the observed frequencies was further hampered by the poor or ambiguous mode identification. Further observations from Kepler are now available but no attempt for mode identification is performed so far. Our computations of the DFT show again very low amplitudes and no clear evidence of power excess. These

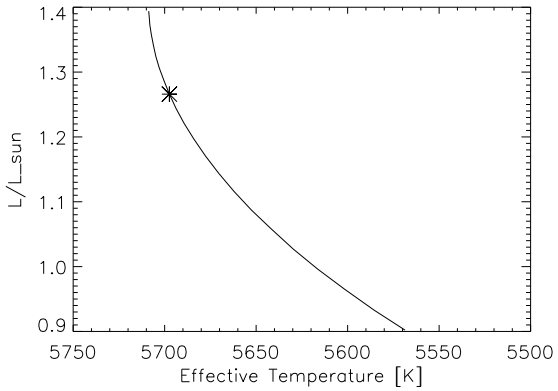

Figure 5.15: Evolutionary track for the best model selected for the star KIC8379927. The asterisk defines the position of the star in the HR diagram characterized by lower value of χ^2.

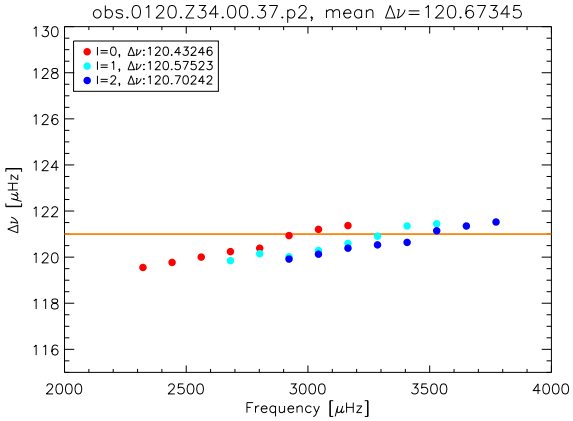

Figure 5.16: Theoretical values of the large frequencies separations compared with the observed mean large separation (121 μHz).

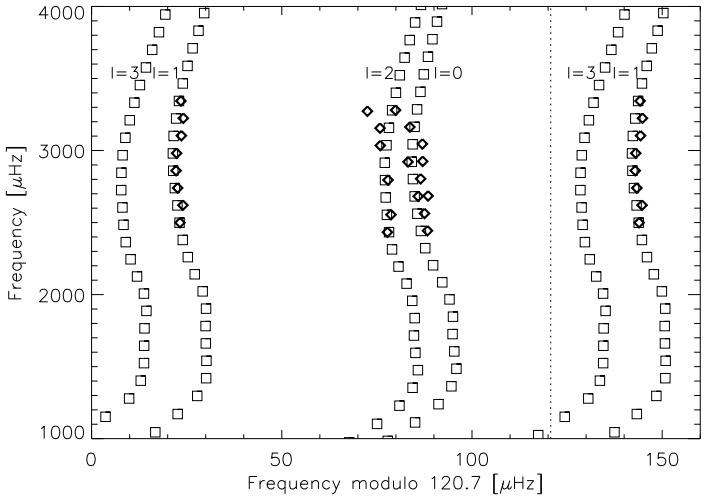

Figure 5.17: Echelle diagram of the theoretical frequencies of the best model computed for the star KIC8379927 (squares) compared with the observed ones (diamonds). The value of the frequency modulo is defined by the dotted vertical line and it is equal to the large separation.

stars behave like a distant Sun, so they are expected to have very low amplitudes and thus weak pulsations. Only the continuous collection of time series from space data will be able to provide unambiguous evidence of solar-like oscillations.

Other two stars of our sample were modelled, namely KIC10644253 and KIC7106245. Their oscillation modes are not yet identified up to now, so we didn't have possibility to test our models. However good perspectives for the star KIC10644253 are foreseen, since it presents a distinct power envelope, as shown in Figure (5.18). Both in the spectrum and in the corresponding smooth it is possible to detect the presence of a hump around 3550 μHz, in agreement with the value listed in Table (5.1). We also attempted to search for

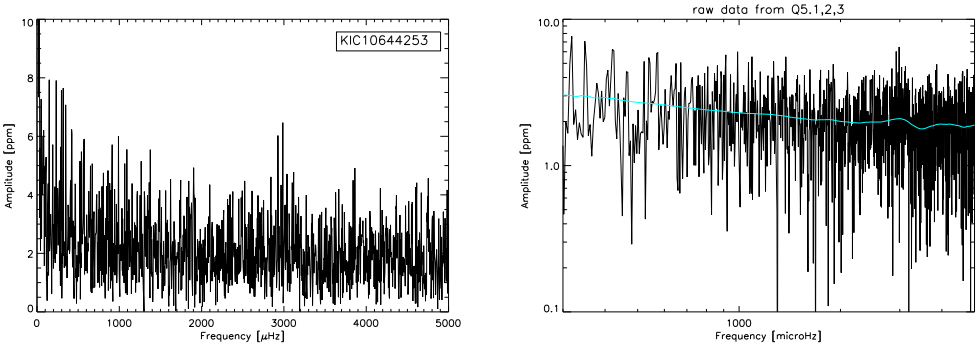

Figure 5.18: *Left panel*: Amplitude spectrum of the star KIC10644253 and the evaluation of its smoothing function (*Right panel*) showing a hump around 3550 μHz.

frequency spacing analysing the comb response function, obtaining $\Delta\nu$ equal to 112 μHz. This result, even if it falls within the error bars, is quite far from the value obtained with

the Kepler pipeline (i.e. 122 μHz). This can be due to an erroneous choice of the peaks used in the computation, because of the quite high value of the noise of the spectrum.

Better results were obtained for the star KIC8379927. Thanks to the stellar modelling and the chi-square minimization test we found a model able to represent within a certain degree the observed frequencies. Table (5.16) shows the global parameters of the best model found.

$M/M_\odot$	Age [Gyr]	R [cm]	$\log g$	T_{eff} [K]	$L/L_\odot$
1.200	4.74	8.037×10^{10}	4.39	5696.5	1.260

Table 5.16: Stellar parameters obtained with the stellar modelling of the solar-like star KIC8379927 and validated by the comparison with the observed frequencies.

Other attempts will be performed, because an improvement of our precision in the determination of the theoretical oscillation frequencies is required. Actually the stellar mass of the best model indicates that KIC8379927 is not properly a solar-twin. The Kepler Input Catalog provides several stellar parameters, e.g, stellar magnitude, effective temperature, surface gravity, metallicity and radius affected by a high degree of uncertainties. This can lead to an erroneous stellar modelling, as shown in the case of KIC3427720, or unexpected results (KIC8379927). This demonstrates that the parameters provided by KIC must be verified with other available in literature, if any, or even with extensive observational campaigns. This fact stresses a very important issue, because it shows the extreme necessity to know reliable values of stellar parameters, in addition to a high accuracy in their determination. Good confidence on the input parameters is for sure a great advantage in stellar modelling and in many other fields. In fact the possibility to obtain accurate determination of fundamental stellar parameters, provided by asteroseismic techniques, is a fundamental step toward exoplanets characterization, especially in consideration of PLATO.

In the next future, further observations of Kepler can yield even more precise measurements and identification of the oscillation frequencies for these objects, affected by small amplitudes. Thanks to that, we expect to improve our determination of stellar paramenters, as well as the determination of the accuracy level of our models.

Conclusions

Asteroseismology unlike traditional techniques, yields quantitative informations on the internal structure of stars through the analysis of stellar oscillation frequencies. The observational scenario of Asteroseismology cannot be better than nowadays, since we are provided by a plenty of valuable incoming data from space satellites like CoRoT and Kepler. Moreover the future might bring further opportunities if the proposed space mission PLATO will flight. Asteroseismology also provides useful indications to several astrophysical fields, such as stellar evolution theories or exoplanetary sciences. In particular, the synergy between the search of extrasolar planets and Asteroseismology is incredibly strong. Satellites mentioned above are working to enhance the number of confirmed exoplanets. However direct and precise informations about the planet properties are still far to be achieved without reliable values of the parent stars parameters. This limiting factor is the reason why Kepler and PLATO inserted in their science cases the asteroseismic observations of planet hosting stars. Nowadays Asteroseismology yields these informations as demonstrated by Mosser et al. 2010 [122], Kallinger et al. 2010 [94] and Metcalfe et al. 2010 [117], which put firm constraints to stellar parameters using the asteroseismic observables and the support of theoretical models.

The PhD project presented in this thesis has been developed in the scenario above mentioned, exploiting the asteroseismic potential provided by space instruments. In particular, the research follows several steps of a space mission project, contributing to the feasibility study of a satellite, passing through the analysis of the incoming data and the use of the results to determine reliable stellar parameters thanks to Asteroseismology.

Part of the work (presented in Chapter 3) was dedicated to the analysis of simulated images provided to us by Dr. Zima through an End-to-End Simulator (see Zima et al. 2010 [158]), created with the aim to study the impact of all the possible sources of noise (photon noise, sky background, readout noise from the detector, instrumental drift and so on) to the images on the focal plane. As first task we have studied the photometric quality of the images, calculating the signal-to-noise ratio for each simulated star in part per million per hour [ppm/h] for all of the 40 telescope units of PLATO, with the aim to compare it with the scientific requirements for the accepted noise levels: 27 ppm/h for the stellar oscillations detection and 80 ppm/h for exoplanets detection.

Brighter stars ($m_V \sim 7 - 8$) show a low level of noise, but in some case this is due to their saturation on the detector. Stars with input magnitude less than $m_V \sim 11$ show a noise level less than 27 ppm/h, while the condition of the 80 ppm/h is fulfilled by stars with magnitude less than $m_V \sim 13$. This kind of analysis allows to select which type of data redution is more suited to perform the better photometry (aperture or weighted mask photometry).

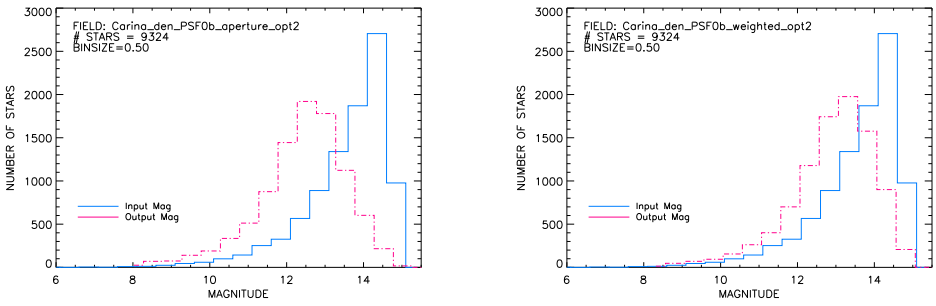

Figure 5.19: Comparison between the two different methods for data reduction: the aperture photometry (left panel) and the weighted mask photometry (right panel). The weighted photometry is significantly less affected by stellar crowding.

The first observing strategy proposed for PLATO involved the use of defocus. We also contributed to a preliminary analysis of the amount of defocusing to apply to the telescopes. However a high concentration of stars in the simulated fields forced to revise the observing strategy. In order to quantify the crowding and to show the problem arose, we estimated the deviation of the luminosity function of the input catalog toward the brighter magnitudes (see Figure (5.19)). This appears to be higher for aperture photometry than weighted mask photometry. The contaminating flux due to the neighbour sources for each star was evaluated, using as input the dimensions of the Point Spread Function and the specified encircled energy. As expected, fainter stars are the most affected by crowding effect, even for the less concentrated simulated field.

Finally, it is described a personal procedure that simulates the time series of the star as observed by PLATO. To obtain this simulation we computed theoretical stellar model and subsequently the corresponding oscillation frequencies. We created the time series as the sum of all the sinusoidal components of the signal. We added the previously analysed noise to our simulation and the amplitude spectrum is extracted (Figure (5.20)). The spectrum

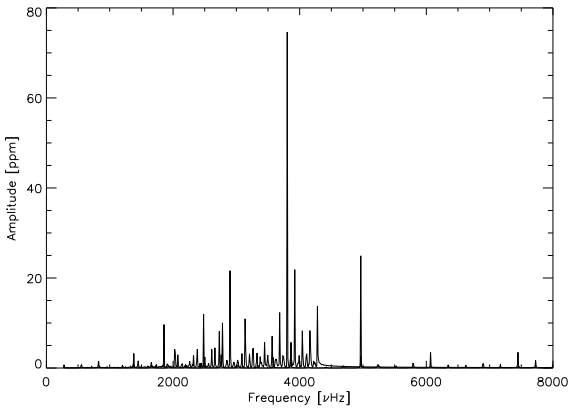

Figure 5.20: Amplitude spectrum of the time series obtained through the sum of the simulated stellar signal and the simulated noise.

of the pure noise shows typical features of white noise, except for two artefacts, maybe due to the algorithm used to simulate the noise. It is important to note that the regular

sampling of both the time series makes the spectra more clean than in the case of a real observation. Nevertheless we find that the instrumental noise doesn't affect in a serious way eventual solar-like oscillations. This tool is useful to assure that these fluctuations can be actually observed by PLATO, and to evaluate the impact of the stellar noise on the detection of a planetary transit.

A series of personal procedures, written in IDL language, aimed to perform seismic analysis of photometric time series are presented, with some applications to Kepler and EXOTIME data. Thanks to these tools we have the possibility, starting from raw data, to perform a statistical analysis of the time series and to extract the power spectrum using the algorithm of Deeming 1975 [62] (namely the Discrete Fourier Transform). One other feature of these procedures is the interactive choice of the time sampling, which allow to automatically select the right Nyquist frequency. The frequencies extraction is then performed through an iterative prewhitening process and a sinusoidal fit of the time series.

These procedures were applied to the Kepler data for a sample of hybrid γ Dor and δ Sct stars, in order to compare the extracted frequencies of those targets among the member of the KASC Working Group 10 (γ Doradus stars). Figure (5.21) left panel, shows the amplitude spectrum obtained for a star, whereas the extracted frequencies are indicated with vertical lines. The right panel of Figure (5.21) shows the amplitude spectra of the residuals, at the end of the iteration process that subtracts for each identified frequency a sinusoidal fit to the time series according to the function: $A\cos(2\pi\nu t_i + \phi)$, where A is the amplitude, ν is the frequency t_i is the temporal cadence and ϕ the phase. Table (5.17) shows the five most important components of the signal detected for KIC001573064 and the relative uncertainties from the formal fit (see Montgomery and O'Donoghue 1999 [121]).

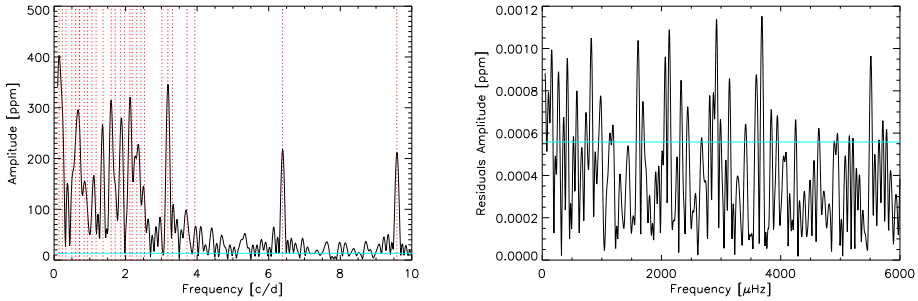

Figure 5.21: Amplitude spectrum of the *gamma* Dor star KIC001573064, using the long cadence time series and amplitude spectrum of the residuals of the same star.

Other features were implemented to our procedures, useful for the analysis of solar-like oscillations. Even in this case we had the opportunity to verify our codes with Kepler data, by using the preliminary observations of three solar-like stars reported by Chaplin et al. 2010 [37]. We modelled the background of the available power spectra through a least-square fit procedure and calculated the value of the large separation by evaluating of the *comb response* function, the tool able to reveal possible periodicities in the power spectrum in the frequency range of the Lorentian envelope (5.22, left panel). Finally the

#	freq [c/d]	δfreq	ampl [ppm]	δampl	phase [rad]	δphase
1	0.1405166	0.0000715	403.0021469	0.5071381	-0.3444051	0.0000962
2	3.1807845	0.0000826	348.7093960	0.5071381	2.7460748	0.0001112
3	2.1205230	0.0000882	326.5478149	0.5071381	1.9415751	0.0001187
4	1.5967794	0.0000929	310.1767091	0.5071381	3.0210462	0.0001250
5	0.7025829	0.0000925	311.3689262	0.5071381	1.5857665	0.0001245

Table 5.17: Frequencies obtained for the star KIC001573064.

echelle diagram in Figure (5.22, right panel) is created for the frequencies extracted by the prewhitening procedure. Small triangles represent all the extracted frequencies, while with larger symbols we indicate the frequencies found also by Chaplin et al. 2010 [37] (diamonds for $l = 0$, asterisks for $l = 1$ and plus for $l = 2$). Departure from the vertical line (as in the case for mode with $l = 1$) is due to the presence of avoided crossings (Aizenmann et al. 1977 [4], clear indicators of stars significantly evolved.

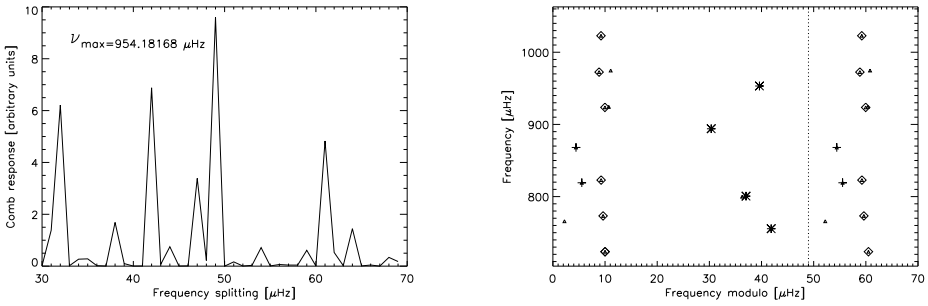

Figure 5.22: Left: Evaluation of the comb response function for a solar-like star KIC11026764 observed by Kepler: the maximum value of this function defines an estimate of the large separation. Right: Echelle diagram of the extracted frequencies for the same target.

Also the data collected personally at the Asiago-Ekar Observatory, in the framework of the EXOTIME project, were used to test and verify the codes, in particular for the Subdwarf B star HS0702+6043. Public softwares aimed to extract oscillation frequencies are also available and they were used during the presented work. However the analysis of different types of data can lead to the development of personal codes, with the advantage to work with tools suited from case to case.

As final topic we show how to use asteroseismic data, obtained thanks to the Kepler satellite, in order to constrain global stellar parameters. Kepler is providing a large amount of light curve for several pulsating classes. Solar-type stars are the most interesting in the framework of Extrasolar planets characterization, particularly important for Kepler's scopes. A small sample of these stars was selected according to the informations of the Kepler Input Catalog with the aim to find the best candidate to be a solar-twin. Using ASTEC and ADIPLS codes (Christensen-Dalsgaard 2008a,b [44], [43]) for the stellar modelling and computation of theoretical pulsation frequencies, we tried to reproduce the observed parameters, starting from large to dense grids of evolutionary models (Figure

(5.23)), and calculated the corresponding theoretical adiabatic pulsations. Through a chi-

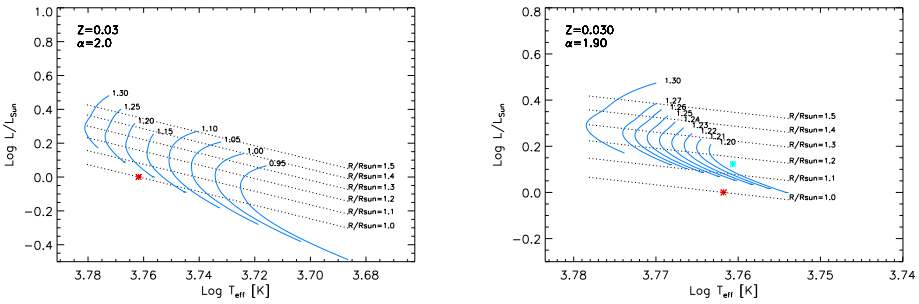

Figure 5.23: Left panel shows the large grid of evolutionary tracks, with a wide range of parameters, whereas the denser grid (right panel) was computed around the model that better represented the observed stellar parameters.

square minimization test, we can select the model that better represents the frequencies obtained by Kepler with the theoretical predictions, and then the parameters of the star (Figure (5.24) and Table (5.18)).

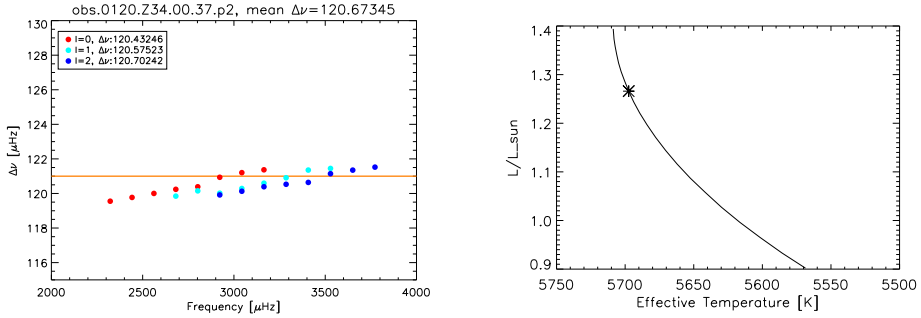

Figure 5.24: Left panel: comparison between the mean large separation obtained with Kepler frequencies and the theoretical ones, obtained with the best model, selected through a chi-square test. Right panel: the evolutionary track for the best model selected for the star KIC8379927. The asterisk define the position of the star in the HR diagram characterized by lower value of χ^2.

$M/M_\odot$	Age [Gyr]	Z	α_{ML}	R [cm]	T_{eff} [K]	$L/L_\odot$	X_c
1.200	4.74001	0.034	1.90	8.03710×10^{10}	5696.5	1.260	3.266×10^{-1}

Table 5.18: Stellar parameters obtained for the solar-like star KIC8379927.

In the next future, further observations of Kepler we can yield even more precise measurement and identification of the oscillation frequencies for these objects, affected by small amplitudes. Furthermore the results of the chi-square test should be optimized. Thanks to that, we expect to improve our determination of stellar paramenters.

The stellar mass of the best model indicates that the target KIC8379927 is not properly a solar-twin. This shows that the parameters provided by KIC must be verified with other

available e.g. in literature, if any. This fact stresses a very important issue, because it shows the extreme necessity to know reliable values of stellar parameters, in addition to a high accuracy in their determination. Asteroseismology can really supply to this gap and help to obtain the required precision for stellar and exoplanets characterization.

Appendix A

Procedures for seismic analysis

In the following Tables are listed the IDL procedures written to perform the seismic analysis already exposed in Chapter 3. For each procedure we define the input and output data as well as a schematic description of their main features.

Procedure's name	Input	Actions	Output
`light_curve.pro`	raw TS	• Instrumental/Airmass trends removal • Normalization • Conversion to [ppm]	TS [ppm]
`statistics.pro`	TS [ppm]	• Histograms of flux and uncertainties • Computation of the variance • Computation of the autocorrelation	plots
`power.pro`	TS [ppm]	• Evaluation of: - Nyquist frequency - temporal distribution - white noise (σ) • Computation of the power spectrum by using `deeming.pro`	PS
`background.pro`	PS	• Smooth of the PS • Binning of the PS • least-square fit with `MPFIT` package[1] with background model function	BKG parameters
`prewhitening.pro`	TS [ppm]	• Computation of the power spectrum through `deeming.pro` and identification of the most important peak • Computation of the periodical function of Eq. (4.23) • Least-square fit with `MPFIT` package[1] between the periodical function and the TS • Subtraction of the best fit from the TS • Iteration of the same process until the maximum peak is higher than 4σ	ν_{osc}

Table A.1: List of acronyms: TS=time series; TS [ppm]= time series converted in parts per million; PS=power spectrum; BKG=background; $\Delta\nu$=large separation; ν_{osc}=oscillation frequencies; 1. *http://www.physics.wisc.edu/∼craigm/idl/idl.html*

.

Procedure's name	Input	Actions	Output
`comb.pro`	PS	• Computation of the CR function according to Eq. (4.28) for each frequency corresponding to a peak $\geq 4\sigma$ in the PS • Computation of the mean value of the maximum of the CR	$\Delta\nu$
`echelle.pro`	ν_{osc} $\Delta\nu$	• Binning of the PS • Overlap of the single bins • Plot of the observed frequencies with the frequency modulo	ED, l

Table A.2: List of acronyms: PS=power spectrum; CR=comb response; $\Delta\nu$=large separation; ν_{osc}=oscillation frequencies; ED=echelle diagram; l=angular degree.

Appendix B

Journal of observations

The journal of observations performed with the 182 cm Telescope at the INAF-Astrophysical Observatory in Asiago-Mt.Ekar in the framework of the EXOTIME project, are listed as follows. We subdivided the three different runs spanned in two years. The name of the images are labelled by a serial number, the date of the observation, the start of each exposure, the exposure time, the Julian Date at the beginning of the exposure, the name of the observed object and the utilized filter.

B.1 March, 12-13, 2008

#	Image	Date	Start	Texp	JD	Object	Filter
1	IMA0018.fits	12/03/08	22:18:07	15.0	2454538.42925	PG1219+534	R
2	IMA0019.fits	12/03/08	22:19:34	15.0	2454538.43025	PG1219+534	R
3	IMA0020.fits	12/03/08	22:21:00	15.0	2454538.43125	PG1219+534	R
4	IMA0021.fits	12/03/08	22:22:25	15.0	2454538.43223	PG1219+534	R
5	IMA0022.fits	12/03/08	22:23:51	15.0	2454538.43323	PG1219+534	R
6	IMA0023.fits	12/03/08	22:25:18	15.0	2454538.43424	PG1219+534	R
7	IMA0024.fits	12/03/08	22:26:43	15.0	2454538.43522	PG1219+534	R
8	IMA0025.fits	12/03/08	22:28:09	15.0	2454538.43622	PG1219+534	R
9	IMA0026.fits	12/03/08	22:29:35	15.0	2454538.43721	PG1219+534	R
10	IMA0027.fits	12/03/08	22:31:17	15.0	2454538.43839	PG1219+534	R
11	IMA0028.fits	12/03/08	22:32:43	15.0	2454538.43939	PG1219+534	R
12	IMA0029.fits	12/03/08	22:34:09	15.0	2454538.44038	PG1219+534	R
13	IMA0030.fits	12/03/08	22:35:36	15.0	2454538.44139	PG1219+534	R
14	IMA0031.fits	12/03/08	22:37:02	15.0	2454538.44238	PG1219+534	R
15	IMA0032.fits	12/03/08	22:38:28	15.0	2454538.44338	PG1219+534	R
16	IMA0033.fits	12/03/08	22:39:53	15.0	2454538.44436	PG1219+534	R
17	IMA0034.fits	12/03/08	22:41:20	15.0	2454538.44537	PG1219+534	R
18	IMA0035.fits	12/03/08	22:42:47	15.0	2454538.44638	PG1219+534	R
19	IMA0036.fits	12/03/08	22:44:29	15.0	2454538.44756	PG1219+534	R
20	IMA0037.fits	12/03/08	22:45:56	15.0	2454538.44856	PG1219+534	R
21	IMA0038.fits	12/03/08	22:47:22	15.0	2454538.44956	PG1219+534	R
22	IMA0039.fits	12/03/08	22:48:48	15.0	2454538.45056	PG1219+534	R
23	IMA0040.fits	12/03/08	22:50:14	15.0	2454538.45155	PG1219+534	R
24	IMA0041.fits	12/03/08	22:51:41	15.0	2454538.45256	PG1219+534	R
25	IMA0042.fits	12/03/08	22:53:07	15.0	2454538.45355	PG1219+534	R
26	IMA0043.fits	12/03/08	22:54:33	15.0	2454538.45455	PG1219+534	R
27	IMA0044.fits	12/03/08	22:55:59	15.0	2454538.45554	PG1219+534	R
28	IMA0045.fits	12/03/08	22:57:39	15.0	2454538.45670	PG1219+534	R
29	IMA0046.fits	12/03/08	22:59:04	15.0	2454538.45769	PG1219+534	R
30	IMA0047.fits	12/03/08	23:00:30	15.0	2454538.45868	PG1219+534	R

31	IMA0048.fits	12/03/08	23:01:56	15.0	2454538.45968	PG1219+534 R
32	IMA0049.fits	12/03/08	23:03:22	15.0	2454538.46067	PG1219+534 R
33	IMA0050.fits	12/03/08	23:04:50	15.0	2454538.46169	PG1219+534 R
34	IMA0051.fits	12/03/08	23:06:17	15.0	2454538.46270	PG1219+534 R
35	IMA0052.fits	12/03/08	23:07:44	15.0	2454538.46370	PG1219+534 R
36	IMA0053.fits	12/03/08	23:09:11	15.0	2454538.46471	PG1219+534 R
37	IMA0054.fits	12/03/08	23:10:53	15.0	2454538.46589	PG1219+534 R
38	IMA0055.fits	12/03/08	23:12:21	15.0	2454538.46691	PG1219+534 R
39	IMA0056.fits	12/03/08	23:13:47	15.0	2454538.46791	PG1219+534 R
40	IMA0057.fits	12/03/08	23:15:14	15.0	2454538.46891	PG1219+534 R
41	IMA0058.fits	12/03/08	23:16:40	15.0	2454538.46991	PG1219+534 R
42	IMA0059.fits	12/03/08	23:18:07	15.0	2454538.47091	PG1219+534 R
43	IMA0060.fits	12/03/08	23:19:33	15.0	2454538.47191	PG1219+534 R
44	IMA0061.fits	12/03/08	23:21:00	15.0	2454538.47292	PG1219+534 R
45	IMA0062.fits	12/03/08	23:22:27	15.0	2454538.47392	PG1219+534 R
46	IMA0063.fits	12/03/08	23:24:10	15.0	2454538.47512	PG1219+534 R
47	IMA0064.fits	12/03/08	23:25:37	15.0	2454538.47612	PG1219+534 R
48	IMA0065.fits	12/03/08	23:27:03	15.0	2454538.47712	PG1219+534 R
49	IMA0066.fits	12/03/08	23:28:30	15.0	2454538.47813	PG1219+534 R
50	IMA0067.fits	12/03/08	23:29:57	15.0	2454538.47913	PG1219+534 R
51	IMA0068.fits	12/03/08	23:31:23	15.0	2454538.48013	PG1219+534 R
52	IMA0069.fits	12/03/08	23:32:50	15.0	2454538.48113	PG1219+534 R
53	IMA0070.fits	12/03/08	23:34:17	15.0	2454538.48214	PG1219+534 R
54	IMA0071.fits	12/03/08	23:35:44	15.0	2454538.48315	PG1219+534 R
55	IMA0072.fits	12/03/08	23:37:25	15.0	2454538.48432	PG1219+534 R
56	IMA0073.fits	12/03/08	23:38:52	15.0	2454538.48532	PG1219+534 R
57	IMA0074.fits	12/03/08	23:40:18	15.0	2454538.48632	PG1219+534 R
58	IMA0075.fits	12/03/08	23:41:44	15.0	2454538.48731	PG1219+534 R
59	IMA0076.fits	12/03/08	23:43:12	15.0	2454538.48833	PG1219+534 R
60	IMA0077.fits	12/03/08	23:44:38	15.0	2454538.48933	PG1219+534 R
61	IMA0078.fits	12/03/08	23:46:04	15.0	2454538.49032	PG1219+534 R
62	IMA0079.fits	12/03/08	23:47:31	15.0	2454538.49133	PG1219+534 R
63	IMA0080.fits	12/03/08	23:48:57	15.0	2454538.49233	PG1219+534 R
64	IMA0081.fits	12/03/08	23:50:38	15.0	2454538.49350	PG1219+534 R
65	IMA0082.fits	12/03/08	23:52:04	15.0	2454538.49449	PG1219+534 R
66	IMA0083.fits	12/03/08	23:53:31	15.0	2454538.49550	PG1219+534 R
67	IMA0084.fits	12/03/08	23:54:57	15.0	2454538.49649	PG1219+534 R
68	IMA0085.fits	12/03/08	23:56:23	15.0	2454538.49749	PG1219+534 R
69	IMA0086.fits	12/03/08	23:57:49	15.0	2454538.49848	PG1219+534 R
70	IMA0087.fits	12/03/08	23:59:18	15.0	2454538.49951	PG1219+534 R
71	IMA0088.fits	13/03/08	00:00:45	15.0	2454538.50052	PG1219+534 R
72	IMA0089.fits	13/03/08	00:02:11	15.0	2454538.50152	PG1219+534 R
73	IMA0090.fits	13/03/08	00:03:52	15.0	2454538.50269	PG1219+534 R
74	IMA0091.fits	13/03/08	00:05:17	15.0	2454538.50367	PG1219+534 R
75	IMA0092.fits	13/03/08	00:06:42	15.0	2454538.50465	PG1219+534 R
76	IMA0093.fits	13/03/08	00:08:09	15.0	2454538.50566	PG1219+534 R
77	IMA0094.fits	13/03/08	00:09:35	15.0	2454538.50666	PG1219+534 R
78	IMA0095.fits	13/03/08	00:11:01	15.0	2454538.50765	PG1219+534 R
79	IMA0096.fits	13/03/08	00:12:27	15.0	2454538.50865	PG1219+534 R
80	IMA0097.fits	13/03/08	00:13:54	15.0	2454538.50965	PG1219+534 R
81	IMA0098.fits	13/03/08	00:15:21	15.0	2454538.51066	PG1219+534 R
82	IMA0099.fits	13/03/08	00:17:03	15.0	2454538.51184	PG1219+534 R
83	IMA0100.fits	13/03/08	00:18:31	15.0	2454538.51286	PG1219+534 R
84	IMA0101.fits	13/03/08	00:19:57	15.0	2454538.51385	PG1219+534 R
85	IMA0102.fits	13/03/08	00:21:23	15.0	2454538.51485	PG1219+534 R
86	IMA0103.fits	13/03/08	00:22:50	15.0	2454538.51586	PG1219+534 R
87	IMA0104.fits	13/03/08	00:24:17	15.0	2454538.51686	PG1219+534 R
88	IMA0105.fits	13/03/08	00:25:43	15.0	2454538.51786	PG1219+534 R
89	IMA0106.fits	13/03/08	00:27:09	15.0	2454538.51885	PG1219+534 R

90	IMA0107.fits	13/03/08	00:28:36	15.0	2454538.51986	PG1219+534	R
91	IMA0108.fits	13/03/08	00:33:59	15.0	2454538.52360	PG1219+534	R
92	IMA0109.fits	13/03/08	00:35:26	15.0	2454538.52461	PG1219+534	R
93	IMA0110.fits	13/03/08	00:36:51	15.0	2454538.52559	PG1219+534	R
94	IMA0111.fits	13/03/08	00:38:18	15.0	2454538.52660	PG1219+534	R
95	IMA0112.fits	13/03/08	00:39:44	15.0	2454538.52759	PG1219+534	R
96	IMA0113.fits	13/03/08	00:41:09	15.0	2454538.52858	PG1219+534	R
97	IMA0114.fits	13/03/08	00:42:36	15.0	2454538.52958	PG1219+534	R
98	IMA0115.fits	13/03/08	00:44:02	15.0	2454538.53058	PG1219+534	R
99	IMA0116.fits	13/03/08	00:45:28	15.0	2454538.53157	PG1219+534	R
100	IMA0117.fits	13/03/08	00:47:09	15.0	2454538.53274	PG1219+534	R
101	IMA0118.fits	13/03/08	00:48:36	15.0	2454538.53375	PG1219+534	R
102	IMA0119.fits	13/03/08	00:50:02	15.0	2454538.53475	PG1219+534	R
103	IMA0120.fits	13/03/08	00:51:28	15.0	2454538.53574	PG1219+534	R
104	IMA0121.fits	13/03/08	00:52:54	15.0	2454538.53674	PG1219+534	R
105	IMA0122.fits	13/03/08	00:54:21	15.0	2454538.53774	PG1219+534	R
106	IMA0123.fits	13/03/08	00:55:46	15.0	2454538.53873	PG1219+534	R
107	IMA0124.fits	13/03/08	00:57:12	15.0	2454538.53972	PG1219+534	R
108	IMA0125.fits	13/03/08	00:58:39	15.0	2454538.54073	PG1219+534	R
109	IMA0126.fits	13/03/08	01:00:19	15.0	2454538.54189	PG1219+534	R
110	IMA0127.fits	13/03/08	01:01:44	15.0	2454538.54287	PG1219+534	R
111	IMA0128.fits	13/03/08	01:03:09	15.0	2454538.54385	PG1219+534	R
112	IMA0129.fits	13/03/08	01:04:36	15.0	2454538.54486	PG1219+534	R
113	IMA0130.fits	13/03/08	01:06:02	15.0	2454538.54586	PG1219+534	R
114	IMA0131.fits	13/03/08	01:07:28	15.0	2454538.54685	PG1219+534	R
115	IMA0132.fits	13/03/08	01:08:56	15.0	2454538.54787	PG1219+534	R
116	IMA0133.fits	13/03/08	01:10:21	15.0	2454538.54885	PG1219+534	R
117	IMA0134.fits	13/03/08	01:11:46	15.0	2454538.54984	PG1219+534	R
118	IMA0135.fits	13/03/08	01:13:29	15.0	2454538.55103	PG1219+534	R
119	IMA0136.fits	13/03/08	01:14:57	15.0	2454538.55205	PG1219+534	R
120	IMA0137.fits	13/03/08	01:16:24	15.0	2454538.55306	PG1219+534	R
121	IMA0138.fits	13/03/08	01:17:50	15.0	2454538.55405	PG1219+534	R
122	IMA0139.fits	13/03/08	01:19:17	15.0	2454538.55506	PG1219+534	R
123	IMA0140.fits	13/03/08	01:20:43	15.0	2454538.55605	PG1219+534	R
124	IMA0141.fits	13/03/08	01:22:10	15.0	2454538.55706	PG1219+534	R
125	IMA0142.fits	13/03/08	01:23:38	15.0	2454538.55808	PG1219+534	R
126	IMA0143.fits	13/03/08	01:25:05	15.0	2454538.55909	PG1219+534	R
127	IMA0144.fits	13/03/08	01:26:45	15.0	2454538.56024	PG1219+534	R
128	IMA0145.fits	13/03/08	01:28:12	15.0	2454538.56125	PG1219+534	R
129	IMA0146.fits	13/03/08	01:29:39	15.0	2454538.56226	PG1219+534	R
130	IMA0147.fits	13/03/08	01:31:05	15.0	2454538.56325	PG1219+534	R
131	IMA0148.fits	13/03/08	01:32:32	15.0	2454538.56426	PG1219+534	R
132	IMA0149.fits	13/03/08	01:33:59	15.0	2454538.56527	PG1219+534	R
133	IMA0150.fits	13/03/08	01:35:26	15.0	2454538.56627	PG1219+534	R
134	IMA0151.fits	13/03/08	01:36:53	15.0	2454538.56728	PG1219+534	R
135	IMA0152.fits	13/03/08	01:38:19	15.0	2454538.56828	PG1219+534	R
136	IMA0153.fits	13/03/08	01:40:03	15.0	2454538.56948	PG1219+534	R
137	IMA0154.fits	13/03/08	01:41:30	15.0	2454538.57049	PG1219+534	R
138	IMA0155.fits	13/03/08	01:42:56	15.0	2454538.57148	PG1219+534	R
139	IMA0156.fits	13/03/08	01:44:22	15.0	2454538.57248	PG1219+534	R
140	IMA0157.fits	13/03/08	01:45:48	15.0	2454538.57347	PG1219+534	R
141	IMA0158.fits	13/03/08	01:47:16	15.0	2454538.57449	PG1219+534	R
142	IMA0159.fits	13/03/08	01:48:42	15.0	2454538.57549	PG1219+534	R
143	IMA0160.fits	13/03/08	01:50:08	15.0	2454538.57648	PG1219+534	R
144	IMA0161.fits	13/03/08	01:51:35	15.0	2454538.57749	PG1219+534	R
145	IMA0162.fits	13/03/08	01:53:16	15.0	2454538.57866	PG1219+534	R
146	IMA0163.fits	13/03/08	01:54:43	15.0	2454538.57966	PG1219+534	R
147	IMA0164.fits	13/03/08	01:56:09	15.0	2454538.58066	PG1219+534	R
148	IMA0165.fits	13/03/08	01:57:36	15.0	2454538.58167	PG1219+534	R

149	IMA0166.fits	13/03/08	01:59:02	15.0	2454538.58266	PG1219+534	R
150	IMA0167.fits	13/03/08	02:00:28	15.0	2454538.58366	PG1219+534	R
151	IMA0168.fits	13/03/08	02:01:55	15.0	2454538.58466	PG1219+534	R
152	IMA0169.fits	13/03/08	02:03:20	15.0	2454538.58565	PG1219+534	R
153	IMA0170.fits	13/03/08	02:04:46	15.0	2454538.58664	PG1219+534	R
154	IMA0171.fits	13/03/08	02:06:28	15.0	2454538.58782	PG1219+534	R
155	IMA0172.fits	13/03/08	02:07:55	15.0	2454538.58883	PG1219+534	R
156	IMA0173.fits	13/03/08	02:09:21	15.0	2454538.58983	PG1219+534	R
157	IMA0174.fits	13/03/08	02:10:47	15.0	2454538.59082	PG1219+534	R
158	IMA0175.fits	13/03/08	02:12:14	15.0	2454538.59183	PG1219+534	R
159	IMA0176.fits	13/03/08	02:13:40	15.0	2454538.59282	PG1219+534	R
160	IMA0177.fits	13/03/08	02:15:06	15.0	2454538.59382	PG1219+534	R
161	IMA0178.fits	13/03/08	02:16:33	15.0	2454538.59483	PG1219+534	R
162	IMA0179.fits	13/03/08	02:17:60	15.0	2454538.59583	PG1219+534	R
163	IMA0180.fits	13/03/08	02:19:40	15.0	2454538.59699	PG1219+534	R
164	IMA0181.fits	13/03/08	02:21:05	15.0	2454538.59797	PG1219+534	R
165	IMA0182.fits	13/03/08	02:22:33	15.0	2454538.59899	PG1219+534	R
166	IMA0183.fits	13/03/08	02:23:58	15.0	2454538.59998	PG1219+534	R
167	IMA0184.fits	13/03/08	02:25:26	15.0	2454538.60100	PG1219+534	R
168	IMA0185.fits	13/03/08	02:26:52	15.0	2454538.60199	PG1219+534	R
169	IMA0186.fits	13/03/08	02:28:20	15.0	2454538.60301	PG1219+534	R
170	IMA0187.fits	13/03/08	02:29:46	15.0	2454538.60400	PG1219+534	R
171	IMA0188.fits	13/03/08	02:31:12	15.0	2454538.60500	PG1219+534	R
172	IMA0189.fits	13/03/08	02:32:54	15.0	2454538.60618	PG1219+534	R
173	IMA0190.fits	13/03/08	02:34:21	15.0	2454538.60719	PG1219+534	R
174	IMA0191.fits	13/03/08	02:35:47	15.0	2454538.60818	PG1219+534	R
175	IMA0192.fits	13/03/08	02:37:13	15.0	2454538.60918	PG1219+534	R
176	IMA0193.fits	13/03/08	02:38:39	15.0	2454538.61017	PG1219+534	R
177	IMA0194.fits	13/03/08	02:40:07	15.0	2454538.61119	PG1219+534	R
178	IMA0195.fits	13/03/08	02:41:33	15.0	2454538.61219	PG1219+534	R
179	IMA0196.fits	13/03/08	02:42:59	15.0	2454538.61318	PG1219+534	R
180	IMA0197.fits	13/03/08	02:44:26	15.0	2454538.61419	PG1219+534	R
181	IMA0198.fits	13/03/08	02:48:35	15.0	2454538.61707	PG1219+534	R
182	IMA0199.fits	13/03/08	02:50:01	15.0	2454538.61807	PG1219+534	R
183	IMA0200.fits	13/03/08	02:51:26	15.0	2454538.61905	PG1219+534	R
184	IMA0201.fits	13/03/08	02:52:53	15.0	2454538.62006	PG1219+534	R
185	IMA0202.fits	13/03/08	02:54:19	15.0	2454538.62105	PG1219+534	R
186	IMA0203.fits	13/03/08	02:55:45	15.0	2454538.62205	PG1219+534	R
187	IMA0204.fits	13/03/08	02:57:11	15.0	2454538.62304	PG1219+534	R
188	IMA0205.fits	13/03/08	02:58:38	15.0	2454538.62405	PG1219+534	R
189	IMA0206.fits	13/03/08	03:00:04	15.0	2454538.62505	PG1219+534	R
190	IMA0207.fits	13/03/08	03:01:45	15.0	2454538.62622	PG1219+534	R
191	IMA0208.fits	13/03/08	03:03:13	15.0	2454538.62723	PG1219+534	R
192	IMA0209.fits	13/03/08	03:04:40	15.0	2454538.62824	PG1219+534	R
193	IMA0210.fits	13/03/08	03:06:08	15.0	2454538.62926	PG1219+534	R
194	IMA0211.fits	13/03/08	03:07:34	15.0	2454538.63025	PG1219+534	R
195	IMA0212.fits	13/03/08	03:09:01	15.0	2454538.63126	PG1219+534	R
196	IMA0213.fits	13/03/08	03:10:27	15.0	2454538.63226	PG1219+534	R
197	IMA0214.fits	13/03/08	03:11:53	15.0	2454538.63325	PG1219+534	R
198	IMA0215.fits	13/03/08	03:13:19	15.0	2454538.63425	PG1219+534	R
199	IMA0216.fits	13/03/08	03:15:02	15.0	2454538.63544	PG1219+534	R
200	IMA0217.fits	13/03/08	03:16:29	15.0	2454538.63645	PG1219+534	R
201	IMA0218.fits	13/03/08	03:17:55	15.0	2454538.63744	PG1219+534	R
202	IMA0219.fits	13/03/08	03:19:21	15.0	2454538.63844	PG1219+534	R
203	IMA0220.fits	13/03/08	03:20:50	15.0	2454538.63947	PG1219+534	R
204	IMA0221.fits	13/03/08	03:22:18	15.0	2454538.64049	PG1219+534	R
205	IMA0222.fits	13/03/08	03:23:43	15.0	2454538.64147	PG1219+534	R
206	IMA0223.fits	13/03/08	03:25:11	15.0	2454538.64249	PG1219+534	R
207	IMA0224.fits	13/03/08	03:26:38	15.0	2454538.64350	PG1219+534	R

208	IMA0225.fits	13/03/08	03:28:19	15.0	2454538.64466	PG1219+534	R
209	IMA0226.fits	13/03/08	03:29:45	15.0	2454538.64566	PG1219+534	R
210	IMA0227.fits	13/03/08	03:31:12	15.0	2454538.64667	PG1219+534	R
211	IMA0228.fits	13/03/08	03:32:38	15.0	2454538.64766	PG1219+534	R
212	IMA0229.fits	13/03/08	03:34:04	15.0	2454538.64866	PG1219+534	R
213	IMA0230.fits	13/03/08	03:35:30	15.0	2454538.64965	PG1219+534	R
214	IMA0231.fits	13/03/08	03:36:58	15.0	2454538.65067	PG1219+534	R
215	IMA0232.fits	13/03/08	03:38:26	15.0	2454538.65169	PG1219+534	R
216	IMA0233.fits	13/03/08	03:39:53	15.0	2454538.65270	PG1219+534	R
217	IMA0234.fits	13/03/08	03:41:34	15.0	2454538.65387	PG1219+534	R
218	IMA0235.fits	13/03/08	03:43:01	15.0	2454538.65487	PG1219+534	R
219	IMA0236.fits	13/03/08	03:44:27	15.0	2454538.65587	PG1219+534	R
220	IMA0237.fits	13/03/08	03:45:53	15.0	2454538.65686	PG1219+534	R
221	IMA0238.fits	13/03/08	03:47:19	15.0	2454538.65786	PG1219+534	R
222	IMA0239.fits	13/03/08	03:48:46	15.0	2454538.65887	PG1219+534	R
223	IMA0240.fits	13/03/08	03:50:12	15.0	2454538.65986	PG1219+534	R
224	IMA0241.fits	13/03/08	03:51:38	15.0	2454538.66086	PG1219+534	R
225	IMA0242.fits	13/03/08	03:53:04	15.0	2454538.66185	PG1219+534	R

#	Image	Date	Start	Texp	JD	Object	Filter
1	IMA0270.fits	13/03/08	18:14:28	30.0	2454539.28328	HS0702+6043	R
2	IMA0276.fits	13/03/08	18:47:55	30.0	2454539.28446	HS0702+6043	R
3	IMA0277.fits	13/03/08	18:49:37	30.0	2454539.28562	HS0702+6043	R
4	IMA0278.fits	13/03/08	18:51:18	30.0	2454539.28678	HS0702+6043	R
5	IMA0279.fits	13/03/08	18:52:58	30.0	2454539.28794	HS0702+6043	R
6	IMA0280.fits	13/03/08	18:54:38	30.0	2454539.28913	HS0702+6043	R
7	IMA0281.fits	13/03/08	18:56:21	30.0	2454539.29030	HS0702+6043	R
8	IMA0282.fits	13/03/08	18:58:02	30.0	2454539.29147	HS0702+6043	R
9	IMA0283.fits	13/03/08	18:59:43	30.0	2454539.29265	HS0702+6043	R
10	IMA0284.fits	13/03/08	19:01:25	30.0	2454539.29399	HS0702+6043	R
11	IMA0285.fits	13/03/08	19:03:21	30.0	2454539.29519	HS0702+6043	R
12	IMA0286.fits	13/03/08	19:05:04	30.0	2454539.29635	HS0702+6043	R
13	IMA0287.fits	13/03/08	19:06:45	30.0	2454539.29753	HS0702+6043	R
14	IMA0288.fits	13/03/08	19:08:27	30.0	2454539.29873	HS0702+6043	R
15	IMA0289.fits	13/03/08	19:10:10	30.0	2454539.29990	HS0702+6043	R
16	IMA0290.fits	13/03/08	19:11:51	30.0	2454539.30109	HS0702+6043	R
17	IMA0291.fits	13/03/08	19:13:34	30.0	2454539.30228	HS0702+6043	R
18	IMA0292.fits	13/03/08	19:15:17	30.0	2454539.30347	HS0702+6043	R
19	IMA0293.fits	13/03/08	19:16:60	30.0	2454539.30480	HS0702+6043	R
20	IMA0294.fits	13/03/08	19:18:55	30.0	2454539.30600	HS0702+6043	R
21	IMA0295.fits	13/03/08	19:20:38	30.0	2454539.30716	HS0702+6043	R
22	IMA0296.fits	13/03/08	19:22:19	30.0	2454539.30834	HS0702+6043	R
23	IMA0297.fits	13/03/08	19:24:01	30.0	2454539.30953	HS0702+6043	R
24	IMA0298.fits	13/03/08	19:25:43	30.0	2454539.31072	HS0702+6043	R
25	IMA0299.fits	13/03/08	19:27:26	30.0	2454539.31189	HS0702+6043	R
26	IMA0300.fits	13/03/08	19:29:07	30.0	2454539.31304	HS0702+6043	R
27	IMA0301.fits	13/03/08	19:30:47	30.0	2454539.31421	HS0702+6043	R
28	IMA0302.fits	13/03/08	19:32:28	30.0	2454539.31558	HS0702+6043	R
29	IMA0303.fits	13/03/08	19:34:26	30.0	2454539.31677	HS0702+6043	R
30	IMA0304.fits	13/03/08	19:36:09	30.0	2454539.31796	HS0702+6043	R
31	IMA0305.fits	13/03/08	19:37:52	30.0	2454539.31914	HS0702+6043	R
32	IMA0306.fits	13/03/08	19:39:34	30.0	2454539.32030	HS0702+6043	R
33	IMA0307.fits	13/03/08	19:41:14	30.0	2454539.32147	HS0702+6043	R
34	IMA0308.fits	13/03/08	19:42:55	30.0	2454539.32265	HS0702+6043	R
35	IMA0309.fits	13/03/08	19:44:37	30.0	2454539.32381	HS0702+6043	R
36	IMA0310.fits	13/03/08	19:46:17	30.0	2454539.32497	HS0702+6043	R
37	IMA0311.fits	13/03/08	19:47:57	30.0	2454539.32633	HS0702+6043	R
38	IMA0312.fits	13/03/08	19:49:55	30.0	2454539.32750	HS0702+6043	R
39	IMA0313.fits	13/03/08	19:51:36	30.0	2454539.32867	HS0702+6043	R

40	IMA0314.fits	13/03/08	19:53:17	30.0	2454539.32983	HS0702+6043	R
41	IMA0315.fits	13/03/08	19:54:57	30.0	2454539.33100	HS0702+6043	R
42	IMA0316.fits	13/03/08	19:56:38	30.0	2454539.33216	HS0702+6043	R
43	IMA0317.fits	13/03/08	19:58:19	30.0	2454539.33333	HS0702+6043	R
44	IMA0318.fits	13/03/08	20:00:00	30.0	2454539.33453	HS0702+6043	R
45	IMA0319.fits	13/03/08	20:01:43	30.0	2454539.33571	HS0702+6043	R
46	IMA0320.fits	13/03/08	20:03:25	30.0	2454539.33704	HS0702+6043	R
47	IMA0321.fits	13/03/08	20:05:20	30.0	2454539.33821	HS0702+6043	R
48	IMA0322.fits	13/03/08	20:07:01	30.0	2454539.33939	HS0702+6043	R
49	IMA0323.fits	13/03/08	20:08:43	30.0	2454539.34057	HS0702+6043	R
50	IMA0324.fits	13/03/08	20:10:25	30.0	2454539.34172	HS0702+6043	R
51	IMA0325.fits	13/03/08	20:12:05	30.0	2454539.34291	HS0702+6043	R
52	IMA0326.fits	13/03/08	20:13:47	30.0	2454539.34407	HS0702+6043	R
53	IMA0327.fits	13/03/08	20:15:28	30.0	2454539.34525	HS0702+6043	R
54	IMA0328.fits	13/03/08	20:17:10	30.0	2454539.34644	HS0702+6043	R
55	IMA0329.fits	13/03/08	20:18:52	30.0	2454539.34780	HS0702+6043	R
56	IMA0330.fits	13/03/08	20:20:50	30.0	2454539.34896	HS0702+6043	R
57	IMA0331.fits	13/03/08	20:22:30	30.0	2454539.35014	HS0702+6043	R
58	IMA0332.fits	13/03/08	20:24:12	30.0	2454539.35133	HS0702+6043	R
59	IMA0333.fits	13/03/08	20:25:55	30.0	2454539.35251	HS0702+6043	R
60	IMA0334.fits	13/03/08	20:27:37	30.0	2454539.35369	HS0702+6043	R
61	IMA0335.fits	13/03/08	20:29:19	30.0	2454539.35488	HS0702+6043	R
62	IMA0336.fits	13/03/08	20:31:02	30.0	2454539.35606	HS0702+6043	R
63	IMA0337.fits	13/03/08	20:32:44	30.0	2454539.35726	HS0702+6043	R
64	IMA0338.fits	13/03/08	20:34:27	30.0	2454539.35862	HS0702+6043	R
65	IMA0339.fits	13/03/08	20:36:25	30.0	2454539.35979	HS0702+6043	R
66	IMA0340.fits	13/03/08	20:38:06	30.0	2454539.36096	HS0702+6043	R
67	IMA0341.fits	13/03/08	20:39:47	30.0	2454539.36212	HS0702+6043	R
68	IMA0342.fits	13/03/08	20:41:27	30.0	2454539.36330	HS0702+6043	R
69	IMA0343.fits	13/03/08	20:43:09	30.0	2454539.36449	HS0702+6043	R
70	IMA0344.fits	13/03/08	20:44:52	30.0	2454539.36568	HS0702+6043	R
71	IMA0345.fits	13/03/08	20:46:35	30.0	2454539.36686	HS0702+6043	R
72	IMA0346.fits	13/03/08	20:48:17	30.0	2454539.36803	HS0702+6043	R
73	IMA0347.fits	13/03/08	20:49:58	30.0	2454539.36937	HS0702+6043	R
74	IMA0348.fits	13/03/08	20:51:54	30.0	2454539.37057	HS0702+6043	R
75	IMA0349.fits	13/03/08	20:53:37	30.0	2454539.37174	HS0702+6043	R
76	IMA0350.fits	13/03/08	20:55:18	30.0	2454539.37291	HS0702+6043	R
77	IMA0351.fits	13/03/08	20:56:59	30.0	2454539.37407	HS0702+6043	R
78	IMA0352.fits	13/03/08	20:58:40	30.0	2454539.37525	HS0702+6043	R
79	IMA0353.fits	13/03/08	21:00:22	30.0	2454539.37645	HS0702+6043	R
80	IMA0354.fits	13/03/08	21:02:05	30.0	2454539.37762	HS0702+6043	R
81	IMA0355.fits	13/03/08	21:03:46	30.0	2454539.37878	HS0702+6043	R
82	IMA0356.fits	13/03/08	21:05:27	30.0	2454539.38013	HS0702+6043	R
83	IMA0357.fits	13/03/08	21:07:23	30.0	2454539.38132	HS0702+6043	R
84	IMA0358.fits	13/03/08	21:09:06	30.0	2454539.38250	HS0702+6043	R
85	IMA0359.fits	13/03/08	21:10:48	30.0	2454539.38368	HS0702+6043	R
86	IMA0360.fits	13/03/08	21:12:30	30.0	2454539.38485	HS0702+6043	R
87	IMA0361.fits	13/03/08	21:14:11	30.0	2454539.38602	HS0702+6043	R
88	IMA0362.fits	13/03/08	21:15:52	30.0	2454539.38719	HS0702+6043	R
89	IMA0363.fits	13/03/08	21:17:33	30.0	2454539.38838	HS0702+6043	R
90	IMA0364.fits	13/03/08	21:19:16	30.0	2454539.38955	HS0702+6043	R
91	IMA0365.fits	13/03/08	21:20:57	30.0	2454539.39219	HS0702+6043	R
92	IMA0366.fits	13/03/08	21:24:45	30.0	2454539.39334	HS0702+6043	R
93	IMA0367.fits	13/03/08	21:26:25	30.0	2454539.39450	HS0702+6043	R
94	IMA0368.fits	13/03/08	21:28:05	30.0	2454539.39569	HS0702+6043	R
95	IMA0369.fits	13/03/08	21:29:48	30.0	2454539.39687	HS0702+6043	R
96	IMA0370.fits	13/03/08	21:31:30	30.0	2454539.39803	HS0702+6043	R
97	IMA0371.fits	13/03/08	21:33:10	30.0	2454539.39920	HS0702+6043	R
98	IMA0372.fits	13/03/08	21:34:51	30.0	2454539.40037	HS0702+6043	R

99	IMA0373.fits	13/03/08	21:36:32	30.0	2454539.40155	HS0702+6043	R
100	IMA0374.fits	13/03/08	21:38:14	30.0	2454539.40293	HS0702+6043	R
101	IMA0375.fits	13/03/08	21:40:13	30.0	2454539.40410	HS0702+6043	R
102	IMA0376.fits	13/03/08	21:41:54	30.0	2454539.40528	HS0702+6043	R
103	IMA0377.fits	13/03/08	21:43:36	30.0	2454539.40646	HS0702+6043	R
104	IMA0378.fits	13/03/08	21:45:18	30.0	2454539.40765	HS0702+6043	R
105	IMA0379.fits	13/03/08	21:47:01	30.0	2454539.40884	HS0702+6043	R
106	IMA0380.fits	13/03/08	21:48:44	30.0	2454539.41002	HS0702+6043	R
107	IMA0381.fits	13/03/08	21:50:26	30.0	2454539.41120	HS0702+6043	R
108	IMA0382.fits	13/03/08	21:52:08	30.0	2454539.41237	HS0702+6043	R
109	IMA0383.fits	13/03/08	21:53:49	30.0	2454539.41374	HS0702+6043	R
110	IMA0384.fits	13/03/08	21:55:47	30.0	2454539.41492	HS0702+6043	R
111	IMA0385.fits	13/03/08	21:57:29	30.0	2454539.41608	HS0702+6043	R
112	IMA0386.fits	13/03/08	21:59:09	30.0	2454539.41723	HS0702+6043	R
113	IMA0387.fits	13/03/08	22:00:49	30.0	2454539.41841	HS0702+6043	R
114	IMA0388.fits	13/03/08	22:02:31	30.0	2454539.41957	HS0702+6043	R
115	IMA0389.fits	13/03/08	22:04:11	30.0	2454539.42073	HS0702+6043	R
116	IMA0390.fits	13/03/08	22:05:51	30.0	2454539.42189	HS0702+6043	R
117	IMA0391.fits	13/03/08	22:07:31	30.0	2454539.42306	HS0702+6043	R
118	IMA0392.fits	13/03/08	22:09:12	30.0	2454539.42441	HS0702+6043	R
119	IMA0393.fits	13/03/08	22:11:09	30.0	2454539.42559	HS0702+6043	R
120	IMA0394.fits	13/03/08	22:12:51	30.0	2454539.42676	HS0702+6043	R
121	IMA0395.fits	13/03/08	22:14:32	30.0	2454539.42794	HS0702+6043	R
122	IMA0396.fits	13/03/08	22:16:14	30.0	2454539.42913	HS0702+6043	R
123	IMA0397.fits	13/03/08	22:17:57	30.0	2454539.43032	HS0702+6043	R
124	IMA0398.fits	13/03/08	22:19:40	30.0	2454539.43150	HS0702+6043	R
125	IMA0399.fits	13/03/08	22:21:22	30.0	2454539.43269	HS0702+6043	R
126	IMA0400.fits	13/03/08	22:23:04	30.0	2454539.43388	HS0702+6043	R
127	IMA0401.fits	13/03/08	22:24:47	30.0	2454539.43524	HS0702+6043	R
128	IMA0402.fits	13/03/08	22:26:45	30.0	2454539.43642	HS0702+6043	R
129	IMA0403.fits	13/03/08	22:28:27	30.0	2454539.43760	HS0702+6043	R
130	IMA0422.fits	14/03/08	01:58:31	35.0	2454539.58230	PG1325+101	R
131	IMA0423.fits	14/03/08	02:00:18	35.0	2454539.58354	PG1325+101	R
132	IMA0424.fits	14/03/08	02:02:05	35.0	2454539.58478	PG1325+101	R
133	IMA0425.fits	14/03/08	02:03:53	35.0	2454539.58603	PG1325+101	R
134	IMA0426.fits	14/03/08	02:05:40	35.0	2454539.58727	PG1325+101	R
135	IMA0427.fits	14/03/08	02:07:26	35.0	2454539.58850	PG1325+101	R
136	IMA0428.fits	14/03/08	02:09:12	35.0	2454539.58972	PG1325+101	R
137	IMA0429.fits	14/03/08	02:10:59	35.0	2454539.59096	PG1325+101	R
138	IMA0430.fits	14/03/08	02:12:46	35.0	2454539.59220	PG1325+101	R
139	IMA0431.fits	14/03/08	02:14:48	35.0	2454539.59361	PG1325+101	R
140	IMA0432.fits	14/03/08	02:16:34	35.0	2454539.59484	PG1325+101	R
141	IMA0433.fits	14/03/08	02:18:20	35.0	2454539.59606	PG1325+101	R
142	IMA0434.fits	14/03/08	02:20:05	35.0	2454539.59728	PG1325+101	R
143	IMA0435.fits	14/03/08	02:21:51	35.0	2454539.59851	PG1325+101	R
144	IMA0436.fits	14/03/08	02:23:37	35.0	2454539.59973	PG1325+101	R
145	IMA0437.fits	14/03/08	02:25:24	35.0	2454539.60097	PG1325+101	R
146	IMA0438.fits	14/03/08	02:27:10	35.0	2454539.60220	PG1325+101	R
147	IMA0439.fits	14/03/08	02:28:56	35.0	2454539.60343	PG1325+101	R
148	IMA0440.fits	14/03/08	02:30:56	35.0	2454539.60481	PG1325+101	R
149	IMA0441.fits	14/03/08	02:32:45	35.0	2454539.60608	PG1325+101	R
150	IMA0442.fits	14/03/08	02:34:32	35.0	2454539.60731	PG1325+101	R
151	IMA0443.fits	14/03/08	02:36:19	35.0	2454539.60855	PG1325+101	R
152	IMA0444.fits	14/03/08	02:38:08	35.0	2454539.60981	PG1325+101	R
153	IMA0445.fits	14/03/08	02:39:56	35.0	2454539.61106	PG1325+101	R
154	IMA0446.fits	14/03/08	02:41:43	35.0	2454539.61230	PG1325+101	R
155	IMA0447.fits	14/03/08	02:43:30	35.0	2454539.61354	PG1325+101	R
156	IMA0448.fits	14/03/08	02:45:17	35.0	2454539.61478	PG1325+101	R
157	IMA0449.fits	14/03/08	02:47:17	35.0	2454539.61617	PG1325+101	R

158	IMA0450.fits	14/03/08	02:49:06	35.0	2454539.61743	PG1325+101	R
159	IMA0451.fits	14/03/08	02:50:54	35.0	2454539.61868	PG1325+101	R
160	IMA0452.fits	14/03/08	02:52:41	35.0	2454539.61992	PG1325+101	R
161	IMA0453.fits	14/03/08	02:54:30	35.0	2454539.62118	PG1325+101	R
162	IMA0454.fits	14/03/08	02:56:16	35.0	2454539.62241	PG1325+101	R
163	IMA0455.fits	14/03/08	02:58:04	35.0	2454539.62366	PG1325+101	R
164	IMA0456.fits	14/03/08	02:59:51	35.0	2454539.62490	PG1325+101	R
165	IMA0457.fits	14/03/08	03:01:40	35.0	2454539.62616	PG1325+101	R
166	IMA0458.fits	14/03/08	03:03:42	35.0	2454539.62757	PG1325+101	R
167	IMA0459.fits	14/03/08	03:05:29	35.0	2454539.62881	PG1325+101	R
168	IMA0460.fits	14/03/08	03:07:18	35.0	2454539.63007	PG1325+101	R
169	IMA0461.fits	14/03/08	03:09:05	35.0	2454539.63131	PG1325+101	R
170	IMA0462.fits	14/03/08	03:10:53	35.0	2454539.63256	PG1325+101	R
171	IMA0463.fits	14/03/08	03:12:41	35.0	2454539.63381	PG1325+101	R
172	IMA0464.fits	14/03/08	03:14:27	35.0	2454539.63503	PG1325+101	R
173	IMA0465.fits	14/03/08	03:16:13	35.0	2454539.63626	PG1325+101	R
174	IMA0466.fits	14/03/08	03:18:01	35.0	2454539.63751	PG1325+101	R
175	IMA0467.fits	14/03/08	03:20:01	35.0	2454539.63890	PG1325+101	R
176	IMA0468.fits	14/03/08	03:21:47	35.0	2454539.64013	PG1325+101	R
177	IMA0469.fits	14/03/08	03:23:35	35.0	2454539.64138	PG1325+101	R
178	IMA0470.fits	14/03/08	03:25:22	35.0	2454539.64262	PG1325+101	R
179	IMA0471.fits	14/03/08	03:27:08	35.0	2454539.64384	PG1325+101	R
180	IMA0472.fits	14/03/08	03:28:55	35.0	2454539.64508	PG1325+101	R
181	IMA0473.fits	14/03/08	03:30:41	35.0	2454539.64631	PG1325+101	R
182	IMA0474.fits	14/03/08	03:32:27	35.0	2454539.64753	PG1325+101	R
183	IMA0475.fits	14/03/08	03:34:14	35.0	2454539.64877	PG1325+101	R
184	IMA0476.fits	14/03/08	03:36:16	35.0	2454539.65019	PG1325+101	R
185	IMA0477.fits	14/03/08	03:38:03	35.0	2454539.65142	PG1325+101	R
186	IMA0478.fits	14/03/08	03:39:50	35.0	2454539.65266	PG1325+101	R
187	IMA0479.fits	14/03/08	03:41:36	35.0	2454539.65389	PG1325+101	R
188	IMA0480.fits	14/03/08	03:43:23	35.0	2454539.65513	PG1325+101	R
189	IMA0481.fits	14/03/08	03:45:10	35.0	2454539.65637	PG1325+101	R
190	IMA0482.fits	14/03/08	03:46:56	35.0	2454539.65759	PG1325+101	R
191	IMA0483.fits	14/03/08	03:48:42	35.0	2454539.65882	PG1325+101	R
192	IMA0484.fits	14/03/08	03:50:29	35.0	2454539.66006	PG1325+101	R
193	IMA0485.fits	14/03/08	03:52:30	35.0	2454539.66146	PG1325+101	R
194	IMA0486.fits	14/03/08	03:54:16	35.0	2454539.66269	PG1325+101	R
195	IMA0487.fits	14/03/08	03:56:03	35.0	2454539.66392	PG1325+101	R
196	IMA0488.fits	14/03/08	03:57:49	35.0	2454539.66515	PG1325+101	R
197	IMA0489.fits	14/03/08	03:59:35	35.0	2454539.66638	PG1325+101	R
198	IMA0490.fits	14/03/08	04:01:23	35.0	2454539.66763	PG1325+101	R
199	IMA0491.fits	14/03/08	04:03:11	35.0	2454539.66888	PG1325+101	R
200	IMA0492.fits	14/03/08	04:04:57	35.0	2454539.67010	PG1325+101	R
201	IMA0493.fits	14/03/08	04:06:43	35.0	2454539.67133	PG1325+101	R
202	IMA0494.fits	14/03/08	04:08:47	35.0	2454539.67277	PG1325+101	R
203	IMA0495.fits	14/03/08	04:10:33	35.0	2454539.67399	PG1325+101	R
204	IMA0496.fits	14/03/08	04:12:21	35.0	2454539.67524	PG1325+101	R
205	IMA0497.fits	14/03/08	04:14:10	35.0	2454539.67650	PG1325+101	R
206	IMA0498.fits	14/03/08	04:15:58	35.0	2454539.67775	PG1325+101	R
207	IMA0499.fits	14/03/08	04:17:46	35.0	2454539.67900	PG1325+101	R
208	IMA0500.fits	14/03/08	04:19:33	35.0	2454539.68024	PG1325+101	R
209	IMA0501.fits	14/03/08	04:21:19	35.0	2454539.68147	PG1325+101	R
210	IMA0502.fits	14/03/08	04:23:05	35.0	2454539.68270	PG1325+101	R
211	IMA0503.fits	14/03/08	04:25:07	35.0	2454539.68411	PG1325+101	R
212	IMA0504.fits	14/03/08	04:26:53	35.0	2454539.68534	PG1325+101	R
213	IMA0505.fits	14/03/08	04:28:39	35.0	2454539.68656	PG1325+101	R
214	IMA0506.fits	14/03/08	04:30:26	35.0	2454539.68780	PG1325+101	R
215	IMA0507.fits	14/03/08	04:32:12	35.0	2454539.68903	PG1325+101	R
216	IMA0508.fits	14/03/08	04:33:58	35.0	2454539.69025	PG1325+101	R

217	IMA0509.fits	14/03/08	04:35:45	35.0	2454539.69149	PG1325+101 R
218	IMA0510.fits	14/03/08	04:37:31	35.0	2454539.69272	PG1325+101 R
219	IMA0511.fits	14/03/08	04:39:18	35.0	2454539.69396	PG1325+101 R

B.2 February, 26-28, 2009

#	Image	Date	Start	Texp	JD	Object	Filter
1	IMA0870.fits	26/02/09	20:35:38	40.0	2454889.35808	HS0702+6043	NONE
2	IMA0871.fits	26/02/09	20:36:40	40.0	2454889.35880	HS0702+6043	NONE
3	IMA0872.fits	26/02/09	20:37:40	40.0	2454889.35949	HS0702+6043	NONE
4	IMA0873.fits	26/02/09	20:38:41	40.0	2454889.36020	HS0702+6043	NONE
5	IMA0874.fits	26/02/09	20:39:42	40.0	2454889.36090	HS0702+6043	NONE
6	IMA0875.fits	26/02/09	20:40:42	40.0	2454889.36160	HS0702+6043	NONE
7	IMA0876.fits	26/02/09	20:41:42	40.0	2454889.36229	HS0702+6043	NONE
8	IMA0877.fits	26/02/09	20:42:42	40.0	2454889.36299	HS0702+6043	NONE
9	IMA0878.fits	26/02/09	20:43:42	40.0	2454889.36368	HS0702+6043	NONE
10	IMA0879.fits	26/02/09	20:44:58	40.0	2454889.36456	HS0702+6043	NONE
11	IMA0880.fits	26/02/09	20:45:59	40.0	2454889.36527	HS0702+6043	NONE
12	IMA0881.fits	26/02/09	20:47:01	40.0	2454889.36598	HS0702+6043	NONE
13	IMA0882.fits	26/02/09	20:48:03	40.0	2454889.36670	HS0702+6043	NONE
14	IMA0883.fits	26/02/09	20:49:05	40.0	2454889.36742	HS0702+6043	NONE
15	IMA0884.fits	26/02/09	20:50:06	40.0	2454889.36812	HS0702+6043	NONE
16	IMA0885.fits	26/02/09	20:51:08	40.0	2454889.36884	HS0702+6043	NONE
17	IMA0886.fits	26/02/09	20:52:010	40.0	2454889.36956	HS0702+6043	NONE
18	IMA0887.fits	26/02/09	20:53:13	40.0	2454889.37029	HS0702+6043	NONE
19	IMA0888.fits	26/02/09	20:54:31	40.0	2454889.37119	HS0702+6043	NONE
20	IMA0889.fits	26/02/09	20:55:48	40.0	2454889.37208	HS0702+6043	NONE
21	IMA0890.fits	26/02/09	20:56:50	40.0	2454889.37280	HS0702+6043	NONE
22	IMA0891.fits	26/02/09	20:57:52	40.0	2454889.37352	HS0702+6043	NONE
23	IMA0892.fits	26/02/09	20:58:54	40.0	2454889.37424	HS0702+6043	NONE
24	IMA0893.fits	26/02/09	20:59:55	40.0	2454889.37494	HS0702+6043	NONE
25	IMA0894.fits	26/02/09	21:00:57	40.0	2454889.37566	HS0702+6043	NONE
26	IMA0895.fits	26/02/09	21:01:60	40.0	2454889.37639	HS0702+6043	NONE
27	IMA0896.fits	26/02/09	21:02:60	40.0	2454889.37708	HS0702+6043	NONE
28	IMA0897.fits	26/02/09	21:04:00	40.0	2454889.37778	HS0702+6043	NONE
29	IMA0898.fits	26/02/09	21:05:18	40.0	2454889.37868	HS0702+6043	NONE
30	IMA0899.fits	26/02/09	21:06:19	40.0	2454889.37939	HS0702+6043	NONE
31	IMA0900.fits	26/02/09	21:07:19	40.0	2454889.38008	HS0702+6043	NONE
32	IMA0901.fits	26/02/09	21:08:19	40.0	2454889.38078	HS0702+6043	NONE
33	IMA0902.fits	26/02/09	21:09:19	40.0	2454889.38147	HS0702+6043	NONE
34	IMA0903.fits	26/02/09	21:10:22	40.0	2454889.38220	HS0702+6043	NONE
35	IMA0904.fits	26/02/09	21:11:23	40.0	2454889.38291	HS0702+6043	NONE
36	IMA0905.fits	26/02/09	21:12:23	40.0	2454889.38360	HS0702+6043	NONE
37	IMA0906.fits	26/02/09	21:13:23	40.0	2454889.38429	HS0702+6043	NONE
38	IMA0907.fits	26/02/09	21:14:38	40.0	2454889.38516	HS0702+6043	NONE

#	Image	Date	Start	Texp	JD	Object	Filter
1	IMA0930.fits	27/02/09	19:51:57	15.0	2454890.32774	HS0702	NONE
2	IMA0931.fits	27/02/09	19:52:48	15.0	2454890.32833	HS0702	NONE
3	IMA0932.fits	27/02/09	19:53:23	15.0	2454890.32874	HS0702	NONE
4	IMA0933.fits	27/02/09	19:53:57	15.0	2454890.32913	HS0702	NONE
5	IMA0934.fits	27/02/09	19:54:32	15.0	2454890.32954	HS0702	NONE
6	IMA0935.fits	27/02/09	19:55:06	15.0	2454890.32993	HS0702	NONE
7	IMA0936.fits	27/02/09	19:55:41	15.0	2454890.33034	HS0702	NONE
8	IMA0937.fits	27/02/09	19:56:15	15.0	2454890.33073	HS0702	NONE
9	IMA0938.fits	27/02/09	19:56:49	15.0	2454890.33112	HS0702	NONE
10	IMA0939.fits	27/02/09	19:57:23	15.0	2454890.33152	HS0702	NONE

11	IMA0940.fits	27/02/09	19:58:13	15.0	2454890.33209	HS0702	NONE
12	IMA0941.fits	27/02/09	19:58:50	15.0	2454890.33252	HS0702	NONE
13	IMA0942.fits	27/02/09	19:59:24	15.0	2454890.33292	HS0702	NONE
14	IMA0943.fits	27/02/09	19:59:58	15.0	2454890.33331	HS0702	NONE
15	IMA0944.fits	27/02/09	20:00:32	15.0	2454890.33370	HS0702	NONE
16	IMA0945.fits	27/02/09	20:01:07	15.0	2454890.33411	HS0702	NONE
17	IMA0946.fits	27/02/09	20:01:42	15.0	2454890.33451	HS0702	NONE
18	IMA0947.fits	27/02/09	20:02:17	15.0	2454890.33492	HS0702	NONE
19	IMA0948.fits	27/02/09	20:02:52	15.0	2454890.33532	HS0702	NONE
20	IMA0949.fits	27/02/09	20:03:41	15.0	2454890.33589	HS0702	NONE
21	IMA0950.fits	27/02/09	20:04:15	15.0	2454890.33628	HS0702	NONE
22	IMA0951.fits	27/02/09	20:04:52	15.0	2454890.33671	HS0702	NONE
23	IMA0952.fits	27/02/09	20:05:27	15.0	2454890.33712	HS0702	NONE
24	IMA0953.fits	27/02/09	20:06:03	15.0	2454890.33753	HS0702	NONE
25	IMA0954.fits	27/02/09	20:06:37	15.0	2454890.33793	HS0702	NONE
26	IMA0955.fits	27/02/09	20:07:13	15.0	2454890.33834	HS0702	NONE
27	IMA0956.fits	27/02/09	20:07:49	15.0	2454890.33876	HS0702	NONE
28	IMA0957.fits	27/02/09	20:08:23	15.0	2454890.33916	HS0702	NONE
29	IMA0958.fits	27/02/09	20:09:11	15.0	2454890.33971	HS0702	NONE
30	IMA0959.fits	27/02/09	20:09:45	15.0	2454890.34010	HS0702	NONE
31	IMA0960.fits	27/02/09	20:10:21	15.0	2454890.34052	HS0702	NONE
32	IMA0961.fits	27/02/09	20:10:56	15.0	2454890.34093	HS0702	NONE
33	IMA0962.fits	27/02/09	20:11:30	15.0	2454890.34132	HS0702	NONE
34	IMA0963.fits	27/02/09	20:12:04	15.0	2454890.34171	HS0702	NONE
35	IMA0964.fits	27/02/09	20:12:40	15.0	2454890.34213	HS0702	NONE
36	IMA0965.fits	27/02/09	20:13:17	15.0	2454890.34256	HS0702	NONE
37	IMA0966.fits	27/02/09	20:13:51	15.0	2454890.34295	HS0702	NONE
38	IMA0967.fits	27/02/09	20:14:42	15.0	2454890.34354	HS0702	NONE
39	IMA0968.fits	27/02/09	20:15:16	15.0	2454890.34394	HS0702	NONE
40	IMA0969.fits	27/02/09	20:15:50	15.0	2454890.34433	HS0702	NONE
41	IMA0970.fits	27/02/09	20:16:26	15.0	2454890.34475	HS0702	NONE
42	IMA0971.fits	27/02/09	20:16:60	15.0	2454890.34514	HS0702	NONE
43	IMA0972.fits	27/02/09	20:17:34	15.0	2454890.34553	HS0702	NONE
44	IMA0973.fits	27/02/09	20:18:08	15.0	2454890.34593	HS0702	NONE
45	IMA0974.fits	27/02/09	20:18:42	15.0	2454890.34632	HS0702	NONE
46	IMA0975.fits	27/02/09	20:19:19	15.0	2454890.34675	HS0702	NONE
47	IMA0976.fits	27/02/09	20:20:09	15.0	2454890.34733	HS0702	NONE
48	IMA0977.fits	27/02/09	20:20:45	15.0	2454890.34774	HS0702	NONE
49	IMA0978.fits	27/02/09	20:21:19	15.0	2454890.34814	HS0702	NONE
50	IMA0979.fits	27/02/09	20:21:54	15.0	2454890.34854	HS0702	NONE
51	IMA0980.fits	27/02/09	20:22:30	15.0	2454890.34896	HS0702	NONE
52	IMA0981.fits	27/02/09	20:23:06	15.0	2454890.34938	HS0702	NONE
53	IMA0982.fits	27/02/09	20:23:42	15.0	2454890.34979	HS0702	NONE
54	IMA0983.fits	27/02/09	20:24:18	15.0	2454890.35021	HS0702	NONE
55	IMA0984.fits	27/02/09	20:24:53	15.0	2454890.35061	HS0702	NONE
56	IMA0985.fits	27/02/09	20:25:42	15.0	2454890.35118	HS0702	NONE
57	IMA0986.fits	27/02/09	20:26:17	15.0	2454890.35159	HS0702	NONE
58	IMA0987.fits	27/02/09	20:26:52	15.0	2454890.35199	HS0702	NONE
59	IMA0988.fits	27/02/09	20:27:27	15.0	2454890.35240	HS0702	NONE
60	IMA0989.fits	27/02/09	20:28:03	15.0	2454890.35281	HS0702	NONE
61	IMA0990.fits	27/02/09	20:28:40	15.0	2454890.35324	HS0702	NONE
62	IMA0991.fits	27/02/09	20:29:16	15.0	2454890.35366	HS0702	NONE
63	IMA0992.fits	27/02/09	20:29:51	15.0	2454890.35406	HS0702	NONE
64	IMA0993.fits	27/02/09	20:30:26	15.0	2454890.35447	HS0702	NONE
65	IMA0994.fits	27/02/09	20:31:17	15.0	2454890.35506	HS0702	NONE
66	IMA0995.fits	27/02/09	20:31:54	15.0	2454890.35549	HS0702	NONE
67	IMA0996.fits	27/02/09	20:32:29	15.0	2454890.35589	HS0702	NONE
68	IMA0997.fits	27/02/09	20:33:03	15.0	2454890.35628	HS0702	NONE
69	IMA0998.fits	27/02/09	20:33:37	15.0	2454890.35668	HS0702	NONE

70	IMA0999.fits	27/02/09	20:34:12	15.0	2454890.35708	HS0702	NONE
71	IMA1000.fits	27/02/09	20:34:47	15.0	2454890.35749	HS0702	NONE
72	IMA1001.fits	27/02/09	20:35:22	15.0	2454890.35789	HS0702	NONE
73	IMA1002.fits	27/02/09	20:35:58	15.0	2454890.35831	HS0702	NONE
74	IMA1003.fits	27/02/09	20:36:48	15.0	2454890.35889	HS0702	NONE
75	IMA1004.fits	27/02/09	20:37:23	15.0	2454890.35929	HS0702	NONE
76	IMA1005.fits	27/02/09	20:37:60	15.0	2454890.35972	HS0702	NONE
77	IMA1006.fits	27/02/09	20:38:36	15.0	2454890.36014	HS0702	NONE
78	IMA1007.fits	27/02/09	20:39:11	15.0	2454890.36054	HS0702	NONE
79	IMA1008.fits	27/02/09	20:39:46	15.0	2454890.36095	HS0702	NONE
80	IMA1009.fits	27/02/09	20:40:21	15.0	2454890.36135	HS0702	NONE
81	IMA1010.fits	27/02/09	20:40:57	15.0	2454890.36177	HS0702	NONE
82	IMA1011.fits	27/02/09	20:41:33	15.0	2454890.36219	HS0702	NONE
83	IMA1012.fits	27/02/09	20:46:35	15.0	2454890.36568	HS0702	NONE
84	IMA1013.fits	27/02/09	20:47:10	15.0	2454890.36609	HS0702	NONE
85	IMA1014.fits	27/02/09	20:47:46	15.0	2454890.36650	HS0702	NONE
86	IMA1015.fits	27/02/09	20:48:22	15.0	2454890.36692	HS0702	NONE
87	IMA1016.fits	27/02/09	20:48:57	15.0	2454890.36733	HS0702	NONE
88	IMA1017.fits	27/02/09	20:49:31	15.0	2454890.36772	HS0702	NONE
89	IMA1018.fits	27/02/09	20:50:06	15.0	2454890.36812	HS0702	NONE
90	IMA1019.fits	27/02/09	20:50:42	15.0	2454890.36854	HS0702	NONE
91	IMA1020.fits	27/02/09	20:51:18	15.0	2454890.36896	HS0702	NONE
92	IMA1021.fits	27/02/09	20:52:010	15.0	2454890.36956	HS0702	NONE
93	IMA1022.fits	27/02/09	20:52:44	15.0	2454890.36995	HS0702	NONE
94	IMA1023.fits	27/02/09	20:53:18	15.0	2454890.37035	HS0702	NONE
95	IMA1024.fits	27/02/09	20:53:53	15.0	2454890.37075	HS0702	NONE
96	IMA1025.fits	27/02/09	20:54:29	15.0	2454890.37117	HS0702	NONE
97	IMA1026.fits	27/02/09	20:55:05	15.0	2454890.37159	HS0702	NONE
98	IMA1027.fits	27/02/09	20:55:41	15.0	2454890.37200	HS0702	NONE
99	IMA1028.fits	27/02/09	20:56:16	15.0	2454890.37241	HS0702	NONE
100	IMA1029.fits	27/02/09	20:56:51	15.0	2454890.37281	HS0702	NONE
101	IMA1030.fits	27/02/09	20:57:42	15.0	2454890.37340	HS0702	NONE
102	IMA1031.fits	27/02/09	20:58:18	15.0	2454890.37382	HS0702	NONE
103	IMA1032.fits	27/02/09	20:58:52	15.0	2454890.37421	HS0702	NONE
104	IMA1033.fits	27/02/09	20:59:27	15.0	2454890.37462	HS0702	NONE
105	IMA1034.fits	27/02/09	21:00:01	15.0	2454890.37501	HS0702	NONE
106	IMA1035.fits	27/02/09	21:00:37	15.0	2454890.37543	HS0702	NONE
107	IMA1036.fits	27/02/09	21:01:13	15.0	2454890.37584	HS0702	NONE
108	IMA1037.fits	27/02/09	21:01:49	15.0	2454890.37626	HS0702	NONE
109	IMA1038.fits	27/02/09	21:02:25	15.0	2454890.37668	HS0702	NONE
110	IMA1039.fits	27/02/09	21:03:15	15.0	2454890.37726	HS0702	NONE
111	IMA1040.fits	27/02/09	21:03:51	15.0	2454890.37767	HS0702	NONE
112	IMA1041.fits	27/02/09	21:04:28	15.0	2454890.37810	HS0702	NONE
113	IMA1042.fits	27/02/09	21:05:04	15.0	2454890.37852	HS0702	NONE
114	IMA1043.fits	27/02/09	21:05:40	15.0	2454890.37894	HS0702	NONE
115	IMA1044.fits	27/02/09	21:06:15	15.0	2454890.37934	HS0702	NONE
116	IMA1045.fits	27/02/09	21:06:51	15.0	2454890.37976	HS0702	NONE
117	IMA1046.fits	27/02/09	21:07:27	15.0	2454890.38017	HS0702	NONE
118	IMA1047.fits	27/02/09	21:08:04	15.0	2454890.38060	HS0702	NONE
119	IMA1048.fits	27/02/09	21:08:55	15.0	2454890.38119	HS0702	NONE
120	IMA1049.fits	27/02/09	21:09:29	15.0	2454890.38159	HS0702	NONE
121	IMA1050.fits	27/02/09	21:10:03	15.0	2454890.38198	HS0702	NONE
122	IMA1051.fits	27/02/09	21:10:38	15.0	2454890.38238	HS0702	NONE
123	IMA1052.fits	27/02/09	21:11:14	15.0	2454890.38280	HS0702	NONE
124	IMA1053.fits	27/02/09	21:11:48	15.0	2454890.38319	HS0702	NONE
125	IMA1054.fits	27/02/09	21:12:23	15.0	2454890.38360	HS0702	NONE
126	IMA1055.fits	27/02/09	21:12:59	15.0	2454890.38402	HS0702	NONE
127	IMA1056.fits	27/02/09	21:13:35	15.0	2454890.38443	HS0702	NONE
128	IMA1057.fits	27/02/09	21:14:25	15.0	2454890.38501	HS0702	NONE

129	IMA1058.fits	27/02/09	21:14:59	15.0	2454890.38541	HS0702	NONE
130	IMA1059.fits	27/02/09	21:15:34	15.0	2454890.38581	HS0702	NONE
131	IMA1060.fits	27/02/09	21:16:010	15.0	2454890.38623	HS0702	NONE
132	IMA1061.fits	27/02/09	21:16:46	15.0	2454890.38664	HS0702	NONE
133	IMA1062.fits	27/02/09	21:17:23	15.0	2454890.38707	HS0702	NONE
134	IMA1063.fits	27/02/09	21:17:58	15.0	2454890.38748	HS0702	NONE
135	IMA1064.fits	27/02/09	21:18:34	15.0	2454890.38789	HS0702	NONE
136	IMA1065.fits	27/02/09	21:19:10	15.0	2454890.38831	HS0702	NONE
137	IMA1066.fits	27/02/09	21:20:02	15.0	2454890.38891	HS0702	NONE
138	IMA1067.fits	27/02/09	21:20:38	15.0	2454890.38933	HS0702	NONE
139	IMA1068.fits	27/02/09	21:21:13	15.0	2454890.38973	HS0702	NONE
140	IMA1069.fits	27/02/09	21:21:48	15.0	2454890.39014	HS0702	NONE
141	IMA1070.fits	27/02/09	21:22:23	15.0	2454890.39054	HS0702	NONE
142	IMA1071.fits	27/02/09	21:22:57	15.0	2454890.39094	HS0702	NONE
143	IMA1072.fits	27/02/09	21:23:33	15.0	2454890.39135	HS0702	NONE
144	IMA1073.fits	27/02/09	21:24:09	15.0	2454890.39177	HS0702	NONE
145	IMA1074.fits	27/02/09	21:24:45	15.0	2454890.39219	HS0702	NONE
146	IMA1075.fits	27/02/09	21:25:36	15.0	2454890.39278	HS0702	NONE
147	IMA1076.fits	27/02/09	21:26:12	15.0	2454890.39319	HS0702	NONE
148	IMA1077.fits	27/02/09	21:26:48	15.0	2454890.39361	HS0702	NONE
149	IMA1078.fits	27/02/09	21:27:22	15.0	2454890.39400	HS0702	NONE
150	IMA1079.fits	27/02/09	21:27:56	15.0	2454890.39440	HS0702	NONE
151	IMA1080.fits	27/02/09	21:28:31	15.0	2454890.39480	HS0702	NONE
152	IMA1081.fits	27/02/09	21:29:07	15.0	2454890.39522	HS0702	NONE
153	IMA1082.fits	27/02/09	21:29:42	15.0	2454890.39563	HS0702	NONE
154	IMA1083.fits	27/02/09	21:30:18	15.0	2454890.39604	HS0702	NONE
155	IMA1084.fits	27/02/09	21:31:08	15.0	2454890.39662	HS0702	NONE
156	IMA1085.fits	27/02/09	21:31:42	15.0	2454890.39701	HS0702	NONE
157	IMA1086.fits	27/02/09	21:32:18	15.0	2454890.39743	HS0702	NONE
158	IMA1087.fits	27/02/09	21:32:55	15.0	2454890.39786	HS0702	NONE
159	IMA1088.fits	27/02/09	21:33:31	15.0	2454890.39828	HS0702	NONE
160	IMA1089.fits	27/02/09	21:34:07	15.0	2454890.39869	HS0702	NONE
161	IMA1090.fits	27/02/09	21:34:43	15.0	2454890.39911	HS0702	NONE
162	IMA1091.fits	27/02/09	21:35:19	15.0	2454890.39953	HS0702	NONE
163	IMA1092.fits	27/02/09	21:35:54	15.0	2454890.39993	HS0702	NONE
164	IMA1093.fits	27/02/09	21:36:46	15.0	2454890.40053	HS0702	NONE
165	IMA1094.fits	27/02/09	21:37:21	15.0	2454890.40094	HS0702	NONE
166	IMA1095.fits	27/02/09	21:37:56	15.0	2454890.40134	HS0702	NONE
167	IMA1096.fits	27/02/09	21:38:32	15.0	2454890.40176	HS0702	NONE
168	IMA1097.fits	27/02/09	21:39:08	15.0	2454890.40218	HS0702	NONE
169	IMA1098.fits	27/02/09	21:39:43	15.0	2454890.40258	HS0702	NONE
170	IMA1099.fits	27/02/09	21:40:19	15.0	2454890.40300	HS0702	NONE
171	IMA1100.fits	27/02/09	21:40:53	15.0	2454890.40339	HS0702	NONE
172	IMA1101.fits	27/02/09	21:41:28	15.0	2454890.40380	HS0702	NONE
173	IMA1102.fits	27/02/09	21:43:49	15.0	2454890.40543	HS0702	NONE
174	IMA1103.fits	27/02/09	21:44:23	15.0	2454890.40582	HS0702	NONE
175	IMA1104.fits	27/02/09	21:44:58	15.0	2454890.40623	HS0702	NONE
176	IMA1105.fits	27/02/09	21:45:34	15.0	2454890.40664	HS0702	NONE
177	IMA1106.fits	27/02/09	21:46:010	15.0	2454890.40706	HS0702	NONE
178	IMA1107.fits	27/02/09	21:46:47	15.0	2454890.40749	HS0702	NONE
179	IMA1108.fits	27/02/09	21:47:22	15.0	2454890.40789	HS0702	NONE
180	IMA1109.fits	27/02/09	21:47:56	15.0	2454890.40829	HS0702	NONE
181	IMA1110.fits	27/02/09	21:48:30	15.0	2454890.40868	HS0702	NONE
182	IMA1111.fits	27/02/09	21:49:22	15.0	2454890.40928	HS0702	NONE
183	IMA1112.fits	27/02/09	21:49:59	15.0	2454890.40971	HS0702	NONE
184	IMA1113.fits	27/02/09	21:50:35	15.0	2454890.41013	HS0702	NONE
185	IMA1114.fits	27/02/09	21:51:010	15.0	2454890.41053	HS0702	NONE
186	IMA1115.fits	27/02/09	21:51:45	15.0	2454890.41094	HS0702	NONE
187	IMA1116.fits	27/02/09	21:52:20	15.0	2454890.41134	HS0702	NONE

188	IMA1117.fits	27/02/09	21:52:55	15.0	2454890.41175	HS0702	NONE
189	IMA1118.fits	27/02/09	21:53:31	15.0	2454890.41216	HS0702	NONE
190	IMA1119.fits	27/02/09	21:54:07	15.0	2454890.41258	HS0702	NONE
191	IMA1120.fits	27/02/09	21:54:58	15.0	2454890.41317	HS0702	NONE
192	IMA1121.fits	27/02/09	21:55:33	15.0	2454890.41358	HS0702	NONE
193	IMA1122.fits	27/02/09	21:56:08	15.0	2454890.41398	HS0702	NONE
194	IMA1123.fits	27/02/09	21:56:43	15.0	2454890.41439	HS0702	NONE
195	IMA1124.fits	27/02/09	21:57:20	15.0	2454890.41481	HS0702	NONE
196	IMA1125.fits	27/02/09	21:57:56	15.0	2454890.41523	HS0702	NONE
197	IMA1126.fits	27/02/09	21:58:31	15.0	2454890.41564	HS0702	NONE
198	IMA1127.fits	27/02/09	21:59:05	15.0	2454890.41603	HS0702	NONE
199	IMA1128.fits	27/02/09	21:59:41	15.0	2454890.41645	HS0702	NONE
200	IMA1129.fits	27/02/09	22:00:33	15.0	2454890.41705	HS0702	NONE
201	IMA1130.fits	27/02/09	22:01:07	15.0	2454890.41744	HS0702	NONE
202	IMA1131.fits	27/02/09	22:01:42	15.0	2454890.41785	HS0702	NONE
203	IMA1132.fits	27/02/09	22:02:18	15.0	2454890.41826	HS0702	NONE
204	IMA1133.fits	27/02/09	22:02:53	15.0	2454890.41867	HS0702	NONE
205	IMA1134.fits	27/02/09	22:03:29	15.0	2454890.41909	HS0702	NONE
206	IMA1135.fits	27/02/09	22:04:06	15.0	2454890.41951	HS0702	NONE
207	IMA1136.fits	27/02/09	22:04:42	15.0	2454890.41993	HS0702	NONE
208	IMA1137.fits	27/02/09	22:05:18	15.0	2454890.42035	HS0702	NONE
209	IMA1138.fits	27/02/09	22:06:09	15.0	2454890.42094	HS0702	NONE
210	IMA1139.fits	27/02/09	22:06:44	15.0	2454890.42134	HS0702	NONE
211	IMA1140.fits	27/02/09	22:07:21	15.0	2454890.42177	HS0702	NONE
212	IMA1141.fits	27/02/09	22:07:57	15.0	2454890.42219	HS0702	NONE
213	IMA1142.fits	27/02/09	22:08:33	15.0	2454890.42260	HS0702	NONE
214	IMA1143.fits	27/02/09	22:09:08	15.0	2454890.42301	HS0702	NONE
215	IMA1144.fits	27/02/09	22:09:43	15.0	2454890.42341	HS0702	NONE
216	IMA1145.fits	27/02/09	22:10:18	15.0	2454890.42382	HS0702	NONE
217	IMA1146.fits	27/02/09	22:10:54	15.0	2454890.42424	HS0702	NONE
218	IMA1147.fits	27/02/09	22:11:44	15.0	2454890.42481	HS0702	NONE
219	IMA1148.fits	27/02/09	22:12:19	15.0	2454890.42522	HS0702	NONE
220	IMA1149.fits	27/02/09	22:12:55	15.0	2454890.42564	HS0702	NONE
221	IMA1150.fits	27/02/09	22:13:31	15.0	2454890.42605	HS0702	NONE
222	IMA1151.fits	27/02/09	22:14:07	15.0	2454890.42647	HS0702	NONE
223	IMA1152.fits	27/02/09	22:14:42	15.0	2454890.42688	HS0702	NONE
224	IMA1153.fits	27/02/09	22:15:18	15.0	2454890.42729	HS0702	NONE
225	IMA1154.fits	27/02/09	22:15:52	15.0	2454890.42769	HS0702	NONE
226	IMA1155.fits	27/02/09	22:16:27	15.0	2454890.42809	HS0702	NONE
227	IMA1156.fits	27/02/09	22:17:18	15.0	2454890.42868	HS0702	NONE
228	IMA1157.fits	27/02/09	22:17:54	15.0	2454890.42910	HS0702	NONE
229	IMA1158.fits	27/02/09	22:18:30	15.0	2454890.42951	HS0702	NONE
230	IMA1159.fits	27/02/09	22:19:05	15.0	2454890.42992	HS0702	NONE
231	IMA1160.fits	27/02/09	22:19:40	15.0	2454890.43032	HS0702	NONE
232	IMA1161.fits	27/02/09	22:20:16	15.0	2454890.43074	HS0702	NONE
233	IMA1162.fits	27/02/09	22:20:52	15.0	2454890.43116	HS0702	NONE
234	IMA1163.fits	27/02/09	22:21:28	15.0	2454890.43157	HS0702	NONE
235	IMA1164.fits	27/02/09	22:22:05	15.0	2454890.43200	HS0702	NONE
236	IMA1165.fits	27/02/09	22:22:56	15.0	2454890.43259	HS0702	NONE
237	IMA1166.fits	27/02/09	22:23:31	15.0	2454890.43300	HS0702	NONE
238	IMA1167.fits	27/02/09	22:24:05	15.0	2454890.43339	HS0702	NONE
239	IMA1168.fits	27/02/09	22:24:40	15.0	2454890.43380	HS0702	NONE
240	IMA1169.fits	27/02/09	22:25:15	15.0	2454890.43420	HS0702	NONE
241	IMA1170.fits	27/02/09	22:25:51	15.0	2454890.43462	HS0702	NONE
242	IMA1171.fits	27/02/09	22:26:26	15.0	2454890.43502	HS0702	NONE
243	IMA1172.fits	27/02/09	22:27:01	15.0	2454890.43543	HS0702	NONE
244	IMA1173.fits	27/02/09	22:27:37	15.0	2454890.43584	HS0702	NONE
245	IMA1174.fits	27/02/09	22:28:27	15.0	2454890.43642	HS0702	NONE
246	IMA1175.fits	27/02/09	22:29:02	15.0	2454890.43683	HS0702	NONE

247	IMA1176.fits	27/02/09	22:29:38	15.0	2454890.43725	HS0702	NONE
248	IMA1177.fits	27/02/09	22:30:15	15.0	2454890.43767	HS0702	NONE
249	IMA1178.fits	27/02/09	22:30:50	15.0	2454890.43808	HS0702	NONE
250	IMA1179.fits	27/02/09	22:31:26	15.0	2454890.43850	HS0702	NONE
251	IMA1180.fits	27/02/09	22:32:02	15.0	2454890.43891	HS0702	NONE
252	IMA1181.fits	27/02/09	22:32:39	15.0	2454890.43934	HS0702	NONE
253	IMA1182.fits	27/02/09	22:33:15	15.0	2454890.43976	HS0702	NONE
254	IMA1183.fits	27/02/09	22:34:06	15.0	2454890.44035	HS0702	NONE
255	IMA1184.fits	27/02/09	22:34:41	15.0	2454890.44075	HS0702	NONE
256	IMA1185.fits	27/02/09	22:35:16	15.0	2454890.44116	HS0702	NONE
257	IMA1186.fits	27/02/09	22:35:51	15.0	2454890.44156	HS0702	NONE
258	IMA1187.fits	27/02/09	22:36:27	15.0	2454890.44198	HS0702	NONE
259	IMA1188.fits	27/02/09	22:37:03	15.0	2454890.44240	HS0702	NONE
260	IMA1189.fits	27/02/09	22:37:39	15.0	2454890.44281	HS0702	NONE
261	IMA1190.fits	27/02/09	22:38:15	15.0	2454890.44323	HS0702	NONE
262	IMA1191.fits	27/02/09	22:38:51	15.0	2454890.44365	HS0702	NONE
263	IMA1192.fits	27/02/09	22:41:14	15.0	2454890.44530	HS0702	NONE
264	IMA1193.fits	27/02/09	22:41:49	15.0	2454890.44571	HS0702	NONE
265	IMA1194.fits	27/02/09	22:42:25	15.0	2454890.44612	HS0702	NONE
266	IMA1195.fits	27/02/09	22:43:00	15.0	2454890.44653	HS0702	NONE
267	IMA1196.fits	27/02/09	22:43:36	15.0	2454890.44694	HS0702	NONE
268	IMA1197.fits	27/02/09	22:44:010	15.0	2454890.44734	HS0702	NONE
269	IMA1198.fits	27/02/09	22:44:47	15.0	2454890.44777	HS0702	NONE
270	IMA1199.fits	27/02/09	22:45:23	15.0	2454890.44818	HS0702	NONE
271	IMA1200.fits	27/02/09	22:45:58	15.0	2454890.44859	HS0702	NONE
272	IMA1201.fits	27/02/09	22:46:47	15.0	2454890.44916	HS0702	NONE
273	IMA1202.fits	27/02/09	22:47:22	15.0	2454890.44956	HS0702	NONE
274	IMA1203.fits	27/02/09	22:47:57	15.0	2454890.44997	HS0702	NONE
275	IMA1204.fits	27/02/09	22:48:33	15.0	2454890.45038	HS0702	NONE
276	IMA1205.fits	27/02/09	22:49:09	15.0	2454890.45080	HS0702	NONE
277	IMA1206.fits	27/02/09	22:49:45	15.0	2454890.45122	HS0702	NONE
278	IMA1207.fits	27/02/09	22:50:20	15.0	2454890.45162	HS0702	NONE
279	IMA1208.fits	27/02/09	22:50:55	15.0	2454890.45203	HS0702	NONE
280	IMA1209.fits	27/02/09	22:51:31	15.0	2454890.45244	HS0702	NONE
281	IMA1210.fits	27/02/09	22:52:22	15.0	2454890.45303	HS0702	NONE
282	IMA1211.fits	27/02/09	22:52:56	15.0	2454890.45343	HS0702	NONE
283	IMA1212.fits	27/02/09	22:53:31	15.0	2454890.45383	HS0702	NONE
284	IMA1213.fits	27/02/09	22:54:05	15.0	2454890.45422	HS0702	NONE
285	IMA1214.fits	27/02/09	22:54:40	15.0	2454890.45463	HS0702	NONE
286	IMA1215.fits	27/02/09	22:55:14	15.0	2454890.45502	HS0702	NONE
287	IMA1216.fits	27/02/09	22:55:48	15.0	2454890.45542	HS0702	NONE
288	IMA1217.fits	27/02/09	22:56:25	15.0	2454890.45584	HS0702	NONE
289	IMA1218.fits	27/02/09	22:57:01	15.0	2454890.45626	HS0702	NONE
290	IMA1219.fits	27/02/09	22:57:52	15.0	2454890.45685	HS0702	NONE
291	IMA1220.fits	27/02/09	22:58:27	15.0	2454890.45726	HS0702	NONE
292	IMA1221.fits	27/02/09	22:59:01	15.0	2454890.45765	HS0702	NONE
293	IMA1222.fits	27/02/09	22:59:35	15.0	2454890.45804	HS0702	NONE
294	IMA1223.fits	27/02/09	23:00:11	15.0	2454890.45846	HS0702	NONE
295	IMA1224.fits	27/02/09	23:00:45	15.0	2454890.45885	HS0702	NONE
296	IMA1225.fits	27/02/09	23:01:19	15.0	2454890.45925	HS0702	NONE
297	IMA1226.fits	27/02/09	23:01:55	15.0	2454890.45966	HS0702	NONE
298	IMA1227.fits	27/02/09	23:02:30	15.0	2454890.46007	HS0702	NONE
299	IMA1228.fits	27/02/09	23:03:19	15.0	2454890.46064	HS0702	NONE
300	IMA1229.fits	27/02/09	23:03:53	15.0	2454890.46103	HS0702	NONE
301	IMA1230.fits	27/02/09	23:04:28	15.0	2454890.46144	HS0702	NONE
302	IMA1231.fits	27/02/09	23:05:02	15.0	2454890.46183	HS0702	NONE
303	IMA1232.fits	27/02/09	23:05:36	15.0	2454890.46222	HS0702	NONE
304	IMA1233.fits	27/02/09	23:06:12	15.0	2454890.46264	HS0702	NONE
305	IMA1234.fits	27/02/09	23:06:47	15.0	2454890.46304	HS0702	NONE

306	IMA1235.fits	27/02/09	23:07:22	15.0	2454890.46345	HS0702	NONE
307	IMA1236.fits	27/02/09	23:07:59	15.0	2454890.46388	HS0702	NONE
308	IMA1237.fits	27/02/09	23:08:47	15.0	2454890.46443	HS0702	NONE
309	IMA1238.fits	27/02/09	23:09:22	15.0	2454890.46484	HS0702	NONE
310	IMA1239.fits	27/02/09	23:09:56	15.0	2454890.46523	HS0702	NONE
311	IMA1240.fits	27/02/09	23:10:31	15.0	2454890.46564	HS0702	NONE
312	IMA1241.fits	27/02/09	23:11:07	15.0	2454890.46605	HS0702	NONE
313	IMA1242.fits	27/02/09	23:11:44	15.0	2454890.46648	HS0702	NONE
314	IMA1243.fits	27/02/09	23:12:19	15.0	2454890.46689	HS0702	NONE
315	IMA1244.fits	27/02/09	23:12:53	15.0	2454890.46728	HS0702	NONE
316	IMA1245.fits	27/02/09	23:13:28	15.0	2454890.46769	HS0702	NONE
317	IMA1246.fits	27/02/09	23:14:18	15.0	2454890.46826	HS0702	NONE
318	IMA1247.fits	27/02/09	23:14:53	15.0	2454890.46867	HS0702	NONE
319	IMA1248.fits	27/02/09	23:15:28	15.0	2454890.46907	HS0702	NONE
320	IMA1249.fits	27/02/09	23:16:04	15.0	2454890.46949	HS0702	NONE
321	IMA1250.fits	27/02/09	23:16:40	15.0	2454890.46991	HS0702	NONE
322	IMA1251.fits	27/02/09	23:17:14	15.0	2454890.47030	HS0702	NONE
323	IMA1252.fits	27/02/09	23:17:48	15.0	2454890.47069	HS0702	NONE
324	IMA1253.fits	27/02/09	23:18:22	15.0	2454890.47109	HS0702	NONE
325	IMA1254.fits	27/02/09	23:18:56	15.0	2454890.47148	HS0702	NONE
326	IMA1255.fits	27/02/09	23:19:46	15.0	2454890.47206	HS0702	NONE
327	IMA1256.fits	27/02/09	23:20:20	15.0	2454890.47245	HS0702	NONE
328	IMA1257.fits	27/02/09	23:20:56	15.0	2454890.47287	HS0702	NONE
329	IMA1258.fits	27/02/09	23:21:31	15.0	2454890.47328	HS0702	NONE
330	IMA1259.fits	27/02/09	23:22:05	15.0	2454890.47367	HS0702	NONE
331	IMA1260.fits	27/02/09	23:22:41	15.0	2454890.47409	HS0702	NONE
332	IMA1261.fits	27/02/09	23:23:15	15.0	2454890.47448	HS0702	NONE
333	IMA1262.fits	27/02/09	23:23:49	15.0	2454890.47487	HS0702	NONE
334	IMA1263.fits	27/02/09	23:24:23	15.0	2454890.47527	HS0702	NONE
335	IMA1264.fits	27/02/09	23:25:12	15.0	2454890.47583	HS0702	NONE
336	IMA1265.fits	27/02/09	23:25:47	15.0	2454890.47624	HS0702	NONE
337	IMA1266.fits	27/02/09	23:26:22	15.0	2454890.47664	HS0702	NONE
338	IMA1267.fits	27/02/09	23:26:56	15.0	2454890.47704	HS0702	NONE
339	IMA1268.fits	27/02/09	23:27:30	15.0	2454890.47743	HS0702	NONE
340	IMA1269.fits	27/02/09	23:28:05	15.0	2454890.47784	HS0702	NONE
341	IMA1270.fits	27/02/09	23:28:39	15.0	2454890.47823	HS0702	NONE
342	IMA1271.fits	27/02/09	23:29:15	15.0	2454890.47865	HS0702	NONE
343	IMA1272.fits	27/02/09	23:29:51	15.0	2454890.47906	HS0702	NONE
344	IMA1273.fits	27/02/09	23:30:41	15.0	2454890.47964	HS0702	NONE
345	IMA1274.fits	27/02/09	23:31:15	15.0	2454890.48003	HS0702	NONE
346	IMA1275.fits	27/02/09	23:31:49	15.0	2454890.48043	HS0702	NONE
347	IMA1276.fits	27/02/09	23:32:23	15.0	2454890.48082	HS0702	NONE
348	IMA1277.fits	27/02/09	23:32:57	15.0	2454890.48122	HS0702	NONE
349	IMA1278.fits	27/02/09	23:33:33	15.0	2454890.48163	HS0702	NONE
350	IMA1279.fits	27/02/09	23:34:09	15.0	2454890.48205	HS0702	NONE
351	IMA1280.fits	27/02/09	23:34:44	15.0	2454890.48245	HS0702	NONE
352	IMA1281.fits	27/02/09	23:35:18	15.0	2454890.48285	HS0702	NONE
353	IMA1282.fits	27/02/09	23:38:11	15.0	2454890.48485	HS0702	NONE
354	IMA1283.fits	27/02/09	23:38:46	15.0	2454890.48525	HS0702	NONE
355	IMA1284.fits	27/02/09	23:39:21	15.0	2454890.48566	HS0702	NONE
356	IMA1285.fits	27/02/09	23:39:57	15.0	2454890.48608	HS0702	NONE
357	IMA1286.fits	27/02/09	23:40:33	15.0	2454890.48649	HS0702	NONE
358	IMA1287.fits	27/02/09	23:41:09	15.0	2454890.48691	HS0702	NONE
359	IMA1288.fits	27/02/09	23:41:43	15.0	2454890.48730	HS0702	NONE
360	IMA1289.fits	27/02/09	23:42:18	15.0	2454890.48771	HS0702	NONE
361	IMA1290.fits	27/02/09	23:42:53	15.0	2454890.48811	HS0702	NONE
362	IMA1291.fits	27/02/09	23:43:43	15.0	2454890.48869	HS0702	NONE
363	IMA1292.fits	27/02/09	23:44:19	15.0	2454890.48911	HS0702	NONE
364	IMA1293.fits	27/02/09	23:44:55	15.0	2454890.48953	HS0702	NONE

365	IMA1294.fits	27/02/09	23:45:31	15.0	2454890.48994	HS0702	NONE
366	IMA1295.fits	27/02/09	23:46:06	15.0	2454890.49035	HS0702	NONE
367	IMA1296.fits	27/02/09	23:46:41	15.0	2454890.49075	HS0702	NONE
368	IMA1297.fits	27/02/09	23:47:17	15.0	2454890.49117	HS0702	NONE
369	IMA1298.fits	27/02/09	23:47:51	15.0	2454890.49156	HS0702	NONE
370	IMA1299.fits	27/02/09	23:48:27	15.0	2454890.49198	HS0702	NONE
371	IMA1300.fits	27/02/09	23:49:18	15.0	2454890.49257	HS0702	NONE
372	IMA1301.fits	27/02/09	23:49:55	15.0	2454890.49300	HS0702	NONE
373	IMA1302.fits	27/02/09	23:50:32	15.0	2454890.49343	HS0702	NONE
374	IMA1303.fits	27/02/09	23:51:07	15.0	2454890.49383	HS0702	NONE
375	IMA1304.fits	27/02/09	23:51:44	15.0	2454890.49426	HS0702	NONE
376	IMA1305.fits	27/02/09	23:52:20	15.0	2454890.49468	HS0702	NONE
377	IMA1306.fits	27/02/09	23:52:56	15.0	2454890.49509	HS0702	NONE
378	IMA1307.fits	27/02/09	23:53:30	15.0	2454890.49549	HS0702	NONE
379	IMA1308.fits	27/02/09	23:54:05	15.0	2454890.49589	HS0702	NONE
380	IMA1309.fits	27/02/09	23:54:55	15.0	2454890.49647	HS0702	NONE
381	IMA1310.fits	27/02/09	23:55:30	15.0	2454890.49687	HS0702	NONE
382	IMA1311.fits	27/02/09	23:56:07	15.0	2454890.49730	HS0702	NONE
383	IMA1312.fits	27/02/09	23:56:43	15.0	2454890.49772	HS0702	NONE
384	IMA1313.fits	27/02/09	23:57:19	15.0	2454890.49814	HS0702	NONE
385	IMA1314.fits	27/02/09	23:57:55	15.0	2454890.49855	HS0702	NONE
386	IMA1315.fits	27/02/09	23:58:30	15.0	2454890.49896	HS0702	NONE
387	IMA1316.fits	27/02/09	23:59:06	15.0	2454890.49938	HS0702	NONE
388	IMA1317.fits	27/02/09	23:59:41	15.0	2454890.49978	HS0702	NONE
389	IMA1318.fits	28/02/09	00:00:31	15.0	2454890.50036	HS0702	NONE
390	IMA1319.fits	28/02/09	00:01:06	15.0	2454890.50076	HS0702	NONE
391	IMA1320.fits	28/02/09	00:01:41	15.0	2454890.50117	HS0702	NONE
392	IMA1321.fits	28/02/09	00:02:18	15.0	2454890.50160	HS0702	NONE
393	IMA1322.fits	28/02/09	00:02:52	15.0	2454890.50199	HS0702	NONE
394	IMA1323.fits	28/02/09	00:03:28	15.0	2454890.50241	HS0702	NONE
395	IMA1324.fits	28/02/09	00:04:03	15.0	2454890.50281	HS0702	NONE
396	IMA1325.fits	28/02/09	00:04:41	15.0	2454890.50325	HS0702	NONE
397	IMA1326.fits	28/02/09	00:05:18	15.0	2454890.50368	HS0702	NONE
398	IMA1327.fits	28/02/09	00:06:09	15.0	2454890.50427	HS0702	NONE
399	IMA1328.fits	28/02/09	00:06:44	15.0	2454890.50468	HS0702	NONE
400	IMA1329.fits	28/02/09	00:07:20	15.0	2454890.50509	HS0702	NONE
401	IMA1330.fits	28/02/09	00:07:57	15.0	2454890.50552	HS0702	NONE
402	IMA1331.fits	28/02/09	00:08:32	15.0	2454890.50593	HS0702	NONE
403	IMA1332.fits	28/02/09	00:09:06	15.0	2454890.50632	HS0702	NONE
404	IMA1333.fits	28/02/09	00:09:40	15.0	2454890.50671	HS0702	NONE
405	IMA1334.fits	28/02/09	00:10:14	15.0	2454890.50711	HS0702	NONE
406	IMA1335.fits	28/02/09	00:10:50	15.0	2454890.50752	HS0702	NONE
407	IMA1336.fits	28/02/09	00:11:40	15.0	2454890.50810	HS0702	NONE
408	IMA1337.fits	28/02/09	00:12:15	15.0	2454890.50851	HS0702	NONE
409	IMA1338.fits	28/02/09	00:12:51	15.0	2454890.50892	HS0702	NONE
410	IMA1339.fits	28/02/09	00:13:27	15.0	2454890.50934	HS0702	NONE
411	IMA1340.fits	28/02/09	00:14:02	15.0	2454890.50975	HS0702	NONE
412	IMA1341.fits	28/02/09	00:14:37	15.0	2454890.51015	HS0702	NONE
413	IMA1342.fits	28/02/09	00:15:11	15.0	2454890.51054	HS0702	NONE
414	IMA1343.fits	28/02/09	00:15:47	15.0	2454890.51096	HS0702	NONE
415	IMA1344.fits	28/02/09	00:16:22	15.0	2454890.51137	HS0702	NONE
416	IMA1345.fits	28/02/09	00:17:12	15.0	2454890.51194	HS0702	NONE
417	IMA1346.fits	28/02/09	00:17:46	15.0	2454890.51234	HS0702	NONE
418	IMA1347.fits	28/02/09	00:18:22	15.0	2454890.51275	HS0702	NONE
419	IMA1348.fits	28/02/09	00:18:58	15.0	2454890.51317	HS0702	NONE
420	IMA1349.fits	28/02/09	00:19:36	15.0	2454890.51361	HS0702	NONE
421	IMA1350.fits	28/02/09	00:20:11	15.0	2454890.51402	HS0702	NONE
422	IMA1351.fits	28/02/09	00:20:47	15.0	2454890.51443	HS0702	NONE
423	IMA1352.fits	28/02/09	00:21:22	15.0	2454890.51484	HS0702	NONE

424	IMA1353.fits	28/02/09	00:21:58	15.0	2454890.51525	HS0702	NONE
425	IMA1354.fits	28/02/09	00:22:51	15.0	2454890.51587	HS0702	NONE
426	IMA1355.fits	28/02/09	00:23:27	15.0	2454890.51628	HS0702	NONE
427	IMA1356.fits	28/02/09	00:24:03	15.0	2454890.51670	HS0702	NONE
428	IMA1357.fits	28/02/09	00:24:39	15.0	2454890.51712	HS0702	NONE
429	IMA1358.fits	28/02/09	00:25:15	15.0	2454890.51753	HS0702	NONE
430	IMA1359.fits	28/02/09	00:25:51	15.0	2454890.51795	HS0702	NONE
431	IMA1360.fits	28/02/09	00:26:26	15.0	2454890.51836	HS0702	NONE
432	IMA1361.fits	28/02/09	00:27:01	15.0	2454890.51876	HS0702	NONE
433	IMA1362.fits	28/02/09	00:27:36	15.0	2454890.51917	HS0702	NONE
434	IMA1363.fits	28/02/09	00:28:26	15.0	2454890.51975	HS0702	NONE
435	IMA1364.fits	28/02/09	00:29:02	15.0	2454890.52016	HS0702	NONE
436	IMA1365.fits	28/02/09	00:29:38	15.0	2454890.52058	HS0702	NONE
437	IMA1366.fits	28/02/09	00:30:14	15.0	2454890.52100	HS0702	NONE
438	IMA1367.fits	28/02/09	00:30:48	15.0	2454890.52139	HS0702	NONE
439	IMA1368.fits	28/02/09	00:31:22	15.0	2454890.52178	HS0702	NONE
440	IMA1369.fits	28/02/09	00:31:58	15.0	2454890.52220	HS0702	NONE
441	IMA1370.fits	28/02/09	00:32:33	15.0	2454890.52260	HS0702	NONE
442	IMA1371.fits	28/02/09	00:33:08	15.0	2454890.52301	HS0702	NONE
443	IMA1372.fits	28/02/09	00:37:37	15.0	2454890.52612	HS0702	NONE
444	IMA1373.fits	28/02/09	00:38:12	15.0	2454890.52653	HS0702	NONE
445	IMA1374.fits	28/02/09	00:38:47	15.0	2454890.52693	HS0702	NONE
446	IMA1375.fits	28/02/09	00:39:22	15.0	2454890.52734	HS0702	NONE
447	IMA1376.fits	28/02/09	00:39:57	15.0	2454890.52774	HS0702	NONE
448	IMA1377.fits	28/02/09	00:40:32	15.0	2454890.52815	HS0702	NONE
449	IMA1378.fits	28/02/09	00:41:07	15.0	2454890.52855	HS0702	NONE
450	IMA1379.fits	28/02/09	00:41:43	15.0	2454890.52897	HS0702	NONE
451	IMA1380.fits	28/02/09	00:42:19	15.0	2454890.52939	HS0702	NONE
452	IMA1381.fits	28/02/09	00:43:10	15.0	2454890.52998	HS0702	NONE
453	IMA1382.fits	28/02/09	00:43:46	15.0	2454890.53039	HS0702	NONE
454	IMA1383.fits	28/02/09	00:44:21	15.0	2454890.53080	HS0702	NONE
455	IMA1384.fits	28/02/09	00:44:56	15.0	2454890.53120	HS0702	NONE
456	IMA1385.fits	28/02/09	00:45:32	15.0	2454890.53162	HS0702	NONE
457	IMA1386.fits	28/02/09	00:46:08	15.0	2454890.53204	HS0702	NONE
458	IMA1387.fits	28/02/09	00:46:43	15.0	2454890.53244	HS0702	NONE
459	IMA1388.fits	28/02/09	00:47:18	15.0	2454890.53285	HS0702	NONE
460	IMA1389.fits	28/02/09	00:47:53	15.0	2454890.53325	HS0702	NONE
461	IMA1390.fits	28/02/09	00:48:43	15.0	2454890.53383	HS0702	NONE
462	IMA1391.fits	28/02/09	00:49:17	15.0	2454890.53422	HS0702	NONE
463	IMA1392.fits	28/02/09	00:49:52	15.0	2454890.53463	HS0702	NONE
464	IMA1393.fits	28/02/09	00:50:28	15.0	2454890.53505	HS0702	NONE
465	IMA1394.fits	28/02/09	00:51:03	15.0	2454890.53545	HS0702	NONE
466	IMA1395.fits	28/02/09	00:51:38	15.0	2454890.53586	HS0702	NONE
467	IMA1396.fits	28/02/09	00:52:13	15.0	2454890.53626	HS0702	NONE
468	IMA1397.fits	28/02/09	00:52:49	15.0	2454890.53668	HS0702	NONE
469	IMA1398.fits	28/02/09	00:53:25	15.0	2454890.53709	HS0702	NONE
470	IMA1399.fits	28/02/09	00:54:16	15.0	2454890.53769	HS0702	NONE
471	IMA1400.fits	28/02/09	00:54:52	15.0	2454890.53810	HS0702	NONE
472	IMA1401.fits	28/02/09	00:55:29	15.0	2454890.53853	HS0702	NONE
473	IMA1402.fits	28/02/09	00:56:06	15.0	2454890.53896	HS0702	NONE
474	IMA1403.fits	28/02/09	00:56:41	15.0	2454890.53936	HS0702	NONE
475	IMA1404.fits	28/02/09	00:57:15	15.0	2454890.53976	HS0702	NONE
476	IMA1405.fits	28/02/09	00:57:50	15.0	2454890.54016	HS0702	NONE
477	IMA1406.fits	28/02/09	00:58:24	15.0	2454890.54056	HS0702	NONE
478	IMA1407.fits	28/02/09	00:59:00	15.0	2454890.54097	HS0702	NONE
479	IMA1408.fits	28/02/09	00:59:51	15.0	2454890.54156	HS0702	NONE
480	IMA1409.fits	28/02/09	01:00:26	15.0	2454890.54197	HS0702	NONE
481	IMA1410.fits	28/02/09	01:01:02	15.0	2454890.54238	HS0702	NONE
482	IMA1411.fits	28/02/09	01:01:39	15.0	2454890.54281	HS0702	NONE

483	IMA1412.fits	28/02/09	01:02:14	15.0	2454890.54322	HS0702	NONE
484	IMA1413.fits	28/02/09	01:02:50	15.0	2454890.54363	HS0702	NONE
485	IMA1414.fits	28/02/09	01:03:25	15.0	2454890.54404	HS0702	NONE
486	IMA1415.fits	28/02/09	01:03:59	15.0	2454890.54443	HS0702	NONE
487	IMA1416.fits	28/02/09	01:04:34	15.0	2454890.54484	HS0702	NONE
488	IMA1417.fits	28/02/09	01:05:23	15.0	2454890.54541	HS0702	NONE
489	IMA1418.fits	28/02/09	01:05:59	15.0	2454890.54582	HS0702	NONE
490	IMA1419.fits	28/02/09	01:06:34	15.0	2454890.54623	HS0702	NONE
491	IMA1420.fits	28/02/09	01:07:08	15.0	2454890.54662	HS0702	NONE
492	IMA1421.fits	28/02/09	01:07:42	15.0	2454890.54701	HS0702	NONE
493	IMA1422.fits	28/02/09	01:08:17	15.0	2454890.54742	HS0702	NONE
494	IMA1423.fits	28/02/09	01:08:52	15.0	2454890.54782	HS0702	NONE
495	IMA1424.fits	28/02/09	01:09:26	15.0	2454890.54822	HS0702	NONE
496	IMA1425.fits	28/02/09	01:09:60	15.0	2454890.54861	HS0702	NONE
497	IMA1426.fits	28/02/09	01:10:50	15.0	2454890.54919	HS0702	NONE
498	IMA1427.fits	28/02/09	01:11:26	15.0	2454890.54961	HS0702	NONE
499	IMA1428.fits	28/02/09	01:12:01	15.0	2454890.55001	HS0702	NONE
500	IMA1429.fits	28/02/09	01:12:37	15.0	2454890.55043	HS0702	NONE
501	IMA1430.fits	28/02/09	01:13:11	15.0	2454890.55082	HS0702	NONE
502	IMA1431.fits	28/02/09	01:13:45	15.0	2454890.55122	HS0702	NONE
503	IMA1432.fits	28/02/09	01:14:21	15.0	2454890.55163	HS0702	NONE
504	IMA1433.fits	28/02/09	01:14:55	15.0	2454890.55203	HS0702	NONE
505	IMA1434.fits	28/02/09	01:15:29	15.0	2454890.55242	HS0702	NONE
506	IMA1435.fits	28/02/09	01:16:18	15.0	2454890.55299	HS0702	NONE
507	IMA1436.fits	28/02/09	01:16:53	15.0	2454890.55339	HS0702	NONE
508	IMA1437.fits	28/02/09	01:17:28	15.0	2454890.55380	HS0702	NONE
509	IMA1438.fits	28/02/09	01:18:02	15.0	2454890.55419	HS0702	NONE
510	IMA1439.fits	28/02/09	01:18:36	15.0	2454890.55458	HS0702	NONE
511	IMA1440.fits	28/02/09	01:19:010	15.0	2454890.55498	HS0702	NONE
512	IMA1441.fits	28/02/09	01:19:45	15.0	2454890.55538	HS0702	NONE
513	IMA1442.fits	28/02/09	01:20:20	15.0	2454890.55579	HS0702	NONE
514	IMA1443.fits	28/02/09	01:20:54	15.0	2454890.55618	HS0702	NONE
515	IMA1444.fits	28/02/09	01:21:43	15.0	2454890.55675	HS0702	NONE
516	IMA1445.fits	28/02/09	01:22:18	15.0	2454890.55715	HS0702	NONE
517	IMA1446.fits	28/02/09	01:22:55	15.0	2454890.55758	HS0702	NONE
518	IMA1447.fits	28/02/09	01:23:31	15.0	2454890.55800	HS0702	NONE
519	IMA1448.fits	28/02/09	01:24:05	15.0	2454890.55839	HS0702	NONE
520	IMA1449.fits	28/02/09	01:24:39	15.0	2454890.55878	HS0702	NONE
521	IMA1450.fits	28/02/09	01:25:13	15.0	2454890.55918	HS0702	NONE
522	IMA1451.fits	28/02/09	01:25:47	15.0	2454890.55957	HS0702	NONE
523	IMA1452.fits	28/02/09	01:26:23	15.0	2454890.55999	HS0702	NONE
524	IMA1453.fits	28/02/09	01:27:12	15.0	2454890.56056	HS0702	NONE
525	IMA1454.fits	28/02/09	01:27:47	15.0	2454890.56096	HS0702	NONE
526	IMA1455.fits	28/02/09	01:28:21	15.0	2454890.56135	HS0702	NONE
527	IMA1456.fits	28/02/09	01:28:57	15.0	2454890.56177	HS0702	NONE
528	IMA1457.fits	28/02/09	01:29:33	15.0	2454890.56219	HS0702	NONE
529	IMA1458.fits	28/02/09	01:30:08	15.0	2454890.56259	HS0702	NONE
530	IMA1459.fits	28/02/09	01:30:42	15.0	2454890.56299	HS0702	NONE
531	IMA1460.fits	28/02/09	01:31:16	15.0	2454890.56338	HS0702	NONE
532	IMA1461.fits	28/02/09	01:31:50	15.0	2454890.56377	HS0702	NONE

B.3 March, 21-22, 2009

#	Image	Date	Start	Texp	JD	Object	Filter
1	IMA0031.fits	21/03/09	20:46:46	30.0	2454912.36581	HS0702	B
2	IMA0032.fits	21/03/09	20:47:45	30.0	2454912.36649	HS0702	B
3	IMA0033.fits	21/03/09	20:48:44	30.0	2454912.36718	HS0702	B
4	IMA0034.fits	21/03/09	20:49:42	30.0	2454912.36785	HS0702	B

5	IMA0035.fits	21/03/09	20:50:41	30.0	2454912.36853	HS0702	B
6	IMA0036.fits	21/03/09	20:51:39	30.0	2454912.36920	HS0702	B
7	IMA0037.fits	21/03/09	20:52:37	30.0	2454912.36987	HS0702	B
8	IMA0038.fits	21/03/09	20:53:35	30.0	2454912.37054	HS0702	B
9	IMA0039.fits	21/03/09	20:54:34	30.0	2454912.37123	HS0702	B
10	IMA0040.fits	21/03/09	20:55:48	30.0	2454912.37208	HS0702	B
11	IMA0041.fits	21/03/09	20:56:45	30.0	2454912.37274	HS0702	B
12	IMA0042.fits	21/03/09	20:57:43	30.0	2454912.37341	HS0702	B
13	IMA0043.fits	21/03/09	20:58:41	30.0	2454912.37409	HS0702	B
14	IMA0044.fits	21/03/09	20:59:38	30.0	2454912.37475	HS0702	B
15	IMA0045.fits	21/03/09	21:00:34	30.0	2454912.37539	HS0702	B
16	IMA0046.fits	21/03/09	21:01:30	30.0	2454912.37604	HS0702	B
17	IMA0047.fits	21/03/09	21:02:27	30.0	2454912.37670	HS0702	B
18	IMA0048.fits	21/03/09	21:03:23	30.0	2454912.37735	HS0702	B
19	IMA0049.fits	21/03/09	21:04:35	30.0	2454912.37818	HS0702	B
20	IMA0050.fits	21/03/09	21:05:33	30.0	2454912.37885	HS0702	B
21	IMA0051.fits	21/03/09	21:06:32	30.0	2454912.37954	HS0702	B
22	IMA0052.fits	21/03/09	21:07:29	30.0	2454912.38020	HS0702	B
23	IMA0053.fits	21/03/09	21:08:27	30.0	2454912.38087	HS0702	B
24	IMA0054.fits	21/03/09	21:09:25	30.0	2454912.38154	HS0702	B
25	IMA0055.fits	21/03/09	21:10:24	30.0	2454912.38222	HS0702	B
26	IMA0056.fits	21/03/09	21:11:22	30.0	2454912.38289	HS0702	B
27	IMA0057.fits	21/03/09	21:12:19	30.0	2454912.38355	HS0702	B
28	IMA0058.fits	21/03/09	21:13:31	30.0	2454912.38439	HS0702	B
29	IMA0059.fits	21/03/09	21:14:28	30.0	2454912.38505	HS0702	B
30	IMA0060.fits	21/03/09	21:15:24	30.0	2454912.38569	HS0702	B
31	IMA0061.fits	21/03/09	21:16:21	30.0	2454912.38635	HS0702	B
32	IMA0062.fits	21/03/09	21:17:18	30.0	2454912.38701	HS0702	B
33	IMA0063.fits	21/03/09	21:18:14	30.0	2454912.38766	HS0702	B
34	IMA0064.fits	21/03/09	21:19:12	30.0	2454912.38833	HS0702	B
35	IMA0065.fits	21/03/09	21:20:010	30.0	2454912.38900	HS0702	B
36	IMA0066.fits	21/03/09	21:21:08	30.0	2454912.38968	HS0702	B
37	IMA0067.fits	21/03/09	21:22:19	30.0	2454912.39050	HS0702	B
38	IMA0068.fits	21/03/09	21:23:16	30.0	2454912.39116	HS0702	B
39	IMA0069.fits	21/03/09	21:24:15	30.0	2454912.39184	HS0702	B
40	IMA0070.fits	21/03/09	21:25:12	30.0	2454912.39250	HS0702	B
41	IMA0071.fits	21/03/09	21:26:10	30.0	2454912.39317	HS0702	B
42	IMA0072.fits	21/03/09	21:27:06	30.0	2454912.39382	HS0702	B
43	IMA0073.fits	21/03/09	21:28:02	30.0	2454912.39447	HS0702	B
44	IMA0074.fits	21/03/09	21:28:59	30.0	2454912.39513	HS0702	B
45	IMA0075.fits	21/03/09	21:29:56	30.0	2454912.39579	HS0702	B
46	IMA0076.fits	21/03/09	21:31:08	30.0	2454912.39662	HS0702	B
47	IMA0077.fits	21/03/09	21:32:06	30.0	2454912.39729	HS0702	B
48	IMA0078.fits	21/03/09	21:33:02	30.0	2454912.39794	HS0702	B
49	IMA0079.fits	21/03/09	21:34:00	30.0	2454912.39861	HS0702	B
50	IMA0080.fits	21/03/09	21:34:57	30.0	2454912.39927	HS0702	B
51	IMA0081.fits	21/03/09	21:35:55	30.0	2454912.39994	HS0702	B
52	IMA0082.fits	21/03/09	21:36:53	30.0	2454912.40061	HS0702	B
53	IMA0083.fits	21/03/09	21:37:51	30.0	2454912.40128	HS0702	B
54	IMA0084.fits	21/03/09	21:38:49	30.0	2454912.40196	HS0702	B
55	IMA0085.fits	21/03/09	21:40:02	30.0	2454912.40280	HS0702	B
56	IMA0086.fits	21/03/09	21:40:60	30.0	2454912.40347	HS0702	B
57	IMA0087.fits	21/03/09	21:41:59	30.0	2454912.40416	HS0702	B
58	IMA0088.fits	21/03/09	21:42:58	30.0	2454912.40484	HS0702	B
59	IMA0089.fits	21/03/09	21:43:56	30.0	2454912.40551	HS0702	B
60	IMA0090.fits	21/03/09	21:44:55	30.0	2454912.40619	HS0702	B
61	IMA0091.fits	21/03/09	21:45:54	30.0	2454912.40687	HS0702	B
62	IMA0092.fits	21/03/09	21:46:52	30.0	2454912.40755	HS0702	B
63	IMA0093.fits	21/03/09	21:47:51	30.0	2454912.40823	HS0702	B

64	IMA0094.fits	21/03/09	21:49:04	30.0	2454912.40907	HS0702	B
65	IMA0095.fits	21/03/09	21:50:02	30.0	2454912.40975	HS0702	B
66	IMA0096.fits	21/03/09	21:51:01	30.0	2454912.41043	HS0702	B
67	IMA0097.fits	21/03/09	21:51:59	30.0	2454912.41110	HS0702	B
68	IMA0098.fits	21/03/09	21:52:57	30.0	2454912.41177	HS0702	B
69	IMA0099.fits	21/03/09	21:53:54	30.0	2454912.41243	HS0702	B
70	IMA0100.fits	21/03/09	21:54:53	30.0	2454912.41311	HS0702	B
71	IMA0101.fits	21/03/09	21:55:51	30.0	2454912.41378	HS0702	B
72	IMA0102.fits	21/03/09	21:56:49	30.0	2454912.41446	HS0702	B
73	IMA0103.fits	21/03/09	21:58:02	30.0	2454912.41530	HS0702	B
74	IMA0104.fits	21/03/09	21:59:01	30.0	2454912.41598	HS0702	B
75	IMA0105.fits	21/03/09	21:59:59	30.0	2454912.41666	HS0702	B
76	IMA0106.fits	21/03/09	22:00:57	30.0	2454912.41733	HS0702	B
77	IMA0107.fits	21/03/09	22:01:57	30.0	2454912.41802	HS0702	B
78	IMA0108.fits	21/03/09	22:02:55	30.0	2454912.41869	HS0702	B
79	IMA0109.fits	21/03/09	22:03:53	30.0	2454912.41936	HS0702	B
80	IMA0110.fits	21/03/09	22:04:53	30.0	2454912.42006	HS0702	B
81	IMA0111.fits	21/03/09	22:05:52	30.0	2454912.42074	HS0702	B
82	IMA0112.fits	21/03/09	22:07:05	30.0	2454912.42159	HS0702	B
83	IMA0113.fits	21/03/09	22:08:02	30.0	2454912.42225	HS0702	B
84	IMA0114.fits	21/03/09	22:09:01	30.0	2454912.42293	HS0702	B
85	IMA0115.fits	21/03/09	22:09:60	30.0	2454912.42361	HS0702	B
86	IMA0116.fits	21/03/09	22:10:58	30.0	2454912.42428	HS0702	B
87	IMA0117.fits	21/03/09	22:11:56	30.0	2454912.42495	HS0702	B
88	IMA0118.fits	21/03/09	22:12:55	30.0	2454912.42564	HS0702	B
89	IMA0119.fits	21/03/09	22:13:53	30.0	2454912.42631	HS0702	B
90	IMA0120.fits	21/03/09	22:14:50	30.0	2454912.42697	HS0702	B
91	IMA0121.fits	21/03/09	22:17:56	30.0	2454912.42912	HS0702	B
92	IMA0122.fits	21/03/09	22:18:53	30.0	2454912.42978	HS0702	B
93	IMA0123.fits	21/03/09	22:19:51	30.0	2454912.43045	HS0702	B
94	IMA0124.fits	21/03/09	22:20:49	30.0	2454912.43112	HS0702	B
95	IMA0125.fits	21/03/09	22:21:48	30.0	2454912.43181	HS0702	B
96	IMA0126.fits	21/03/09	22:22:46	30.0	2454912.43248	HS0702	B
97	IMA0127.fits	21/03/09	22:23:44	30.0	2454912.43315	HS0702	B
98	IMA0128.fits	21/03/09	22:24:43	30.0	2454912.43383	HS0702	B
99	IMA0129.fits	21/03/09	22:25:42	30.0	2454912.43451	HS0702	B
100	IMA0130.fits	21/03/09	22:26:55	30.0	2454912.43536	HS0702	B
101	IMA0131.fits	21/03/09	22:27:52	30.0	2454912.43602	HS0702	B
102	IMA0132.fits	21/03/09	22:28:51	30.0	2454912.43670	HS0702	B
103	IMA0133.fits	21/03/09	22:29:48	30.0	2454912.43736	HS0702	B
104	IMA0134.fits	21/03/09	22:30:46	30.0	2454912.43803	HS0702	B
105	IMA0135.fits	21/03/09	22:31:45	30.0	2454912.43872	HS0702	B
106	IMA0136.fits	21/03/09	22:32:43	30.0	2454912.43939	HS0702	B
107	IMA0137.fits	21/03/09	22:33:41	30.0	2454912.44006	HS0702	B
108	IMA0138.fits	21/03/09	22:34:38	30.0	2454912.44072	HS0702	B
109	IMA0139.fits	21/03/09	22:35:52	30.0	2454912.44157	HS0702	B
110	IMA0140.fits	21/03/09	22:36:50	30.0	2454912.44225	HS0702	B
111	IMA0141.fits	21/03/09	22:37:49	30.0	2454912.44293	HS0702	B
112	IMA0142.fits	21/03/09	22:38:47	30.0	2454912.44360	HS0702	B
113	IMA0143.fits	21/03/09	22:39:46	30.0	2454912.44428	HS0702	B
114	IMA0144.fits	21/03/09	22:40:44	30.0	2454912.44495	HS0702	B
115	IMA0145.fits	21/03/09	22:41:42	30.0	2454912.44562	HS0702	B
116	IMA0146.fits	21/03/09	22:42:40	30.0	2454912.44630	HS0702	B
117	IMA0147.fits	21/03/09	22:43:38	30.0	2454912.44697	HS0702	B
118	IMA0148.fits	21/03/09	22:44:51	30.0	2454912.44781	HS0702	B
119	IMA0149.fits	21/03/09	22:45:49	30.0	2454912.44848	HS0702	B
120	IMA0150.fits	21/03/09	22:46:48	30.0	2454912.44917	HS0702	B
121	IMA0151.fits	21/03/09	22:47:46	30.0	2454912.44984	HS0702	B
122	IMA0152.fits	21/03/09	22:48:44	30.0	2454912.45051	HS0702	B

123	IMA0153.fits	21/03/09	22:49:43	30.0	2454912.45119	HS0702	B
124	IMA0154.fits	21/03/09	22:50:42	30.0	2454912.45187	HS0702	B
125	IMA0155.fits	21/03/09	22:51:41	30.0	2454912.45256	HS0702	B
126	IMA0156.fits	21/03/09	22:52:39	30.0	2454912.45323	HS0702	B
127	IMA0157.fits	21/03/09	22:53:54	30.0	2454912.45410	HS0702	B
128	IMA0158.fits	21/03/09	22:54:52	30.0	2454912.45477	HS0702	B
129	IMA0159.fits	21/03/09	22:55:50	30.0	2454912.45544	HS0702	B
130	IMA0160.fits	21/03/09	22:56:48	30.0	2454912.45611	HS0702	B
131	IMA0161.fits	21/03/09	22:57:46	30.0	2454912.45678	HS0702	B
132	IMA0162.fits	21/03/09	22:58:44	30.0	2454912.45745	HS0702	B
133	IMA0163.fits	21/03/09	22:59:42	30.0	2454912.45813	HS0702	B
134	IMA0164.fits	21/03/09	23:00:40	30.0	2454912.45880	HS0702	B
135	IMA0165.fits	21/03/09	23:01:38	30.0	2454912.45947	HS0702	B
136	IMA0166.fits	21/03/09	23:02:50	30.0	2454912.46030	HS0702	B
137	IMA0167.fits	21/03/09	23:03:48	30.0	2454912.46097	HS0702	B
138	IMA0168.fits	21/03/09	23:04:46	30.0	2454912.46164	HS0702	B
139	IMA0169.fits	21/03/09	23:05:44	30.0	2454912.46231	HS0702	B
140	IMA0170.fits	21/03/09	23:06:42	30.0	2454912.46299	HS0702	B
141	IMA0171.fits	21/03/09	23:07:40	30.0	2454912.46366	HS0702	B
142	IMA0172.fits	21/03/09	23:08:39	30.0	2454912.46434	HS0702	B
143	IMA0173.fits	21/03/09	23:09:37	30.0	2454912.46501	HS0702	B
144	IMA0174.fits	21/03/09	23:10:34	30.0	2454912.46567	HS0702	B
145	IMA0175.fits	21/03/09	23:11:48	30.0	2454912.46653	HS0702	B
146	IMA0176.fits	21/03/09	23:12:45	30.0	2454912.46719	HS0702	B
147	IMA0177.fits	21/03/09	23:13:42	30.0	2454912.46785	HS0702	B
148	IMA0178.fits	21/03/09	23:14:40	30.0	2454912.46852	HS0702	B
149	IMA0179.fits	21/03/09	23:15:39	30.0	2454912.46920	HS0702	B
150	IMA0180.fits	21/03/09	23:16:37	30.0	2454912.46987	HS0702	B
151	IMA0181.fits	21/03/09	23:17:35	30.0	2454912.47054	HS0702	B
152	IMA0182.fits	21/03/09	23:18:32	30.0	2454912.47120	HS0702	B
153	IMA0183.fits	21/03/09	23:19:31	30.0	2454912.47189	HS0702	B
154	IMA0184.fits	21/03/09	23:20:44	30.0	2454912.47273	HS0702	B
155	IMA0185.fits	21/03/09	23:21:42	30.0	2454912.47340	HS0702	B
156	IMA0186.fits	21/03/09	23:22:41	30.0	2454912.47409	HS0702	B
157	IMA0187.fits	21/03/09	23:23:40	30.0	2454912.47477	HS0702	B
158	IMA0188.fits	21/03/09	23:24:38	30.0	2454912.47544	HS0702	B
159	IMA0189.fits	21/03/09	23:25:36	30.0	2454912.47611	HS0702	B
160	IMA0190.fits	21/03/09	23:26:35	30.0	2454912.47679	HS0702	B
161	IMA0191.fits	21/03/09	23:27:32	30.0	2454912.47745	HS0702	B
162	IMA0192.fits	21/03/09	23:28:30	30.0	2454912.47813	HS0702	B
163	IMA0193.fits	21/03/09	23:29:43	30.0	2454912.47897	HS0702	B
164	IMA0194.fits	21/03/09	23:30:41	30.0	2454912.47964	HS0702	B
165	IMA0195.fits	21/03/09	23:31:38	30.0	2454912.48030	HS0702	B
166	IMA0196.fits	21/03/09	23:32:36	30.0	2454912.48097	HS0702	B
167	IMA0197.fits	21/03/09	23:33:34	30.0	2454912.48164	HS0702	B
168	IMA0198.fits	21/03/09	23:34:33	30.0	2454912.48233	HS0702	B
169	IMA0199.fits	21/03/09	23:35:31	30.0	2454912.48300	HS0702	B
170	IMA0200.fits	21/03/09	23:36:29	30.0	2454912.48367	HS0702	B
171	IMA0201.fits	21/03/09	23:37:27	30.0	2454912.48434	HS0702	B
172	IMA0202.fits	21/03/09	23:38:40	30.0	2454912.48519	HS0702	B
173	IMA0203.fits	21/03/09	23:39:38	30.0	2454912.48586	HS0702	B
174	IMA0204.fits	21/03/09	23:40:37	30.0	2454912.48654	HS0702	B
175	IMA0205.fits	21/03/09	23:41:36	30.0	2454912.48722	HS0702	B
176	IMA0206.fits	21/03/09	23:42:34	30.0	2454912.48789	HS0702	B
177	IMA0207.fits	21/03/09	23:43:32	30.0	2454912.48856	HS0702	B
178	IMA0208.fits	21/03/09	23:44:30	30.0	2454912.48924	HS0702	B
179	IMA0209.fits	21/03/09	23:45:30	30.0	2454912.48993	HS0702	B
180	IMA0210.fits	21/03/09	23:46:28	30.0	2454912.49060	HS0702	B
181	IMA0211.fits	21/03/09	23:51:09	30.0	2454912.49385	HS0702	B

182	IMA0212.fits	21/03/09	23:52:07	30.0	2454912.49453	HS0702	B
183	IMA0213.fits	21/03/09	23:53:05	30.0	2454912.49520	HS0702	B
184	IMA0214.fits	21/03/09	23:54:03	30.0	2454912.49587	HS0702	B
185	IMA0215.fits	21/03/09	23:55:01	30.0	2454912.49654	HS0702	B
186	IMA0216.fits	21/03/09	23:55:60	30.0	2454912.49722	HS0702	B
187	IMA0217.fits	21/03/09	23:56:59	30.0	2454912.49791	HS0702	B
188	IMA0218.fits	21/03/09	23:57:58	30.0	2454912.49859	HS0702	B
189	IMA0219.fits	21/03/09	23:58:56	30.0	2454912.49926	HS0702	B
190	IMA0220.fits	22/03/09	00:00:11	30.0	2454912.50013	HS0702	B
191	IMA0221.fits	22/03/09	00:01:09	30.0	2454912.50080	HS0702	B
192	IMA0222.fits	22/03/09	00:02:07	30.0	2454912.50147	HS0702	B
193	IMA0223.fits	22/03/09	00:03:05	30.0	2454912.50214	HS0702	B
194	IMA0224.fits	22/03/09	00:04:04	30.0	2454912.50282	HS0702	B
195	IMA0225.fits	22/03/09	00:05:01	30.0	2454912.50348	HS0702	B
196	IMA0226.fits	22/03/09	00:05:59	30.0	2454912.50416	HS0702	B
197	IMA0227.fits	22/03/09	00:06:57	30.0	2454912.50483	HS0702	B
198	IMA0228.fits	22/03/09	00:07:56	30.0	2454912.50551	HS0702	B
199	IMA0229.fits	22/03/09	00:09:08	30.0	2454912.50634	HS0702	B
200	IMA0230.fits	22/03/09	00:10:06	30.0	2454912.50701	HS0702	B
201	IMA0231.fits	22/03/09	00:11:05	30.0	2454912.50770	HS0702	B
202	IMA0232.fits	22/03/09	00:12:04	30.0	2454912.50838	HS0702	B
203	IMA0233.fits	22/03/09	00:13:02	30.0	2454912.50905	HS0702	B
204	IMA0234.fits	22/03/09	00:14:00	30.0	2454912.50972	HS0702	B
205	IMA0235.fits	22/03/09	00:15:00	30.0	2454912.51042	HS0702	B
206	IMA0236.fits	22/03/09	00:15:58	30.0	2454912.51109	HS0702	B
207	IMA0237.fits	22/03/09	00:16:56	30.0	2454912.51176	HS0702	B
208	IMA0238.fits	22/03/09	00:18:010	30.0	2454912.51262	HS0702	B
209	IMA0239.fits	22/03/09	00:19:09	30.0	2454912.51330	HS0702	B
210	IMA0240.fits	22/03/09	00:20:07	30.0	2454912.51397	HS0702	B
211	IMA0241.fits	22/03/09	00:21:05	30.0	2454912.51464	HS0702	B
212	IMA0242.fits	22/03/09	00:22:04	30.0	2454912.51532	HS0702	B
213	IMA0243.fits	22/03/09	00:23:03	30.0	2454912.51601	HS0702	B
214	IMA0244.fits	22/03/09	00:24:02	30.0	2454912.51669	HS0702	B
215	IMA0245.fits	22/03/09	00:24:60	30.0	2454912.51736	HS0702	B
216	IMA0246.fits	22/03/09	00:26:00	30.0	2454912.51806	HS0702	B
217	IMA0247.fits	22/03/09	00:27:12	30.0	2454912.51889	HS0702	B
218	IMA0248.fits	22/03/09	00:28:09	30.0	2454912.51955	HS0702	B
219	IMA0249.fits	22/03/09	00:29:06	30.0	2454912.52021	HS0702	B
220	IMA0250.fits	22/03/09	00:30:05	30.0	2454912.52089	HS0702	B
221	IMA0251.fits	22/03/09	00:31:03	30.0	2454912.52156	HS0702	B
222	IMA0252.fits	22/03/09	00:32:01	30.0	2454912.52223	HS0702	B
223	IMA0253.fits	22/03/09	00:33:00	30.0	2454912.52292	HS0702	B
224	IMA0254.fits	22/03/09	00:33:59	30.0	2454912.52360	HS0702	B
225	IMA0255.fits	22/03/09	00:34:57	30.0	2454912.52427	HS0702	B
226	IMA0256.fits	22/03/09	00:36:11	30.0	2454912.52513	HS0702	B
227	IMA0257.fits	22/03/09	00:37:11	30.0	2454912.52582	HS0702	B
228	IMA0258.fits	22/03/09	00:38:09	30.0	2454912.52649	HS0702	B
229	IMA0259.fits	22/03/09	00:39:07	30.0	2454912.52716	HS0702	B
230	IMA0260.fits	22/03/09	00:40:05	30.0	2454912.52784	HS0702	B
231	IMA0261.fits	22/03/09	00:41:04	30.0	2454912.52852	HS0702	B
232	IMA0262.fits	22/03/09	00:42:01	30.0	2454912.52918	HS0702	B
233	IMA0263.fits	22/03/09	00:42:59	30.0	2454912.52985	HS0702	B
234	IMA0264.fits	22/03/09	00:43:57	30.0	2454912.53052	HS0702	B
235	IMA0265.fits	22/03/09	00:45:010	30.0	2454912.53137	HS0702	B
236	IMA0266.fits	22/03/09	00:46:08	30.0	2454912.53204	HS0702	B
237	IMA0267.fits	22/03/09	00:47:06	30.0	2454912.53271	HS0702	B
238	IMA0268.fits	22/03/09	00:48:04	30.0	2454912.53338	HS0702	B
239	IMA0269.fits	22/03/09	00:49:04	30.0	2454912.53407	HS0702	B
240	IMA0270.fits	22/03/09	00:50:03	30.0	2454912.53476	HS0702	B

241	IMA0271.fits	22/03/09	00:51:01	30.0	2454912.53543	HS0702	B
242	IMA0272.fits	22/03/09	00:51:59	30.0	2454912.53610	HS0702	B
243	IMA0273.fits	22/03/09	00:52:58	30.0	2454912.53678	HS0702	B
244	IMA0274.fits	22/03/09	00:54:11	30.0	2454912.53763	HS0702	B
245	IMA0275.fits	22/03/09	00:55:09	30.0	2454912.53830	HS0702	B
246	IMA0276.fits	22/03/09	00:56:08	30.0	2454912.53898	HS0702	B
247	IMA0277.fits	22/03/09	00:57:06	30.0	2454912.53965	HS0702	B
248	IMA0278.fits	22/03/09	00:58:04	30.0	2454912.54032	HS0702	B
249	IMA0279.fits	22/03/09	00:59:03	30.0	2454912.54101	HS0702	B
250	IMA0280.fits	22/03/09	01:00:02	30.0	2454912.54169	HS0702	B
251	IMA0281.fits	22/03/09	01:00:60	30.0	2454912.54236	HS0702	B
252	IMA0282.fits	22/03/09	01:01:58	30.0	2454912.54303	HS0702	B
253	IMA0283.fits	22/03/09	01:03:13	30.0	2454912.54390	HS0702	B
254	IMA0284.fits	22/03/09	01:04:11	30.0	2454912.54457	HS0702	B
255	IMA0285.fits	22/03/09	01:05:010	30.0	2454912.54525	HS0702	B
256	IMA0286.fits	22/03/09	01:06:09	30.0	2454912.54594	HS0702	B
257	IMA0287.fits	22/03/09	01:07:08	30.0	2454912.54662	HS0702	B
258	IMA0288.fits	22/03/09	01:08:06	30.0	2454912.54729	HS0702	B
259	IMA0289.fits	22/03/09	01:09:04	30.0	2454912.54796	HS0702	B
260	IMA0290.fits	22/03/09	01:10:02	30.0	2454912.54863	HS0702	B
261	IMA0291.fits	22/03/09	01:11:01	30.0	2454912.54932	HS0702	B
262	IMA0292.fits	22/03/09	01:12:14	30.0	2454912.55016	HS0702	B
263	IMA0293.fits	22/03/09	01:13:11	30.0	2454912.55082	HS0702	B
264	IMA0294.fits	22/03/09	01:14:09	30.0	2454912.55149	HS0702	B
265	IMA0295.fits	22/03/09	01:15:08	30.0	2454912.55218	HS0702	B
266	IMA0296.fits	22/03/09	01:16:05	30.0	2454912.55284	HS0702	B
267	IMA0297.fits	22/03/09	01:17:03	30.0	2454912.55351	HS0702	B
268	IMA0298.fits	22/03/09	01:18:01	30.0	2454912.55418	HS0702	B
269	IMA0299.fits	22/03/09	01:19:00	30.0	2454912.55486	HS0702	B
270	IMA0300.fits	22/03/09	01:19:59	30.0	2454912.55554	HS0702	B
271	IMA0301.fits	22/03/09	01:25:26	30.0	2454912.55933	HS0702	B
272	IMA0302.fits	22/03/09	01:26:25	30.0	2454912.56001	HS0702	B
273	IMA0303.fits	22/03/09	01:27:23	30.0	2454912.56068	HS0702	B
274	IMA0304.fits	22/03/09	01:28:22	30.0	2454912.56137	HS0702	B
275	IMA0305.fits	22/03/09	01:29:20	30.0	2454912.56204	HS0702	B
276	IMA0306.fits	22/03/09	01:30:19	30.0	2454912.56272	HS0702	B
277	IMA0307.fits	22/03/09	01:31:17	30.0	2454912.56339	HS0702	B
278	IMA0308.fits	22/03/09	01:32:15	30.0	2454912.56406	HS0702	B
279	IMA0309.fits	22/03/09	01:33:12	30.0	2454912.56472	HS0702	B
280	IMA0310.fits	22/03/09	01:34:25	30.0	2454912.56557	HS0702	B
281	IMA0311.fits	22/03/09	01:35:24	30.0	2454912.56625	HS0702	B
282	IMA0312.fits	22/03/09	01:36:23	30.0	2454912.56693	HS0702	B
283	IMA0313.fits	22/03/09	01:37:22	30.0	2454912.56762	HS0702	B
284	IMA0314.fits	22/03/09	01:38:21	30.0	2454912.56830	HS0702	B
285	IMA0315.fits	22/03/09	01:39:19	30.0	2454912.56897	HS0702	B
286	IMA0316.fits	22/03/09	01:40:17	30.0	2454912.56964	HS0702	B
287	IMA0317.fits	22/03/09	01:41:16	30.0	2454912.57032	HS0702	B
288	IMA0318.fits	22/03/09	01:42:15	30.0	2454912.57101	HS0702	B
289	IMA0319.fits	22/03/09	01:43:29	30.0	2454912.57186	HS0702	B
290	IMA0320.fits	22/03/09	01:44:28	30.0	2454912.57255	HS0702	B
291	IMA0321.fits	22/03/09	01:45:26	30.0	2454912.57322	HS0702	B
292	IMA0322.fits	22/03/09	01:46:24	30.0	2454912.57389	HS0702	B
293	IMA0323.fits	22/03/09	01:47:22	30.0	2454912.57456	HS0702	B
294	IMA0324.fits	22/03/09	01:48:20	30.0	2454912.57523	HS0702	B
295	IMA0325.fits	22/03/09	01:49:19	30.0	2454912.57591	HS0702	B
296	IMA0326.fits	22/03/09	01:50:16	30.0	2454912.57657	HS0702	B
297	IMA0327.fits	22/03/09	01:51:14	30.0	2454912.57725	HS0702	B
298	IMA0328.fits	22/03/09	01:52:27	30.0	2454912.57809	HS0702	B
299	IMA0329.fits	22/03/09	01:53:27	30.0	2454912.57878	HS0702	B

300	IMA0330.fits	22/03/09	01:54:25	30.0	2454912.57946	HS0702	B
301	IMA0331.fits	22/03/09	01:55:23	30.0	2454912.58013	HS0702	B
302	IMA0332.fits	22/03/09	01:56:21	30.0	2454912.58080	HS0702	B
303	IMA0333.fits	22/03/09	01:57:20	30.0	2454912.58148	HS0702	B
304	IMA0334.fits	22/03/09	01:58:19	30.0	2454912.58216	HS0702	B
305	IMA0335.fits	22/03/09	01:59:17	30.0	2454912.58284	HS0702	B
306	IMA0336.fits	22/03/09	02:00:16	30.0	2454912.58352	HS0702	B
307	IMA0337.fits	22/03/09	02:01:28	30.0	2454912.58435	HS0702	B
308	IMA0338.fits	22/03/09	02:02:26	30.0	2454912.58502	HS0702	B
309	IMA0339.fits	22/03/09	02:03:25	30.0	2454912.58571	HS0702	B
310	IMA0340.fits	22/03/09	02:04:24	30.0	2454912.58639	HS0702	B
311	IMA0341.fits	22/03/09	02:05:23	30.0	2454912.58707	HS0702	B
312	IMA0342.fits	22/03/09	02:06:21	30.0	2454912.58774	HS0702	B
313	IMA0343.fits	22/03/09	02:07:19	30.0	2454912.58841	HS0702	B
314	IMA0344.fits	22/03/09	02:08:18	30.0	2454912.58910	HS0702	B
315	IMA0345.fits	22/03/09	02:09:16	30.0	2454912.58977	HS0702	B
316	IMA0346.fits	22/03/09	02:10:31	30.0	2454912.59064	HS0702	B
317	IMA0347.fits	22/03/09	02:11:28	30.0	2454912.59130	HS0702	B
318	IMA0348.fits	22/03/09	02:12:27	30.0	2454912.59198	HS0702	B
319	IMA0349.fits	22/03/09	02:13:26	30.0	2454912.59266	HS0702	B
320	IMA0350.fits	22/03/09	02:14:25	30.0	2454912.59334	HS0702	B
321	IMA0351.fits	22/03/09	02:15:23	30.0	2454912.59402	HS0702	B
322	IMA0352.fits	22/03/09	02:16:22	30.0	2454912.59470	HS0702	B
323	IMA0353.fits	22/03/09	02:17:21	30.0	2454912.59538	HS0702	B
324	IMA0354.fits	22/03/09	02:18:19	30.0	2454912.59605	HS0702	B
325	IMA0355.fits	22/03/09	02:19:32	30.0	2454912.59690	HS0702	B
326	IMA0356.fits	22/03/09	02:20:30	30.0	2454912.59757	HS0702	B
327	IMA0357.fits	22/03/09	02:21:27	30.0	2454912.59823	HS0702	B
328	IMA0358.fits	22/03/09	02:22:25	30.0	2454912.59890	HS0702	B
329	IMA0359.fits	22/03/09	02:23:23	30.0	2454912.59957	HS0702	B
330	IMA0360.fits	22/03/09	02:24:22	30.0	2454912.60025	HS0702	B
331	IMA0361.fits	22/03/09	02:25:20	30.0	2454912.60093	HS0702	B
332	IMA0362.fits	22/03/09	02:26:19	30.0	2454912.60161	HS0702	B
333	IMA0363.fits	22/03/09	02:27:17	30.0	2454912.60228	HS0702	B
334	IMA0364.fits	22/03/09	02:28:30	30.0	2454912.60312	HS0702	B
335	IMA0365.fits	22/03/09	02:29:29	30.0	2454912.60381	HS0702	B
336	IMA0366.fits	22/03/09	02:30:27	30.0	2454912.60448	HS0702	B
337	IMA0367.fits	22/03/09	02:31:26	30.0	2454912.60516	HS0702	B
338	IMA0368.fits	22/03/09	02:32:24	30.0	2454912.60583	HS0702	B
339	IMA0369.fits	22/03/09	02:33:21	30.0	2454912.60649	HS0702	B
340	IMA0370.fits	22/03/09	02:34:19	30.0	2454912.60716	HS0702	B
341	IMA0371.fits	22/03/09	02:35:18	30.0	2454912.60785	HS0702	B
342	IMA0372.fits	22/03/09	02:36:16	30.0	2454912.60852	HS0702	B
343	IMA0373.fits	22/03/09	02:37:29	30.0	2454912.60936	HS0702	B
344	IMA0374.fits	22/03/09	02:38:27	30.0	2454912.61003	HS0702	B
345	IMA0375.fits	22/03/09	02:39:26	30.0	2454912.61072	HS0702	B
346	IMA0376.fits	22/03/09	02:40:24	30.0	2454912.61139	HS0702	B
347	IMA0377.fits	22/03/09	02:41:22	30.0	2454912.61206	HS0702	B
348	IMA0378.fits	22/03/09	02:42:21	30.0	2454912.61274	HS0702	B
349	IMA0379.fits	22/03/09	02:43:21	30.0	2454912.61344	HS0702	B
350	IMA0380.fits	22/03/09	02:44:19	30.0	2454912.61411	HS0702	B
351	IMA0381.fits	22/03/09	02:45:37	30.0	2454912.61501	HS0702	B

#	Image	Date	Start	Texp	JD	Object	Filter
1	IMA0407.fits	22/03/09	21:25:37	30.0	2454913.39279	HS0702	B
2	IMA0408.fits	22/03/09	21:26:35	30.0	2454913.39346	HS0702	B
3	IMA0409.fits	22/03/09	21:27:32	30.0	2454913.39412	HS0702	B
4	IMA0410.fits	22/03/09	21:28:30	30.0	2454913.39479	HS0702	B
5	IMA0411.fits	22/03/09	21:29:29	30.0	2454913.39547	HS0702	B

6	IMA0412.fits	22/03/09	21:30:27	30.0	2454913.39615	HS0702	B
7	IMA0413.fits	22/03/09	21:31:25	30.0	2454913.39682	HS0702	B
8	IMA0414.fits	22/03/09	21:32:22	30.0	2454913.39748	HS0702	B
9	IMA0415.fits	22/03/09	21:33:36	30.0	2454913.39833	HS0702	B
10	IMA0416.fits	22/03/09	21:34:33	30.0	2454913.39899	HS0702	B
11	IMA0417.fits	22/03/09	21:35:31	30.0	2454913.39966	HS0702	B
12	IMA0418.fits	22/03/09	21:36:29	30.0	2454913.40034	HS0702	B
13	IMA0419.fits	22/03/09	21:37:27	30.0	2454913.40101	HS0702	B
14	IMA0420.fits	22/03/09	21:38:23	30.0	2454913.40166	HS0702	B
15	IMA0421.fits	22/03/09	21:39:21	30.0	2454913.40233	HS0702	B
16	IMA0422.fits	22/03/09	21:40:21	30.0	2454913.40302	HS0702	B
17	IMA0423.fits	22/03/09	21:41:18	30.0	2454913.40368	HS0702	B
18	IMA0424.fits	22/03/09	21:42:31	30.0	2454913.40453	HS0702	B
19	IMA0425.fits	22/03/09	21:43:28	30.0	2454913.40519	HS0702	B
20	IMA0426.fits	22/03/09	21:44:26	30.0	2454913.40586	HS0702	B
21	IMA0427.fits	22/03/09	21:45:24	30.0	2454913.40653	HS0702	B
22	IMA0428.fits	22/03/09	21:46:22	30.0	2454913.40720	HS0702	B
23	IMA0429.fits	22/03/09	21:47:20	30.0	2454913.40787	HS0702	B
24	IMA0430.fits	22/03/09	21:48:17	30.0	2454913.40853	HS0702	B
25	IMA0431.fits	22/03/09	21:49:16	30.0	2454913.40921	HS0702	B
26	IMA0432.fits	22/03/09	21:50:14	30.0	2454913.40988	HS0702	B
27	IMA0433.fits	22/03/09	21:51:27	30.0	2454913.41073	HS0702	B
28	IMA0434.fits	22/03/09	21:52:25	30.0	2454913.41140	HS0702	B
29	IMA0435.fits	22/03/09	21:53:23	30.0	2454913.41207	HS0702	B
30	IMA0436.fits	22/03/09	21:54:21	30.0	2454913.41274	HS0702	B
31	IMA0437.fits	22/03/09	21:55:19	30.0	2454913.41341	HS0702	B
32	IMA0438.fits	22/03/09	21:56:18	30.0	2454913.41410	HS0702	B
33	IMA0439.fits	22/03/09	21:57:16	30.0	2454913.41477	HS0702	B
34	IMA0440.fits	22/03/09	21:58:14	30.0	2454913.41544	HS0702	B
35	IMA0441.fits	22/03/09	21:59:11	30.0	2454913.41610	HS0702	B
36	IMA0442.fits	22/03/09	22:00:25	30.0	2454913.41696	HS0702	B
37	IMA0443.fits	22/03/09	22:01:22	30.0	2454913.41762	HS0702	B
38	IMA0444.fits	22/03/09	22:02:19	30.0	2454913.41828	HS0702	B
39	IMA0445.fits	22/03/09	22:03:17	30.0	2454913.41895	HS0702	B
40	IMA0446.fits	22/03/09	22:04:15	30.0	2454913.41962	HS0702	B
41	IMA0447.fits	22/03/09	22:05:13	30.0	2454913.42029	HS0702	B
42	IMA0448.fits	22/03/09	22:06:11	30.0	2454913.42096	HS0702	B
43	IMA0449.fits	22/03/09	22:07:08	30.0	2454913.42162	HS0702	B
44	IMA0450.fits	22/03/09	22:08:07	30.0	2454913.42230	HS0702	B
45	IMA0451.fits	22/03/09	22:09:20	30.0	2454913.42315	HS0702	B
46	IMA0452.fits	22/03/09	22:10:18	30.0	2454913.42382	HS0702	B
47	IMA0453.fits	22/03/09	22:11:16	30.0	2454913.42449	HS0702	B
48	IMA0454.fits	22/03/09	22:12:15	30.0	2454913.42517	HS0702	B
49	IMA0455.fits	22/03/09	22:13:13	30.0	2454913.42584	HS0702	B
50	IMA0456.fits	22/03/09	22:14:11	30.0	2454913.42652	HS0702	B
51	IMA0457.fits	22/03/09	22:15:08	30.0	2454913.42718	HS0702	B
52	IMA0458.fits	22/03/09	22:16:07	30.0	2454913.42786	HS0702	B
53	IMA0459.fits	22/03/09	22:17:05	30.0	2454913.42853	HS0702	B
54	IMA0460.fits	22/03/09	22:18:18	30.0	2454913.42938	HS0702	B
55	IMA0461.fits	22/03/09	22:19:15	30.0	2454913.43003	HS0702	B
56	IMA0462.fits	22/03/09	22:20:14	30.0	2454913.43072	HS0702	B
57	IMA0463.fits	22/03/09	22:21:12	30.0	2454913.43139	HS0702	B
58	IMA0464.fits	22/03/09	22:22:010	30.0	2454913.43206	HS0702	B
59	IMA0465.fits	22/03/09	22:23:08	30.0	2454913.43273	HS0702	B
60	IMA0466.fits	22/03/09	22:24:06	30.0	2454913.43340	HS0702	B
61	IMA0467.fits	22/03/09	22:25:04	30.0	2454913.43407	HS0702	B
62	IMA0468.fits	22/03/09	22:26:02	30.0	2454913.43475	HS0702	B
63	IMA0469.fits	22/03/09	22:27:15	30.0	2454913.43559	HS0702	B
64	IMA0470.fits	22/03/09	22:28:13	30.0	2454913.43626	HS0702	B

65	IMA0471.fits	22/03/09	22:29:11	30.0	2454913.43693	HS0702	B
66	IMA0472.fits	22/03/09	22:30:09	30.0	2454913.43760	HS0702	B
67	IMA0473.fits	22/03/09	22:31:06	30.0	2454913.43826	HS0702	B
68	IMA0474.fits	22/03/09	22:32:05	30.0	2454913.43895	HS0702	B
69	IMA0475.fits	22/03/09	22:33:03	30.0	2454913.43962	HS0702	B
70	IMA0476.fits	22/03/09	22:34:01	30.0	2454913.44029	HS0702	B
71	IMA0477.fits	22/03/09	22:34:59	30.0	2454913.44096	HS0702	B
72	IMA0478.fits	22/03/09	22:36:12	30.0	2454913.44181	HS0702	B
73	IMA0479.fits	22/03/09	22:37:09	30.0	2454913.44247	HS0702	B
74	IMA0480.fits	22/03/09	22:38:07	30.0	2454913.44314	HS0702	B
75	IMA0481.fits	22/03/09	22:39:06	30.0	2454913.44382	HS0702	B
76	IMA0482.fits	22/03/09	22:40:04	30.0	2454913.44449	HS0702	B
77	IMA0483.fits	22/03/09	22:41:02	30.0	2454913.44516	HS0702	B
78	IMA0484.fits	22/03/09	22:42:00	30.0	2454913.44583	HS0702	B
79	IMA0485.fits	22/03/09	22:42:58	30.0	2454913.44650	HS0702	B
80	IMA0486.fits	22/03/09	22:43:56	30.0	2454913.44718	HS0702	B
81	IMA0487.fits	22/03/09	22:45:09	30.0	2454913.44802	HS0702	B
82	IMA0488.fits	22/03/09	22:46:06	30.0	2454913.44868	HS0702	B
83	IMA0489.fits	22/03/09	22:47:05	30.0	2454913.44936	HS0702	B
84	IMA0490.fits	22/03/09	22:48:02	30.0	2454913.45002	HS0702	B
85	IMA0491.fits	22/03/09	22:49:00	30.0	2454913.45069	HS0702	B
86	IMA0492.fits	22/03/09	22:49:58	30.0	2454913.45137	HS0702	B
87	IMA0493.fits	22/03/09	22:50:56	30.0	2454913.45204	HS0702	B
88	IMA0494.fits	22/03/09	22:51:55	30.0	2454913.45272	HS0702	B
89	IMA0495.fits	22/03/09	22:52:52	30.0	2454913.45338	HS0702	B
90	IMA0496.fits	22/03/09	22:57:26	30.0	2454913.45655	HS0702	B
91	IMA0497.fits	22/03/09	22:58:23	30.0	2454913.45721	HS0702	B
92	IMA0498.fits	22/03/09	22:59:20	30.0	2454913.45787	HS0702	B
93	IMA0499.fits	22/03/09	23:00:19	30.0	2454913.45855	HS0702	B
94	IMA0500.fits	22/03/09	23:01:17	30.0	2454913.45922	HS0702	B
95	IMA0501.fits	22/03/09	23:02:15	30.0	2454913.45990	HS0702	B
96	IMA0502.fits	22/03/09	23:03:11	30.0	2454913.46054	HS0702	B
97	IMA0503.fits	22/03/09	23:04:09	30.0	2454913.46122	HS0702	B
98	IMA0504.fits	22/03/09	23:05:07	30.0	2454913.46189	HS0702	B
99	IMA0505.fits	22/03/09	23:06:20	30.0	2454913.46273	HS0702	B
100	IMA0506.fits	22/03/09	23:07:18	30.0	2454913.46340	HS0702	B
101	IMA0507.fits	22/03/09	23:08:16	30.0	2454913.46407	HS0702	B
102	IMA0508.fits	22/03/09	23:09:14	30.0	2454913.46475	HS0702	B
103	IMA0509.fits	22/03/09	23:10:12	30.0	2454913.46542	HS0702	B
104	IMA0510.fits	22/03/09	23:11:11	30.0	2454913.46610	HS0702	B
105	IMA0511.fits	22/03/09	23:12:09	30.0	2454913.46677	HS0702	B
106	IMA0512.fits	22/03/09	23:13:06	30.0	2454913.46743	HS0702	B
107	IMA0513.fits	22/03/09	23:14:04	30.0	2454913.46810	HS0702	B
108	IMA0514.fits	22/03/09	23:15:17	30.0	2454913.46895	HS0702	B
109	IMA0515.fits	22/03/09	23:16:14	30.0	2454913.46961	HS0702	B
110	IMA0516.fits	22/03/09	23:17:12	30.0	2454913.47028	HS0702	B
111	IMA0517.fits	22/03/09	23:18:10	30.0	2454913.47095	HS0702	B
112	IMA0518.fits	22/03/09	23:19:09	30.0	2454913.47163	HS0702	B
113	IMA0519.fits	22/03/09	23:20:06	30.0	2454913.47229	HS0702	B
114	IMA0520.fits	22/03/09	23:21:04	30.0	2454913.47296	HS0702	B
115	IMA0521.fits	22/03/09	23:22:03	30.0	2454913.47365	HS0702	B
116	IMA0522.fits	22/03/09	23:23:01	30.0	2454913.47432	HS0702	B
117	IMA0523.fits	22/03/09	23:24:15	30.0	2454913.47517	HS0702	B
118	IMA0524.fits	22/03/09	23:25:13	30.0	2454913.47584	HS0702	B
119	IMA0525.fits	22/03/09	23:26:12	30.0	2454913.47653	HS0702	B
120	IMA0526.fits	22/03/09	23:27:10	30.0	2454913.47720	HS0702	B
121	IMA0527.fits	22/03/09	23:28:08	30.0	2454913.47787	HS0702	B
122	IMA0528.fits	22/03/09	23:29:05	30.0	2454913.47853	HS0702	B
123	IMA0529.fits	22/03/09	23:30:04	30.0	2454913.47921	HS0702	B

124	IMA0530.fits	22/03/09	23:31:02	30.0	2454913.47988	HS0702	B
125	IMA0531.fits	22/03/09	23:31:60	30.0	2454913.48056	HS0702	B
126	IMA0532.fits	22/03/09	23:33:12	30.0	2454913.48139	HS0702	B
127	IMA0533.fits	22/03/09	23:34:11	30.0	2454913.48207	HS0702	B
128	IMA0534.fits	22/03/09	23:35:09	30.0	2454913.48274	HS0702	B
129	IMA0535.fits	22/03/09	23:36:07	30.0	2454913.48341	HS0702	B
130	IMA0536.fits	22/03/09	23:37:04	30.0	2454913.48407	HS0702	B
131	IMA0537.fits	22/03/09	23:38:03	30.0	2454913.48476	HS0702	B
132	IMA0538.fits	22/03/09	23:39:01	30.0	2454913.48543	HS0702	B
133	IMA0539.fits	22/03/09	23:39:59	30.0	2454913.48610	HS0702	B
134	IMA0540.fits	22/03/09	23:40:57	30.0	2454913.48677	HS0702	B
135	IMA0541.fits	22/03/09	23:42:10	30.0	2454913.48762	HS0702	B
136	IMA0542.fits	22/03/09	23:43:07	30.0	2454913.48828	HS0702	B
137	IMA0543.fits	22/03/09	23:44:05	30.0	2454913.48895	HS0702	B
138	IMA0544.fits	22/03/09	23:45:04	30.0	2454913.48963	HS0702	B
139	IMA0545.fits	22/03/09	23:46:02	30.0	2454913.49030	HS0702	B
140	IMA0546.fits	22/03/09	23:46:60	30.0	2454913.49097	HS0702	B
141	IMA0547.fits	22/03/09	23:47:58	30.0	2454913.49164	HS0702	B
142	IMA0548.fits	22/03/09	23:48:56	30.0	2454913.49231	HS0702	B
143	IMA0549.fits	22/03/09	23:49:54	30.0	2454913.49299	HS0702	B
144	IMA0550.fits	22/03/09	23:51:07	30.0	2454913.49383	HS0702	B
145	IMA0551.fits	22/03/09	23:52:04	30.0	2454913.49449	HS0702	B
146	IMA0552.fits	22/03/09	23:53:02	30.0	2454913.49516	HS0702	B
147	IMA0553.fits	22/03/09	23:53:59	30.0	2454913.49582	HS0702	B
148	IMA0554.fits	22/03/09	23:54:57	30.0	2454913.49649	HS0702	B
149	IMA0555.fits	22/03/09	23:55:54	30.0	2454913.49715	HS0702	B
150	IMA0556.fits	22/03/09	23:56:53	30.0	2454913.49784	HS0702	B
151	IMA0557.fits	22/03/09	23:57:51	30.0	2454913.49851	HS0702	B
152	IMA0558.fits	22/03/09	23:58:49	30.0	2454913.49918	HS0702	B
153	IMA0559.fits	23/03/09	00:00:03	30.0	2454913.50003	HS0702	B
154	IMA0560.fits	23/03/09	00:01:02	30.0	2454913.50072	HS0702	B
155	IMA0561.fits	23/03/09	00:02:00	30.0	2454913.50139	HS0702	B
156	IMA0562.fits	23/03/09	00:02:58	30.0	2454913.50206	HS0702	B
157	IMA0563.fits	23/03/09	00:03:56	30.0	2454913.50273	HS0702	B
158	IMA0564.fits	23/03/09	00:04:55	30.0	2454913.50341	HS0702	B
159	IMA0565.fits	23/03/09	00:05:53	30.0	2454913.50409	HS0702	B
160	IMA0566.fits	23/03/09	00:06:51	30.0	2454913.50476	HS0702	B
161	IMA0567.fits	23/03/09	00:07:49	30.0	2454913.50543	HS0702	B
162	IMA0568.fits	23/03/09	00:09:02	30.0	2454913.50627	HS0702	B
163	IMA0569.fits	23/03/09	00:09:59	30.0	2454913.50693	HS0702	B
164	IMA0570.fits	23/03/09	00:10:56	30.0	2454913.50759	HS0702	B
165	IMA0571.fits	23/03/09	00:11:54	30.0	2454913.50826	HS0702	B
166	IMA0572.fits	23/03/09	00:12:53	30.0	2454913.50895	HS0702	B
167	IMA0573.fits	23/03/09	00:13:50	30.0	2454913.50961	HS0702	B
168	IMA0574.fits	23/03/09	00:14:48	30.0	2454913.51028	HS0702	B
169	IMA0575.fits	23/03/09	00:15:45	30.0	2454913.51094	HS0702	B
170	IMA0576.fits	23/03/09	00:16:44	30.0	2454913.51162	HS0702	B
171	IMA0577.fits	23/03/09	00:17:56	30.0	2454913.51245	HS0702	B
172	IMA0578.fits	23/03/09	00:18:54	30.0	2454913.51313	HS0702	B
173	IMA0579.fits	23/03/09	00:19:52	30.0	2454913.51380	HS0702	B
174	IMA0580.fits	23/03/09	00:20:51	30.0	2454913.51448	HS0702	B
175	IMA0581.fits	23/03/09	00:21:49	30.0	2454913.51515	HS0702	B
176	IMA0582.fits	23/03/09	00:22:45	30.0	2454913.51580	HS0702	B
177	IMA0583.fits	23/03/09	00:23:43	30.0	2454913.51647	HS0702	B
178	IMA0584.fits	23/03/09	00:24:41	30.0	2454913.51714	HS0702	B
179	IMA0585.fits	23/03/09	00:25:37	30.0	2454913.51779	HS0702	B
180	IMA0586.fits	23/03/09	00:33:07	30.0	2454913.52300	HS0702	B
181	IMA0587.fits	23/03/09	00:34:05	30.0	2454913.52367	HS0702	B
182	IMA0588.fits	23/03/09	00:35:04	30.0	2454913.52435	HS0702	B

183	IMA0589.fits	23/03/09	00:36:02	30.0	2454913.52502	HS0702	B
184	IMA0590.fits	23/03/09	00:37:00	30.0	2454913.52569	HS0702	B
185	IMA0591.fits	23/03/09	00:37:58	30.0	2454913.52637	HS0702	B
186	IMA0592.fits	23/03/09	00:38:56	30.0	2454913.52704	HS0702	B
187	IMA0593.fits	23/03/09	00:39:54	30.0	2454913.52771	HS0702	B
188	IMA0594.fits	23/03/09	00:40:52	30.0	2454913.52838	HS0702	B
189	IMA0595.fits	23/03/09	00:42:06	30.0	2454913.52924	HS0702	B
190	IMA0596.fits	23/03/09	00:43:04	30.0	2454913.52991	HS0702	B
191	IMA0597.fits	23/03/09	00:44:02	30.0	2454913.53058	HS0702	B
192	IMA0598.fits	23/03/09	00:45:00	30.0	2454913.53125	HS0702	B
193	IMA0599.fits	23/03/09	00:45:58	30.0	2454913.53192	HS0702	B
194	IMA0600.fits	23/03/09	00:46:56	30.0	2454913.53259	HS0702	B
195	IMA0601.fits	23/03/09	00:47:54	30.0	2454913.53326	HS0702	B
196	IMA0602.fits	23/03/09	00:48:52	30.0	2454913.53394	HS0702	B
197	IMA0603.fits	23/03/09	00:49:50	30.0	2454913.53461	HS0702	B
198	IMA0604.fits	23/03/09	00:51:04	30.0	2454913.53546	HS0702	B
199	IMA0605.fits	23/03/09	00:52:00	30.0	2454913.53611	HS0702	B
200	IMA0606.fits	23/03/09	00:52:58	30.0	2454913.53678	HS0702	B
201	IMA0607.fits	23/03/09	00:53:56	30.0	2454913.53745	HS0702	B
202	IMA0608.fits	23/03/09	00:54:55	30.0	2454913.53814	HS0702	B
203	IMA0609.fits	23/03/09	00:55:51	30.0	2454913.53878	HS0702	B
204	IMA0610.fits	23/03/09	00:56:48	30.0	2454913.53944	HS0702	B
205	IMA0611.fits	23/03/09	00:57:46	30.0	2454913.54012	HS0702	B
206	IMA0612.fits	23/03/09	00:58:44	30.0	2454913.54079	HS0702	B
207	IMA0613.fits	23/03/09	00:59:56	30.0	2454913.54162	HS0702	B
208	IMA0614.fits	23/03/09	01:00:54	30.0	2454913.54229	HS0702	B
209	IMA0615.fits	23/03/09	01:01:53	30.0	2454913.54297	HS0702	B
210	IMA0616.fits	23/03/09	01:02:51	30.0	2454913.54365	HS0702	B
211	IMA0617.fits	23/03/09	01:03:49	30.0	2454913.54432	HS0702	B
212	IMA0618.fits	23/03/09	01:04:46	30.0	2454913.54498	HS0702	B
213	IMA0619.fits	23/03/09	01:05:45	30.0	2454913.54566	HS0702	B
214	IMA0620.fits	23/03/09	01:06:43	30.0	2454913.54633	HS0702	B
215	IMA0621.fits	23/03/09	01:07:41	30.0	2454913.54700	HS0702	B
216	IMA0622.fits	23/03/09	01:08:54	30.0	2454913.54785	HS0702	B
217	IMA0623.fits	23/03/09	01:09:52	30.0	2454913.54852	HS0702	B
218	IMA0624.fits	23/03/09	01:10:50	30.0	2454913.54919	HS0702	B
219	IMA0625.fits	23/03/09	01:11:47	30.0	2454913.54985	HS0702	B
220	IMA0626.fits	23/03/09	01:12:45	30.0	2454913.55052	HS0702	B
221	IMA0627.fits	23/03/09	01:13:44	30.0	2454913.55120	HS0702	B
222	IMA0628.fits	23/03/09	01:14:42	30.0	2454913.55188	HS0702	B
223	IMA0629.fits	23/03/09	01:15:40	30.0	2454913.55255	HS0702	B
224	IMA0630.fits	23/03/09	01:16:37	30.0	2454913.55321	HS0702	B
225	IMA0631.fits	23/03/09	01:17:51	30.0	2454913.55406	HS0702	B
226	IMA0632.fits	23/03/09	01:18:48	30.0	2454913.55472	HS0702	B
227	IMA0633.fits	23/03/09	01:19:46	30.0	2454913.55539	HS0702	B
228	IMA0634.fits	23/03/09	01:20:44	30.0	2454913.55606	HS0702	B
229	IMA0635.fits	23/03/09	01:21:43	30.0	2454913.55675	HS0702	B
230	IMA0636.fits	23/03/09	01:22:41	30.0	2454913.55742	HS0702	B
231	IMA0637.fits	23/03/09	01:23:39	30.0	2454913.55809	HS0702	B
232	IMA0638.fits	23/03/09	01:24:36	30.0	2454913.55875	HS0702	B
233	IMA0639.fits	23/03/09	01:25:35	30.0	2454913.55943	HS0702	B
234	IMA0640.fits	23/03/09	01:26:49	30.0	2454913.56029	HS0702	B
235	IMA0641.fits	23/03/09	01:27:47	30.0	2454913.56096	HS0702	B
236	IMA0642.fits	23/03/09	01:28:46	30.0	2454913.56164	HS0702	B
237	IMA0643.fits	23/03/09	01:29:44	30.0	2454913.56231	HS0702	B
238	IMA0644.fits	23/03/09	01:30:42	30.0	2454913.56299	HS0702	B
239	IMA0645.fits	23/03/09	01:31:40	30.0	2454913.56366	HS0702	B
240	IMA0646.fits	23/03/09	01:32:37	30.0	2454913.56432	HS0702	B
241	IMA0647.fits	23/03/09	01:33:36	30.0	2454913.56500	HS0702	B

242	IMA0648.fits	23/03/09	01:34:33	30.0	2454913.56566	HS0702	B
243	IMA0649.fits	23/03/09	01:35:46	30.0	2454913.56650	HS0702	B
244	IMA0650.fits	23/03/09	01:36:45	30.0	2454913.56719	HS0702	B
245	IMA0651.fits	23/03/09	01:37:43	30.0	2454913.56786	HS0702	B
246	IMA0652.fits	23/03/09	01:38:41	30.0	2454913.56853	HS0702	B
247	IMA0653.fits	23/03/09	01:39:39	30.0	2454913.56920	HS0702	B
248	IMA0654.fits	23/03/09	01:40:37	30.0	2454913.56987	HS0702	B
249	IMA0655.fits	23/03/09	01:41:35	30.0	2454913.57054	HS0702	B
250	IMA0656.fits	23/03/09	01:42:33	30.0	2454913.57122	HS0702	B
251	IMA0657.fits	23/03/09	01:43:31	30.0	2454913.57189	HS0702	B
252	IMA0658.fits	23/03/09	01:44:45	30.0	2454913.57274	HS0702	B
253	IMA0659.fits	23/03/09	01:45:42	30.0	2454913.57340	HS0702	B
254	IMA0660.fits	23/03/09	01:46:41	30.0	2454913.57409	HS0702	B
255	IMA0661.fits	23/03/09	01:47:39	30.0	2454913.57476	HS0702	B
256	IMA0662.fits	23/03/09	01:48:39	30.0	2454913.57545	HS0702	B
257	IMA0663.fits	23/03/09	01:49:37	30.0	2454913.57612	HS0702	B
258	IMA0664.fits	23/03/09	01:50:35	30.0	2454913.57679	HS0702	B
259	IMA0665.fits	23/03/09	01:51:33	30.0	2454913.57747	HS0702	B
260	IMA0666.fits	23/03/09	01:52:32	30.0	2454913.57815	HS0702	B
261	IMA0667.fits	23/03/09	01:53:44	30.0	2454913.57898	HS0702	B
262	IMA0668.fits	23/03/09	01:54:42	30.0	2454913.57965	HS0702	B
263	IMA0669.fits	23/03/09	01:55:40	30.0	2454913.58032	HS0702	B
264	IMA0670.fits	23/03/09	01:56:39	30.0	2454913.58101	HS0702	B
265	IMA0671.fits	23/03/09	01:57:37	30.0	2454913.58168	HS0702	B
266	IMA0672.fits	23/03/09	01:58:35	30.0	2454913.58235	HS0702	B
267	IMA0673.fits	23/03/09	01:59:33	30.0	2454913.58302	HS0702	B
268	IMA0674.fits	23/03/09	02:00:32	30.0	2454913.58370	HS0702	B
269	IMA0675.fits	23/03/09	02:01:31	30.0	2454913.58439	HS0702	B
270	IMA0676.fits	23/03/09	02:03:25	30.0	2454913.58571	HS0702	B
271	IMA0677.fits	23/03/09	02:04:24	30.0	2454913.58639	HS0702	B
272	IMA0678.fits	23/03/09	02:05:22	30.0	2454913.58706	HS0702	B
273	IMA0679.fits	23/03/09	02:06:21	30.0	2454913.58774	HS0702	B
274	IMA0680.fits	23/03/09	02:07:20	30.0	2454913.58843	HS0702	B
275	IMA0681.fits	23/03/09	02:08:18	30.0	2454913.58910	HS0702	B
276	IMA0682.fits	23/03/09	02:09:16	30.0	2454913.58977	HS0702	B
277	IMA0683.fits	23/03/09	02:10:15	30.0	2454913.59045	HS0702	B
278	IMA0684.fits	23/03/09	02:11:14	30.0	2454913.59113	HS0702	B
279	IMA0685.fits	23/03/09	02:12:27	30.0	2454913.59198	HS0702	B
280	IMA0686.fits	23/03/09	02:13:26	30.0	2454913.59266	HS0702	B
281	IMA0687.fits	23/03/09	02:14:24	30.0	2454913.59333	HS0702	B
282	IMA0688.fits	23/03/09	02:15:23	30.0	2454913.59402	HS0702	B
283	IMA0689.fits	23/03/09	02:16:21	30.0	2454913.59469	HS0702	B
284	IMA0690.fits	23/03/09	02:17:19	30.0	2454913.59536	HS0702	B
285	IMA0691.fits	23/03/09	02:18:18	30.0	2454913.59604	HS0702	B
286	IMA0692.fits	23/03/09	02:19:17	30.0	2454913.59672	HS0702	B
287	IMA0693.fits	23/03/09	02:20:15	30.0	2454913.59740	HS0702	B

Bibliography

[1] C. Aerts. Asteroseismology. Catholic University of Leuven, Belgium, 2004.

[2] C. Aerts, J. Christensen-Dalsgaard, and D. W. Kurtz. *Asteroseismology*. 2010.

[3] S. Aigrain, F. Favata, and G. Gilmore. Characterising stellar micro-variability for planetary transit searches. *A&A*, 414:1139–1152, February 2004.

[4] M. Aizenman, P. Smeyers, and A. Weigert. Avoided Crossing of Modes of Non-radial Stellar Oscillations. *A&A*, 58:41–+, June 1977.

[5] C. Allende Prieto and D. L. Lambert. Fundamental parameters of stars (Allende Prieto+, 1999). *VizieR Online Data Catalog*, 335:20555–+, October 1999.

[6] R. Alonso, M. Auvergne, A. Baglin, M. Ollivier, C. Moutou, D. Rouan, H. J. Deeg, S. Aigrain, J. M. Almenara, M. Barbieri, P. Barge, W. Benz, P. Bordé, F. Bouchy, R. de La Reza, M. Deleuil, R. Dvorak, A. Erikson, M. Fridlund, M. Gillon, P. Gondoin, T. Guillot, A. Hatzes, G. Hébrard, P. Kabath, L. Jorda, H. Lammer, A. Léger, A. Llebaria, B. Loeillet, P. Magain, M. Mayor, T. Mazeh, M. Pätzold, F. Pepe, F. Pont, D. Queloz, H. Rauer, A. Shporer, J. Schneider, B. Stecklum, S. Udry, and G. Wuchterl. Transiting exoplanets from the CoRoT space mission. II. CoRoT-Exo-2b: a transiting planet around an active G star. *A&A*, 482:L21–L24, May 2008.

[7] T. Arentoft, H. Kjeldsen, T. R. Bedding, M. Bazot, J. Christensen-Dalsgaard, T. H. Dall, C. Karoff, F. Carrier, P. Eggenberger, D. Sosnowska, R. A. Wittenmyer, M. Endl, T. S. Metcalfe, S. Hekker, S. Reffert, R. P. Butler, H. Bruntt, L. L. Kiss, S. J. O'Toole, E. Kambe, H. Ando, H. Izumiura, B. Sato, M. Hartmann, A. Hatzes, F. Bouchy, B. Mosser, T. Appourchaux, C. Barban, G. Berthomieu, R. A. Garcia, E. Michel, J. Provost, S. Turck-Chièze, M. Martić, J.-C. Lebrun, J. Schmitt, J.-L. Bertaux, A. Bonanno, S. Benatti, R. U. Claudi, R. Cosentino, S. Leccia, S. Frandsen, K. Brogaard, L. Glowienka, F. Grundahl, and E. Stempels. A Multisite Campaign to Measure Solar-like Oscillations in Procyon. I. Observations, Data Reduction, and Slow Variations. *ApJ*, 687:1180–1190, November 2008.

[8] A. Baglin, G. Vauclair, and The COROT Team. The Space Stellar Photometry Mission COROT: Asteroseismology and Search for Extrasolar Planets. *Journal of Astrophysics and Astronomy*, 21:319–+, June 2000.

[9] L. A. Balona, K. Krisciunas, and A. W. J. Cousins. Gamma-Doradus - Evidence for a New Class of Pulsating Star. *MNRAS*, 270:905–+, October 1994.

[10] C. Barban, J. M. Matthews, J. De Ridder, F. Baudin, R. Kuschnig, A. Mazumdar, R. Samadi, D. B. Guenther, A. F. J. Moffat, S. M. Rucinski, D. Sasselov, G. A. H. Walker, and W. W. Weiss. Detection of solar-like oscillations in the red giant star ϵ Ophiuchi by MOST spacebased photometry. *A&A*, 468:1033–1038, June 2007.

[11] C. Barbieri, G. Romano, S. di Serego, and M. Zambon. Survey of the optical variability of compact extragalactic objects. I - The field of 3 C 345. *A&A*, 59:419–426, August 1977.

[12] P. Barge, A. Baglin, M. Auvergne, H. Rauer, A. Léger, J. Schneider, F. Pont, S. Aigrain, J.-M. Almenara, R. Alonso, M. Barbieri, P. Bordé, F. Bouchy, H. J. Deeg, D. La Reza, M. Deleuil, R. Dvorak, A. Erikson, M. Fridlund, M. Gillon, P. Gondoin, T. Guillot, A. Hatzes, G. Hebrard, L. Jorda, P. Kabath, H. Lammer, A. Llebaria, B. Loeillet, P. Magain, T. Mazeh, C. Moutou, M. Ollivier, M. Pätzold, D. Queloz, D. Rouan, A. Shporer, and G. Wuchterl. Transiting exoplanets from the CoRoT space mission. I. CoRoT-Exo-1b: a low-density short-period planet around a G0V star. *A&A*, 482:L17–L20, May 2008.

[13] S. Basu and J. Christensen-Dalsgaard. Equation of state and helioseismic inversions. *ApJ*, 322:L5–L8, June 1997.

[14] G. K. Batchelor. *The Theory of Homogeneous Turbulence*. The Theory of Homogeneous Turbulence, Cambridge: Cambridge University Press, 1953, 1953.

[15] M. Bazot, F. Bouchy, H. Kjeldsen, S. Charpinet, M. Laymand, and S. Vauclair. Asteroseismology of α Centauri A. Evidence of rotational splitting. *A&A*, 470:295–302, July 2007.

[16] M. Bazot, S. Vauclair, F. Bouchy, and N. C. Santos. Seismic analysis of the planet-hosting star μ Arae. *ApJ*, 440:615–621, September 2005.

[17] T. R. Bedding, D. Huber, D. Stello, Y. P. Elsworth, S. Hekker, T. Kallinger, S. Mathur, B. Mosser, H. L. Preston, J. Ballot, C. Barban, A. M. Broomhall, D. L. Buzasi, W. J. Chaplin, R. A. García, M. Gruberbauer, S. J. Hale, J. De Ridder, S. Frandsen, W. J. Borucki, T. Brown, J. Christensen-Dalsgaard, R. L. Gilliland, J. M. Jenkins, H. Kjeldsen, D. Koch, K. Belkacem, L. Bildsten, H. Bruntt, T. L. Campante, S. Deheuvels, A. Derekas, M.-A. Dupret, M.-J. Goupil, A. Hatzes, G. Houdek, M. J. Ireland, C. Jiang, C. Karoff, L. L. Kiss, Y. Lebreton, A. Miglio, J. Montalbán, A. Noels, I. W. Roxburgh, V. Sangaralingam, I. R. Stevens, M. D. Suran, N. J. Tarrant, and A. Weiss. Solar-like Oscillations in Low-luminosity Red Giants: First Results from Kepler. *ApJl*, 713:L176–L181, April 2010.

[18] T. R. Bedding and H. Kjeldsen. Solar-like Oscillations. *Publications of the Astronomical Society of Australia*, 20:203–212, 2003.

[19] T. R. Bedding, H. Kjeldsen, F. Bouchy, H. Bruntt, R. P. Butler, D. L. Buzasi, J. Christensen-Dalsgaard, S. Frandsen, J.-C. Lebrun, M. Martić, and J. Schou. The non-detection of oscillations in Procyon by MOST: Is it really a surprise? *A&A*, 432:L43–L48, March 2005.

[20] T. R. Bedding, H. Kjeldsen, R. P. Butler, C. McCarthy, G. W. Marcy, S. J. O'Toole, C. G. Tinney, and J. T. Wright. Oscillation Frequencies and Mode Lifetimes in α Centauri A. *ApJ*, 614:380–385, October 2004.

[21] T. R. Bedding, H. Kjeldsen, T. L. Campante, T. Appourchaux, A. Bonanno, W. J. Chaplin, R. A. Garcia, M. Martić, B. Mosser, R. P. Butler, H. Bruntt, L. L. Kiss, S. J. O'Toole, E. Kambe, H. Ando, H. Izumiura, B. Sato, M. Hartmann, A. Hatzes, C. Barban, G. Berthomieu, E. Michel, J. Provost, S. Turck-Chièze, J.-C. Lebrun, J. Schmitt, J.-L. Bertaux, S. Benatti, R. U. Claudi, R. Cosentino, S. Leccia, S. Frandsen, K. Brogaard, L. Glowienka, F. Grundahl, E. Stempels, T. Arentoft, M. Bazot, J. Christensen-Dalsgaard, T. H. Dall, C. Karoff, J. Lundgreen-Nielsen, F. Carrier, P. Eggenberger, D. Sosnowska, R. A. Wittenmyer, M. Endl, T. S. Metcalfe, S. Hekker, and S. Reffert. A Multi-Site Campaign to Measure Solar-Like Oscillations in Procyon. II. Mode Frequencies. *ApJ*, 713:935–949, April 2010.

[22] S. Benatti. Search for solar-like oscillations in μ Herculis with the radial velocities technique, 2007.

[23] S. Benatti, M. Bonavita, R. U. Claudi, S. Desidera, M. Endl, and M. Barbieri. Search for Massive Earths Around SARG Asteroseismology Targets. In D. Fischer, F. A. Rasio, S. E. Thorsett, & A. Wolszczan, editor, *Astronomical Society of the Pacific Conference Series*, volume 398 of *Astronomical Society of the Pacific Conference Series*, pages 37–+, 2008.

[24] S. Benatti, R. Silvotti, R. U. Claudi, S. Schuh, R. Lutz, S.-L. Kim, R. Janulis, M. Paparò, A. Baran, and R. Østensen. The EXOTIME project: a status report on PG 1325+101 (QQ Vir). *ArXiv e-prints*, December 2010.

[25] M. Billeres, G. Fontaine, P. Brassard, S. Charpinet, J. Liebert, R. A. Saffer, and G. Vauclair. Discovery of p-mode Instabilities in the Hot Subdwarf B Star PG 1047+003. *ApJ*, 487:L81+, September 1997.

[26] P. Bloomfield. *Fourier analysis of time series: an introduction*. 1976.

[27] E. Böhm-Vitense. Über die Wasserstoffkonvektionszone in Sternen verschiedener Effektivtemperaturen und Leuchtkräfte. Mit 5 Textabbildungen. *ZAp*, 46:108–+, 1958.

[28] A. Bonanno, S. Benatti, R. Claudi, S. Desidera, R. Gratton, S. Leccia, and L. Paternò. Detection of Solar-like Oscillations in the G5 Subgiant μ Her. *ApJ*, 676:1248–1253, April 2008.

[29] W. Borucki, D. Koch, N. Batalha, D. Caldwell, J. Christensen-Dalsgaard, W. D. Cochran, E. Dunham, T. N. Gautier, J. Geary, R. Gilliland, J. Jenkins, H. Kjeldsen, J. J. Lissauer, and J. Rowe. KEPLER: Search for Earth-Size Planets in the Habitable Zone. In *IAU Symposium*, volume 253 of *IAU Symposium*, pages 289–299, February 2009.

[30] F. Bouchy, M. Bazot, N. C. Santos, S. Vauclair, and D. Sosnowska. Asteroseismology of the planet-hosting star μ Arae. I. The acoustic spectrum. *A&A*, 440:609–614, September 2005.

[31] F. Bouchy, D. Queloz, M. Deleuil, B. Loeillet, A. P. Hatzes, S. Aigrain, R. Alonso, M. Auvergne, A. Baglin, P. Barge, W. Benz, P. Bordé, H. J. Deeg, R. de La Reza, R. Dvorak, A. Erikson, M. Fridlund, P. Gondoin, T. Guillot, G. Hébrard, L. Jorda, H. Lammer, A. Léger, A. Llebaria, P. Magain, M. Mayor, C. Moutou, M. Ollivier, M. Pätzold, F. Pepe, F. Pont, H. Rauer, D. Rouan, J. Schneider, A. H. M. J. Triaud, S. Udry, and G. Wuchterl. Transiting exoplanets from the CoRoT space mission. III. The spectroscopic transit of CoRoT-Exo-2b with SOPHIE and HARPS. *A&A*, 482:L25–L28, May 2008.

[32] M. Breger and F. Beichbuchner. γ Doradus and δ Scuti stars: cousins or twins? *A&A*, 313:851–856, September 1996.

[33] T. M. Brown, R. L. Gilliland, R. W. Noyes, and L. W. Ramsey. Detection of possible p-mode oscillations on Procyon. *ApJ*, 368:599–609, February 1991.

[34] R. P. Butler, T. R. Bedding, H. Kjeldsen, C. McCarthy, S. J. O'Toole, C. G. Tinney, G. W. Marcy, and J. T. Wright. Ultra-High-Precision Velocity Measurements of Oscillations in α Centauri A. *ApJl*, 600:L75–L78, January 2004.

[35] F. Carrier and P. Eggenberger. Asteroseismology of the visual binary 70 Ophiuchi. *A&A*, 450:695–699, May 2006.

[36] C. Catala and PLATO Consortium. PLATO: PLAnetary Transits and Oscillations of stars. *Journal of Physics Conference Series*, 118(1):012040–+, October 2008.

[37] W. J. Chaplin, T. Appourchaux, Y. Elsworth, R. A. García, G. Houdek, C. Karoff, T. S. Metcalfe, J. Molenda-Żakowicz, M. J. P. F. G. Monteiro, M. J. Thompson, T. M. Brown, J. Christensen-Dalsgaard, R. L. Gilliland, H. Kjeldsen, W. J. Borucki, D. Koch, J. M. Jenkins, J. Ballot, S. Basu, M. Bazot, T. R. Bedding, O. Benomar, A. Bonanno, I. M. Brandão, H. Bruntt, T. L. Campante, O. L. Creevey, M. P. Di Mauro, G. Doğan, S. Dreizler, P. Eggenberger, L. Esch, S. T. Fletcher, S. Frandsen, N. Gai, P. Gaulme, R. Handberg, S. Hekker, R. Howe, D. Huber, S. G. Korzennik, J. C. Lebrun, S. Leccia, M. Martic, S. Mathur, B. Mosser, R. New, P.-O. Quirion, C. Régulo, I. W. Roxburgh, D. Salabert, J. Schou, S. G. Sousa, D. Stello, G. A. Verner, T. Arentoft, C. Barban, K. Belkacem, S. Benatti, K. Biazzo, P. Boumier, P. A. Bradley, A.-M. Broomhall, D. L. Buzasi, R. U. Claudi, M. S. Cunha, F. D'Antona, S. Deheuvels, A. Derekas, A. García Hernández, M. S. Giampapa, M. J. Goupil, M. Gruberbauer, J. A. Guzik, S. J. Hale, M. J. Ireland, L. L. Kiss, I. N. Kitiashvili, K. Kolenberg, H. Korhonen, A. G. Kosovichev, F. Kupka, Y. Lebreton, B. Leroy, H.-G. Ludwig, S. Mathis, E. Michel, A. Miglio, J. Montalbán, A. Moya, A. Noels, R. W. Noyes, P. L. Pallé, L. Piau, H. L. Preston, T. Roca Cortés, M. Roth, K. H. Sato, J. Schmitt, A. M. Serenelli, V. Silva Aguirre, I. R. Stevens, J. C. Suárez, M. D. Suran, R. Trampedach, S. Turck-Chièze, K. Uytterhoeven, R. Ventura, and P. A. Wilson. The Asteroseismic Potential of Kepler: First Results for Solar-Type Stars. *ApJl*, 713:L169–L175, April 2010.

[38] S. Charpinet, G. Fontaine, P. Brassard, P. Chayer, F. J. Rogers, C. A. Iglesias, and B. Dorman. A Driving Mechanism for the Newly Discovered Class of Pulsating Subdwarf B Stars. *ApJ*, 483:L123+, July 1997.

[39] S. Charpinet, G. Fontaine, P. Brassard, and B. Dorman. The Potential of Asteroseismology for Hot, Subdwarf B Stars: A New Class of Pulsating Stars? *ApJ*, 471:L103+, November 1996.

[40] J. Christensen-Dalsgaard. Some aspects of the theory of solar oscillations. *Geophys. Astrophys. Fluid Dynamics*, 62:123–152, 1991.

[41] J. Christensen-Dalsgaard. Helioseismology. *Review of Modern Physics*, Oct 2002.

[42] J. Christensen-Dalsgaard. Lecture Notes on Stellar Oscillations. Fifth Edition. May 2003.

[43] J. Christensen-Dalsgaard. ADIPLS - the Aarhus adiabatic oscillation package. *ApSS*, 316:113–120, August 2008.

[44] J. Christensen-Dalsgaard. ASTEC - the Aarhus STellar Evolution Code. *ApSS*, 316:13–24, August 2008.

[45] J. Christensen-Dalsgaard, T. R. Bedding, and H. Kjeldsen. Modeling solar-like oscillations in η Bootis. *ApJ*, 443:L29–L32, April 1995.

[46] J. Christensen-Dalsgaard, W. Dappen, S. V. Ajukov, E. R. Anderson, H. M. Antia, S. Basu, V. A. Baturin, G. Berthomieu, B. Chaboyer, S. M. Chitre, A. N. Cox, P. Demarque, J. Donatowicz, W. A. Dziembowski, M. Gabriel, D. O. Gough, D. B. Guenther, J. A. Guzik, J. W. Harvey, F. Hill, G. Houdek, C. A. Iglesias, A. G. Kosovichev, J. W. Leibacher, P. Morel, C. R. Proffitt, J. Provost, J. Reiter, E. J. Rhodes, Jr., F. J. Rogers, I. W. Roxburgh, M. J. Thompson, and R. K. Ulrich. The Current State of Solar Modeling. *Science*, 272:1286–1292, May 1996.

[47] J. Christensen-Dalsgaard, F. W. W. Dilke, and D. O. Gough. The stability of a solar model to non-radial oscillations. *MNRAS*, 169:429–445, December 1974.

[48] J. Christensen-Dalsgaard and S. Frandsen. Stellar 5 min oscillations. *SoPh*, 82:469–486, January 1983.

[49] J. Christensen-Dalsgaard and D. O. Gough. On the dipolar f mode of stellar oscillation. *MNRAS*, 326:1115–1121, September 2001.

[50] J. Christensen-Dalsgaard and G. Houdek. Prospects for asteroseismology. *ApSS*, 328:51–66, July 2010.

[51] J. Christensen-Dalsgaard and F. Perez Hernandez. The phase function for stellar acoustic oscillations. I - Theory. *MNRAS*, 257:62–88, July 1992.

[52] Kjeldsen H. Mattei J.A. Christensen-Dalsgaard, J. Solar-like oscillations of Semiregular Variables. *ApJ*, 562:L141–L144, December 2001.

[53] R. U. Claudi, A. Bonanno, S. Leccia, R. Ventura, S. Desidera, R. Gratton, R. Cosentino, L. Paternò, and M. Endl. Asteroseismology of Procyon A with SARG at TNG. *A&A*, 429:L17–L20, January 2005.

[54] G. Cowling, T. The non-radial oscillations of polytropic stars. *MNRAS*, 101:367–375, 1941.

[55] Giuli R. T. Cox, J. P. *Principles of stellar structure*. 1968.

[56] J.P. Cox. The linear theory: Initiation of pulsational instability in stars. *IAUS*, 28:3–+, 1967.

[57] J.P. Cox. Pulsationg stars. *Reports on Progress in Physics*, 37:563–698, 1974.

[58] M. S. Cunha, C. Aerts, J. Christensen-Dalsgaard, A. Baglin, L. Bigot, T. M. Brown, C. Catala, O. L. Creevey, A. Domiciano de Souza, P. Eggenberger, P. J. V. Garcia, F. Grundahl, P. Kervella, D. W. Kurtz, P. Mathias, A. Miglio, M. J. P. F. G. Monteiro, G. Perrin, F. P. Pijpers, D. Pourbaix, A. Quirrenbach, K. Rousselet-Perraut, T. C. Teixeira, F. Thévenin, and M. J. Thompson. Asteroseismology and interferometry. *A&Ar*, 14:217–360, November 2007.

[59] J. Cuypers. New observations and frequency analysis of the Beta Cephei star Tau1 LUPI. *A&As*, 69:445–449, June 1987.

[60] J. De Ridder, T. Arentoft, and H. Kjeldsen. Modelling space-based high-precision photometry for asteroseismic applications. *MNRAS*, 365:595–605, January 2006.

[61] J. De Ridder, C. Barban, F. Baudin, F. Carrier, A. P. Hatzes, S. Hekker, T. Kallinger, W. W. Weiss, A. Baglin, M. Auvergne, R. Samadi, P. Barge, and M. Deleuil. Non-radial oscillation modes with long lifetimes in giant stars. *Nat.*, 459:398–400, May 2009.

[62] T. J. Deeming. Fourier Analysis with Unequally-Spaced Data. *ApSS*, 36:137–158, August 1975.

[63] S. Deheuvels, H. Bruntt, E. Michel, C. Barban, G. Verner, C. Régulo, B. Mosser, S. Mathur, P. Gaulme, R. A. Garcia, P. Boumier, T. Appourchaux, R. Samadi, C. Catala, F. Baudin, A. Baglin, M. Auvergne, I. W. Roxburgh, and F. Pérez Hernández. Seismic and spectroscopic characterization of the solar-like pulsating CoRoT target HD 49385. *A&A*, 515:A87+, June 2010.

[64] S. Desidera, R. G. Gratton, M. Endl, M. Barbieri, R. U. Claudi, R. Cosentino, S. Lucatello, F. Marzari, and S. Scuderi. A search for planets in the metal-enriched binary HD 219542. *A&A*, 405:207–221, July 2003.

[65] F.-L. Deubner and D. Gough. Helioseismology: Oscillations as a Diagnostic of the Solar Interior. *ARA&A*, 22:593–619, 1984.

[66] S. Dreizler, S. L. Schuh, J. L. Deetjen, H. Edelmann, and U. Heber. HS0702+6043 - A new large amplitude sdB variable at the cool end of the instability region. *A&A*, 386:249–255, April 2002.

[67] M.-A. Dupret, A. Grigahcène, R. Garrido, M. Gabriel, and R. Scuflaire. Convection-pulsation coupling. II. Excitation and stabilization mechanisms in δ Sct and γ Dor stars. *A&A*, 435:927–939, June 2005.

[68] T. L. Duvall, Jr. A dispersion law for solar oscillations. *Nature*, 300:242–+, November 1982.

[69] M. Endl, M. Kürster, and S. Els. The planet search program at the ESO Coudé Echelle spectrometer. I. Data modeling technique and radial velocity precision tests. *A&A*, 362:585–594, October 2000.

[70] S. Frandsen, F. Carrier, C. Aerts, D. Stello, T. Maas, M. Burnet, H. Bruntt, T. C. Teixeira, J. R. de Medeiros, F. Bouchy, H. Kjeldsen, F. Pijpers, and J. Christensen-Dalsgaard. Detection of Solar-like oscillations in the G7 giant star xi Hya. *A&A*, 394:L5–L8, October 2002.

[71] R. A. García, C. Régulo, R. Samadi, J. Ballot, C. Barban, O. Benomar, W. J. Chaplin, P. Gaulme, T. Appourchaux, S. Mathur, B. Mosser, T. Toutain, G. A. Verner, M. Auvergne, A. Baglin, F. Baudin, P. Boumier, H. Bruntt, C. Catala, S. Deheuvels, Y. Elsworth, S. J. Jiménez-Reyes, E. Michel, F. Pérez Hernández, I. W. Roxburgh, and D. Salabert. Solar-like oscillations with low amplitude in the CoRoT target HD 181906. *A&A*, 506:41–50, October 2009.

[72] P. Gaulme, T. Appourchaux, and P. Boumier. Mode width fitting with a simple Bayesian approach. Application to CoRoT targets HD 181420 and HD 49933. *A&A*, 506:7–14, October 2009.

[73] D. O. Gough. Linear adiabatic stellar pulsation. In J. Zahn, J. P & Zinn-Justin and Amsterdam Elsevier, editors, *Astrophysical fluid dynamics, Les Houches Session XLVII*, pages 399–560, 1993.

[74] R. G. Gratton, G. Bonanno, P. Bruno, A. Cali, R. U. Claudi, R. Cosentino, S. Desidera, F. Diego, G. Farisato, G. Martorana, M. Rebeschini, and S. Scuderi. SARG: the high resolution spectrograph of TNG. *Experimental Astronomy*, 12:107–143, 2001.

[75] G. Grec, E. Fossat, and M. A. Pomerantz. Full-disk observations of solar oscillations from the geographic South Pole - Latest results. *SolPhys*, 82:55–66, January 1983.

[76] E. M. Green, G. Fontaine, E. A. Hyde, B.-Q. For, and P. Chayer. Systematics of Hot Subdwarfs Obtained from a Large Low Resolution Survey. In U. Heber, C. S. Jeffery, & R. Napiwotzki, editor, *Hot Subdwarf Stars and Related Objects*, volume 392 of *Astronomical Society of the Pacific Conference Series*, pages 75–+, 2008.

[77] E. M. Green, G. Fontaine, M. D. Reed, K. Callerame, I. R. Seitenzahl, B. A. White, E. A. Hyde, R. Østensen, O. Cordes, P. Brassard, S. Falter, E. J. Jeffery, S. Dreizler, S. L. Schuh, M. Giovanni, H. Edelmann, J. Rigby, and A. Bronowska. Discovery of A New Class of Pulsating Stars: Gravity-Mode Pulsators among Subdwarf B Stars. *ApJl*, 583:L31–L34, January 2003.

[78] N. Grevesse, A. Noels, and A. J. Sauval. A revision of the solar abundance of dysprosium. *A&A*, 271:587–+, April 1993.

[79] A. Grigahcène, V. Antoci, L. Balona, G. Catanzaro, J. Daszyńska-Daszkiewicz, J. A. Guzik, G. Handler, G. Houdek, D. W. Kurtz, M. Marconi, M. J. P. F. G. Monteiro, A. Moya, V. Ripepi, J.-C. Suárez, K. Uytterhoeven, W. J. Borucki, T. M. Brown, J. Christensen-Dalsgaard, R. L. Gilliland, J. M. Jenkins, H. Kjeldsen, D. Koch, S. Bernabei, P. Bradley, M. Breger, M. Di Criscienzo, M.-A. Dupret, R. A. García, A. García Hernández, J. Jackiewicz, A. Kaiser, H. Lehmann, S. Martín-Ruiz, P. Mathias, J. Molenda-Żakowicz, J. M. Nemec, J. Nuspl, M. Paparó, M. Roth, R. Szabó, M. D. Suran, and R. Ventura. Hybrid γ Doradus-δ Scuti Pulsators: New Insights into the Physics of the Oscillations from Kepler Observations. *ApJl*, 713:L192–L197, April 2010.

[80] A. Grigahcène, K. Uytterhoeven, V. Antoci, L. Balona, G. Catanzaro, J. Daszyńska-Daszkiewicz, J. A. Guzik, G. Handler, G. Houdek, D. W. Kurtz, M. Marconi, M. J. P. F. G. Monteiro, A. Moya, V. Ripepi, J.-C. Suárez, W. J. Borucki, T. M. Brown, J. Christensen-Dalsgaard, R. L. Gilliland, J. M. Jenkins, H. Kjeldsen, D. Koch, S. Bernabei, P. Bradley, M. Breger, M. Di Criscienzo, M.-A. Dupret, R. A. García, A. García Hernández, J. Jackiewicz, A. Kaiser, H. Lehmann, S. Martín-Ruiz, P. Mathias, J. Molenda-Żakowicz, J. M. Nemec, J. Nuspl, M. Paparó, M. Roth, R. Szabó, M. D. Suran, and R. Ventura. Kepler observations: Light shed on the hybrid γ Doradus - δ Scuti pulsation phenomenon. *Astron. Nachr*, 331, 2010.

[81] D. B. Guenther, T. Kallinger, M. Gruberbauer, D. Huber, W. W. Weiss, R. Kuschnig, P. Demarque, F. Robinson, J. M. Matthews, A. F. J. Moffat, S. M. Rucinski, D. Sasselov, and G. A. H. Walker. The Nature of p-modes and Granulation in Procyon: New MOST Photometry and New Yale Convection Models. *ApJ*, 687:1448–1459, November 2008.

[82] Z. Han, P. Podsiadlowski, P. F. L. Maxted, and T. R. Marsh. The origin of subdwarf B stars - II. *MNRAS*, 341:669–691, May 2003.

[83] G. Handler and R. R. Shobbrook. On the relationship between the δ Scuti and γ Doradus pulsators. *MNRAS*, 333:251–262, June 2002.

[84] J. Harvey. High-resolution helioseismology. In E. Rolfe & B. Battrick, editor, *Future Missions in Solar, Heliospheric & Space Plasma Physics*, volume 235 of *ESA Special Publication*, pages 199–208, June 1985.

[85] S. Hekker, C. Barban, F. Baudin, J. De Ridder, T. Kallinger, T. Morel, W. J. Chaplin, and Y. Elsworth. Oscillation mode lifetimes of red giants observed during the initial and first anticentre long run of CoRoT. *A&A*, 520:A60+, September 2010.

[86] S. Hekker, A.-M. Broomhall, W. J. Chaplin, Y. P. Elsworth, S. T. Fletcher, R. New, T. Arentoft, P.-O. Quirion, and H. Kjeldsen. The Octave (Birmingham-Sheffield Hallam) automated pipeline for extracting oscillation parameters of solar-like main-sequence stars. *MNRAS*, 402:2049–2059, March 2010.

[87] J. Holmberg, B. Nordstrom, and J. Andersen. Geneva-Copenhagen Survey of Solar neighbourhood III (Holmberg+, 2009). *VizieR Online Data Catalog*, 5130:0–+, July 2009.

[88] G. Houdek, N. J. Balmforth, J. Christensen-Dalsgaard, and D. O. Gough. Amplitudes of stochastically excited oscillations in main-sequence stars. *A&A*, 351:582–596, November 1999.

[89] S. B. Howell. Two-dimensional aperture photometry - Signal-to-noise ratio of point-source observations and optimal data-extraction techniques. *PASP*, 101:616–622, June 1989.

[90] S. B. Howell. Introduction to Differential Time-Series Astronomical Photometry Using Charged-Coupled Devices. In S. B. Howell, editor, *Astronomical CCD Observing and Reduction Techniques*, volume 23 of *Astronomical Society of the Pacific Conference Series*, pages 105–+, 1992.

[91] D. Huber, T. R. Bedding, D. Stello, B. Mosser, S. Mathur, T. Kallinger, S. Hekker, Y. P. Elsworth, D. L. Buzasi, J. De Ridder, R. L. Gilliland, H. Kjeldsen, W. J. Chaplin, R. A. García, S. J. Hale, H. L. Preston, T. R. White, W. J. Borucki, J. Christensen-Dalsgaard, B. D. Clarke, J. M. Jenkins, and D. Koch. Asteroseismology of Red Giants from the First Four Months of Kepler Data: Global Oscillation Parameters for 800 Stars. *ApJ*, 723:1607–1617, November 2010.

[92] C. A. Iglesias and F. J. Rogers. Updated Opal Opacities. *ApJ*, 464:943–+, June 1996.

[93] T. Kallinger, D. B. Guenther, J. M. Matthews, W. W. Weiss, D. Huber, R. Kuschnig, A. F. J. Moffat, S. M. Rucinski, and D. Sasselov. Nonradial p-modes in the G9.5 giant ϵ Ophiuchi? Pulsation model fits to MOST photometry. *A&A*, 478:497–505, February 2008.

[94] T. Kallinger, B. Mosser, S. Hekker, D. Huber, D. Stello, S. Mathur, S. Basu, T. R. Bedding, W. J. Chaplin, J. De Ridder, Y. P. Elsworth, S. Frandsen, R. A. García, M. Gruberbauer, J. M. Matthews, W. J. Borucki, H. Bruntt, J. Christensen-Dalsgaard, R. L. Gilliland, H. Kjeldsen, and D. G. Koch. Asteroseismology of red giants from the first four months of Kepler data: Fundamental stellar parameters. *A&A*, 522:A1+, November 2010.

[95] S.D. Kawaler. Structure and evolution of pulsating hot subdwarfs. *Astron. Nach.*, 331, 2010.

[96] D. Kilkenny, C. Koen, D. O'Donoghue, and R. S. Stobie. A new class of rapidly pulsating star - I. EC 14026-2647, the class prototype. *MNRAS*, 285:640–644, March 1997.

[97] D. Kilkenny, R. S. Stobie, D. O'Donoghue, C. Koen, N. Hambly, H. MacGillivray, and A. E. Lynas-Gray. Three new pulsating sdB stars from the Edinburgh-Cape survey. *MNRAS*, 367:1603–1608, April 2006.

[98] Bedding T.R. Christensen-Dalsgaard J. Kjeldsen, H. Asteroseismology - Studying stellar structure. *AIPC*, 1043:365, 2008.

[99] H. Kjeldsen and T. R. Bedding. Amplitudes of stellar oscillations: the implications for asteroseismology. *A&A*, 293:87–106, January 1995.

[100] H. Kjeldsen, T. R. Bedding, R. P. Butler, J. Christensen-Dalsgaard, L. L. Kiss, C. McCarthy, G. W. Marcy, C. G. Tinney, and J. T. Wright. Solar-like Oscillations in α Centauri B. *ApJ*, 635:1281–1290, December 2005.

[101] H. Kjeldsen, T. R. Bedding, M. Viskum, and S. Frandsen. Solarlike oscillations in eta Boo. *AJ*, 109:1313–1319, March 1995.

[102] L. D. Landau and E. M. Lifshitz. *Fluid Mechanics*. Pergamon Press, London, 1959.

[103] D. W. Latham, T. M. Brown, D. G. Monet, M. Everett, G. A. Esquerdo, and C. W. Hergenrother. The Kepler Input Catalog. In *Bulletin of the American Astronomical Society*, volume 37 of *Bulletin of the American Astronomical Society*, pages 1340–+, December 2005.

[104] M. Laymand and S. Vauclair. Asteroseismology of exoplanets host stars: the special case of ι Horologii (HD 17051). *A&A*, 463:657–662, February 2007.

[105] Montalbán J. Lebreton, Y. Stellar ages from asteroseismology. *IAUS*, 258, 2009.

[106] S. Leccia, H. Kjeldsen, A. Bonanno, R. U. Claudi, R. Ventura, and L. Paternò. Seismology of Procyon A: determination of mode frequencies, amplitudes, lifetimes, and granulation noise. *A&A*, 464:1059–1067, March 2007.

[107] J. W. Lee, S.-L. Kim, C.-H. Kim, R. H. Koch, C.-U. Lee, H.-I. Kim, and J.-H. Park. The sdB+M Eclipsing System HW Virginis and its Circumbinary Planets. *AJ*, 137:3181–3190, February 2009.

[108] A. Léger, D. Rouan, J. Schneider, P. Barge, M. Fridlund, B. Samuel, M. Ollivier, E. Guenther, M. Deleuil, H. J. Deeg, M. Auvergne, R. Alonso, S. Aigrain, A. Alapini, J. M. Almenara, A. Baglin, M. Barbieri, H. Bruntt, P. Bordé, F. Bouchy, J. Cabrera, C. Catala, L. Carone, S. Carpano, S. Csizmadia, R. Dvorak, A. Erikson, S. Ferraz-Mello, B. Foing, F. Fressin, D. Gandolfi, M. Gillon, P. Gondoin, O. Grasset, T. Guillot, A. Hatzes, G. Hébrard, L. Jorda, H. Lammer, A. Llebaria, B. Loeillet, M. Mayor, T. Mazeh, C. Moutou, M. Pätzold, F. Pont, D. Queloz, H. Rauer, S. Renner, R. Samadi, A. Shporer, C. Sotin, B. Tingley, G. Wuchterl, M. Adda, P. Agogu, T. Appourchaux, H. Ballans, P. Baron, T. Beaufort, R. Bellenger, R. Berlin, P. Bernardi, D. Blouin, F. Baudin, P. Bodin, L. Boisnard, L. Boit, F. Bonneau, S. Borzeix, R. Briet, J.-T. Buey, B. Butler, D. Cailleau, R. Cautain, P.-Y. Chabaud, S. Chaintreuil, F. Chiavassa, V. Costes, V. Cuna Parrho, F. de Oliveira Fialho, M. Decaudin, J.-M. Defise, S. Djalal, G. Epstein, G.-E. Exil, C. Fauré, T. Fenouillet, A. Gaboriaud, A. Gallic, P. Gamet, P. Gavalda, E. Grolleau, R. Gruneisen, L. Gueguen, V. Guis, V. Guivarc'h, P. Guterman, D. Hallouard, J. Hasiba, F. Heuripeau, G. Huntzinger, H. Hustaix, C. Imad, C. Imbert, B. Johlander, M. Jouret, P. Journoud, F. Karioty, L. Kerjean, V. Lafaille, L. Lafond, T. Lam-Trong, P. Landiech, V. Lapeyrere, T. Larqué, P. Laudet, N. Lautier, H. Lecann, L. Lefevre, B. Leruyet, P. Levacher, A. Magnan, E. Mazy, F. Mertens, J.-M. Mesnager, J.-C. Meunier, J.-P. Michel, W. Monjoin, D. Naudet, K. Nguyen-Kim, J.-L. Orcesi, H. Ottacher, R. Perez, G. Peter, P. Plasson, J.-Y. Plesseria, B. Pontet, A. Pradines, C. Quentin, J.-L. Reynaud, G. Rolland, F. Rollenhagen, R. Romagnan, N. Russ, R. Schmidt, N. Schwartz, I. Sebbag, G. Sedes, H. Smit, M. B. Steller, W. Sunter, C. Surace, M. Tello, D. Tiphène, P. Toulouse, B. Ulmer, O. Vandermarcq, E. Vergnault, A. Vuillemin, and P. Zanatta. Transiting exoplanets from the CoRoT space mission. VIII. CoRoT-7b: the first super-Earth with measured radius. *A&A*, 506:287–302, October 2009.

[109] P. Lenz and M. Breger. Period04: A software package to extract multiple frequencies from real data. In J. Zverko, J. Ziznovsky, S. J. Adelman, & W. W. Weiss, editor, *The A-Star Puzzle*, volume 224 of *IAU Symposium*, pages 786–790, December 2004.

[110] G. L. Loumos and T. J. Deeming. Spurious results from Fourier analysis of data with closely spaced frequencies. *ApSS*, 56:285–291, July 1978.

[111] M. Martić, J. Schmitt, J.-C. Lebrun, C. Barban, P. Connes, F. Bouchy, E. Michel, A. Baglin, T. Appourchaux, and J.-L. Bertaux. Evidence for global pressure oscillations on Procyon. *A&A*, 351:993–1002, November 1999.

[112] E. Masana, C. Jordi, and I. Ribas. Effective temperatures and radii of stars (Masana+, 2006). *VizieR Online Data Catalog*, 345:735–+, January 2006.

[113] S. Mathur, R. A. García, C. Catala, H. Bruntt, B. Mosser, T. Appourchaux, J. Ballot, O. L. Creevey, P. Gaulme, S. Hekker, D. Huber, C. Karoff, L. Piau, C. Régulo, I. W. Roxburgh, D. Salabert, G. A. Verner, M. Auvergne, A. Baglin, W. J. Chaplin, Y. Elsworth, E. Michel, R. Samadi, K. Sato, and D. Stello. The solar-like CoRoT target HD 170987: spectroscopic and seismic observations. *A&A*, 518:A53+, July 2010.

[114] J. M. Matthews, R. Kusching, D. B. Guenther, G. A. H. Walker, A. F. J. Moffat, S. M. Rucinski, D. Sasselov, and W. W. Weiss. No stellar p-mode oscillations in space-based photometry of Procyon. *Nature*, 430:51–53, July 2004.

[115] M. Mayor, X. Bonfils, T. Forveille, X. Delfosse, S. Udry, J.-L. Bertaux, H. Beust, F. Bouchy, C. Lovis, F. Pepe, C. Perrier, D. Queloz, and N. C. Santos. The HARPS search for southern extra-solar planets. XVIII. An Earth-mass planet in the GJ 581 planetary system. *A&A*, 507:487–494, November 2009.

[116] W. J. Merline. Precise Velocity Observation of K-Giants: Evidence for Solar-Like Oscillations in Arcturus. In J. B. Hearnshaw & C. D. Scarfe, editor, *IAU Colloq. 170: Precise Stellar Radial Velocities*, volume 185 of *Astronomical Society of the Pacific Conference Series*, pages 187–+, 1999.

[117] T. S. Metcalfe, M. J. P. F. G. Monteiro, M. J. Thompson, J. Molenda-Żakowicz, T. Appourchaux, W. J. Chaplin, G. Doğan, P. Eggenberger, T. R. Bedding, H. Bruntt, O. L. Creevey, P.-O. Quirion, D. Stello, A. Bonanno, V. Silva Aguirre, S. Basu, L. Esch, N. Gai, M. P. Di Mauro, A. G. Kosovichev, I. N. Kitiashvili, J. C. Suárez, A. Moya, L. Piau, R. A. García, J. P. Marques, A. Frasca, K. Biazzo, S. G. Sousa, S. Dreizler, M. Bazot, C. Karoff, S. Frandsen, P. A. Wilson, T. M. Brown, J. Christensen-Dalsgaard, R. L. Gilliland, H. Kjeldsen, T. L. Campante, S. T. Fletcher, R. Handberg, C. Régulo, D. Salabert, J. Schou, G. A. Verner, J. Ballot, A.-M. Broomhall, Y. Elsworth, S. Hekker, D. Huber, S. Mathur, R. New, I. W. Roxburgh, K. H. Sato, T. R. White, W. J. Borucki, D. G. Koch, and J. M. Jenkins. A Precise Asteroseismic Age and Radius for the Evolved Sun-like Star KIC 11026764. *ApJ*, 723:1583–1598, November 2010.

[118] E. Michel, A. Baglin, M. Auvergne, C. Catala, R. Samadi, F. Baudin, T. Appourchaux, C. Barban, W. W. Weiss, G. Berthomieu, P. Boumier, M.-A. Dupret, R. A. Garcia, M. Fridlund, R. Garrido, M.-J. Goupil, H. Kjeldsen, Y. Lebreton, B. Mosser, A. Grotsch-Noels, E. Janot-Pacheco, J. Provost, I. W. Roxburgh, A. Thoul, T. Toutain, D. Tiphène, S. Turck-Chieze, S. D. Vauclair, G. P. Vauclair, C. Aerts, G. Alecian, J. Ballot, S. Charpinet, A.-M. Hubert, F. Lignières, P. Mathias, M. J. P. F. G. Monteiro, C. Neiner, E. Poretti, J. Renan de Medeiros, I. Ribas, M. L. Rieutord, T. R. Cortés, and K. Zwintz. CoRoT Measures Solar-Like Oscillations and Granulation in Stars Hotter Than the Sun. *Science*, 322:558–, October 2008.

[119] A. Miglio, J. Montalbán, F. Baudin, P. Eggenberger, A. Noels, S. Hekker, J. De Ridder, W. Weiss, and A. Baglin. Probing populations of red giants in the galactic disk with CoRoT. *A&A*, 503:L21–L24, September 2009.

[120] E. Miller-Ricci, J. F. Rowe, D. Sasselov, J. M. Matthews, D. B. Guenther, R. Kuschnig, A. F. J. Moffat, S. M. Rucinski, G. A. H. Walker, and W. W. Weiss. MOST Space-based Photometry of the Transiting Exoplanet System HD 209458: Transit Timing to Search for Additional Planets. *ApJ*, 682:586–592, July 2008.

[121] M. H. Montgomery and D. O'donoghue. A derivation of the errors for least squares fitting to time series data. *Delta Scuti Star Newsletter*, 13:28–+, July 1999.

[122] B. Mosser, K. Belkacem, M.-J. Goupil, A. Miglio, T. Morel, C. Barban, F. Baudin, S. Hekker, R. Samadi, J. De Ridder, W. Weiss, M. Auvergne, and A. Baglin. Red-giant seismic properties analyzed with CoRoT. *A&A*, 517:A22+, July 2010.

[123] R. Østensen. Observational Asteroseismology of Hot Subdwarf Stars. *Astron. Nach.*, 331, 2010.

[124] R. Østensen, U. Heber, R. Silvotti, J.-E. Solheim, S. Dreizler, and H. Edelmann. Four new subdwarf B pulsators. *A&A*, 378:466–476, November 2001.

[125] R. Østensen, J.-E. Solheim, U. Heber, R. Silvotti, S. Dreizler, and H. Edelmann. Detection of pulsations in three subdwarf B stars. *A&A*, 368:175–182, March 2001.

[126] R. H. Østensen, R. Silvotti, S. Charpinet, R. Oreiro, G. Handler, E. M. Green, S. Bloemen, U. Heber, B. T. Gänsicke, T. R. Marsh, D. W. Kurtz, J. H. Telting, M. D. Reed, S. D. Kawaler, C. Aerts, C. Rodríguez-López, M. Vučković, T. A. Ottosen, T. Liimets, A. C. Quint, V. van Grootel, S. K. Randall, R. L. Gilliland, H. Kjeldsen, J. Christensen-Dalsgaard, W. J. Borucki, D. Koch, and E. V. Quintana. First Kepler results on compact pulsators - I. Survey target selection and the first pulsators. *MNRAS*, 409:1470–1486, December 2010.

[127] F. Pepe, M. Mayor, G. Rupprecht, G. Avila, P. Ballester, J.-L. Beckers, W. Benz, J.-L. Bertaux, F. Bouchy, B. Buzzoni, C. Cavadore, S. Deiries, H. Dekker, B. Delabre, S. D'Odorico, W. Eckert, J. Fischer, M. Fleury, M. George, A. Gilliotte, D. Gojak, J.-C. Guzman, F. Koch, D. Kohler, H. Kotzlowski, D. Lacroix, J. Le Merrer, J.-L. Lizon, G. Lo Curto, A. Longinotti, D. Megevand, L. Pasquini, P. Petitpas, M. Pichard, D. Queloz, J. Reyes, P. Richaud, J.-P. Sivan, D. Sosnowska, R. Soto, S. Udry, E. Ureta, A. van Kesteren, L. Weber, U. Weilenmann, A. Wicenec, G. Wieland, J. Christensen-Dalsgaard, D. Dravins, A. Hatzes, M. Kürster, F. Paresce, and A. Penny. HARPS: ESO's coming planet searcher. Chasing exoplanets with the La Silla 3.6-m telescope. *The Messenger*, 110:9–14, December 2002.

[128] F. P. Pijipers. *The physics in Asteroseismology.* 2003.

[129] M. D. Reed, J. R. Eggen, S. L. Harms, J. H. Telting, R. H. Østensen, S. J. O'Toole, D. M. Terndrup, A.-Y. Zhou, R. L. Kienenberger, and U. Heber. Time-series spectroscopy and photometry of the pulsating subdwarf B star PG 1219+534 (KY UMa). *A&A*, 493:175–183, January 2009.

[130] P. Reegen. SigSpec. I. Frequency- and phase-resolved significance in Fourier space. *A&A*, 467:1353–1371, June 2007.

[131] C. Régulo and T. Roca Cortés. Stellar p-mode oscillations signal in Procyon A from MOST data. *A&A*, 444:L5–L8, December 2005.

[132] H. Robe. Les oscillations non radiales des polytropes. 1968.

[133] F. J. Rogers and A. Nayfonov. Updated and Expanded OPAL Equation-of-State Tables: Implications for Helioseismology. *ApJ*, 576:1064–1074, September 2002.

[134] I. W. Roxburgh and S. V. Vorontsov. . *A&A*, 2007.

[135] H. Saio, R. Kuschnig, A. Gautschy, C. Cameron, G. A. H. Walker, J. M. Matthews, D. B. Guenther, A. F. J. Moffat, S. M. Rucinski, D. Sasselov, and W. W. Weiss. MOST Detects g- and p-Modes in the B Supergiant HD 163899 (B2 Ib/II). *ApJ*, 650:1111–1118, October 2006.

[136] N. C. Santos, F. Bouchy, M. Mayor, F. Pepe, D. Queloz, S. Udry, C. Lovis, M. Bazot, W. Benz, J.-L. Bertaux, G. Lo Curto, X. Delfosse, C. Mordasini, D. Naef, J.-P. Sivan, and S. Vauclair. The HARPS survey for southern extra-solar planets. II. A 14 Earth-masses exoplanet around μ Arae. *A&A*, 426:L19–L23, October 2004.

[137] S. Schuh, J. Huber, S. Dreizler, U. Heber, S. J. O'Toole, E. M. Green, and G. Fontaine. HS 0702+6043: a star showing both short-period p-mode and long-period g-mode oscillations. *A&A*, 445:L31–L34, January 2006.

[138] S. Schuh, R. Silvotti, R. Lutz, B. Loeptien, E. M. Green, R. H. Østensen, S. Leccia, S.-L. Kim, G. Fontaine, S. Charpinet, M. Francœur, S. Randall, C. Rodríguez-López, V. van Grootel, A. P. Odell, M. Paparó, Z. Bognár, P. Pápics, T. Nagel, B. Beeck, M. Hundertmark, T. Stahn, S. Dreizler, F. V. Hessman, M. Dall'Ora, D. Mancini, F. Cortecchia, S. Benatti, R. Claudi, and R. Janulis. EXOTIME: searching for planets around pulsating subdwarf B stars. *ApSS*, pages 130–+, March 2010.

[139] R. Scuflaire and A. Thoul. *Stellar stability and Asteroseismology*. 2002.

[140] R. Silvotti, A. Bonanno, S. Bernabei, G. Fontaine, S. Charpinet, S. Leccia, H. Kjeldsen, R. Janulis, A. Frasca, R. Østensen, S.-L. Kim, B.-G. Park, X. Jiang, M. D. Reed, R. S. Patterson, K. M. Gietzen, P. J. Clark, G. W. Wolf, Y. Lipkin, L. Formiggini, E. Leibowitz, T. D. Oswalt, M. Rudkin, K. Johnston, P. Brassard, P. Chayer, E. M. Green, and P. Bergeron. The rapidly pulsating subdwarf B star PG 1325+101. I. Oscillation modes from multisite observations. *A&A*, 459:557–564, November 2006.

[141] R. Silvotti, R. Østensen, U. Heber, J.-E. Solheim, S. Dreizler, and M. Altmann. PG 1325+101 and PG 2303+019: Two new large amplitude subdwarf B pulsators. *A&A*, 383:239–243, January 2002.

[142] R. Silvotti, S. Schuh, R. Janulis, J.-E. Solheim, S. Bernabei, R. Østensen, T. D. Oswalt, I. Bruni, R. Gualandi, A. Bonanno, G. Vauclair, M. Reed, C.-W. Chen, E. Leibowitz, M. Paparo, A. Baran, S. Charpinet, N. Dolez, S. Kawaler, D. Kurtz, P. Moskalik, R. Riddle, and S. Zola. A giant planet orbiting the 'extreme horizontal branch' star V391 Pegasi. *Nat.*, 449:189–191, September 2007.

[143] P. Smeyers and A. Moya. The asymptotic representation of higher-order g^+-modes in stars with a convective core. *A&A*, 465:509–524, April 2007.

[144] N. Soker. Can Planets Influence the Horizontal Branch Morphology? *AJ*, 116:1308–1313, September 1998.

[145] J. H. Steffen, N. M. Batalha, W. J. Borucki, L. A. Buchhave, D. A. Caldwell, W. D. Cochran, M. Endl, D. C. Fabrycky, F. Fressin, E. B. Ford, J. J. Fortney, M. J. Haas, M. J. Holman, S. B. Howell, H. Isaacson, J. M. Jenkins, D. Koch, D. W. Latham, J. J. Lissauer, A. V. Moorhead, R. C. Morehead, G. Marcy, P. J. MacQueen, S. N. Quinn, D. Ragozzine, J. F. Rowe, D. D. Sasselov, S. Seager, G. Torres, and W. F. Welsh. Five Kepler Target Stars That Show Multiple Transiting Exoplanet Candidates. *ApJ*, 725:1226–1241, December 2010.

[146] D. Stello, S. Basu, H. Bruntt, B. Mosser, I. R. Stevens, T. M. Brown, J. Christensen-Dalsgaard, R. L. Gilliland, H. Kjeldsen, T. Arentoft, J. Ballot, C. Barban, T. R. Bedding, W. J. Chaplin, Y. P. Elsworth, R. A. García, M.-J. Goupil, S. Hekker, D. Huber, S. Mathur, S. Meibom, V. Sangaralingam, C. S. Baldner, K. Belkacem, K. Biazzo, K. Brogaard, J. C. Suárez, F. D'Antona, P. Demarque, L. Esch, N. Gai, F. Grundahl, Y. Lebreton, B. Jiang, N. Jevtic, C. Karoff, A. Miglio, J. Molenda-Żakowicz, J. Montalbán, A. Noels, T. Roca Cortés, I. W. Roxburgh, A. M. Serenelli, V. Silva Aguirre, C. Sterken,

P. Stine, R. Szabó, A. Weiss, W. J. Borucki, D. Koch, and J. M. Jenkins. Detection of Solar-like Oscillations from Kepler Photometry of the Open Cluster NGC 6819. *ApJl*, 713:L182–L186, April 2010.

[147] D. Stello, W. J. Chaplin, S. Basu, Y. Elsworth, and T. R. Bedding. The relation between $\Delta\nu$ and ν_{max} for solar-like oscillations. *MNRAS*, 400:L80–L84, November 2009.

[148] P. B. Stetson. On the growth-curve method for calibrating stellar photometry with CCDs. *PASP*, 102:932–948, August 1990.

[149] A. A. Suchkov, V. V. Makarov, and W. Voges. ROSAT View of Hipparcos F Stars. *ApJ*, 595:1206–1221, October 2003.

[150] M. Tassoul. Asymptotic approximations for stellar nonradial pulsations. *ApJS*, 43:469–490, August 1980.

[151] T. Toutain and C. Froehlich. Characteristics of solar p-modes - Results from the IPHIR experiment. *A&A*, 257:287–297, April 1992.

[152] W. Unno, Y. Osaki, H. Ando, H. Saio, and H. Shibahashi. *Nonradial oscillations of stars*. Nonradial oscillations of stars, Tokyo: University of Tokyo Press, 1989, 2nd ed., 1989.

[153] G. Walker, J. Matthews, R. Kuschnig, R. Johnson, S. Rucinski, J. Pazder, G. Burley, A. Walker, K. Skaret, R. Zee, S. Grocott, K. Carroll, P. Sinclair, D. Sturgeon, and J. Harron. The MOST Asteroseismology Mission: Ultraprecise Photometry from Space. *PASP*, 115:1023–1035, September 2003.

[154] R. M. Warner. *Spectral analysis of time-series data*. Methodology in the social sciences, David A. Kenny, Series Editor, The Guilford Press, 1998.

[155] D. E. Winget and Clemens J. C. Provencal J. Kleinman S. J. Bradley P. A. Wood M. A. Claver C. F. Frueh M. L. Grauer A. D. Hine B. P. Hansen C. J. Fontaine G. Achilleos N. Wickramasinghe D. D. Marar T. M. K. Seetha S. Ashoka B. N. O'Donoghue D. Warner B. Kurtz D. W. Buckley D. A. Brickhill J. Vauclair G. Dolez N. Chevreton M. Barstow M. A. Solheim J. E. Kanaan A. Kepler S. O. Henry G. W. Kawaler S. D. Nather, R. E. Asteroseismology of the DOV star PG 1159-035 with the whole earth telescope. *AJ*, 378:326, 1991.

[156] D. E. Winget and Clemens J. C. Provencal J. L. Kleinman S. J. Bradley P. A. Claver C. F. Dixson J. S. Montgomery M. H. Hansen C. J. Hine B. P. Birch P. Candy M. Marar T. M. K. Seetha S. Ashoka B. N. Leibowitz E. M. O'Donoghue D. Warner B. Buckley D. A. H. Tripe P. Vauclair G. Dolez N. Chevreton M. Serre T. Garrido R. Kepler S. O. Kanaan A. Augusteijn T. Wood M. A. Bergeron P. Grauer A. D. Nather, R. E. Whole Earth telescope observations of the DBV white dwarf GD 358. *AJ*, 430:839, 1994.

[157] C. O. Wright, M. P. Egan, K. E. Kraemer, and S. D. Price. The Tycho-2 Spectral Type Catalog (Wright+, 2003). *VizieR Online Data Catalog*, 3231:0–+, October 2002.

[158] W. Zima, T. Arentoft, J. De Ridder, S. Salmon, C. Catala, H. Kjeldsen, and C. Aerts. The PLATO End-to-End CCD Simulator – Modelling space-based ultra-high precision CCD photometry for the assessment study of the PLATO Mission. *ArXiv e-prints*, April 2010.